ARTICLE　　　　　　　　　　　　　　　　　　　　　　　　　　　**Open Access**

Essential role of microglial transforming growth factor-β1 in antidepressant actions of (*R*)-ketamine and the novel antidepressant TGF-β1

Kai Zhang[1,5], Chun Yang[1,6], Lijia Chang[1], Akemi Sakamoto[2], Toru Suzuki[3], Yuko Fujita[1], Youge Qu[1], Siming Wang[1], Yaoyu Pu[1], Yunfei Tan (iD)[1], Xingming Wang[1], Tamaki Ishima[1], Yukihiko Shirayama[1,4], Masahiko Hatano[2], Kenji F. Tanaka (iD)[3] and Kenji Hashimoto (iD)[1]

Abstract
In rodent models of depression, (*R*)-ketamine has greater potency and longer-lasting antidepressant effects than (*S*)-ketamine; however, the precise molecular mechanisms underlying the antidepressant actions of (*R*)-ketamine remain unknown. Using RNA-sequencing analysis, we identified novel molecular targets that contribute to the different antidepressant effects of the two enantiomers. Either (*R*)-ketamine (10 mg/kg) or (*S*)-ketamine (10 mg/kg) was administered to susceptible mice after chronic social defeat stress (CSDS). RNA-sequencing analysis of prefrontal cortex (PFC) and subsequent GSEA (gene set enrichment analysis) revealed that transforming growth factor (TGF)-β signaling might contribute to the different antidepressant effects of the two enantiomers. (*R*)-ketamine, but not (*S*)-ketamine, ameliorated the reduced expressions of *Tgfb1* and its receptors (*Tgfbr1* and *Tgfbr2*) in the PFC and hippocampus of CSDS susceptible mice. Either pharmacological inhibitors (i.e., RepSox and SB431542) or neutralizing antibody of TGF-β1 blocked the antidepressant effects of (*R*)-ketamine in CSDS susceptible mice. Moreover, depletion of microglia by the colony-stimulating factor 1 receptor (CSF1R) inhibitor PLX3397 blocked the antidepressant effects of (*R*)-ketamine in CSDS susceptible mice. Similar to (*R*)-ketamine, the recombinant TGF-β1 elicited rapid and long-lasting antidepressant effects in animal models of depression. Our data implicate a novel microglial TGF-β1-dependent mechanism underlying the antidepressant effects of (*R*)-ketamine in rodents with depression-like phenotype. Moreover, TGF-β1 and its receptor agonists would likely constitute a novel rapid-acting and sustained antidepressant in humans.

Introduction

In 1990, Trullas and Skolnick[1] demonstrated that *N*-methyl-D-aspartate receptor (NMDAR) antagonists such as (+)-MK-801 showed antidepressant-like effects in rodents. In 2000, Berman et al.[2] demonstrated the rapid-acting and sustained antidepressant effects of the NMDAR antagonist ketamine in patients with major depressive disorder (MDD). Subsequently, several groups replicated the robust antidepressant effects of ketamine in treatment-resistant patients with either MDD or bipolar disorder[3–10]. Interestingly, ketamine rapidly reduced suicidal thoughts in depressed patients with suicidal ideation within 1 day and for up to 1 week[11,12]. In addition, it is suggested that suicidal thoughts may be related to symptoms of anhedonia independent of other depressive symptoms[13]. Meta-analyses revealed that ketamine has rapid-acting and sustained antidepressant effects and anti-suicidal ideation effects in treatment-resistant patients with depression[14–16]. Importantly, meta-analyses showed that the effect sizes of ketamine are larger than those of

Correspondence: Kenji Hashimoto (hashimoto@faculty.chiba-u.jp)
[1]Division of Clinical Neuroscience, Chiba University Center for Forensic Mental Health, Chiba 260-8670, Japan
[2]Department of Biomedical Science, Chiba University Graduate School of Medicine, Chiba 260-8670, Japan
Full list of author information is available at the end of the article.

other NMDAR antagonists[14,15], suggesting that NMDAR blockade is not a sole mechanism of antidepressant action for ketamine. The collective rapid-acting and sustained antidepressant actions of ketamine in depressed patients are serendipitous in the field of psychiatry;[17–19] however, the precise molecular and cellular mechanisms underlying antidepressant effects of ketamine remain to be elucidated[20–25]. Off-label use of ketamine is popular in the United States (US), although the adverse side-effects (i.e., psychotomimetic effects, dissociation, and abuse liability) of ketamine remain to be resolved[26,27].

Ketamine (Ki = 0.53 μM for NMDAR), also known as (R, S)-ketamine, is a racemic mixture that contains equal amounts of (R)-ketamine (or arketamine) (Ki = 1.4 μM for NMDAR) and (S)-ketamine (or esketamine) (Ki = 0.30 μM for NMDAR)[24]. Preclinical data have shown that (R)-ketamine displays greater potency and longer -lasting antidepressant effects than (S)-ketamine in rodent models of depression[28–34], suggesting that NMDARs do not play a major role in the robust antidepressant effects of ketamine[24]. Importantly, in both rodents and monkey, the side-effects of (R)-ketamine were lower than were those of (R,S)-ketamine and (S)-ketamine[29,35–38]. In addition, in humans, the incidence of psychotomimetic side-effects of (S)-ketamine (0.45 mg/kg) was higher than that of (R)-ketamine (1.8 mg/kg), although the dose of (S)-ketamine was lower than was that of (R)-ketamine[39]. Though (S)-ketamine produced psychotic reactions, including depersonalization and hallucinations, the same dosage of (R)-ketamine did not induce psychotic symptoms in the healthy subjects, and most of them experienced a state of relaxation[40]. These results indicate that (S)-ketamine contributes to the acute side-effects of ketamine, whereas (R)-ketamine may not be associated with these side-effects[22,24]. On 5 March 2019, the US Food & Drug Administration approved (S)-ketamine nasal spray for treatment-resistant depressed patients. Due to the risk of serious adverse effects, (S)-ketamine nasal spray can be obtained only through a restricted distribution system under the Risk Evaluation and Mitigation Strategy. A clinical trial of (R)-ketamine in humans is underway[24]. Meanwhile, little is known about the precise molecular mechanisms underlying the different antidepressant effects of the two enantiomers[24,25,41,42].

The aim of this study was to identify the novel molecular mechanisms underlying the antidepressant effects of (R)-ketamine in animal models of depression. First, we conducted RNA-sequencing analysis of the prefrontal cortex (PFC) of chronic social defeat stress (CSDS) susceptible mice treated with either (R)-ketamine or (S)-ketamine, as PFC contributes to the antidepressant actions of ketamine and its enantiomers[29,43,44]. Second, we studied the effects of pharmacological inhibitors and a neutralizing antibody of the novel target in the antidepressant effects of (R)-ketamine. Finally, we investigated whether the novel molecule (i.e., TGF-β) has rapid-acting and sustained antidepressant effects in rodent models of depression.

Materials and methods
Animals
Male adult C57BL/6 mice, aged 8 weeks (body weight 20–25 g, Japan SLC, Inc., Hamamatsu, Japan), male CD1 mice, aged 14 weeks (body weight 40–45 g, Japan SLC, Inc., Hamamatsu, Japan) were used in the experiments. Male Sprague-Dawley rats, aged 7 weeks (body weight 200–230 g, Charles-River Japan, Co., Tokyo, Japan) were used for learned helplessness (LH) model. No blinding for animal experiments was done. Animals were housed under controlled temperature and 12 h light/dark cycles (lights on between 07:00–19:00), with ad libitum food and water. The study was approved by the Chiba University Institutional Animal Care and Use Committee.

Compounds and treatment
(R)-ketamine hydrochloride and (S)-ketamine hydrochloride were prepared by recrystallization of (R,S)-ketamine (Ketalar®, ketamine hydrochloride, Daiichi Sankyo Pharmaceutical Ltd., Tokyo, Japan) and D-(-)-tartaric acid (or L− (+)-tartaric acid), respectively[28]. The purity of these enantiomers was determined by a high-performance liquid chromatography (CHIRALPAK® IA, Column size: 250 × 4.6 mm, Mobile phase: n-hexane/dichloromethane/ diethylamine (75/25/0.1), Daicel Corporation, Tokyo, Japan)[28]. The dose (10 mg/kg as hydrochloride salt) of (R)-ketamine and (S)-ketamine was selected as reported previously[28,29,32–35]. RepSox (10 mg/kg, i.p., a TGF-β1 receptor inhibitor; Selleck Chemicals, Co., Ltd, Houston, TX, USA), SB431542 (10 μM, 2 μl, i.c.v., a TGF-β1 receptor inhibitor; Tocris Bioscience, Ltd., Bristol, UK), neutralized TGF-β antibody (Catalog #: MAB1835–500; R&D System, Inc. Minneapolis, MN), and mouse IgG1 control antibody (Catalog #: MAB002; R&D System, Inc. Minneapolis, MN) were used. Recombinant mouse TGF-β1 (Catalog #: 7666-MB-005; R&D System, Inc. Minneapolis, MN) and recombinant mouse TGF-β2 (Catalog #: 302-B2; R&D System, Inc. Minneapolis, MN) were used as previously reported[45,46]. PLX3397 [Pexidartinib: a colony-stimulating factor 1 receptor (CSF1R) inhibitor, MedChemExpress Co., Ltd., Monmouth Junction, NJ] was used to decrease microglia in the brain. LPS (Catalog #: L-4130, serotype 0111:B4, Sigma-Aldrich, St Louis, MO, USA) was used for inflammation model of depression. Other reagents were purchased commercially.

CSDS model and LPS-induced model
The procedure of CSDS was performed as previously reported[29,32–34,47]. Detailed methods were shown in the supplemental information.

RNA-sequencing analysis

(R)-Ketamine (10 mg/kg) or (S)-ketamine (10 mg/kg) was administered intraperitoneally (i.p.) to susceptible mice after CSDS (Fig. 1a). PFC was collected 3 days after a single administration. RNA-sequencing analysis of PFC samples was performed at Tataka Bio Inc. (Kusatsu, Shiga, Japan). Analysis of the biological functions was performed using gene set enrichment analysis (GSEA)(http://software.broadinstitute.org/gsea/index.jsp).
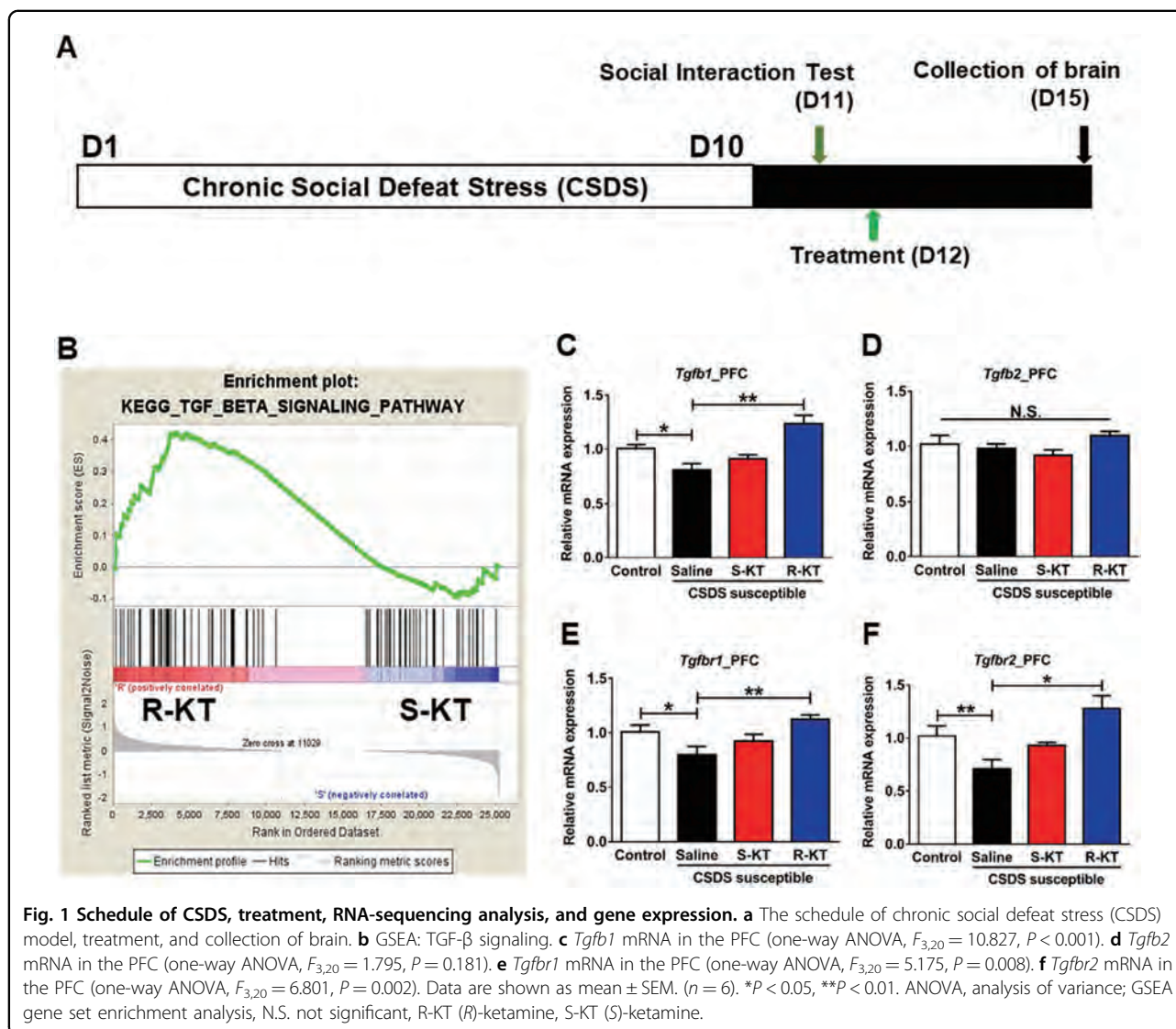
Gene expression analysis by quantitative real-time PCR

Control mice and CSDS susceptible mice were sacrificed 3 days after intraperitoneal (i.p.) administration of saline (10 ml/kg), (R)-ketamine (10 mg/kg), or (S)-ketamine (10 mg/kg). The PFC and hippocampus were quickly dissected on ice from whole brain since these brain regions play a key role in antidepressant effects of (R)-ketamine[44]. Detailed methods were shown in the supplemental information.

Inhibition of TGF-β1 inhibitors and neutralizing antibody

To examine the role of TGF-β1 in the antidepressant effects of (R)-ketamine, two inhibitors (RepSox and SB431542) of TGF-β receptor 1 were used. RepSox (10 mg/kg, i.p.) or vehicle (10 ml/kg, i.p.) was injected 30 min before i.p. administration of (R)-ketamine (10 mg/kg) in CSDS susceptible mice. SB431542 (10 μM, 2 μl, i.c.v.) or vehicle (2 μl, i.c.v.) was injected 30 min before i.p. administration of (R)-ketamine (10 mg/kg) in CSDS susceptible mice. The neutralizing antibody of TGF-β1 (1 μg/ml, 2 μL, i.c.v.) or control antibody (1 μg/ml, 2 μL, i.c.v.) was injected 30 min before i.p. administration of (R)-ketamine (10 mg/kg) in CSDS susceptible mice. Subsequently, behavioral tests were performed.

Fig. 1 Schedule of CSDS, treatment, RNA-sequencing analysis, and gene expression. a The schedule of chronic social defeat stress (CSDS) model, treatment, and collection of brain. **b** GSEA: TGF-β signaling. **c** *Tgfb1* mRNA in the PFC (one-way ANOVA, $F_{3,20} = 10.827$, $P < 0.001$). **d** *Tgfb2* mRNA in the PFC (one-way ANOVA, $F_{3,20} = 1.795$, $P = 0.181$). **e** *Tgfbr1* mRNA in the PFC (one-way ANOVA, $F_{3,20} = 5.175$, $P = 0.008$). **f** *Tgfbr2* mRNA in the PFC (one-way ANOVA, $F_{3,20} = 6.801$, $P = 0.002$). Data are shown as mean ± SEM. ($n = 6$). *$P < 0.05$, **$P < 0.01$. ANOVA, analysis of variance; GSEA gene set enrichment analysis, N.S. not significant, R-KT (R)-ketamine, S-KT (S)-ketamine.

Depletion of microglia by PLX3397

PLX3397 was reported to eliminate microglia in the brain[48–50]. For preliminary experiment, PLX3397 (10 μM or 100 μM, 2 μl, i.c.v.) or vehicle [10% dimethyl sulfoxide (DMSO) and 90% (sulfobutylether-β-cyclodextrin)(SBE-β-CD)] was administered to mice under isoflurane anesthesia. The PFC was collected 6, 12, and 24 h after i.c.v. infusion, and Western blot analysis of Iba1 in the PFC was performed.

To examine the effects of microglia depletion, PLX3397 (100 μM, 2 μl, i.c.v.) or vehicle (10% DMSO and 90% SBE-β-CD) was administered to mice under isoflurane anesthesia. PFC was collected 24 h after injection. Right PFC and left PFC were used for FACS analysis and Western blot of Iba1, respectively.

To examine the effects of microglia depletion on antidepressant effects of (R)-ketamine, PLX3397 (100 μM, 2 μl, i.c.v.) or vehicle (10% DMSO and 90% SBE-β-CD) was administered to CSDS susceptible mice under isoflurane anesthesia. Saline (10 ml/kg) or (R)-ketamine (10 mg/kg) was administered i.p. 24 h after injection of PLX3397 or vehicle. Subsequently, behavioral tests were performed.

Antidepressant effects of TGF-β1 in a CSDS model

Effects of recombinant TGF-β1 in a CSDS model, LPS model, and LH model were examined. Saline (2 μL, i.c.v.) or (R)-ketamine (1 mg/ml, 2 μL, i.c.v.) was administered to CSDS susceptible mice. Saline (2 μL, i.c.v.) was administered to control mice. Subsequently, behavioral tests were performed.

Antidepressant effects of TGF-β1 in a LPS-induced inflammation model

Inflammation model by lipopolysaccharide (LPS) was performed as previously reported[51–53]. Saline (10 ml/kg) or LPS (0.5 mg/kg) was administered i.p. to mice. Under isoflurane anesthesia, saline (2 μl, i.c.v.) or TGF-β1 (10 ng/μl, 2 μl, i.c.v.) was administered to mice 23 hrs after LPS administration. The locomotion and FST were performed 1 and 3 h after injection, respectively.

For intranasal administration, saline (15 μl) or TGF-β1 (1.5 μg, 15 μl) was administered to mice 23 hrs after LPS administration, as previously reported[38]. Mice were restrained by hand, and saline or TGF-β1 was administered intranasally into awake mice using Eppendorf micropipette (Eppendorf Japan, Tokyo, Japan). The locomotion and FST were performed 1 and 3 h after injection, respectively.

Behavioral tests

Behavioral tests including locomotion, tail suspension test (TST), forced swimming test (FST), and one % sucrose preference test (SPT) were performed as previously reported[28,29,32–34]. Detailed methods were shown in the supplemental information.

Learned helplessness (LH) model

Rat LH paradigm was performed as previously reported[44,54]. Detailed methods were shown in the supplemental information.

Western blot analysis of Iba1

Western blot analysis was performed as reported previously[29,34,51,52]. Detailed methods were shown in the supplemental information.

Double staining by in situ hybridization and immunohistochemistry

Mice were deeply anesthetized with isoflurane and sodium pentobarbital, and transcardially perfused with 4% paraformaldehyde in 0.1 M phosphate buffer (pH 7.4). The brains were further immersed in the same fixative overnight, cryoprotected in 20% sucrose/phosphate-buffered saline (PBS), and frozen by liquid nitrogen. The brains were sectioned coronally on a cryostat (CM3050S; Leica Biosystems, Germany) at 25 μm thickness. The cryosections were treated with proteinase K (40 μg/ml; Merck). After they were washed and acetylated, sections were incubated with a digoxigenin (DIG)-labeled mouse *Tgfb1* (cat#: G430055L01), *Tgfbr1* (cat#: F630025J19), or *Tgfbr2* (cat#: I420016D17) cRNA probes (DNAFORM, Yokohama, Kanagawa, Japan). After the sections were washed in buffers with serial differences in stringency, they were incubated with an alkaline phosphatase-conjugated anti-DIG antibody (1:5000; Roche, Japan). The cRNA probes were visualized with freshly prepared colorimetric substrate (NBT/BCIP; Roche, Japan). After visualized, sections were incubated with primary antibodies overnight at RT. All antibodies were diluted in PBS with 0.1% Triton X-100. The following antibodies were used: anti-Iba1 (cat#: 019–19741, 1:1000, rabbit, polyclonal; Wako, Japan), and anti-S100b (cat#: ab52642, 1:200, rabbit, monoclonal; Abcam, Cambridge, UK). the sections were sequentially incubated with anti-rabbit IgG biotinylated secondary antibodies (1:250, goat, polyclonal; Vector Laboratories, USA) for 90 min at room temperature (RT), an avidin-biotin complex (Vector Laboratories, USA) for 30 min at RT, and then the colorimetric reactions were developed with DAB (3,3′-diaminobenzidine) (ImmPACT DAB; Vector Laboratories, USA). Images of the sections were captured using a light microscope (BZ-X710; Keyence, Japan).

FACS analysis

Mouse PFC tissues were mashed and passed through a 70 μm mesh to prepare single cell suspension then subjected for FACS analysis. Cells were stained with

monoclonal antibodies against cell surface antigens at 4 °C for 30 min, then washed with PBS. In indicated cells, cells were fixed and permeabilized using FoxP3 staining buffer set (Invitrogen) according to the manufacturer instruction. Then intracellular antigens were stained with indicated antibodies at room temperature for 30 min. The following antibodies were used for staining; anti TMEM119-PE (Abcam, Cambridge, UK), allophycocyanin conjugated anti CD11b (BD Bioscience, Franklin Lakes, NJ), anti Iba1-FITC (Abcam), anti TGF-β-allophycocyanin (BioLegend, San Diego, CA). The stained cells were analyzed using FACSCantII and FlowJo software (BD).

Statistical analysis

The data show as the mean ± standard error of the mean (S.E.M.). Analysis was performed using PASW Statistics 20 (formerly SPSS Statistics; SPSS). The data were analyzed using Student t-test or the one-way analysis of variance (ANOVA), followed by post hoc Tukey test. The P-values < 0.05 were considered statistically significant.

Results

RNA-sequencing analysis of PFC samples

To identify the novel molecular targets for the antidepressant effects of (R)-ketamine, we collected PFC samples 3 days after either (R)-ketamine (10 mg/kg) or (S)-ketamine (10 mg/kg) were administered to CSDS susceptible mice. We performed RNA-sequencing analysis of PFC samples from animals treated with either (R)-ketamine or (S)-ketamine (Fig. 1a). GSEA revealed that TGF-β signaling might be involved in the differential antidepressant effects of the two enantiomers (Fig. 1b). We found reduced expression of *Tgfb1* and its receptors (*Tgfbr1* and *Tgfbr2*) in the PFC and hippocampus from CSDS susceptible mice (Fig. 1c–f **and** Fig. S1). Conversely, the expression of *Tgfb2* in the PFC and the hippocampus did not differ in the four groups (Fig. 1c–f and Fig. S1).
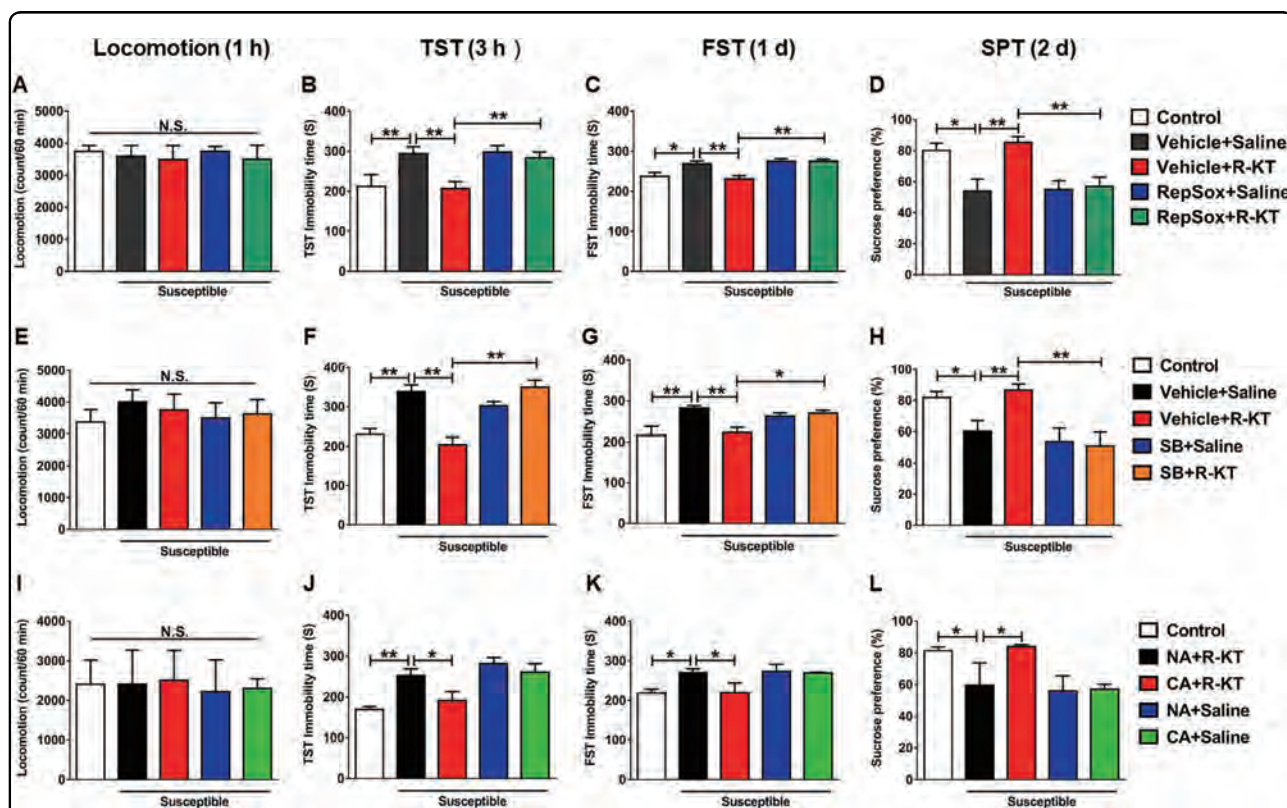

Fig. 2 Effects of TGF-β1 inhibitors (RepSox and SB431542) and neutralizing TGF-β1 antibody on antidepressant effects of (R)-ketamine in CSDS model. a Locomotion (1 h, one-way ANOVA, $F_{4,35} = 0.146$, $P = 0.964$). **b** TST (3 h, one-way ANOVA, $F_{4,35} = 5.439$, $P = 0.002$). **c** FST (1 day, one-way ANOVA, $F_{4,35} = 2.919$, $P = 0.035$). **d** SPT (2 days, one-way ANOVA, $F_{4,35} = 7.011$, $P < 0.001$). Data are shown as mean ± SEM. ($n = 8$). *$P < 0.05$, **$P < 0.01$. **e** Locomotion (1 h, one-way ANOVA, $F_{4,35} = 0.299$, $P = 0.877$). **f** TST (3 h, one-way ANOVA, $F_{4,35} = 16.586$, $P < 0.001$). **g** FST (1 day, one-way ANOVA, $F_{4,35} = 4.686$, $P = 0.004$). **h** SPT (2 day, one-way ANOVA, $F_{4,35} = 6.161$, $P = 0.001$). **i** Locomotion (1 h, one-way ANOVA, $F_{4,25} = 0.020$, $P = 0.999$). **j** TST (3 h, one-way ANOVA, $F_{4,35} = 8.165$, $P < 0.001$). **k** FST (1 day, one-way ANOVA, $F_{4,35} = 4.012$, $P = 0.015$). **l** SPT (2 day, one-way ANOVA, $F_{4,35} = 3.872$, $P = 0.021$). Data are shown as mean ± SEM. ($n = 8$). *$P < 0.05$, **$P < 0.01$. ANOVA analysis of variance, CA control antibody, FST forced swimming test, NA neutralizing antibody, N.S. not significant, R-KT (R)-ketamine, SB SB431542, SPT sucrose preference test, TST tail suspension test.

Interestingly, (*R*)-ketamine (10 mg/kg), but not (*S*)-ketamine (10 mg/kg), significantly ameliorated the reduced expression of these genes (Fig. 1c–f and Fig. S1).

Effects of TGF-β1 inhibitors and neutralizing antibody in the antidepressant effects of (*R*)-ketamine

To study the role of TGF-β1 in the antidepressant effects of (*R*)-ketamine, we used two TGF-β receptor 1 inhibitors: RepSox and SB431542. Pretreatment with RepSox (10 mg/kg, i.p., 30 min) significantly blocked the antidepressant effects of (*R*)-ketamine in CSDS susceptible mice (Fig. 2a–d). Likewise, pretreatment with SB431542 (10 μM, 2 μl, i.c.v., 30 min) significantly blocked the antidepressant effects of (*R*)-ketamine in CSDS susceptible mice (Fig. 2e–h). Moreover, pretreatment with neutralizing antibody of TGF-β1 (1 μg/ml, 2 μL, i.c.v., 30 min) significantly blocked the antidepressant effects of (*R*)-ketamine in CSDS susceptible mice (Fig. 2i–l). These findings indicate that TGF-β1 might contribute to the antidepressant effects of (*R*)-ketamine in CSDS susceptible mice.

Role of microglial TGF-β1

TGF-β1 is constitutively expressed in microglia into adulthood[55]. An earlier study demonstrated that TGF-β1 was necessary for the in vitro development of microglia and that microglia were absent in the brain of TGF-β1-deficient mice[56], suggesting that TGF-β1 plays a key role in microglia. Microglia rely on cytokine signaling, such as activation of CSF1R and TGF-β1, for their survival[57]. In situ hybridization with cell-type marker immunostaining revealed high expression of *Tgfb1* and its receptors (*Tgfbr1* and *Tgfbr2*) in microglia, but not in astrocytes, in mouse brain PFC (Fig. 3).

To examine whether microglia TGF-β1 contributes to the antidepressant effects of (*R*)-ketamine, we studied the impact of microglial depletion on the antidepressant effects of (*R*)-ketamine. Preliminary experimentation revealed that i.c.v. injection of PLX3397, a potent CSF1R inhibitor, reduced the Iba1 protein in the mouse PFC (Fig. S2). In this study, we used the time (24 h) of PLX3397 (100 μM, 2 μl, i.c.v.). Using FACS analysis, we analyzed the expression of both Iba1 and TGF-β1 in TMEM119$^+$CD11b$^+$ microglia in the PFC. Pretreatment with PLX3397 significantly reduced the expression of both TGF-β1 and Iba1 in TMEM119$^+$CD11b$^+$ microglia (Fig. 4a–c). Furthermore, Western blot analysis revealed that PLX3397 injection reduced Iba1 protein in the PFC (Fig. 4d). These findings indicate partial depletion of microglia by PLX3397 in the PFC.

Next, we studied the impact of PLX3397 on the antidepressant effects of (*R*)-ketamine in CSDS susceptible mice (Fig. 5a). There were no changes in locomotion among the five groups (Fig. 5b). Findings from the TST and the forced swim test (FST), showed that PLX3397 significantly blocked the antidepressant effects of (*R*)-ketamine for increased immobility time of both TST and FST (Fig. 5c, d). In the SPT, PLX3397 significantly blocked the effects of (*R*)-ketamine for reduced sucrose preference in CSDS susceptible mice (Fig. 5e). Collectively, partial depletion of microglia by PLX3397 significantly blocked the antidepressant effects of (*R*)-ketamine in CSDS susceptible mice (Fig. 5). These findings indicate that microglia-expressing molecules, including TGF-β1 and its receptors, contribute to the antidepressant effects of (*R*)-ketamine in a CSDS model.

Antidepressant effects of TGF-β1 in rodent models of depression

Finally, we studied whether mouse recombinant TGF-β1 has antidepressant effects in three animal models of depression. First, we studied the effects of TGF-β1 and TGF-β2 in the CSDS model (Fig. 6a). There were no changes in locomotion in the four groups (Fig. 6b, h). A single i.c.v. injection of (*R*)-ketamine (1 mg/ml, 2 μl) produced rapid and sustained antidepressant effects in CSDS susceptible mice, consistent with the previous report[58]. Similar to (*R*)-ketamine, i.c.v. infusion of TGF-β1 (10 ng/ml, 2 μl) significantly the increased

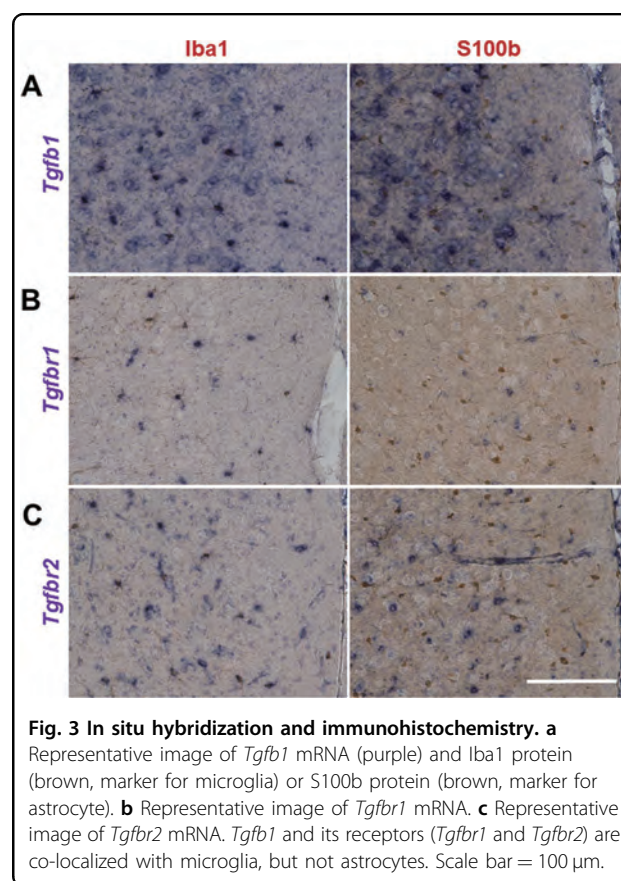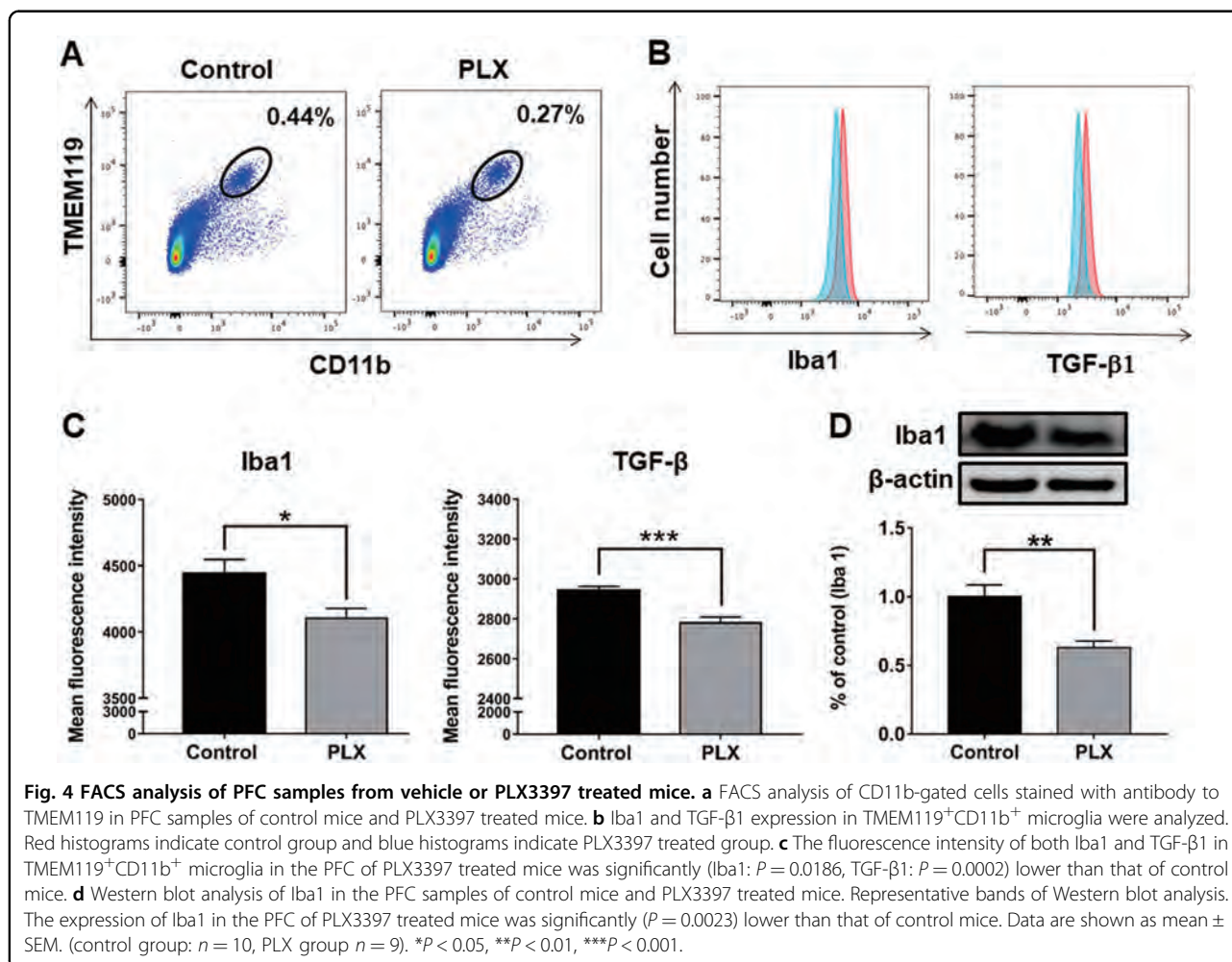**Fig. 3 In situ hybridization and immunohistochemistry. a** Representative image of *Tgfb1* mRNA (purple) and Iba1 protein (brown, marker for microglia) or S100b protein (brown, marker for astrocyte). **b** Representative image of *Tgfbr1* mRNA. **c** Representative image of *Tgfbr2* mRNA. *Tgfb1* and its receptors (*Tgfbr1* and *Tgfbr2*) are co-localized with microglia, but not astrocytes. Scale bar = 100 μm.

Fig. 4 FACS analysis of PFC samples from vehicle or PLX3397 treated mice. a FACS analysis of CD11b-gated cells stained with antibody to TMEM119 in PFC samples of control mice and PLX3397 treated mice. **b** Iba1 and TGF-β1 expression in TMEM119⁺CD11b⁺ microglia were analyzed. Red histograms indicate control group and blue histograms indicate PLX3397 treated group. **c** The fluorescence intensity of both Iba1 and TGF-β1 in TMEM119⁺CD11b⁺ microglia in the PFC of PLX3397 treated mice was significantly (Iba1: $P = 0.0186$, TGF-β1: $P = 0.0002$) lower than that of control mice. **d** Western blot analysis of Iba1 in the PFC samples of control mice and PLX3397 treated mice. Representative bands of Western blot analysis. The expression of Iba1 in the PFC of PLX3397 treated mice was significantly ($P = 0.0023$) lower than that of control mice. Data are shown as mean ± SEM. (control group: $n = 10$, PLX group $n = 9$). *$P < 0.05$, **$P < 0.01$, ***$P < 0.001$.

immobility time of both TST and FST in CSDS susceptible mice (Fig. 6c, d). In the SPT, i.c.v. infusion of TGF-β1 significantly the reduced sucrose preference in CSDS susceptible mice (Fig. 6e-g). Interestingly, we detected the beneficial effects of TGF-β1 seven days after a single injection (Fig. 6g), indicating long-lasting antidepressant effects of TGF-β1. Conversely, TGF-β2 (10 ng/ml, 2 μl) did not produce antidepressant effects in CSDS susceptible mice, though (R)-ketamine (1 mg/ml, 2 μl) produced rapid and sustained antidepressant effects in the same model (Fig. 6h–l).

Moreover, a single i.c.v. infusion of TGF-β1 (10 ng/ml, 2 μl) significantly attenuated the increased immobility time of FST in LPS (0.5 mg/kg)-treated mice (Fig. 7a–c). In addition, a single intranasal administration of TGF-β1 (1.5 μg, 15 μl) significantly attenuated the increased immobility time of FST in LPS-treated mice (Fig. 7d–f). In a rat LH model, bilateral i.c.v. infusion of TGF-β1 (250 ng/side) significantly reduced the failure number and latency of LH rats 4 days after i.c.v. injection (Fig. 7g–i). These findings indicate that

recombinant TGF-β1 has ketamine-like robust antidepressant effects in rodent models of depression.

Discussion

The main findings of this study are as follows: First, RNA-sequencing and GSEA revealed the role of TGF-β signaling in the beneficial antidepressant effects of (R)-ketamine compared with (S)-ketamine. RT-PCR revealed reduced expression of *Tgfb1* and its receptors (*Tgfbr1* and *Tgfbr2*) in the PFC and the hippocampus from CSDS susceptible mice. Furthermore, (R)-ketamine, but not (S)-ketamine, attenuated the reduced expression of these genes in the PFC and the hippocampus of CSDS susceptible mice. Second, pharmacological inhibitors and neutralizing antibody of TGF-β1 blocked the antidepressant effects of (R)-ketamine in CSDS susceptible mice, indicating a role of TGF-β1 signaling in the antidepressant effects of (R)-ketamine. Third, partial depletion of microglia by PLX3397 blocked antidepressant effects of (R)-ketamine in CSDS susceptible mice, indicating a role of microglia in the antidepressant
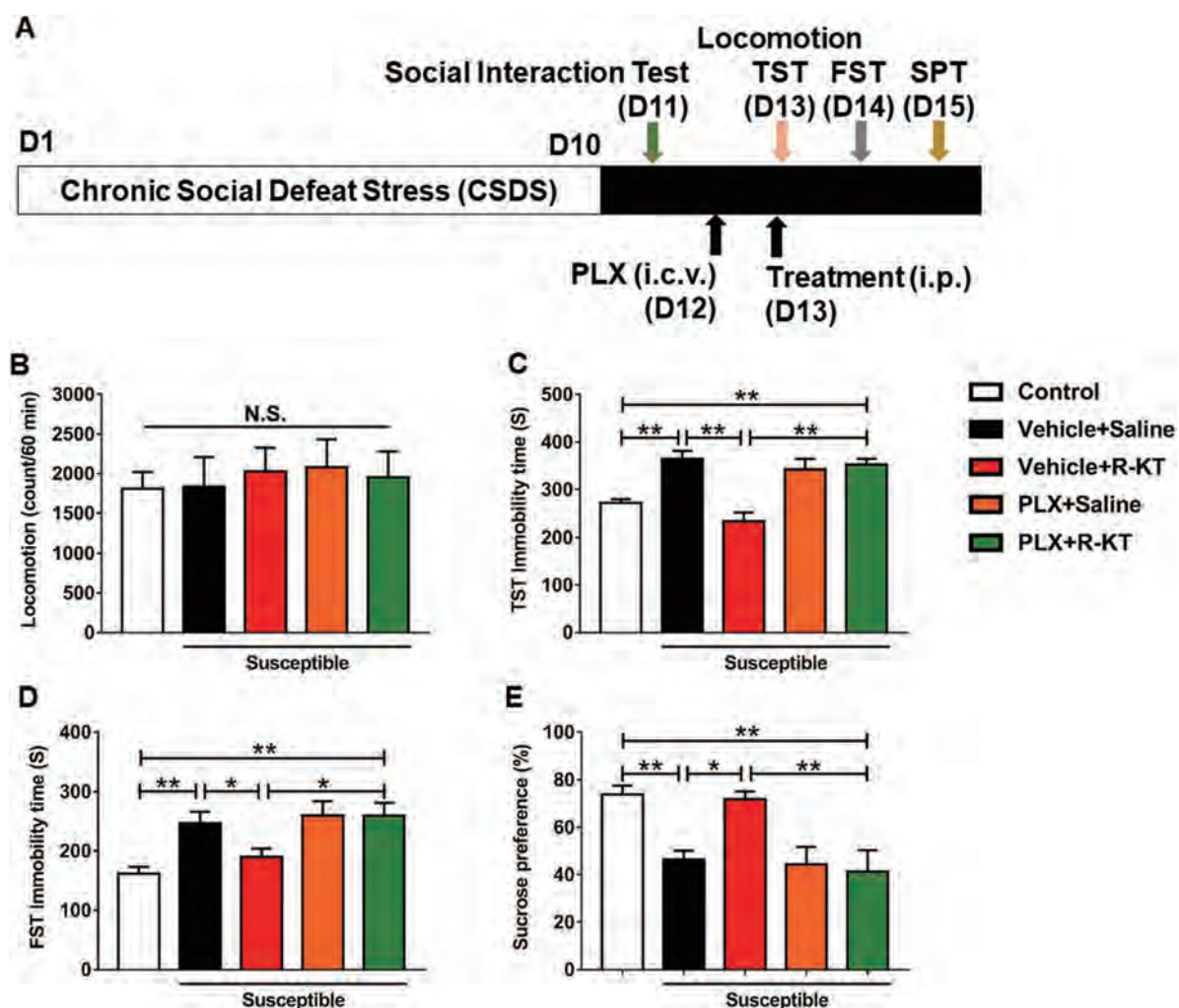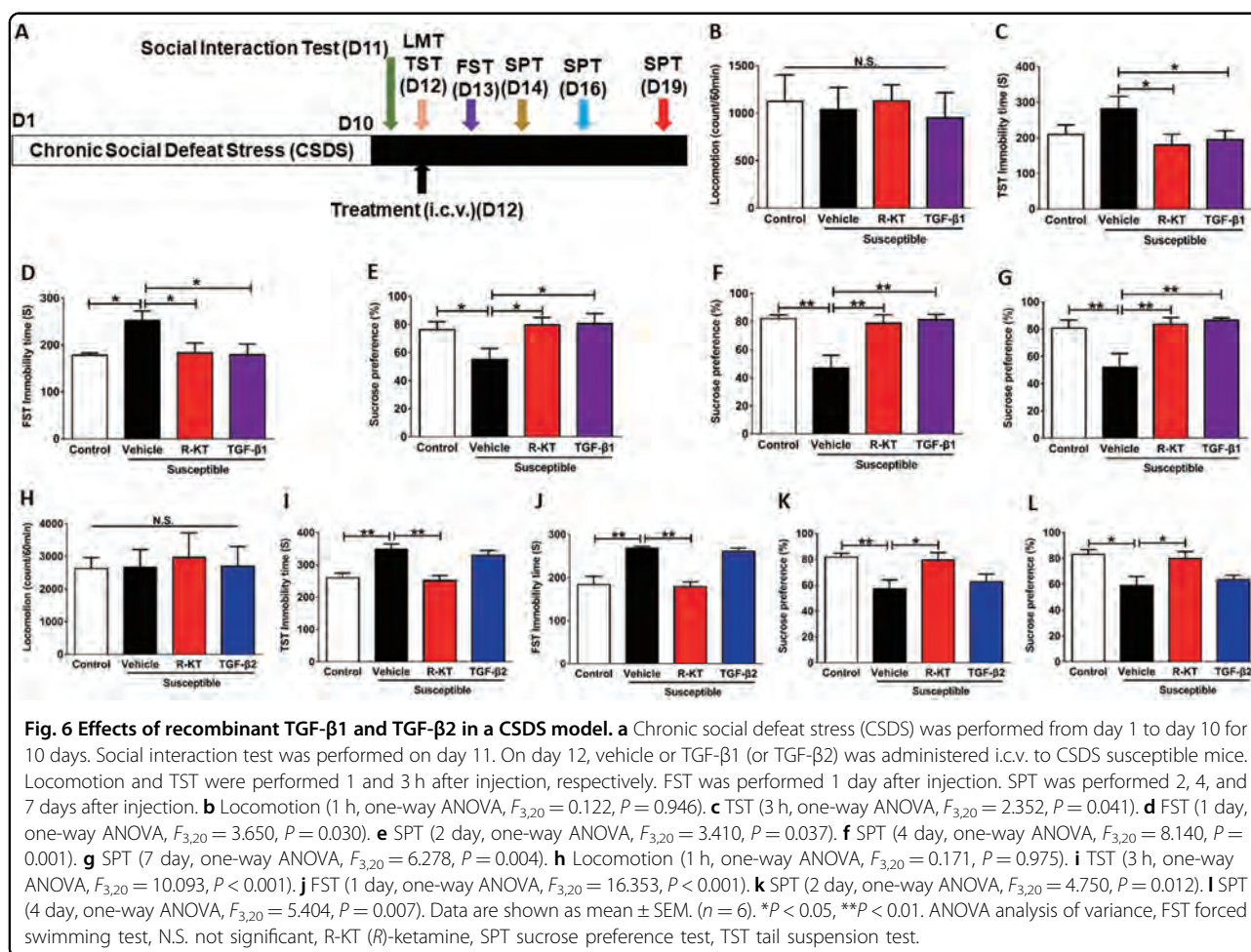
Fig. 5 Effects of PLX3397 on antidepressant effects of (*R*)-ketamine in a CSDS model. a Chronic social defeat stress (CSDS) was performed from day 1 to day 10 for 10 days. Social interaction test was performed on day 11. On day 12, vehicle or PLX3397 was administered i.c.v. to CSDS susceptible mice. On day 13, saline or (*R*)-ketamine (10 mg/kg) was administered i.p. 24 h after injection of PLX3397. Locomotion and FST were performed 1 and 3 h after injection, respectively. FST and SPT were performed 1 and 2 days after injection, respectively. **b** Locomotion (1 h, one-way ANOVA, $F_{4,35} = 0.226$, $P = 0.921$). **c** TST (3 h, one-way ANOVA, $F_{4,35} = 13.706$, $P < 0.001$). **d** FST (1 day, one-way ANOVA, $F_{4,35} = 5.362$, $P = 0.005$). **e** SPT (2 day, one-way ANOVA, $F_{4,35} = 6.045$, $P = 0.003$). Data are shown as mean ± SEM. (*n* = 8). *$P < 0.05$, **$P < 0.01$. ANOVA analysis of variance, FST forced swimming test, N.S. not significant, PLX PLX3397, R-KT (*R*)-ketamine, SPT sucrose preference test, TST tail suspension test.

effects of (*R*)-ketamine. Lastly, recombinant TGF-β1 elicited rapid-acting and long-lasting antidepressant effects in CSDS, LPS, and LH models of depression. Overall, it appears likely that (*R*)-ketamine can exert antidepressant effects by normalizing microglial TGF-β1 signaling in the PFC and the hippocampus of CSDS susceptible mice. Furthermore, TGF-β1 has ketamine-like antidepressant effects in rodent models.

Microglia are the only cell type that express CSF1R. CSF1R knockout mice are devoid of microglia[59]. Moreover, it has been reported that repeated treatment with CSF1R inhibitors, such as PLX3397, cause a dramatic reduction in the number of microglia within the adult brain[48–50].

Interestingly, microglia are absent in the brains of central nervous system TGF-β1 knockout mice[56]. Thus, microglia in the adult brain are physiologically dependent upon CSF1R and TGF-β1 signaling[57]. In this study, a single i.c.v. injection of PLX3397 produced significant reduction of Iba1 and TGF-β1 in the PFC, suggesting partial depletion of microglia in the PFC. Interestingly, pretreatment of PLX3397 significantly blocked the antidepressant effects of (*R*)-ketamine in CSDS susceptible mice. Overall, it appears likely that microglial TGF-β1 in the PFC might contribute to the antidepressant effects of (*R*)-ketamine.

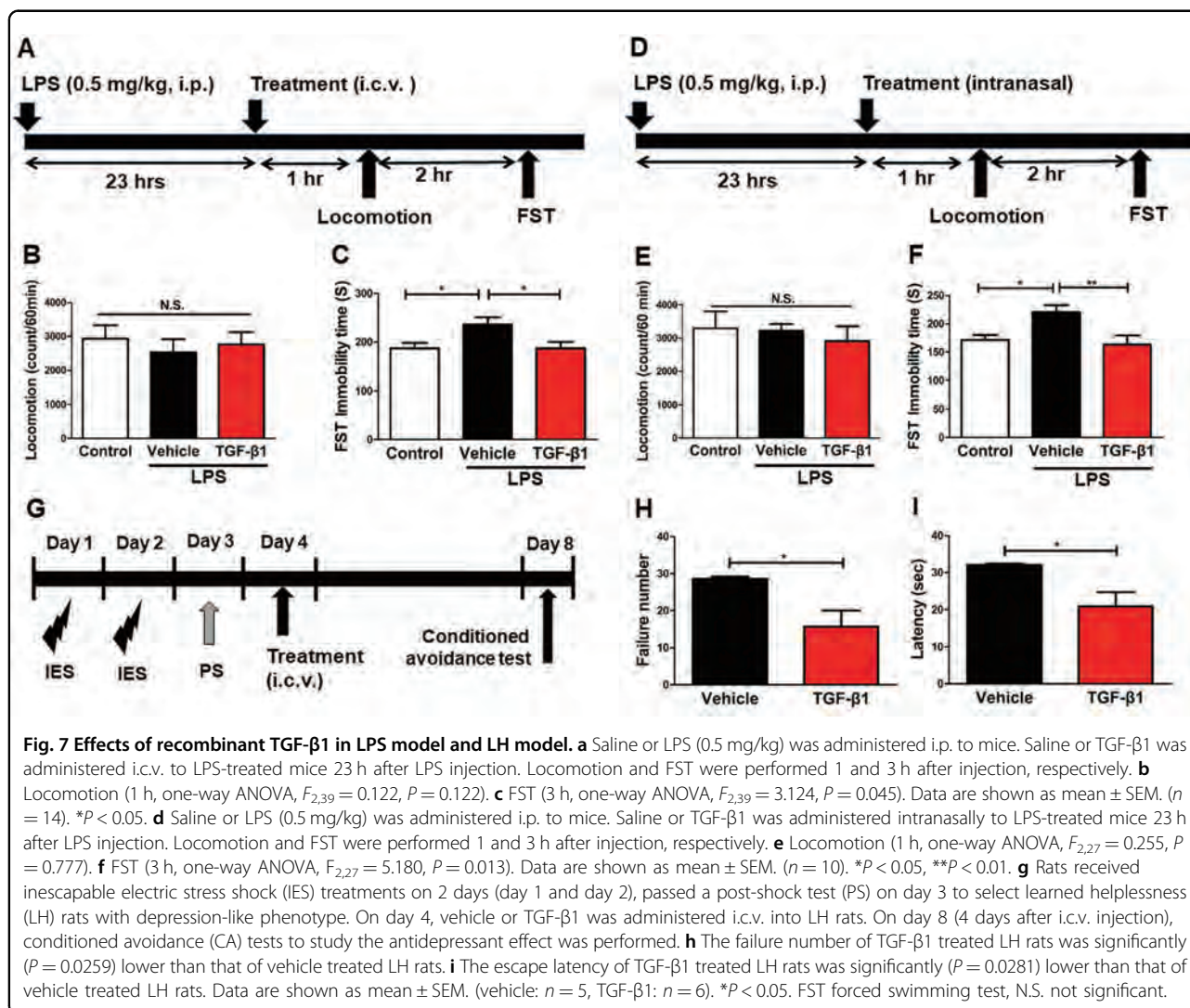In this study, i.c.v. infusion of TGF-β1 produced rapid-acting and long-lasting antidepressant effects in a CSDS

Fig. 6 Effects of recombinant TGF-β1 and TGF-β2 in a CSDS model. a Chronic social defeat stress (CSDS) was performed from day 1 to day 10 for 10 days. Social interaction test was performed on day 11. On day 12, vehicle or TGF-β1 (or TGF-β2) was administered i.c.v. to CSDS susceptible mice. Locomotion and TST were performed 1 and 3 h after injection, respectively. FST was performed 1 day after injection. SPT was performed 2, 4, and 7 days after injection. **b** Locomotion (1 h, one-way ANOVA, $F_{3,20} = 0.122$, $P = 0.946$). **c** TST (3 h, one-way ANOVA, $F_{3,20} = 2.352$, $P = 0.041$). **d** FST (1 day, one-way ANOVA, $F_{3,20} = 3.650$, $P = 0.030$). **e** SPT (2 day, one-way ANOVA, $F_{3,20} = 3.410$, $P = 0.037$). **f** SPT (4 day, one-way ANOVA, $F_{3,20} = 8.140$, $P = 0.001$). **g** SPT (7 day, one-way ANOVA, $F_{3,20} = 6.278$, $P = 0.004$). **h** Locomotion (1 h, one-way ANOVA, $F_{3,20} = 0.171$, $P = 0.975$). **i** TST (3 h, one-way ANOVA, $F_{3,20} = 10.093$, $P < 0.001$). **j** FST (1 day, one-way ANOVA, $F_{3,20} = 16.353$, $P < 0.001$). **k** SPT (2 day, one-way ANOVA, $F_{3,20} = 4.750$, $P = 0.012$). **l** SPT (4 day, one-way ANOVA, $F_{3,20} = 5.404$, $P = 0.007$). Data are shown as mean ± SEM. ($n = 6$). *$P < 0.05$, **$P < 0.01$. ANOVA analysis of variance, FST forced swimming test, N.S. not significant, R-KT (R)-ketamine, SPT sucrose preference test, TST tail suspension test.

model, an LPS-induced model, and an LH model. Notably, we detected the antidepressant effects of TGF-β1 in a CSDS model and an LH model 7 days and 4 days after a single dose, respectively. Collectively, the antidepressant effects of TGF-β1 in these models are similar to those of (R)-ketamine, suggesting that TGF-β1 has (R)-ketamine-like long-lasting antidepressant effects. Taylor et al[60]. showed that a single i.c.v. injection of TGF-β1 4 h after intracerebral hemorrhage (ICH) produced complete recovery of motor function at 24 h, and that this recovery persisted for at least one week. Furthermore, i.c.v. injection of TGF-β1 alleviated *N*-methyl-4-phenylpyridinium ion (MPP⁺)-induced microglial inflammatory response and dopaminergic neuronal loss in the substantia nigra, indicating that TGF-β1 plays a role in the pathology of Parkinson's disease (PD). Collectively, it is possible that TGF-β1 can produce rapid and long-lasting beneficial effects in several models, such as depression, ICH, and PD.

Notably, intranasal administration of TGF-β1 has rapid-acting antidepressant effects in LPS-treated mice. A previous study showed that intranasal administration of TGF-β1 ameliorated neurodegeneration in the mouse

brain after β-amyloid$_{1-42}$ injection[44]. It has also been reported that TGF-β1 administered intranasally entered several brain regions, such as the PFC and the hippocampus, of control adult mice, whereas no increase was observed in the blood and peripheral organs[61], indicating good permeability of the blood brain barrier for TGF-β1. It is also reported that CSDS alters blood brain barrier integrity through loss of tight junction protein Cldn5[62]. In addition, TGF-β1 might be free of the psychotomimetic side-effects of ketamine and its potential for abuse in humans, as TGF-β1 does not interact with NMDAR in the brain. Therefore, it is likely that intranasal administration of TGF-β1 would be a novel potential therapeutic approach for depression.

This study has some limitations. In this study, we used the CSF1R inhibitor to delete microglia in the brain although the partial depletion of microglia was detected. It is of great interest to investigate the role of microglia in the antidepressant effects of (R)-ketamine using CSF1R knockout mice since CSF1R knockout mice are devoid of microglia[59]. Furthermore, it is also of interest to investigate the role of microglial TGF-β1 in the antidepressant

Fig. 7 Effects of recombinant TGF-β1 in LPS model and LH model. a Saline or LPS (0.5 mg/kg) was administered i.p. to mice. Saline or TGF-β1 was administered i.c.v. to LPS-treated mice 23 h after LPS injection. Locomotion and FST were performed 1 and 3 h after injection, respectively. **b** Locomotion (1 h, one-way ANOVA, $F_{2,39} = 0.122$, $P = 0.122$). **c** FST (3 h, one-way ANOVA, $F_{2,39} = 3.124$, $P = 0.045$). Data are shown as mean ± SEM. ($n = 14$). *$P < 0.05$. **d** Saline or LPS (0.5 mg/kg) was administered i.p. to mice. Saline or TGF-β1 was administered intranasally to LPS-treated mice 23 h after LPS injection. Locomotion and FST were performed 1 and 3 h after injection, respectively. **e** Locomotion (1 h, one-way ANOVA, $F_{2,27} = 0.255$, $P = 0.777$). **f** FST (3 h, one-way ANOVA, $F_{2,27} = 5.180$, $P = 0.013$). Data are shown as mean ± SEM. ($n = 10$). *$P < 0.05$, **$P < 0.01$. **g** Rats received inescapable electric stress shock (IES) treatments on 2 days (day 1 and day 2), passed a post-shock test (PS) on day 3 to select learned helplessness (LH) rats with depression-like phenotype. On day 4, vehicle or TGF-β1 was administered i.c.v. into LH rats. On day 8 (4 days after i.c.v. injection), conditioned avoidance (CA) tests to study the antidepressant effect was performed. **h** The failure number of TGF-β1 treated LH rats was significantly ($P = 0.0259$) lower than that of vehicle treated LH rats. **i** The escape latency of TGF-β1 treated LH rats was significantly ($P = 0.0281$) lower than that of vehicle treated LH rats. Data are shown as mean ± SEM. (vehicle: $n = 5$, TGF-β1: $n = 6$). *$P < 0.05$. FST forced swimming test, N.S. not significant.

effects of (*R*)-ketamine using TGF-β1 knockout mice since microglia were absent in the brain of TGF-β1 knockout mice[56].

In conclusion, this study shows that TGF-β1 in the microglia might contribute to the antidepressant effects of (*R*)-ketamine in animal models of depression. Furthermore, similar to (*R*)-ketamine, TGF-β1 seems to rapid-acting and long-lasting antidepressant effects. Therefore, it is likely that TGF-β1 would be a new rapid-acting and sustained antidepressant.

Author details
[1]Division of Clinical Neuroscience, Chiba University Center for Forensic Mental Health, Chiba 260-8670, Japan. [2]Department of Biomedical Science, Chiba University Graduate School of Medicine, Chiba 260-8670, Japan. [3]Department of Neuropsychiatry, Keio University School of Medicine, Tokyo 160-8585, Japan. [4]Department of Psychiatry, Teikyo University Chiba Medical Center, Chiba 299-0111, Japan. [5]Present address: Department of Psychiatry, Chaohu Hospital of Anhui Medical University, Hefei 238000, China. [6]Present address: Department of Anesthesiology and Perioperative Medicine, The First Affiliated Hospital of Nanjing Medical University, Nanjing 210029, China

Conflict of interest
K. H. is an inventor on the filed patent on "The use of (*R*)-ketamine in the treatment of psychiatric diseases" and "Transforming growth factor β1 in the treatment of depression". Other authors declare no conflict of interest.

Publisher's note
Springer Nature remains neutral with regard to jurisdictional claims in published maps and institutional affiliations.

Supplementary Information accompanies this paper at (https://doi.org/10.1038/s41398-020-0733-x).

References

1. Trullas, R. & Skolnick, P. Functional antagonists at the NMDA receptor complex exhibit antidepressant actions. *Eur. J. Pharm.* **185**, 1–10 (1990).
2. Berman, R. M. et al. Antidepressant effects of ketamine in depressed patients. *Biol. Psychiatry* **47**, 351–354 (2000).
3. Zarate, C. A. Jr et al. A randomized trial of an N-methyl-D-aspartate antagonist in treatment-resistant major depression. *Arch. Gen. Psychiatry* **63**, 856–864 (2006).
4. Murrough, J. W. et al. Antidepressant efficacy of ketamine in treatment-resistant major depression: a two-site randomized controlled trial. *Am. J. Psychiatry* **170**, 1134–1142 (2013).
5. Diazgranados, N. et al. A randomized add-on trial of an N-methyl-D-aspartate antagonist in treatment-resistant bipolar depression. *Arch. Gen. Psychiatry* **67**, 793–802 (2010).
6. Zarate, C. A. Jr et al. Replication of ketamine's antidepressant efficacy in bipolar depression: a randomized controlled add-on trial. *Biol. Psychiatry* **71**, 939–946 (2012).
7. Singh, J. B. et al. A double-blind, randomized, placebo-controlled, dose-frequency study of intravenous ketamine in patients with treatment-resistant depression. *Am. J. Psychiatry* **173**, 816–826 (2016).
8. Su, T. P. et al. Dose-related effects of adjunctive ketamine in Taiwanese patients with treatment-resistant depression. *Neuropsychopharmacology* **42**, 2482–2492 (2017).
9. Phillips, J. L. et al. Single, repeated, and maintenance ketamine infusions for treatment-resistant depression: a randomized controlled trial. *Am. J. Psychiatry* **176**, 401–409 (2019).
10. Fava, M. et al. Double-blind, placebo-controlled, dose-ranging trial of intravenous ketamine as adjunctive therapy in treatment-resistant depression (TRD). *Mol. Psychiatry* https://doi.org/10.1038/s41380-018-0256-5 (2018).
11. Murrough, J. W. et al. Ketamine for rapid reduction of suicidal ideation: a randomized controlled trial. *Psychol. Med* **45**, 3571–3580 (2015).
12. Grunebaum, M. F. et al. Ketamine for rapid reduction of suicidal thoughts in major depression: A midazolam-controlled randomized clinical trial. *Am. J. Psychiatry* **175**, 327–335 (2018).
13. Ballard, E. D. et al. Anhedonia as a clinical correlate of suicidal thoughts in clinical ketamine trials. *J. Affect. Disord.* **218**, 195–200 (2017).
14. Newport, D. J. et al. Ketamine and other NMDA antagonists: early clinical trials and possible mechanisms in depression. *Am. J. Psychiatry* **172**, 950–966 (2015).
15. Kishimoto, T. et al. Single-dose infusion ketamine and non-ketamine N-methyl-D-aspartate receptor antagonists for unipolar and bipolar depression: a meta-analysis of efficacy, safety and time trajectories. *Psychol. Med.* **46**, 1459–1472 (2016).
16. Wilkinson, S. T. et al. The effect of a single dose of intravenous ketamine on suicidal ideation: a systematic review and individual participant data meta-analysis. *Am. J. Psychiatry* **175**, 150–158 (2018).
17. Duman, R. S. Ketamine and rapid-acting antidepressants: a new era in the battle against depression and suicide. *F1000Res* **7**, F1000 (2018).
18. Krystal, J. H., Abdallah, C. G., Sanacora, G., Charney, D. & Duman, R. S. Ketamine: a paradigm shift for depression research and treatment. *Neuron* **101**, 774–778 (2019).
19. Zhang, K. & Hashimoto, K. An update on ketamine and its two enantiomers as rapid-acting antidepressants. *Expert Rev. Neurother.* **19**, 83–92 (2019).
20. Monteggia, L. M. & Zarate, C. Jr Antidepressant actions of ketamine: from molecular mechanisms to clinical practice. *Curr. Opin. Neurobiol.* **30**, 139–143 (2015).
21. Murrough, J. W., Abdallah, C. G. & Mathew, S. J. Targeting glutamate signaling in depression: progress and prospects. *Nat. Rev. Drug Discov.* **16**, 472–486 (2017).
22. Zanos, P. et al. Ketamine and ketamine metabolites pharmacology: Insights into therapeutic mechanisms. *Pharm. Rev.* **70**, 621–660 (2018).
23. Gould, T. D., Zarate, C. A. Jr & Thompson, S. M. Molecular pharmacology and neurobiology of rapid-acting antidepressants. *Annu. Rev. Pharm. Toxicol.* **59**, 213–236 (2019).
24. Hashimoto, K. Rapid-acting antidepressant ketamine, its metabolites and other candidates: a historical overview and future perspective. *Psychiatry Clin. Neurosci.* **73**, 613–627 (2019).
25. Yang, C., Yang, J., Luo, A. & Hashimoto, K. Molecular and cellular mechanisms underlying the antidepressant effects of ketamine enantiomers and its metabolites. *Transl. Psychiatry* **9**, 280 (2019).
26. Sanacora, G. et al. A consensus statement on the use of ketamine in the treatment of mood disorders. *JAMA Psychiatry* **74**, 399–405 (2017).
27. Reardon, S. "Party drug" turned antidepressant approaches approval. *Nat. Rev. Drug Discov.* **17**, 773–775 (2018).
28. Zhang, J. C., Li, S. X. & Hashimoto, K. R (-)-ketamine shows greater potency and longer lasting antidepressant effects than S(+)-ketamine. *Pharm. Biochem. Behav.* **116**, 137–141 (2014).
29. Yang, C. et al. R-ketamine: a rapid-onset and sustained antidepressant without psychotomimetic side effects. *Transl. Psychiatry* **5**, e632 (2015).
30. Zanos, P. et al. NMDAR inhibition-independent antidepressant actions of ketamine metabolites. *Nature* **533**, 481–486 (2016).
31. Fukumoto, K. et al. Antidepressant potential of (R)-ketamine in rodent models: Comparison with (S)-ketamine. *J. Pharm. Exp. Ther.* **361**, 9–16 (2017).
32. Yang, C. et al. (R)-Ketamine shows greater potency and longer lasting antidepressant effects than its metabolite (2R,6R)-hydroxynorketamine. *Biol. Psychiatry* **82**, e43–e44 (2017).
33. Yang, C. et al. Possible role of the gut microbiota-brain axis in the antidepressant effects of (R)-ketamine in a social defeat stress model. *Transl. Psychiatry* **7**, 1294 (2017).
34. Yang, C. et al. Mechanistic target of rapamycin-independent antidepressant effects of (R)-ketamine in a social defeat stress model. *Biol. Psychiatry* **83**, 18–28 (2018).
35. Yang, C., Han, M., Zhang, J. C., Ren, Q. & Hashimoto, K. Loss of parvalbumin-immunoreactivity in mouse brain regions after repeated intermittent administration of esketamine, but not R-ketamine. *Psychiatry Res.* **239**, 281–283 (2016).
36. Hashimoto, K., Kakiuchi, T., Ohba, H., Nishiyama, S. & Tsukada, H. Reduction of dopamine D$_{2/3}$ receptor binding in the striatum after a single administration of esketamine, but not R-ketamine: a PET study in conscious monkeys. *Eur. Arch. Psychiatry Clin. Neurosci.* **267**, 173–176 (2017).
37. Tian, Z., Dong, C., Fujita, A., Fujita, Y. & Hashimoto, K. Expression of heat shock protein HSP-70 in the retrosplenial cortex of rat brain after administration of (R, S)-ketamine and (S)-ketamine, but not (R)-ketamine. *Pharm. Biochem. Behav.* **172**, 17–21 (2018).
38. Chang, L. et al. Comparison of antidepressant and side effects in mice after intranasal administration of (R,S)-ketamine, (R)-ketamine, and (S)-ketamine. *Pharm. Biochem. Behav.* **181**, 53–59 (2019).
39. Mathisen, L. C., Skjelbred, P., Skoglund, L. A. & Oye, I. Effect of ketamine, an NMDA receptor inhibitor, in acute and chronic orofacial pain. *Pain* **61**, 215–220 (1995).
40. Vollenweider, F. X., Leenders, K. L., Oye, I., Hell, D. & Angst, J. Differential psychopathology and patterns of cerebral glucose utilisation produced by (S)- and (R)-ketamine in healthy volunteers using positron emission tomography (PET). *Eur. Neuropsychopharmacol.* **7**, 25–38 (1997).
41. Hashimoto, K. R-ketamine: a rapid-onset and sustained antidepressant without risk of brain toxicity. *Psychol. Med.* **46**, 2449–2451 (2016).
42. Hashimoto, K. Ketamine's antidepressant action: beyond NMDA receptor inhibition. *Expert Opin. Ther. Targets* **20**, 1389–1392 (2016).
43. Fuchikami, M. et al. Optogenetic stimulation of infralimbic PFC reproduces ketamine's rapid and sustained antidepressant actions. *Proc. Natl Acad. Sci. USA* **112**, 8106–8111 (2015).
44. Shirayama, Y. & Hashimoto, K. Effects of a single bilateral infusion of R-ketamine in the rat brain regions of a learned helplessness model of depression. *Eur. Arch. Psychiatry Clin. Neurosci.* **267**, 177–182 (2017).
45. Chen, J. H., Ke, K. F., Lu, J. H., Qiu, Y. H. & Peng, Y. P. Protection of TGF-β1 against neuroinflammation and neurodegeneration in Aβ$_{1-42}$-induced Alzheimer's disease model rats. *PLoS ONE* **10**, e0116549 (2015).
46. Chen, X., Liu, Z., Cao, B. B., Qiu, Y. H. & Peng, Y. P. TGF-β1 neuroprotection via inhibition of microglial activation in a rat model of Parkinson's disease. *J. Neuroimmune Pharm.* **12**, 433–446 (2017).
47. Golden, S. A., Covington, H. E. R. 3rd, Berton, O. & Russo, S. J. A standardized protocol for repeated social defeat stress in mice. *Nat. Protoc.* **6**, 1183–1191 (2011).
48. Elmore, M. R. et al. Colony-stimulating factor 1 receptor signaling is necessary for microglia viability, unmasking a microglia progenitor cell in the adult brain. *Neuron* **82**, 380–397 (2014).
49. Tang, Y. et al. Interaction between astrocytic colony stimulating factor and its receptor on microglia mediates central sensitization and behavioral hypersensitivity in chronic post ischemic pain model. *Brain Behav. Immun.* **68**, 248–260 (2018).
50. Liang, Y. J. et al. Contribution of microglial reaction to increased nociceptive responses in high-fat-diet (HFD)-induced obesity in male mice. *Brain Behav. Immun.* **80**, 777–792 (2019).

51. Zhang, J. C. et al. Antidepressant effects of TrkB ligands on depression-like behavior and dendritic changes in mice after inflammation. *Int J. Neuropsychopharmacol.* **18**, pyu077 (2014).

52. Ma, M. et al. Antidepressant effects of combination of brexpiprazole and fluoxetine on depression-like behavior and dendritic changes in mice after inflammation. *Psychopharmacology* **234**, 525–533 (2017).

53. Zhang, K. & Hashimoto, K. Lack of opioid system in the antidepressant actions of ketamine. *Biol. Psychiatry* **85**, e25–e27 (2019).

54. Shirayama, Y. & Hashimoto, K. Lack of antidepressant effects of (2R,6R)-hydroxynorketamine in a rat learned helplessness model: comparison with (R)-ketamine. *Int J. Neuropsychopharmacol.* **21**, 84–88 (2018).

55. Kiefer, R., Streit, W. J., Toyka, K. V., Kreutzberg, G. W. & Hartung, H. P. Transforming growth factor-β1: a lesion-associated cytokines of the nervous system. *Int J. Dev. Neurosci.* **13**, 331–339 (1995).

56. Butovsky, O. et al. Identification of a unique TGF-β-dependent molecular and functional signature in microglia. *Nat. Neurosci.* **17**, 131–143 (2014).

57. Priller, J. & Prinz, M. Targeting microglia in brain disorders. *Science* **365**, 32–33 (2019).

58. Zhang, K, Fujita, Y. & Hashimoto, K. Lack of metabolism in (R)-ketamine's antidepressant actions in a chronic social defeat stress model. *Sci. Rep.* **8**, 4007 (2018).

59. Erblich, B., Zhu, L., Etgen, A. M., Dobrenis, K. & Pollard, J. W. Absence of colony stimulation factor-1 receptor results in loss of microglia, disrupted brain development and olfactory deficits. *PLoS ONE* **6**, e26317 (2011).

60. Taylor, R. A. et al. TGF-β1 modulates microglial phenotype and promotes recovery after intracerebral hemorrhage. *J. Clin. Invest.* **127**, 280–292 (2017).

61. Ma, Y. P. et al. Intranasally delivered TGF-β1 enters brain and regulates gene expressions of its receptors in rats. *Brain Res. Bull.* **74**, 271–277 (2007).

62. Menard, C. et al. Social defeat induces neurovascular pathology promoting depression. *Nat. Neurosci.* **20**, 1752–1760 (2017).

Correction

The authors note that the author name Debin Wang should instead appear as Debin Wan. The corrected author line appears below. The online version has been corrected.

Yaoyu Pu, Jun Yang, Lijia Chang, Youge Qu, Siming Wang, Kai Zhang, Zhongwei Xiong, Jiancheng Zhang, Yunfei Tan, Xingming Wang, Yuko Fujita, Tamaki Ishima, Debin Wan, Sung Hee Hwang, Bruce D. Hammock, and Kenji Hashimoto

CORRECTION

Maternal glyphosate exposure causes autism-like behaviors in offspring through increased expression of soluble epoxide hydrolase

Yaoyu Pu[a], Jun Yang[b], Lijia Chang[a], Youge Qu[a], Siming Wang[a], Kai Zhang[a], Zhongwei Xiong[a], Jiancheng Zhang[a], Yunfei Tan[a], Xingming Wang[a], Yuko Fujita[a], Tamaki Ishima[a], Debin Wan[b], Sung Hee Hwang[b], Bruce D. Hammock[b,1], and Kenji Hashimoto[a,1]

[a]Division of Clinical Neuroscience, Chiba University Center for Forensic Mental Health, 260-8670 Chiba, Japan; and [b]Department of Entomology and Nematology and UC Davis Comprehensive Cancer Center, University of California, Davis, CA 95616

Epidemiological studies suggest that exposure to herbicides during pregnancy might increase risk for autism spectrum disorder (ASD) in offspring. However, the precise mechanisms underlying the risk of ASD by herbicides such as glyphosate remain unclear. Soluble epoxide hydrolase (sEH) in the metabolism of polyunsaturated fatty acids is shown to play a key role in the development of ASD in offspring after maternal immune activation. Here, we found ASD-like behavioral abnormalities in juvenile offspring after maternal exposure to high levels of formulated glyphosate. Furthermore, we found higher levels of sEH in the prefrontal cortex (PFC), hippocampus, and striatum of juvenile offspring, and oxylipin analysis showed decreased levels of epoxy-fatty acids such as 8 (9)-EpETrE in the blood, PFC, hippocampus, and striatum of juvenile offspring after maternal glyphosate exposure, supporting increased activity of sEH in the offspring. Moreover, we found abnormal composition of gut microbiota and short-chain fatty acids in fecal samples of juvenile offspring after maternal glyphosate exposure. Interestingly, oral administration of TPPU (an sEH inhibitor) to pregnant mothers from E5 to P21 prevented ASD-like behaviors such as social interaction deficits and increased grooming time in the juvenile offspring after maternal glyphosate exposure. These findings suggest that maternal exposure to high levels of glyphosate causes ASD-like behavioral abnormalities and abnormal composition of gut microbiota in juvenile offspring, and that increased activity of sEH might play a role in ASD-like behaviors in offspring after maternal glyphosate exposure. Therefore, sEH may represent a target for ASD in offspring after maternal stress from occupational exposure to contaminants.

glyphosate | gut microbiota | soluble epoxide hydrolase

Autism spectrum disorder (ASD) is a developmental disorder characterized by social and communication impairments, combined with limited or focused interests and repetitive behaviors (1, 2). Although the prevalence of ASD has been rising since the 1980s, the detailed reasons underlying this rise remain unknown (3, 4). In addition to genetic factors, accumulating evidence supports a significant contribution of environmental factors in ASD etiology (1, 2, 5, 6). Environmental factors, including exposures to synthetic chemicals during pregnancy and lactation, are suggested to play a role in the development of ASD. These chemicals include selective serotonin reuptake inhibitors (SSRIs), pesticides, phthalates, polychlorinated biphenyls, solvents, air pollutants, fragrances, and heavy metals (6–8).

Glyphosate [N-(phosphonomethyl)glycine] is the active ingredient in Roundup and other herbicides, and, because of its efficacy, excellent environmental profile, and low toxicity, it is the most widely used herbicide in the world (9, 10). Interestingly, a positive correlation was reported between the rise of glyphosate usage on corn and soy crops in the United States over the years 1995 to 2010 and the increase in ASD rates over the same

period as reported in the US public school system (11–13). A recent population-based case-control study in California showed that the risk of ASD was associated with the use of glyphosate (odds ratio = 1.16) (14). For ASD with intellectual disability, estimated odds ratio were higher (by about 30%) with prenatal exposure to glyphosate (odds ratio = 1.33) (14). These reports suggest that possible relationships between glyphosate and ASD should be explored in animal models.

Epidemiological studies implicate prenatal environmental factors, including maternal immune activation (MIA), playing a key role in the etiology of developmental disorders such as ASD (15–19). There are a number of positive associations between maternal infections or inflammatory biomarkers and ASD (15, 16, 20). Collectively, MIA during pregnancy can increase the risk of developmental disorders such as ASD in offspring.

Epoxy fatty acids (EpFAs) are produced from the corresponding polyunsaturated fatty acids by cytochrome P450 enzymes. Epoxyeicosatrienoic acids (EpETrEs) and epoxydocosapentaenoic acids (EpDPEs) are produced from arachidonic acid and docosahexaenoic acid (DHA), respectively. EpETrEs, EpDPEs, and some other EpFAs have potent antiinflammatory properties. However,

---

Significance

Maternal exposure to high levels of the herbicide glyphosate may increase the risk for autism spectrum disorder (ASD) in offspring; however, the underlying mechanisms remain largely unknown. Maternal glyphosate exposure during pregnancy and lactation caused ASD-like behavioral abnormalities and abnormal composition of gut microbiota in murine male offspring. Soluble epoxide hydrolase (sEH) in the brain of offspring after maternal glyphosate exposure was higher than controls. Treatment with an sEH inhibitor from pregnancy to weaning prevented the onset of ASD-like behavioral abnormalities in offspring after maternal glyphosate exposure. The glyphosate exposures used here exceed any reasonable dietary, environmental, or occupational exposure, but they indicate that increased sEH plays a role in ASD-like behaviors in offspring.

---

these lipid mediators are metabolized rapidly into their corresponding diols by soluble epoxide hydrolase (sEH), and inhibition of sEH enhances the beneficial effects of EpFAs (21–24). Accumulating evidence demonstrate a key role of sEH in multiple animal models, including depression, ASD, schizophrenia, and Parkinson's disease (25–32). Recently, we reported that sEH in the prefrontal cortex (PFC) plays a key role in the development of ASD-like behavioral abnormalities in juvenile offspring after MIA (30). However, there is no previous report showing the role of sEH in the pathogenesis of ASD in offspring after maternal exposure to formulated glyphosate.

The purpose of this study was to examine the role of sEH in the pathogenesis of ASD in offspring after maternal glyphosate exposure. First, we examined whether maternal glyphosate exposure causes ASD-like behavioral abnormalities in juvenile offspring. Second, we examined whether expression of sEH is altered in the brain regions of juvenile offspring after maternal glyphosate exposure. Furthermore, we performed oxylipin analysis of blood and brain regions from juvenile offspring. Moreover, we measured levels of *N*-methyl-D-aspartate receptor (NMDAR)-related amino acids in the blood and brain from juvenile offspring since NMDAR-related amino acids were altered in patients with ASD (33–36). Third, we performed 16S rRNA analysis and measurement of short-chain fatty acids of fecal samples in juvenile off\spring after maternal glyphosate exposure since abnormal composition of gut microbiota is shown in patients with ASD (36–40). Finally, we examined whether treatment with TPPU [1-trifluoromethoxyphenyl-3-(1-propionylpiperidin-4-yl)urea] (40–42), a potent sEH inhibitor, in pregnant mice from pregnancy to weaning could prevent behavioral abnormalities in juvenile offspring after maternal glyphosate exposure.

Results

General and Behavioral Data of Mother and Juvenile Offspring after Maternal Glyphosate Exposure.
First, we examined whether maternal glyphosate exposure could affect the general and behavioral outcomes in male offspring (*SI Appendix*, Fig. S1*A*). Previous studies used drinking water containing 1% Roundup [0.38% (wt/vol) glyphosate] during pregnancy and lactation (43, 44). For this study, water or formulated glyphosate [0.039% (wt/vol) glyphosate] were given to pregnant mice from E5 to P21 (weaning). The mortality of pregnant mice at the highest concentration (0.39%) in our hands was 100%, although the mortality of lower concentrations (0.039% and 0.098%) was 0% (*SI Appendix*, Table S1), even though the 0.39% concentration has been previously used in other studies (43, 44). This discrepancy may have been due to different formulations of glyphosate or mouse strain differences (ddy vs. ICR) between the studies. Body weight of pregnant mice was increased gradually after maternal glyphosate (0.039 to 0.293%) exposure, whereas body weight of pregnant mice treated with the high concentration (0.39%) did not increase (*SI Appendix*, Fig. S1*B*). The mortality of offspring in the 0.039% glyphosate group was 0%, and juvenile offspring after maternal 0.039% glyphosate exposure did not show any behavioral abnormality such as locomotion, social interaction deficits in a three-chamber test, and depression-like phenotype in the forced swimming test (*SI Appendix*, Fig. S1 *C–E* and Table S1). In contrast, we found social interaction deficits in juvenile offspring after maternal 0.098% glyphosate exposure. Therefore, we used 0.098% glyphosate in the subsequent experiments. This concentration corresponded with 1/80th of the glyphosate no-observed-adverse-effect level, as reported previously (45).

Body weight of glyphosate-exposed mothers was significantly lower than that of water-exposed mothers at E17 (Fig. 1 *A* and *B*). On P21 (weaning), we could detect blood levels of glyphosate in the mothers treated with 0.098% glyphosate and their offspring, although glyphosate was not detected in the dams and offspring of the water-treated group (Fig. 1 *A* and *C*). Locomotion

and prepulse inhibition (PPI; for psychosis) were not different between the two groups (Fig. 1 *D* and *F*). In the novel object recognition test (NORT), offspring after maternal glyphosate exposure showed cognitive deficits (Fig. 1*E*). In the three-chamber test, juvenile offspring after maternal glyphosate exposure showed social interaction deficits compared to the water-treated group (Fig. 1*G*). The data suggest that maternal exposure to glyphosate in a commercial formation (*SI Appendix, Supplementary Material* for composition) causes ASD-like cognitive deficits and social interaction deficits in juvenile offspring.

Increased Expression of sEH in the Brain of Juvenile Offspring after Maternal Glyphosate Exposure.
We measured the expression of sEH in the brain since increased expression of sEH in the PFC plays a role in the ASD-like behaviors after MIA (30). Protein levels of sEH in the PFC and striatum, but not hippocampus, from mothers treated with glyphosate were significantly higher than those of water-treated mice (Fig. 1*H*). Protein levels of sEH in the PFC, hippocampus, and striatum from juvenile offspring (P28) after maternal glyphosate exposure were significantly higher than those of water-treated mice (Fig. 1*I*). Furthermore, gene expression of sEH (or *Ephx2*) mRNA in the PFC, hippocampus, and striatum from juvenile offspring (P28) after maternal glyphosate exposure was significantly higher than those of water-treated mice (Fig. 1*J*).

Next, we performed parvalbumin (PV) immunohistochemistry in the brain from juvenile mice (Fig. 1*K*). PV immunoreactivity in the prelimbic (PrL), but not IL (infralimbic), of medial PFC in the offspring of maternal glyphosate exposure was significantly lower than that of the water-treated group (Fig. 1*K*).

Oxylipin Analysis of Blood and Brain Regions.
Using oxylipin analysis, we measured the levels of eicosanoid metabolites in the blood, PFC, hippocampus, and striatum from juvenile offspring (P28) after maternal glyphosate exposure (*SI Appendix*, Fig. S2 and Tables S2–S5). Blood levels of many epoxides were significantly lower in juvenile offspring after maternal glyphosate exposure (*SI Appendix*, Table S2). We found higher levels of 8 (9)-EpETrE [8,9-epoxy-5Z,11Z,14Z-eicosatrienoic acid] compared to other EpFAs in the mouse brain. Levels of 8 (9)-EpETrE in the PFC, hippocampus, and striatum were significantly lower in juvenile offspring (P28) after maternal glyphosate exposure (Fig. 2 and *SI Appendix*, Tables S3–S5). Lower levels of 8 (9)-EpETrE in the brain regions from juvenile offspring after maternal glyphosate exposure support the increased expression of sEH in these regions. In contrast, tissue levels of other EpFAs in the PFC, hippocampus, and striatum from juvenile offspring after maternal glyphosate exposure were significantly higher than those of control mice (*SI Appendix*, Tables S3–S5).

Measurement of Amino Acids in the Blood and Brain.
Next, we measured levels of NMDAR-related amino acids (i.e., glutamate, glutamine, glycine, D-serine, L-serine, GABA) in the plasma and brains of juvenile offspring (P28) after maternal glyphosate exposure. Maternal glyphosate exposure caused significant reductions of glutamate in the plasma and brain regions. In addition, maternal glyphosate exposure caused significant reductions of other amino acids (i.e., glycine, L-serine, GABA) in the PFC (*SI Appendix*, Table S6). The data suggest abnormalities in NMDAR-related neurotransmission in the PFC of juvenile offspring after maternal glyphosate exposure.

16S rRNA Analysis and Measurement of Short-Chain Fatty Acids of Fecal Samples of Juvenile Offspring after Maternal Glyphosate Exposure.
We performed 16S rRNA analysis of fecal samples of offspring (P28). Maternal glyphosate exposure caused abnormal composition of gut microbiota in juvenile offspring (Fig. 3). At the species level, the relative abundance of *Eubacterium plexicaudatum*,
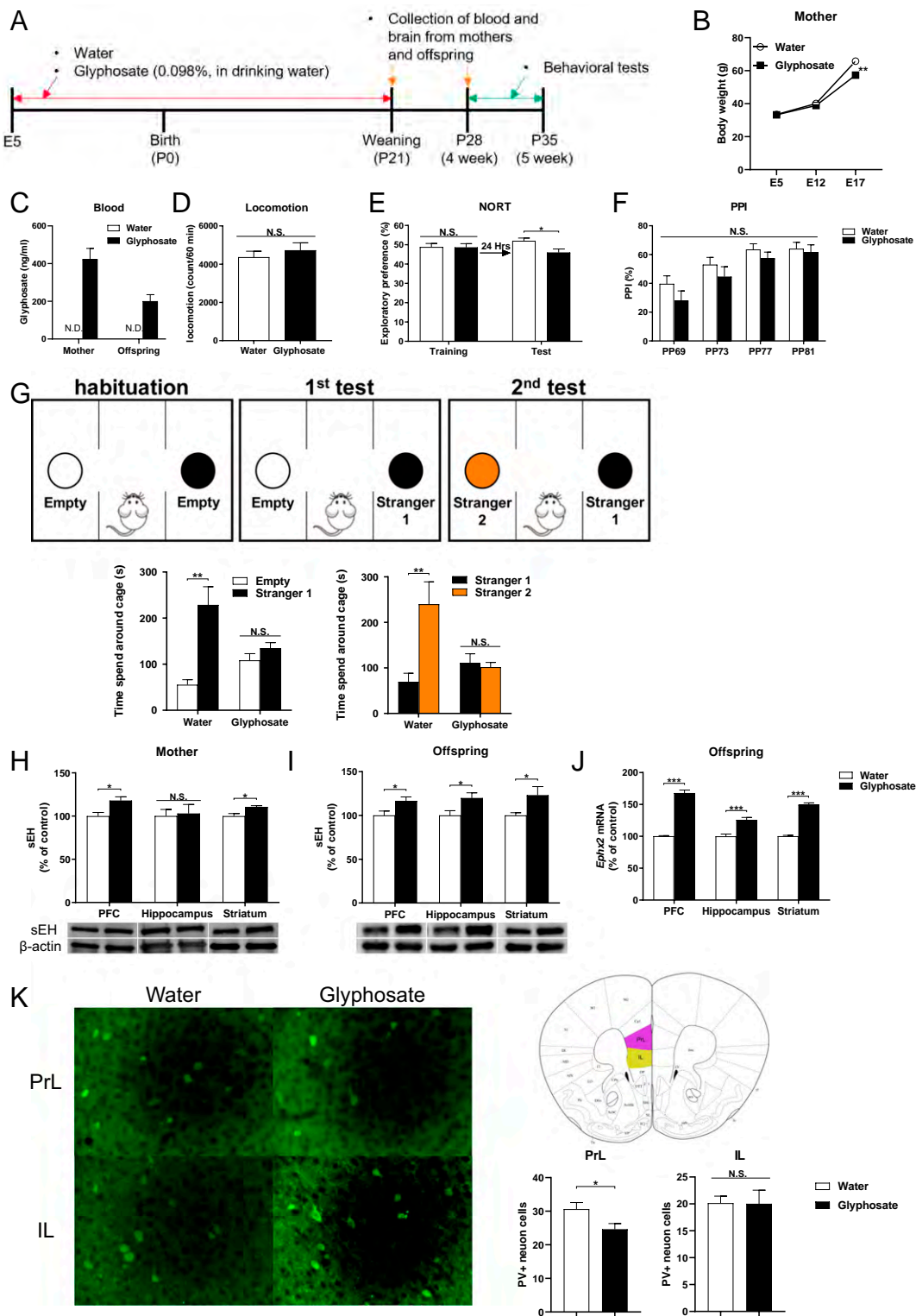
11754 | www.pnas.org/cgi/doi/10.1073/pnas.1922287117
-188-
Pu et al.

Fig. 1. Social interaction deficits, increased expression of sEH, and decreased PV immunoreactivity in the brain from juvenile offspring after maternal glyphosate exposure. (*A*) Schedule of treatment, behavioral tests, and sample collection. (*B*) Change of body weight of pregnant mothers (*n* = 6). (*C*) Blood levels of glyphosate in the mothers and offspring at P21. Data are shown as mean ± SEM (mother *n* = 7, offspring n = 10). (*D*) Locomotion. Data are shown as mean ± SEM (*n* = 7 or 8). (*E*) Novel object recognition test (NORT). Data are shown as mean ± SEM (*n* = 8). (*F*) Prepulse inhibition (PPI) test. Data are shown as mean ± SEM (*n* = 8). (*G*) Three-chamber social interaction test. (*Left*) Two-way ANOVA (glyphosate, $F_{1,22}$ = 4.747, *P* = 0.040; stranger, $F_{1,22}$ = 141.2, *P* < 0.001; interaction, $F_{1,22}$ = 76.77, *P* < 0.001). (*Right*) Two-way ANOVA (glyphosate, $F_{1,22}$ = 9.760, *P* = 0.005; stranger, $F_{1,22}$ = 26.75, *P* < 0.001; interaction, $F_{1,22}$ = 33.38, *P* < 0.001). Data are shown as mean ± SEM (*n* = 4 or 5). (*I*) Protein expression of sEH in the PFC, hippocampus, and striatum of mothers. Data are shown as mean ± SEM (*n* = 4 or 5). (*I*) Protein expression of sEH in the PFC, hippocampus, and striatum from juvenile offspring (P28). Data are shown as mean ± SEM (*n* = 10). (*J*) Gene expression of *Ephx2* mRNA in the mouse brain regions from juvenile offspring (P28). Data are shown as mean ± SEM (*n* = 8). (*K*) PV immunoreactivity in the prelimbic area (PrL) and infralimbic (IL) of mPFC. The values represent the mean ± SEM (*n* = 8; **P* < 0.05, ***P* < 0.01, ****P* < 0.001 compared to control group by Student *t* test). N.S., not significant.
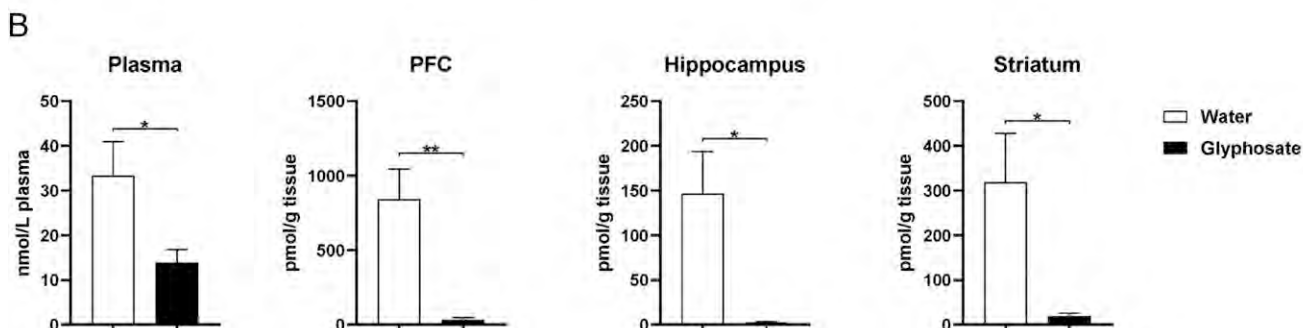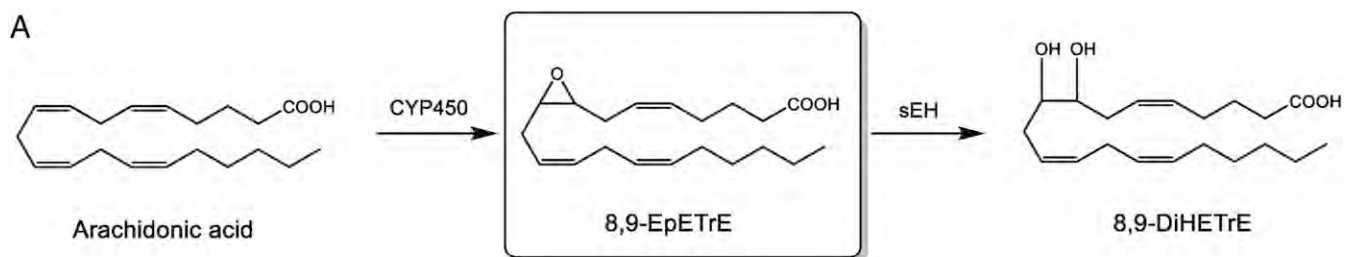
Fig. 2. Oxylipin analysis of blood and brain regions. (*A*) Arachidonic acid is metabolized to 8,9-EpETrE by several cytochrome P450 enzymes. Subsequently, 8,9-EpETrE is metabolized to 8,9-DiHETrE by sEH. (*B*) Levels of 8,9-EpETrE in the plasma, PFC, hippocampus, and striatum from juvenile offspring (P28). The values represent the mean ± SEM ($n = 8$ to 10; *$P < 0.05$, **$P < 0.01$ compared to control group by Student t test).

Lachnospiraceae bacterium 538, and *Clostridium tertium* was significantly lower in the juvenile offspring after maternal glyphosate exposure compared to the water-treated group (Fig. 3). In contrast, the relative abundance of *Clostridium* sp. *Clone-1*, *Enterorhabdus muris*, *Clostridium* sp. *Clone-46*, and *Butyricimonas virosa* was significantly higher in juvenile offspring after maternal glyphosate exposure compared to the water-treated group (Fig. 3). Furthermore, levels of acetic acid in the fecal samples of the offspring were significantly increased after maternal glyphosate exposure (Fig. 3). Other short-chain fatty acids including propionic acid, butyric acid, and valeric acid were not different. The data suggest that maternal exposure to formulated glyphosate causes abnormal composition of gut microbiota in juvenile offspring.

Effects of TPPU on ASD-Like Behaviors in Juvenile Offspring of Maternal Glyphosate Exposure. Water or glyphosate was given to pregnant mice from E5 to P21. In addition, the pregnant mice were orally administered vehicle (5 mL/kg/d) or vehicle and TPPU (3 mg/kg/d) from E5 to P21. Behavioral tests such as grooming test and three-chamber social interaction test were performed from P28 to P35 (Fig. 4*A*). Body weight was significantly increased in TPPU-treated glyphosate-exposed mothers compared to vehicle-treated glyphosate exposure mothers (Fig. 4*B*). Treatment with TPPU significantly ameliorated the increased grooming time of juvenile offspring after maternal glyphosate exposure (Fig. 4*C*). In the three-chamber social interaction test, treatment with TPPU significantly improved social interaction deficits in juvenile offspring after maternal glyphosate exposure (Fig. 4*D*).

Discussion

The present results demonstrate a role of sEH in the onset of ASD-like behaviors in murine offspring after maternal glyphosate exposure. The major findings of the present study are as follows. First, exposure to high levels (0.098%) of glyphosate during pregnancy and lactation caused ASD-like behaviors in juvenile offspring. Second, expression of sEH protein in the PFC, hippocampus, and

striatum from juvenile offspring after maternal glyphosate exposure was higher than that of the control group. Oxylipin analysis showed a marked reduction of 8 (9)-EpETrE in the plasma, PFC, hippocampus, and striatum from juvenile offspring after maternal glyphosate exposure, supporting higher levels of sEH in these regions. Third, maternal glyphosate exposure caused reduced PV immunoreactivity in the prelimbic of medial PFC in the offspring compared to the water-treated group. Furthermore, maternal glyphosate exposure caused significant alterations of NMDAR-related amino acids in the blood and brain of offspring. Fourth, maternal glyphosate exposure caused significant abnormal composition of gut microbiota and increased levels of acetic acid in the fecal samples from juvenile offspring. Finally, repeated treatment with TPPU in glyphosate-treated pregnant mice from pregnancy (E5) to weaning (P21) prevented the onset of ASD-like behaviors (i.e., increased grooming time and social interaction deficits) in juvenile offspring after maternal glyphosate exposure. Collectively, these findings suggest that the sEH enzyme plays a key role in the development of ASD-like behavioral abnormalities in offspring after maternal glyphosate exposure, and that sEH inhibitors may prove to be promising prophylactic or therapeutic drugs for ASD.

In this study, we found increased expression of sEH protein in the PFC of juvenile offspring after maternal glyphosate exposure, consistent with our report using MIA (30). Thus, it seems that increases in the sEH in the PFC and other regions (hippocampus and striatum) might play a role in the behavioral and biochemical abnormalities seen in juvenile offspring after maternal glyphosate exposure. Previously, we reported higher levels of *EPHX2* mRNA in the postmortem brain samples from ASD patients (30). These findings suggest that increased metabolism of EpFAs to the corresponding diols by increased sEH may play a role in the pathogenesis of ASD, although further detailed studies on how maternal glyphosate exposure induces abnormalities in the eicosanoid metabolism by sEH and behavioral abnormalities in offspring are needed.

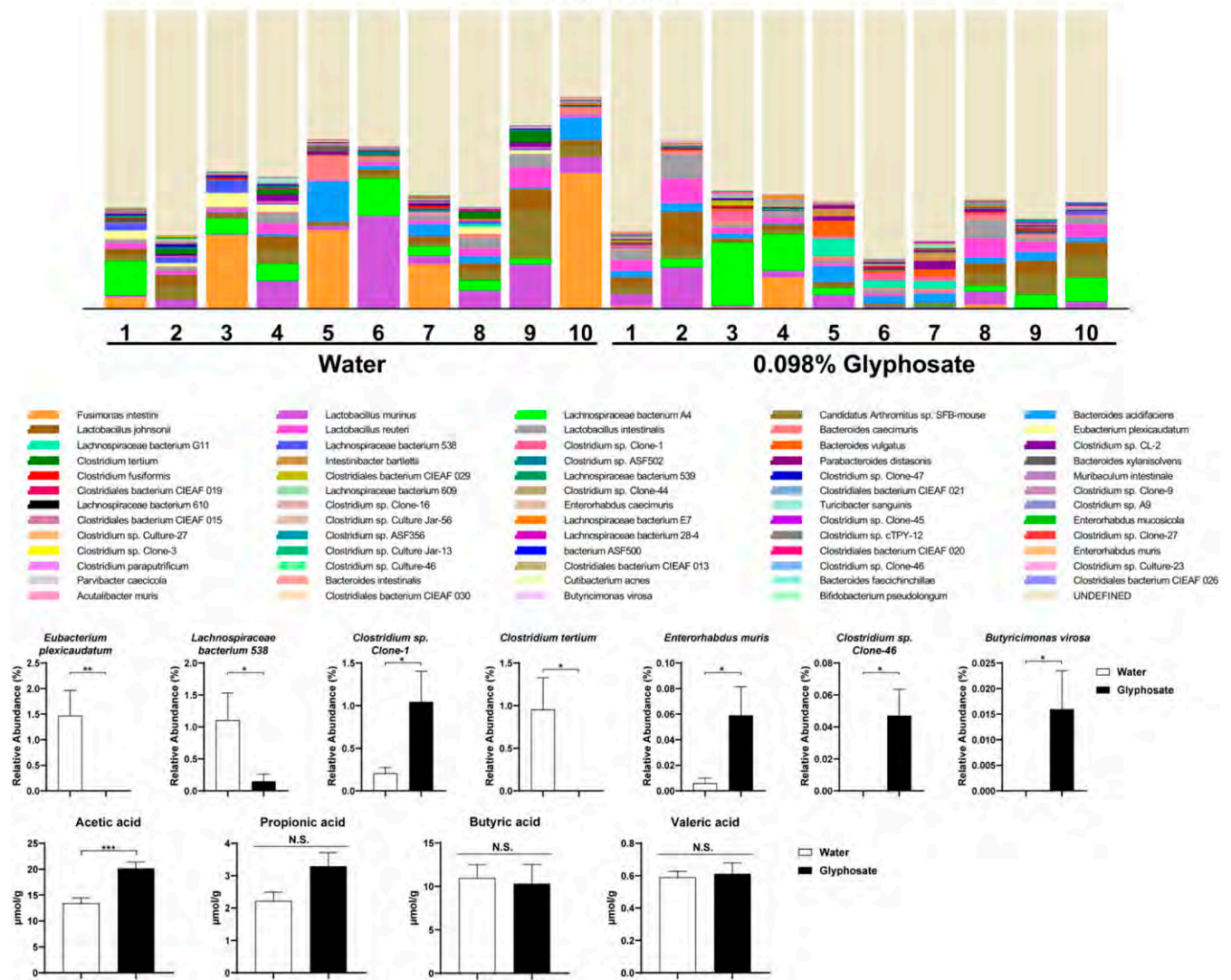We found decreased levels of many EpFAs including 8 (9)-EpETrE in the blood of juvenile offspring after maternal

-190-

Fig. 3. Composition of gut microbiota in fecal samples of juvenile offspring. (*A*) Histogram of microbiota at species level of offspring (P28). (*B*) Several bacteria were significantly altered in the offspring after maternal glyphosate exposure. Data are shown as mean ± SEM (*n* = 10; *$P < 0.05$, **$P < 0.01$ compared to control group by Student *t* test).

glyphosate exposure compared to the water-treated group. Interestingly, tissue levels of 8 (9)-EpETrE, the abundant EpFA in the brain, were significantly lower in the PFC, hippocampus, and striatum from juvenile offspring after maternal glyphosate exposure than those of control mice, supporting an increased activity of sEH in these brain regions. The data on 8 (9)-EpETrE are consistent with our previous report using MIA model of ASD (30). Although the precise mechanisms underlying the relationship between 8 (9)-EpETrE and sEH in the brain from juvenile offspring after maternal glyphosate exposure are currently unclear, it seems that low levels of 8 (9)-EpETrE by increased levels of sEH in the brain may be involved in behavioral abnormalities of offspring after maternal glyphosate exposure. By contrast, other EpFAs were significantly higher in the brain regions of juvenile offspring after maternal glyphosate exposure than those of the water-treated group, although tissue levels of sEH in the brain regions were increased after maternal glyphosate exposure. Although the reasons underlying this discrepancy are currently unknown, it seems that multiple pathways may contribute to formation and degradation of EpFAs in the brain regions.

It is recognized that mechanism of action of glyphosate is to disrupt the shikimate pathway, which is absent from human cells. However, human gut microbiomes contain the shikimate pathway, which plays a key role in the synthesis of aromatic amino acids in both plants and microbiomes (11, 46–48). Therefore, it is suggested that exposure to glyphosate can affect gut microbiota in humans (6, 49). In this study, we found abnormal composition of gut microbiota such as *Clostridium* in juvenile offspring after maternal glyphosate exposure. A recent review pointed an interaction between *Clostridium* bacteria and ASD (50). In addition, we found higher levels of acetic acid in fecal samples of juvenile offspring after maternal glyphosate exposure. It is reported that fecal levels of acetic acid in children with ASD were higher than those in controls (51). It seems that increased intestinal permeability by acetic acid might play a role in fecal production of acetic acid since acetic acid plays a role in gut epithelial barrier function (51). Given the crucial role of gut microbiota in ASD pathogenesis (39, 52, 53), abnormal composition of gut microbiota may be, in part, involved in the ASD-like behaviors in offspring after maternal glyphosate exposure. At present, specific
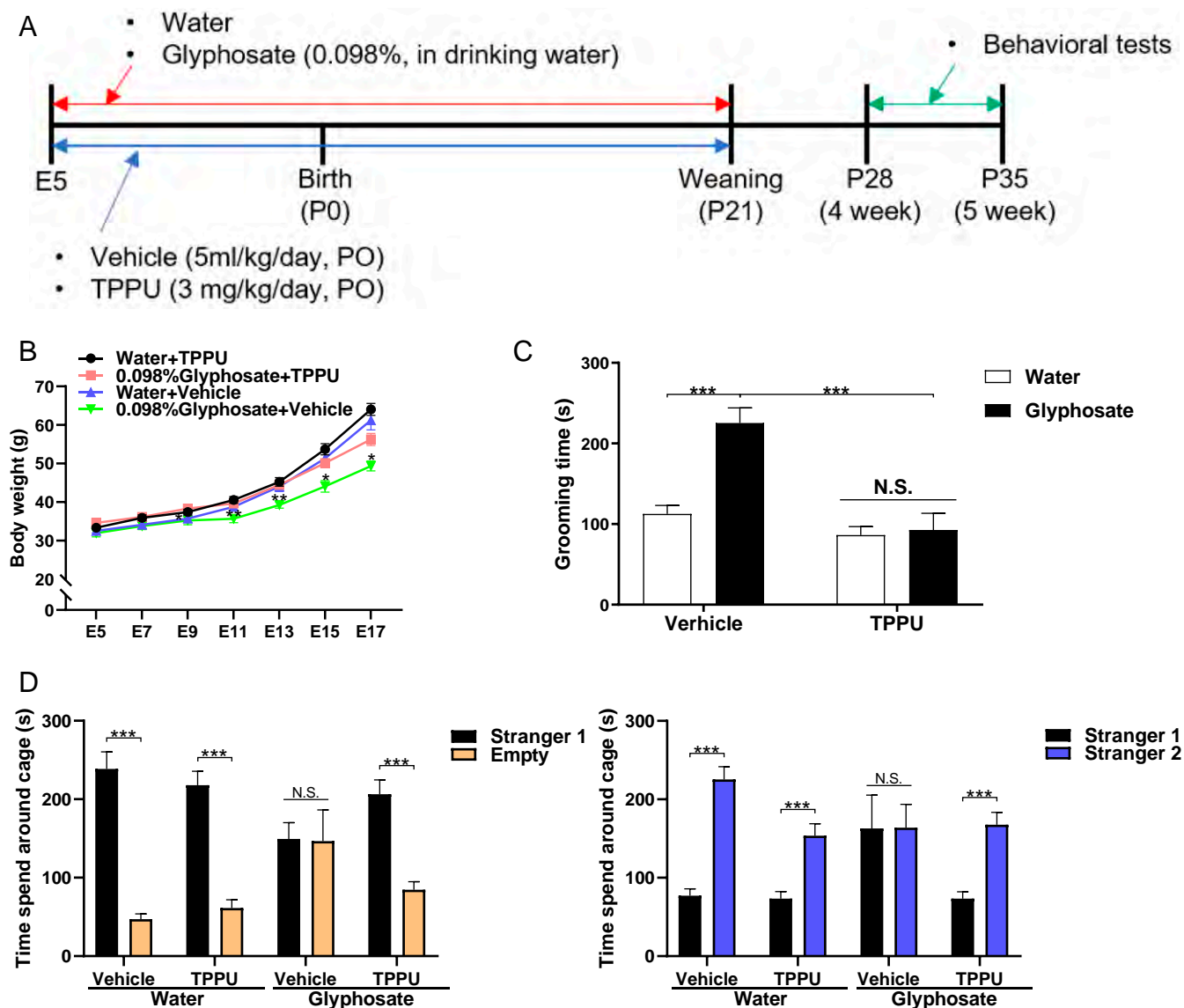
Fig. 4. Effects of TPPU on ASD-like behavioral abnormalities in juvenile offspring after maternal glyphosate exposure. (*A*) Schedule of treatment and behavioral tests. Water or glyphosate (0.098%) was given to pregnant mice. Vehicle (5 mL/kg/d) or TPPU (3 mg/kg/d) was administered orally to pregnant mice from E5 to P21. Subsequently, all mice received normal water. Grooming test and three-chamber social interaction test were performed from P28 to P35. (*B*) Change of body weight of mothers (n = 5 or 6). Two-way ANOVA (glyphosate, $F_{1,17}$ = 7.66, P = 0.013; TPPU, $F_{1,17}$ = 9.14, P = 0.008; interaction, $F_{1,17}$ = 1.59, P = 0.225). (*C*) Grooming test. Treatment with TPPU significantly attenuated the increased grooming time in juvenile offspring after maternal glyphosate exposure. Two-way ANOVA (glyphosate, $F_{1,36}$ = 14.19, P = 0.001; TPPU, $F_{1,36}$ = 25.34, P < 0.001; interaction, $F_{1,36}$ = 11.31, P = 0.002). Data are shown as mean ± SEM (n = 10; ***P < 0.01 compared to glyphosate + vehicle group). (*D*) Three-chamber social interaction test. (*Left*) Three-way ANOVA (glyphosate, $F_{1,56}$ = 9.948, P = 0.003; TPPU, $F_{1,56}$ = 0.301, P = 0.585; stranger, $F_{1,56}$ = 135.27, P < 0.001; interaction [glyphosate × TPPU], $F_{1,56}$ = 0.845, P = 0.362; interaction [glyphosate × stranger], $F_{1,56}$ = 38.61, P < 0.001; interaction [TPPU × stranger], $F_{1,56}$ = 3.593, P = 0.063; interaction [glyphosate × TPPU × stranger], $F_{1,56}$ = 11.06, P = 0.002). (*Right*) Three-way ANOVA (glyphosate, $F_{1,56}$ = 4.168, P = 0.046; TPPU, $F_{1,56}$ = 21.96, P < 0.001; stranger, $F_{1,56}$ = 104.28, P < 0.001; interaction [glyphosate × TPPU], $F_{1,56}$ = 1.902, P = 0.173; interaction [TPPU × stranger], $F_{1,56}$ = 3.870, P = 0.054; interaction [glyphosate × stranger], $F_{1,56}$ = 13.10, P = 0.001; interaction [glyphosate × TPPU × stranger], $F_{1,56}$ = 19.69, P < 0.001). Data are shown as mean ± SEM (n = 8; ***P < 0.01). N.S., not significant.

bacteria that can cause ASD were not yet identified. Therefore, further study on the role of gut microbiota on glyphosate-induced ASD is needed.

Maternal exposure to 0.098% glyphosate causes ASD-like behaviors and abnormal composition of gut microbiota in juvenile offspring. Although it is exceptionally unlikely that such exposure could be reached during human pregnancy, maternal exposure to high levels of technical glyphosate could have detrimental side effects in offspring. A cohort study on measurement of blood (or urine) levels of glyphosate in pregnant mothers who have offspring with or without ASD is of interest.

Although the current animal data do not necessarily translate to humans, further study connecting animal data with the findings from epidemiological studies is needed to identify the detailed mechanisms of action of glyphosate exposure for ASD pathogenesis.

In conclusion, this study suggests that maternal exposure to high levels of formulated glyphosate might play a role in the etiology of ASD-like behaviors in murine offspring through increased activity of sEH in the brain, and sEH inhibitors could be a useful tool to dissect the mechanism. However, a recent comprehensive review on human exposure to glyphosate indicates

-192-

that human exposure approaching these levels is exceptionally unlikely (54).

Materials and Methods

Details of the experimental protocols, including animals, maternal glyphosate exposure, measurement of glyphosate in the blood, oxylipin analysis, Western blot analysis, RT-PCR, behavioral tests, treatment of TPPU, immunohistochemistry, measurement of amino acids, gut microbiota analysis, and statistical analysis, are given in the *SI Appendix*.

1. M. C. Lai, M. V. Lombardo, S. Baron-Cohen, Autism. *Lancet* **383**, 896–910 (2014).
2. C. Lord, M. Elsabbagh, G. Baird, J. Veenstra-Vanderweele, Autism spectrum disorder. *Lancet* **392**, 508–520 (2018).
3. S. N. Hansen, D. E. Schendel, E. T. Parner, Explaining the increase in the prevalence of autism spectrum disorders: The proportion attributable to changes in reporting practices. *JAMA Pediatr.* **169**, 56–62 (2015).
4. J. Baio et al., Prevalence of autism spectrum disorder among children aged 8 years–autism and developmental disabilities monitoring network, 11 sites, United States, 2014. *MMWR Surveill. Summ.* **67**, 1–23 (2018).
5. J. Hallmayer et al., Genetic heritability and shared environmental factors among twin pairs with autism. *Arch. Gen. Psychiatry* **68**, 1095–1102 (2011).
6. L. A. Sealey et al., Environmental factors in the development of autism spectrum disorders. *Environ. Int.* **88**, 288–298 (2016).
7. S. K. Sagiv et al., Prenatal organophosphate pesticide exposure and traits related to autism spectrum disorders in a population living in proximity to agriculture. *Environ. Health Perspect.* **126**, 047012 (2018).
8. J. Y. Kim et al., Environmental risk factors and biomarkers for autism spectrum disorder: An umbrella review of the evidence. *Lancet Psychiatry* **6**, 590–600 (2019).
9. S. M. Bradberry, A. T. Proudfoot, J. A. Vale, Glyphosate poisoning. *Toxicol. Rev.* **23**, 159–167 (2004).
10. L. D. Kier, D. J. Kirkland, Review of genotoxicity studies of glyphosate and glyphosate-based formulations. *Crit. Rev. Toxicol.* **43**, 283–315 (2013).
11. A. Samsel, S. Seneff, Glyphosate, pathways to modern diseases II: Celiac sprue and gluten intolerance. *Interdiscip. Toxicol.* **6**, 159–184 (2013).
12. N. L. Swanson, A. Leu, J. Abrahamson, B. Wallet, Genetically engineered crops, glyphosate and the deterioration of health in the United States of America. *J. Org. Syst.* **9**, 6–37 (2014).
13. A. Samsel, S. Seneff, Glyphosate, pathways to modern diseases III: Manganese, neurological diseases, and associated pathologies. *Surg. Neurol. Int.* **6**, 45 (2015).
14. O. S. von Ehrenstein et al., Prenatal and infant exposure to ambient pesticides and autism spectrum disorder in children: Population based case-control study. *BMJ* **364**, l962 (2019).
15. M. L. Estes, A. K. McAllister, Maternal immune activation: Implications for neuropsychiatric disorders. *Science* **353**, 772–777 (2016).
16. H. Y. Jiang et al., Maternal infection during pregnancy and risk of autism spectrum disorders: A systematic review and meta-analysis. *Brain Behav. Immun.* **58**, 165–172 (2016).
17. M. Careaga, T. Murai, M. D. Bauman, Maternal immune activation and autism spectrum disorder: From rodents to nonhuman and human primates. *Biol. Psychiatry* **81**, 391–401 (2017).
18. O. Zerbo et al., Association between influenza infection and vaccination during pregnancy and risk of autism spectrum disorder. *JAMA Pediatr.* **171**, e163609 (2017).
19. K. Hashimoto, Recent advances in the early intervention in schizophrenia: Future direction from preclinical findings. *Curr. Psychiatry Rep.* **21**, 75 (2019).
20. A. S. Brown, U. Meyer, Maternal immune activation and neuropsychiatric illness: A translational research perspective. *Am. J. Psychiatry* **175**, 1073–1083 (2018).
21. C. Morisseau, B. D. Hammock, Epoxide hydrolases: Mechanisms, inhibitor designs, and biological roles. *Annu. Rev. Pharmacol. Toxicol.* **45**, 311–333 (2005).
22. J. D. Imig, B. D. Hammock, Soluble epoxide hydrolase as a therapeutic target for cardiovascular diseases. *Nat. Rev. Drug Discov.* **8**, 794–805 (2009).
23. C. Morisseau, B. D. Hammock, Impact of soluble epoxide hydrolase and epoxyeicosanoids on human health. *Annu. Rev. Pharmacol. Toxicol.* **53**, 37–58 (2013).
24. K. Hashimoto, Role of soluble epoxide hydrolase in metabolism of PUFAs in psychiatric and neurological disorders. *Front. Pharmacol.* **10**, 36 (2019).
25. Q. Ren et al., Gene deficiency and pharmacological inhibition of soluble epoxide hydrolase confers resilience to repeated social defeat stress. *Proc. Natl. Acad. Sci. U.S.A.* **113**, E1944–E1952 (2016).
26. K. Hashimoto, Soluble epoxide hydrolase: A new therapeutic target for depression. *Expert Opin. Ther. Targets* **20**, 1149–1151 (2016).
27. K. M. Wagner, C. B. McReynolds, W. K. Schmidt, B. D. Hammock, Soluble epoxide hydrolase as a therapeutic target for pain, inflammatory and neurodegenerative diseases. *Pharmacol. Ther.* **180**, 62–76 (2017).
28. W. Swardfager et al., Metabolic/inflammatory/vascular comorbidity in psychiatric disorders; soluble epoxide hydrolase (sEH) as a possible new target. *Neurosci. Biobehav. Rev.* **87**, 56–66 (2018).
29. Q. Ren et al., Soluble epoxide hydrolase plays a key role in the pathogenesis of Parkinson's disease. *Proc. Natl. Acad. Sci. U.S.A.* **115**, E5815–E5823 (2018).
30. M. Ma et al., Key role of soluble epoxide hydrolase in the neurodevelopmental disorders of offspring after maternal immune activation. *Proc. Natl. Acad. Sci. U.S.A.* **116**, 7083–7088 (2019).
31. K. Hashimoto, Understanding the link between maternal infections and neurodevelopmental disorders in offspring: The role of abnormalities in metabolism of polyunsaturated fatty acids. *Brain Behav. Immun.* **81**, 4–5 (2019).
32. J. Atone, K. Wagner, K. Hashimoto, B. D. Hammock, Cytochrome P450 derived epoxidized fatty acids as a therapeutic tool against neuroinflammatory diseases. *Prostaglandins Other Lipid Mediat.* **147**, 106385 (2020).
33. A. Shinohe et al., Increased serum levels of glutamate in adult patients with autism. *Prog. Neuropsychopharmacol. Biol. Psychiatry* **30**, 1472–1477 (2006).
34. C. Shimmura et al., Alteration of plasma glutamate and glutamine levels in children with high-functioning autism. *PLoS One* **6**, e25340 (2011).
35. Z. Zheng, T. Zhu, Y. Qu, D. Mu, Blood glutamate levels in autism spectrum disorder: A systematic review and meta-analysis. *PLoS One* **11**, e0158688 (2016).
36. M. Wang et al., Alterations in gut glutamate metabolism associated with changes in gut microbiota composition in children with autism spectrum disorder. *mSystems* **4**, e00321-18 (2019).
37. A. Tomova et al., Gastrointestinal microbiota in children with autism in Slovakia. *Physiol. Behav.* **138**, 179–187 (2015).
38. H. E. Vuong, E. Y. Hsiao, Emerging roles for the gut microbiome in autism spectrum disorder. *Biol. Psychiatry* **81**, 411–423 (2017).
39. F. Liu et al., Altered composition and function of intestinal microbiota in autism spectrum disorders: A systematic review. *Transl. Psychiatry* **9**, 43 (2019).
40. M. Xu, X. Xu, J. Li, F. Li, Association between gut microbiota and autism spectrum disorder: A systematic review and meta-analysis. *Front. Psychiatry* **10**, 473 (2019).
41. T. E. Rose et al., 1-Aryl-3-(1-acylpiperidin-4-yl)urea inhibitors of human and murine soluble epoxide hydrolase: Structure-activity relationships, pharmacokinetics, and reduction of inflammatory pain. *J. Med. Chem.* **53**, 7067–7075 (2010).
42. A. I. Ostermann et al., Oral treatment of rodents with soluble epoxide hydrolase inhibitor 1-trifluoromethoxyphenyl-3-(1-propionylpiperidin-4-yl)urea (TPPU): Bioavailability, resulting drug levels and modulation of oxylipin pattern. *Prostaglandins Other Lipid Mediat.* **121**, 131–137 (2015).
43. H. Ji, L. Xu, Z. Wang, X. Fan, L. Wu, Differential microRNA expression in the prefrontal cortex of mouse offspring induced by glyphosate exposure during pregnancy and lactation. *Exp. Ther. Med.* **15**, 2457–2467 (2018).
44. N. Yu et al., Circular RNA expression profiles in hippocampus from mice with perinatal glyphosate exposure. *Biochem. Biophys. Res. Commun.* **501**, 838–845 (2018).
45. G. M. Williams, R. Kroes, I. C. Munro, Safety evaluation and risk assessment of the herbicide Roundup and its active ingredient, glyphosate, for humans. *Regul. Toxicol. Pharmacol.* **31**, 117–165 (2000).
46. K. M. Herrmann, L. M. Weaver, The shikimate pathway. *Annu. Rev. Plant Physiol. Plant Mol. Biol.* **50**, 473–503 (1999).
47. H. Maeda, N. Dudareva, The shikimate pathway and aromatic amino acid biosynthesis in plants. *Annu. Rev. Plant Biol.* **63**, 73–105 (2012).
48. A. Samsel, S. Seneff, Glyphosate's suppression of cytochrome P450 enzymes and amino acid biosynthesis by the gut microbiome: Pathways to modern diseases. *Entropy* **15**, 1416–1463 (2013).
49. L. Rueda-Ruzafa, F. Cruz, P. Roman, D. Cardona, Gut microbiota and neurological effects of glyphosate. *Neurotoxicology* **75**, 1–8 (2019).
50. I. Argou-Cardozo, F. Zeidán-Chuliá, Clostridium bacteria and autism spectrum conditions: A systematic review and hypothetical contribution of environmental glyphosate levels. *Med. Sci.* **6**, 29 (2018).
51. L. Wang et al., Elevated fecal short chain fatty acid and ammonia concentrations in children with autism spectrum disorder. *Dig. Dis. Sci.* **57**, 2096–2102 (2012).
52. J. F. Cryan et al., The micribiota-gut-brain axis. *Physiol. Rev.* **99**, 1877–2013 (2019).
53. E. Sherwin, S. R. Bordenstein, J. L. Quinn, T. G. Dinan, J. F. Cryan, Microbiota and the social brain. *Science* **366**, eaar2016 (2019).
54. K. R. Solomon, Estimated exposure to glyphosate in humans via environmental, occupational, and dietary pathways: An updated review of the scientific literature. *Pest Manag. Sci.*, 10.1002/ps.5717 (2019).

NEUROSCIENCE

A key role of the subdiaphragmatic vagus nerve in the depression-like phenotype and abnormal composition of gut microbiota in mice after lipopolysaccharide administration

Jiancheng Zhang[1,2], Li Ma[1], Lijia Chang[1], Yaoyu Pu[1], Youge Qu[1] and Kenji Hashimoto[1]

Abstract

The vagus nerve plays a role in the cross talk between the brain and gut microbiota, which could be involved in depression. The subdiaphragmatic vagus nerve serves as a major modulatory pathway between the brain and gut microbiota. Here, we investigated the effects of subdiaphragmatic vagotomy (SDV) on the depression-like phenotype and the abnormal composition of gut microbiota in mice after lipopolysaccharide (LPS) administration. LPS caused a depression-like phenotype, inflammation, increase in spleen weight, and downregulation of synaptic proteins in the medial prefrontal cortex (mPFC) in the sham-operated mice. In contrast, LPS did not produce a depression-like phenotype and downregulated synaptic proteins in the mPFC after SDV. The spleen weight and plasma levels of pro-inflammatory cytokines in the SDV + LPS group were lower than those of the sham + LPS group. Interestingly, there were positive correlations between the plasma levels of pro-inflammatory cytokines and spleen weight, suggesting a relationship between inflammatory events and spleen weight. Furthermore, LPS led to significant alterations in gut microbiota diversity in sham-operated mice, but not SDV-operated mice. In an unweighted UniFrac PCoA, the dots representing the sham + LPS group were located far away from the dots representing the other three groups. Our results suggest that LPS produces a depression-like phenotype, increases spleen weight, triggers inflammation, downregulates synaptic proteins in the mPFC, and leads to abnormal composition of gut microbiota via the subdiaphragmatic vagus nerve. It is likely that the vagus nerve plays a crucial role in the brain–gut–microbiota axis.

Introduction

Depression, a common mental disorder, affects 264 million people worldwide and places great pressure on the global burden of disease[1]. Although inflammation plays a crucial role in the pathogenesis of depression[2–8], the precise mechanisms underlying inflammation-related depression are not fully understood. Meta-analyses showed that patients with depression exhibit higher expression levels of pro-inflammatory cytokines, including interleukin-6 (IL-6) and the tumor necrosis factor-α (TNF-α), compared with healthy control subjects[9–16].

Interestingly, we reported previously that alterations of peripheral IL-6, but not cerebral IL-6, might lead to resilience rather than susceptibility to inescapable electric stress in a rat model of learned helplessness[17]; moreover, we showed that blockage of the IL-6 receptor in the periphery produced rapid-acting sustained antidepressant effects in a murine model of chronic social defeat stress (CSDS)[18]. Thus, it is likely that inflammation in the periphery plays an important role in depression-like phenotypes in rodents.

Correspondence: Kenji Hashimoto (hashimoto@faculty.chiba-u.jp)
[1]Division of Clinical Neuroscience, Chiba University Center for Forensic Mental Health, Chiba 260-8670, Japan
[2]Department of Critical Care Medicine, Union Hospital, Tongji Medical College, Huazhong University of Science and Technology, Wuhan 430022, PR China

The peripheral administration of a bacterial endotoxin (lipopolysaccharide (LPS)) induces depression-like behaviors after triggering inflammation in rodents[2,19]. Therefore, the LPS-induced depression model has been widely used as an inflammatory model of depression in rodents[20–25]. The spleen, which is a large immune organ, plays an essential role in systemic immune function. Recently, we demonstrated a notable increase in splenic size and weight in CSDS-susceptible mice compared with non-CSDS control mice and CSDS-resilient mice[26], suggesting a role for the brain–spleen axis in stress-induced depression.

Accumulating evidence suggests that the brain–gut–microbiota axis plays an important role in the pathogenesis of depression, as the composition of gut microbiota in patients with depression is altered compared with healthy control subjects[27–29]. Preclinical studies showed that abnormal composition of gut microbiota might contribute to the depression-like behaviors detected in rodents[30–39]. Interestingly, it is suggested that the communication between the brain and the endogenous and exogenous microorganisms in the gut is modulated by the vagus nerve system[40–46]. The ingestion of beneficial bacteria alleviated stress-induced anxiety and depression-like behaviors via the subdiaphragmatic vagus nerve; moreover, these antidepressant-like effects were abolished after subdiaphragmatic vagotomy (SDV)[46]. SDV blocked the depression-like phenotype after intraperitoneal injection of recombinant IL-1β or LPS[47], suggesting a role for the subdiaphragmatic vagus nerve in LPS-induced depression-like phenotypes in rodents. However, no study has demonstrated the role of the subdiaphragmatic vagus nerve in the effects of the brain–gut–microbiota axis and brain–spleen axis on LPS-induced depression-like phenotype.

Given the key role of inflammation in depression, the present study was undertaken to investigate whether the subdiaphragmatic vagus nerve plays a role in the depression-like phenotype and gut microbiota composition observed in mice after LPS administration. Furthermore, we measured the plasma levels of pro-inflammatory cytokines (i.e., IL-6 and TNF-α) and synaptic proteins [i.e., α-amino-3-hydroxy-5-methyl-4-isoxazolepropionic acid receptor A1 (GluA1) and the postsynaptic density-95 (PSD-95) protein] in the medial prefrontal cortex (mPFC). In addition, we investigated whether SDV affects the depression-like phenotype, spleen weight, synaptic protein expression in the mPFC, and gut microbiota composition in LPS-treated mice.

Materials and method
Animals

Forty adult male C57BL/6 mice (aged 8 weeks, body weighing 20–25 g) were purchased from Japan SLC Inc. (Hamamatsu, Japan). Mice were housed under controlled conditions for temperature and humidity with a 12 h light/dark cycle (lights on from 07 to 19 h) and were allowed free access to food (CE-2; CLEA Japan, Inc., Tokyo, Japan) and water. All experiments using mice were carried out in strict accordance with the recommendations in the Guide for the Care and Use of Laboratory Animals of the National Institutes of Health, USA, and were approved by the Chiba University Institutional Animal Care and Use Committee (Permission number: 1-427). Animals were deeply anaesthetized with inhaled isoflurane and rapidly killed by cervical dislocation. All efforts were made to minimize animal suffering.

Subdiaphragmatic vagotomy (SDV)

Bilateral SDV was performed under anesthesia with 5% isoflurane. Briefly, a 1 cm right transverse abdominal incision was made 0.5 cm below the xiphisternum, starting from the linea alba. The liver was carefully retracted with a small cotton pellet dampened with sterile normal saline and the costal arc was pulled using a vascular clamp, to expose the esophagus. The dorsal and ventral branches of the vagus nerve were exposed along the subdiaphragmatic esophagus under a surgical microscope (Leica, Heidelberg, Germany). Fourteen days after the operation, the observation of an increased stomach size indicated a successful SDV. For sham surgery, the trunk of the vagus nerve was gently exposed but not cut. In all mice that were subjected to SDV, particular care was taken to avoid any injuries to the subdiaphragmatic esophagus. The mice that underwent bilateral SDV were allowed to recover for 14 days.

Grouping and behavioral tests

The mice were randomly divided into four groups ($n = 10$/group). Saline (10 ml/kg), or LPS (0.5 mg/kg, Sigma-Aldrich Japan, Tokyo, Japan) was given intraperitoneally (i.p.) to mice subjected to SDV or sham surgery (day 15) (Fig. 1a). The locomotion test (LMT) and forced swimming test (FST) were performed 22 and 24 h after a single injection of saline or LPS.

The mice were deeply anesthetized with inhaled isoflurane (5%) 24 h after the injection of saline or LPS. Blood was collected via cardiac puncture, placed into tubes containing ethylenediaminetetraacetic acid, and immediately centrifuged at $3000 \times g$ for 3 min at 4 °C, to obtain plasma, and then stored at −80 °C until bioanalysis. The bilateral mPFC was collected rapidly and stored at −80 °C until bioanalysis. The weight of spleens was recorded immediately after spleen removal[26].

The LMT and FST were performed as described previously[21,25,48,49]. An automated animal movement analysis system (SCANET MV-40; MELQUEST
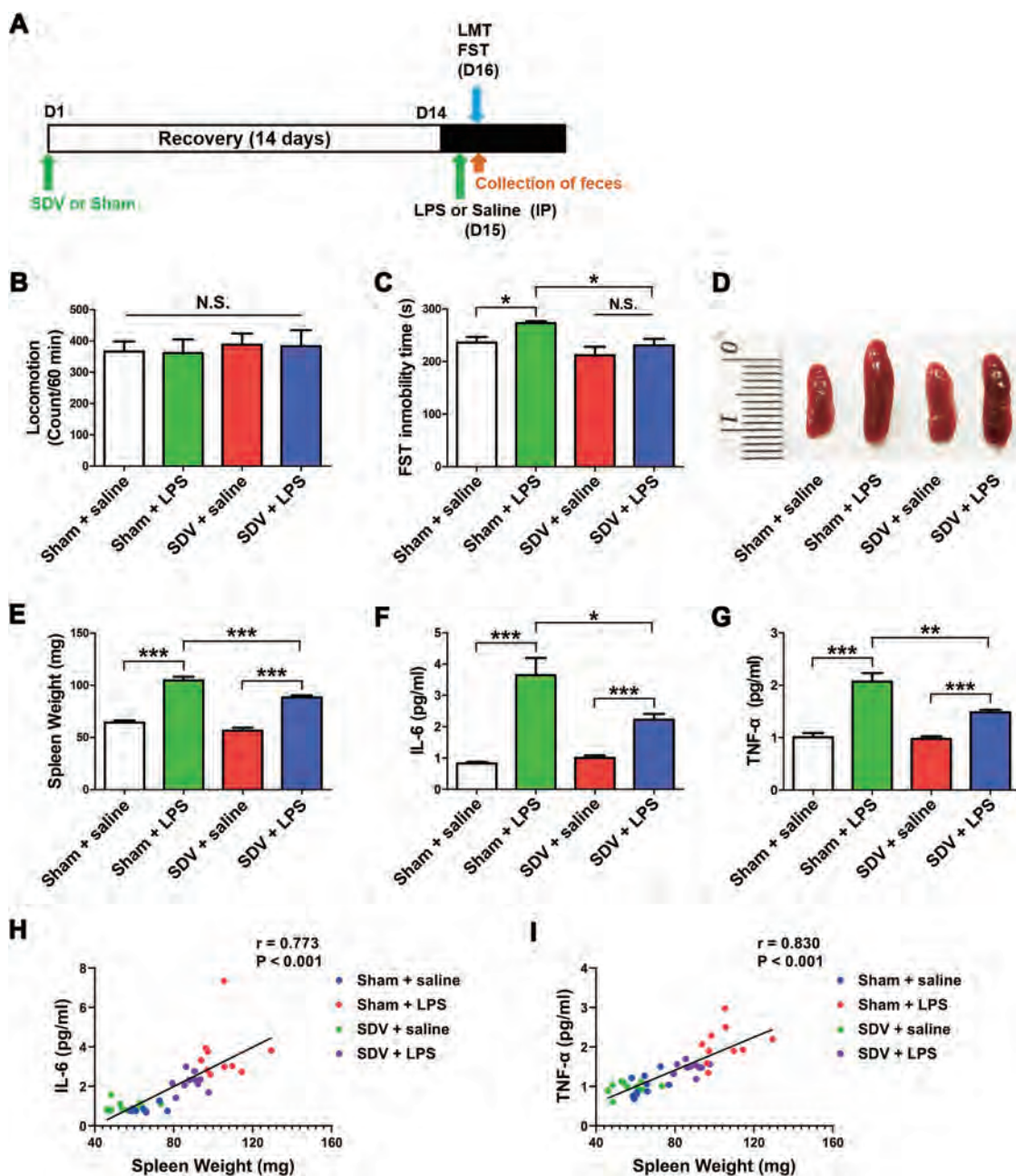
Fig. 1 Effects of SDV on depression-like phenotype, spleen weight and inflammatory cytokines after LPS treatment. a Treatment schedule. Adult mice were subjected to subdiaphragmatic vagotomy (SDV) and then allowed to recovery for 14 days. On day 15, mice were intraperitoneally (i.p.) injected with lipopolysaccharides (LPS, 0.5 mg/kg) or saline (10 ml/kg). On day 16, fresh feces were collected. Locomotion test and forced swimming test (FST) were performed 22 and 24 h after a single injection of saline or LPS. Blood and brain samples (prefrontal cortex) were collected after behavioral tests (**b**) Locomotion test (LMT). (tow-way ANOVA: LPS: $F_{1,36} = 0.014$, $P = 0.907$; SDV: $F_{1,36} = 0.271$, $P = 0.606$; interaction: $F_{1,36} = 0.000$, $P = 0.996$). **c** FST (two-way ANOVA: LPS: $F_{1,36} = 5.666$, $P = 0.0243$; SDV: $F_{1,36} = 8.126$, $P = 0.0081$; interaction: $F_{1,36} = 0.617$, $P = 0.439$). **d** Representative picture of spleen. **e** Spleen weight (two-way ANOVA: LPS: $F_{1,36} = 197.7$, $P < 0.0001$; SDV: $F_{1,36} = 21.84$, $P < 0.0001$; interaction: $F_{1,36} = 2.756$, $P = 0.106$). **f** Plasma levels of IL-6. (two-way ANOVA: LPS: $F_{1,36} = 58.34$, $P < 0.0001$; SDV: $F_{1,36} = 5.507$, $P = 0.0253$; interaction: $F_{1,36} = 9.131$, $P = 0.0049$). **g** Plasma levels of TNF-α (two-way ANOVA: LPS: $F_{1,36} = 74.43$, $P < 0.0001$; SDV: $F_{1,36} = 9.243$, $P = 0.0047$; interaction: $F_{1,36} = 9.850$, $P = 0.0036$). The data represent mean ± S.E.M. ($n = 10$). *$P < 0.05$, **$P < 0.01$, ***$P < 0.0001$; N.S. not significant. **h** There was a positive correlation ($r = 0.773$, $P < 0.001$) between spleen weight and plasma IL-6. i There was a positive correlation ($r = 0.830$, $P < 0.001$) between spleen weight and plasma TNF-α.

Co., Ltd, Toyama, Japan) was used to measure the locomotor activity of mice. The cumulative ambulatory activity counts were recorded continuously over a period of 60 min after the mice were placed in the experimental cages (56 cm (length) × 56 cm (width) × 33 cm (height)). The cages were cleaned between the testing sessions. The FST was performed using an automated forced-swim apparatus (SCANET MV-40; MELQUEST Co., Ltd, Toyama, Japan). The mice were individually placed into a cylinder (23 cm (diameter) × 31 cm (height)) with a water depth of 15 cm (water temperature, 23 ± 1 °C). The immobility time was recorded and calculated by the analytical software of the apparatus throughout a 6 min observation time.

Enzyme-linked immunosorbent assay (ELISA)

The plasma expression levels of IL-6 (Cat Number: 88-7064, Invitrogen, Camarillo, CA, USA) and TNF-α (Cat Number: 88-7324, Invitrogen, Camarillo, CA, USA) were measured using commercial ELISA kits, as per the manufacturer's instructions.

Western blotting

Tissue samples from the mPFC and hippocampus were homogenized in ice-cold Laemmli lysis buffer and centrifuged at $3000 \times g$ for 10 min at 4 °C, to collect the supernatants. Proteins were quantified using a bicinchoninic acid protein assay kit (Bio-Rad, Hercules, CA). The samples were then mixed with an equal volume of loading buffer (125 mM Tris/HCl, pH 6.8, 20% glycerol, 0.1% bromophenol blue, 10% β-mercaptoethanol, and 4% sodium dodecyl sulfate) and boiled for 5 min at 95 °C. Proteins were separated using 10% sodium dodecyl sulfate polyacrylamide gel electrophoresis (SDS–PAGE) (Mini-PROTEAN® TGX™ Precast Gel; Bio-Rad) and then transferred onto polyvinylidene difluoride membranes using a Trans Blot Mini Cell apparatus (Bio-Rad). The membranes were blocked with 5% skim milk in TBS containing 0.1% Tween 20 (TBST) for 1 h at room temperature, followed by incubation with primary antibodies against PSD-95 (1:1000, Cat Number: 51-6900, Invitrogen, Camarillo, CA, USA), GluA1 (1:1,000, Cat Number: ab31232, Abcam, Cambridge, MA, USA), and β-actin (1:10,000, Sigma-Aldrich Co., Ltd, St Louis, MO, USA) overnight at 4 °C. After three washes with TBST, the membranes were incubated with a horseradish peroxidase-conjugated anti-rabbit or anti-mouse antibody (1:5000) for 1 h at room temperature. After three washes in TBST, the bands were visualized using enhanced chemiluminescence plus the Western Blotting Detection system (GE Healthcare Bioscience) and captured by a ChemiDoc™ Touch Imaging System (170-01401; Bio-Rad Laboratories, Hercules, CA). The images were subjected to grey-scale analysis using the Image Lab™ 3.0 software (Bio-Rad Laboratories).

Collection of fecal samples and 16S rRNA analysis

Fresh fecal samples of mice were collected before the LMT. The fecal samples were placed into sterilized screw-cap microtubes immediately after defecation and were stored at −80 °C until use. The 16S rRNA analyses of fecal samples were performed at MyMetagenome Co., Ltd (Tokyo, Japan), as reported previously[38,49].

Statistical analysis

Data are expressed as the mean ± standard error of the mean (S.E.M). Data were analyzed using two-way analysis of variance (ANOVA) followed by post-hoc Tukey's multiple comparison tests. Correlation was analyzed by Pearson's correlation. Significance was set at $P < 0.05$. Statistical analyses were performed using the SPSS version 20.0 software (SPSS, Tokyo, Japan).
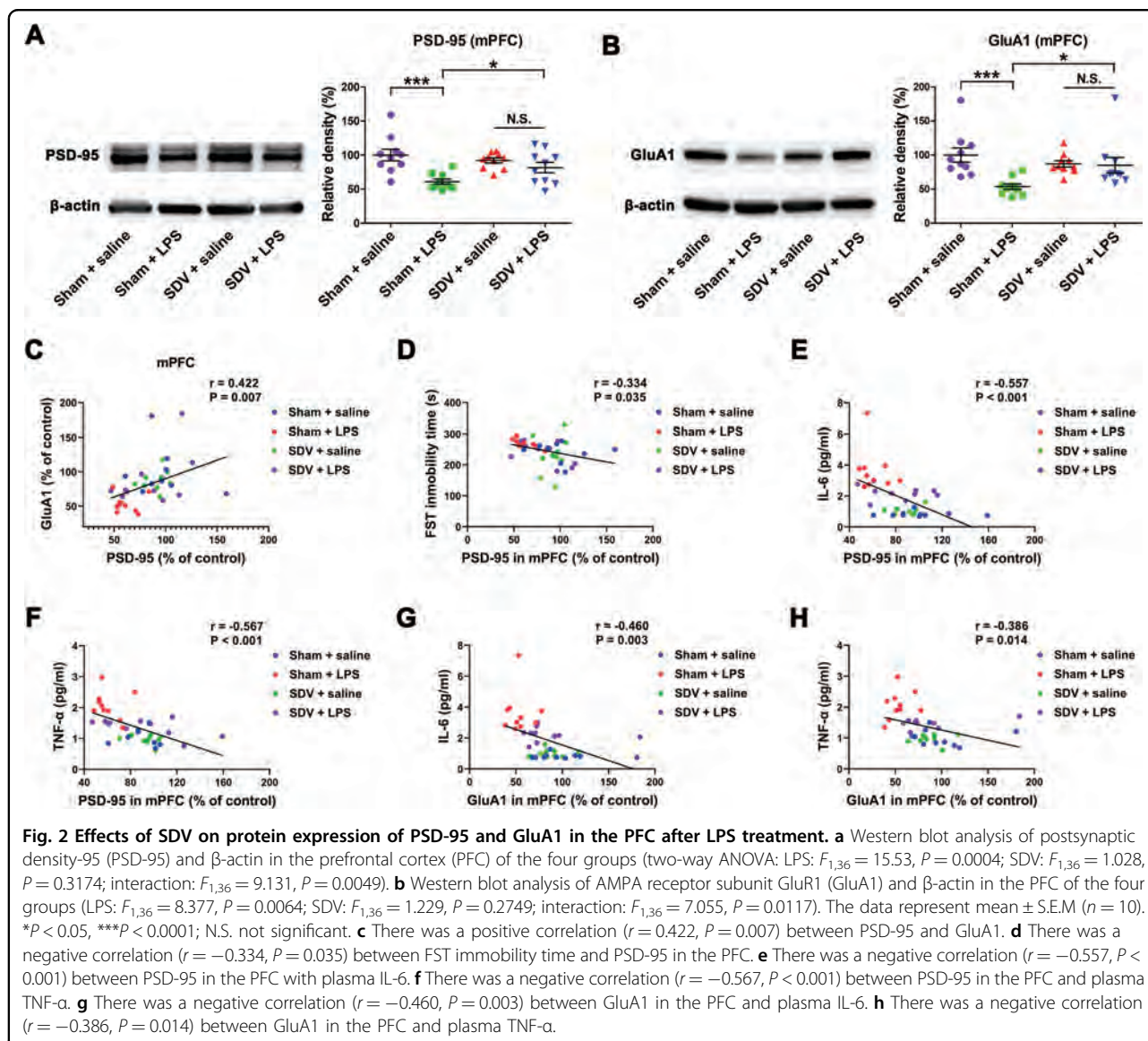
Results

Effects of SDV on the depression-like phenotype, spleen weight, and inflammatory cytokines after LPS treatment

First, we studied the effects of SDV on the depression-like phenotype, spleen weight, and increased inflammatory cytokines observed in mice after LPS treatment (Fig. 1a). No difference was found in locomotor activity among the four groups (Fig. 1b). A significant difference in the immobility time in the FST, as analyzed by two-way ANOVA, was observed among the four groups (Fig. 1c). LPS significantly increased the immobility time in the FST in sham-operated mice, but not in mice subjected to SDV (Fig. 1c). Interestingly, SDV significantly attenuated the increased immobility time in the FST observed in LPS-treated mice.

A two-way ANOVA of the spleen weight data revealed a significant difference in this parameter among the four groups (Fig. 1d, e). LPS significantly increased the spleen weight in both sham-operated and SVD-operated mice. However, the spleen weight of LPS-treated mice subjected to SDV was significantly lower than that of LPS-treated mice subjected to sham operation.

A two-way ANOVA revealed significant differences in the plasma expression of IL-6 and TNF-α among the four groups (Fig. 1f, g). LPS significantly increased the plasma levels of IL-6 and TNF-α in both sham-operated and SDV-operated mice. However, the plasma levels of IL-6 and TNF-α in the SDV + LPS group were significantly lower than those of the sham + LPS group. Interestingly, positive correlations between spleen weight and plasma IL-6 (or plasma TNF-α) levels were observed in the four groups (Fig. 1h, i). Thus, LPS-induced inflammation in the periphery is associated with increased splenic volume and weight.

Fig. 2 Effects of SDV on protein expression of PSD-95 and GluA1 in the PFC after LPS treatment. a Western blot analysis of postsynaptic density-95 (PSD-95) and β-actin in the prefrontal cortex (PFC) of the four groups (two-way ANOVA: LPS: $F_{1,36} = 15.53$, $P = 0.0004$; SDV: $F_{1,36} = 1.028$, $P = 0.3174$; interaction: $F_{1,36} = 9.131$, $P = 0.0049$). **b** Western blot analysis of AMPA receptor subunit GluR1 (GluA1) and β-actin in the PFC of the four groups (LPS: $F_{1,36} = 8.377$, $P = 0.0064$; SDV: $F_{1,36} = 1.229$, $P = 0.2749$; interaction: $F_{1,36} = 7.055$, $P = 0.0117$). The data represent mean ± S.E.M ($n = 10$). *$P < 0.05$, ***$P < 0.0001$; N.S. not significant. **c** There was a positive correlation ($r = 0.422$, $P = 0.007$) between PSD-95 and GluA1. **d** There was a negative correlation ($r = -0.334$, $P = 0.035$) between FST immobility time and PSD-95 in the PFC. **e** There was a negative correlation ($r = -0.557$, $P < 0.001$) between PSD-95 in the PFC with plasma IL-6. **f** There was a negative correlation ($r = -0.567$, $P < 0.001$) between PSD-95 in the PFC and plasma TNF-α. **g** There was a negative correlation ($r = -0.460$, $P = 0.003$) between GluA1 in the PFC and plasma IL-6. **h** There was a negative correlation ($r = -0.386$, $P = 0.014$) between GluA1 in the PFC and plasma TNF-α.

Effects of SDV on the expression of PSD-95 and GluA1 in the brain after LPS treatment

Two-way ANOVA showed a significant difference in the levels of expression of the PSD-95 and GluA1 proteins in the mPFC among the four groups (Fig. 2a, b). LPS significantly decreased the expression of PSD-95 and GluA1 in the mPFC in sham-operated mice, but not in mice subjected to SDV.

Positive correlations were detected between PSD-95 and GluA1 in the mPFC of the four groups (Fig. 2c). Furthermore, there was a negative correlation between the immobility time in the FST and PSD-95 levels in the mPFC in the four groups (Fig. 2d). In turn, there were negative correlations between plasma IL-6 (or TNF-α) levels and PSD-95 (or GluA1) expression in the mPFC in the four groups (Fig. 2e–h). Thus, LPS-induced

inflammation is associated with the depression-like phenotype and reduced expression of synaptic proteins in the mPFC.

Composition of gut microbiota

The composition of the gut microbiota was investigated in the four groups. α-diversity, defined as the gut microbiota richness, can be measured using different indices, including the Chao1 index, Shannon index, and ACE index. A two-way ANOVA revealed significant differences in the Chao1 and Shannon indices among the four groups (Fig. 3a–c). A two-way ANOVA showed an absence of significant differences in the ACE index among the four groups (Fig. 3d). Regarding β-diversity, principal coordinate analysis plots of Bray–Curtis dissimilarity between the four groups showed that the dots representing the
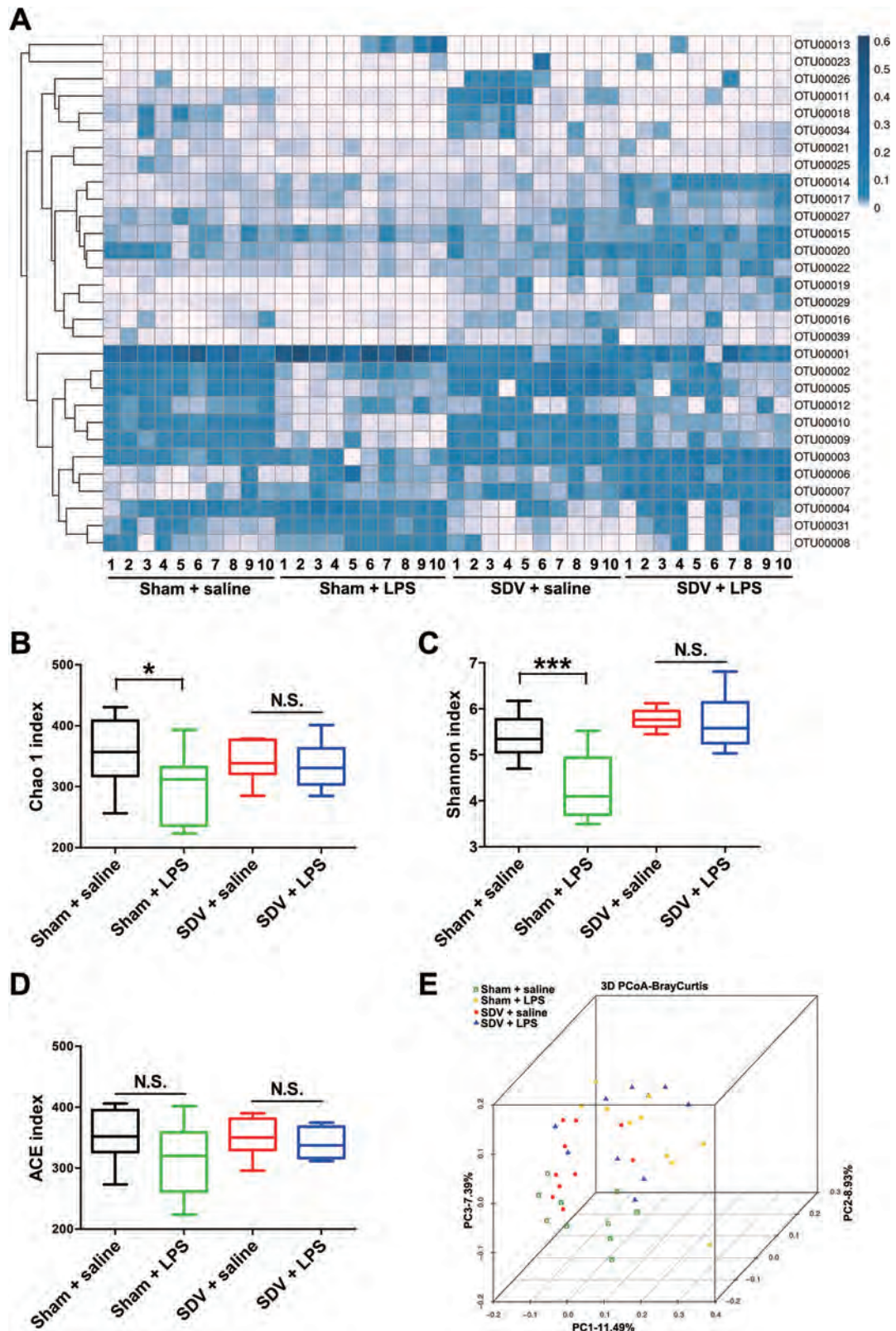
Fig. 3 α-diversity and β-diversity in gut microbiota. a Heat map of differential levels of bacteria between the four groups. b Chao1 index. c Shannon index. d ACE index. e PCoA analysis of gut bacteria data (Bray–Curtis dissimilarity). The data represent mean ± S.E.M. ($n = 10$). *$P < 0.05$, ***$P < 0.0001$; N.S. not significant.
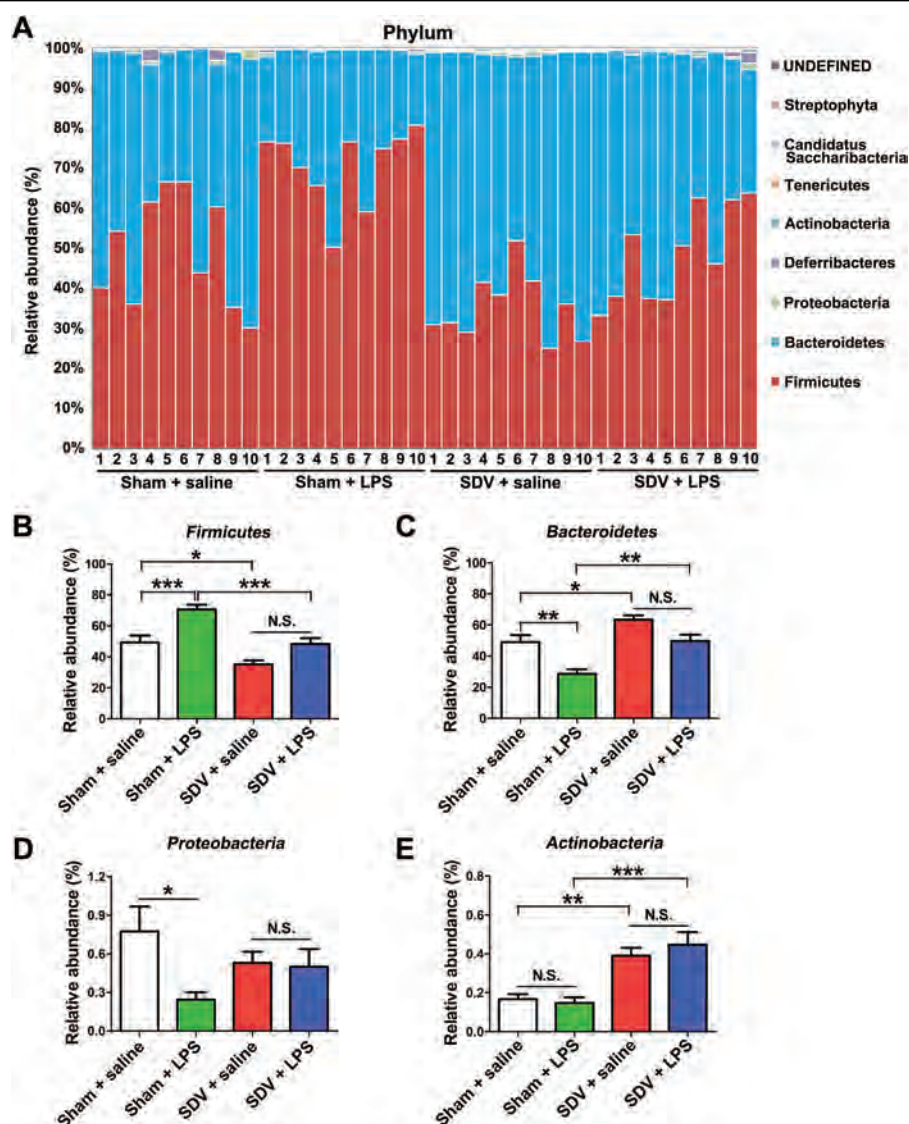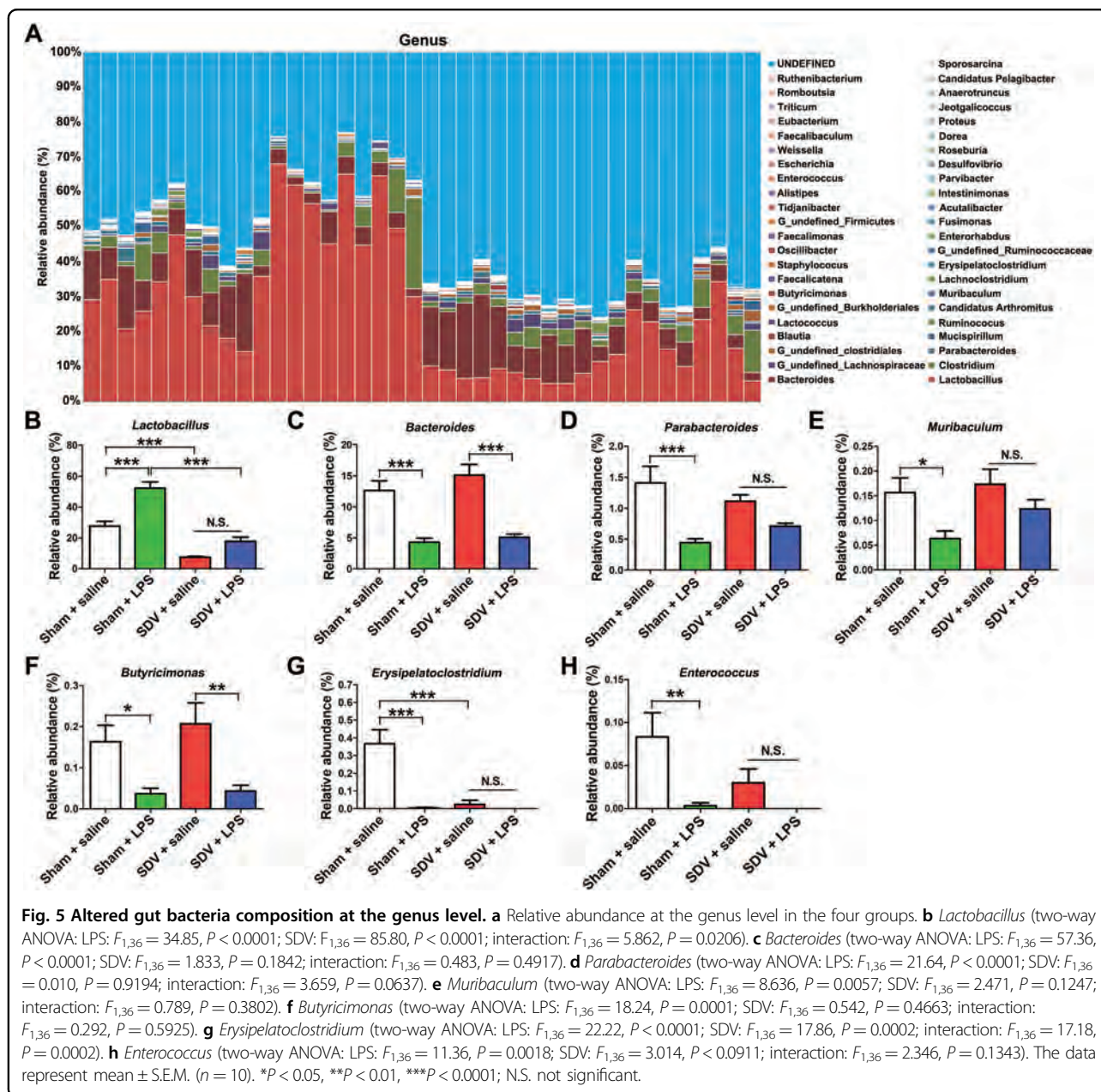
Fig. 4 Altered gut bacteria composition at the phylum level. a Relative abundance at the phylum level in the four groups. **b** *Firmicutes* (two-way ANOVA: LPS: $F_{1,36} = 24.11$, $P < 0.0001$; SDV: $F_{1,36} = 26.94$, $P < 0.0001$; interaction: $F_{1,36} = 1.324$, $P = 0.2575$). **c** *Bacteroidetes* (two-way ANOVA: LPS: $F_{1,36} = 21.37$, $P < 0.0001$; SDV: $F_{1,36} = 23.49$, $P < 0.0001$; interaction: $F_{1,36} = 0.853$, $P = 0.3619$). **d** *Proteobacteria* (two-way ANOVA: LPS: $F_{1,36} = 4.683$, $P = 0.0372$; SDV: $F_{1,36} = 0.003$, $P = 0.9592$; interaction: $F_{1,36} = 3.733$, $P = 0.0612$). **e** *Actinobacteria* (two-way ANOVA: LPS: $F_{1,36} = 0.180$, $P = 0.6739$; SDV: $F_{1,36} = 36.67$, $P < 0.0001$; interaction: $F_{1,36} = 0.787$, $P = 0.3809$). The data represent mean ± S.E.M. ($n = 10$). *$P < 0.05$, **$P < 0.01$, ***$P < 0.0001$; N.S. not significant.

sham + LPS group were far from the dots representing the other three groups (Fig. 3e).

At the phylum level, *Firmicutes* were most abundant in the sham + LPS group (Fig. 4a, b). The abundance of *Firmicutes* was more pronounced in the sham + LPS group than it was in the sham + saline and SDV + LPS groups (Fig. 4b). In contrast, *Bacteroidetes* were also an abundant phylum in these samples. The abundance of *Bacteroidetes* was lower in the sham + LPS group than it was in the sham + saline and SDV + LPS groups (Fig. 4c). The levels of *Proteobacteria* in the sham-operated mice were decreased

after treatment with LPS (Fig. 4d), whereas *Actinobacteria* levels in the sham and SDV-operated mice were not altered after treatment with LPS (Fig. 4e). Moreover, there were no differences in the abundance of *Firmicutes*, *Bacteroidetes*, *Proteobacteria*, and *Actinobacteria* between the SDV + saline group and the SDV + LPS group (Fig. 4b–e). Interestingly, the abundance of *Firmicutes* in the SDV + saline group was lower than that in the sham + saline group, whereas the abundance of *Bacteroidetes* and *Actinobacteria* was higher in the SDV + saline group than it was in the sham + saline group (Fig. 4b–d).

Fig. 5 Altered gut bacteria composition at the genus level. a Relative abundance at the genus level in the four groups. **b** *Lactobacillus* (two-way ANOVA: LPS: $F_{1,36} = 34.85$, $P < 0.0001$; SDV: $F_{1,36} = 85.80$, $P < 0.0001$; interaction: $F_{1,36} = 5.862$, $P = 0.0206$). **c** *Bacteroides* (two-way ANOVA: LPS: $F_{1,36} = 57.36$, $P < 0.0001$; SDV: $F_{1,36} = 1.833$, $P = 0.1842$; interaction: $F_{1,36} = 0.483$, $P = 0.4917$). **d** *Parabacteroides* (two-way ANOVA: LPS: $F_{1,36} = 21.64$, $P < 0.0001$; SDV: $F_{1,36} = 0.010$, $P = 0.9194$; interaction: $F_{1,36} = 3.659$, $P = 0.0637$). **e** *Muribaculum* (two-way ANOVA: LPS: $F_{1,36} = 8.636$, $P = 0.0057$; SDV: $F_{1,36} = 2.471$, $P = 0.1247$; interaction: $F_{1,36} = 0.789$, $P = 0.3802$). **f** *Butyricimonas* (two-way ANOVA: LPS: $F_{1,36} = 18.24$, $P = 0.0001$; SDV: $F_{1,36} = 0.542$, $P = 0.4663$; interaction: $F_{1,36} = 0.292$, $P = 0.5925$). **g** *Erysipelatoclostridium* (two-way ANOVA: LPS: $F_{1,36} = 22.22$, $P < 0.0001$; SDV: $F_{1,36} = 17.86$, $P = 0.0002$; interaction: $F_{1,36} = 17.18$, $P = 0.0002$). **h** *Enterococcus* (two-way ANOVA: LPS: $F_{1,36} = 11.36$, $P = 0.0018$; SDV: $F_{1,36} = 3.014$, $P < 0.0911$; interaction: $F_{1,36} = 2.346$, $P = 0.1343$). The data represent mean ± S.E.M. ($n = 10$). *$P < 0.05$, **$P < 0.01$, ***$P < 0.0001$; N.S. not significant.

At the genus level, both LPS treatment and SDV altered the fecal microbiota composition (Fig. 5a). LPS significantly increased *Lactobacillus* abundance in the sham-operated mice, but not in the SDV-operated mice (Fig. 5b). In contrast, LPS significantly decreased the abundance of *Bacteroides*, *Parabacteroides*, *Muribaculum*, *Butyricimonas*, *Erysipelatoclostridium*, and *Enterococcus* in the sham-operated mice (Fig. 5c–h). However, LPS did not alter the abundance of *Parabacteroides*, *Muribaculum*, *Erysipelatoclostridium*, and *Enterococcus* in the SDV-operated mice (Fig. 5d, e, g, h).

The composition of gut microbiota at the species level in the four groups is shown in Fig. 6a. The abundance of *Lactobacillus murinus*, *Lactobacillus johnsonii*, and *Lactobacillus reuteri* in the sham-operated mice was increased after LPS administration, whereas the abundance of *Muribaculum intestinale*, *[Clostridium] cocleatum*, *Parabacteroides goldsteinii*, *Parabacteroides distasonis*, and *Enterococcus faecalis* in the sham-operated mice was decreased after LPS treatment (Fig. 6). Interestingly, there were no differences in the abundance of *L. murinus*, *L. johnsonii*, *M. intestinale*, *[C.] cocleatum*, *P. goldsteinii*, *P. distasonis*, and *E. faecalis* between the SDV + saline group and the SDV + LPS group (Fig. 6).

Fig. 6 Altered gut bacteria composition at the species level. a Relative abundance at the species level in the four groups. **b** *Lactobacillus murinus* (two-way ANOVA: LPS: $F_{1,36} = 16.64$, $P = 0.0002$; SDV: $F_{1,36} = 66.09$, $P < 0.0001$; interaction: $F_{1,36} = 5.849$, $P = 0.02085$). **c** *Lactobacillus johnsonii* (two-way ANOVA: LPS: $F_{1,36} = 12.13$, $P = 0.0013$; SDV: $F_{1,36} = 9.196$, $P = 0.0045$; interaction: $F_{1,36} = 0.212$, $P = 0.6479$). **d** *Lactobacillus reuteri*. (two-way ANOVA: LPS: $F_{1,36} = 21.04$, $P < 0.0001$; SDV: $F_{1,36} = 16.75$, $P = 0.0012$; interaction: $F_{1,36} = 0.469$, $P = 0.4977$). **e** *Muribaculum intestinale* (two-way ANOVA: LPS: $F_{1,36} = 8.636$, $P = 0.0057$; SDV: $F_{1,36} = 2.471$, $P = 0.1247$; interaction: $F_{1,36} = 0.789$, $P = 0.3802$). **f** *[Clostridium] cocleatum* (two-way ANOVA: LPS: $F_{1,36} = 22.22$, $P < 0.0001$; SDV: $F_{1,36} = 17.86$, $P = 0.0002$; interaction: $F_{1,36} = 17.18$, $P = 0.0002$). **g** *Parabacteroides goldsteinii* (two-way ANOVA: LPS: $F_{1,36} = 11.98$, $P = 0.0014$; SDV: $F_{1,36} = 0.479$, $P = 0.4932$; interaction: $F_{1,36} = 6.444$, $P = 0.0156$). **h** *Parabacteroides distasonis* (two-way ANOVA: LPS: $F_{1,36} = 6.288$, $P = 0.0168$; SDV: $F_{1,36} = 0.959$, $P = 0.3340$; interaction: $F_{1,36} = 3.929$, $P = 0.0551$). **i** *Enterococcus faecalis* (two-way ANOVA: LPS: $F_{1,36} = 8.907$, $P = 0.0051$; SDV: $F_{1,36} = 0.990$, $P = 0.3265$; interaction: $F_{1,36} = 0.557$, $P = 0.4604$). The data represent mean ± S.E.M. ($n = 10$). *$P < 0.05$, **$P < 0.01$, ***$P < 0.0001$; N.S. not significant.

Correlations between spleen weight and the abundance of gut microbiota

There were positive correlations between spleen weight and the abundance of *Firmicutes*, *Proteobacteria*, *Lactobacillus*, *L. murinus*, *L. johnsonii*, and *L. reuteri* among the four groups (Fig. 7a, c, d, g, h, i). In contrast, there were negative correlations between spleen weight and the abundance of *Bacteroidetes*, *Parabacteroides*, *Muribaculum*, *M. intestinale*, and *P. distasonis* among the groups (Fig. 7b, e, f, j, k).

Discussion

The major findings of this study were as follows. First, LPS (0.5 mg/kg) caused a depression-like phenotype, inflammation, and downregulation of synaptic proteins (i.e., PSD-95 and GluA1) in the mPFC in the sham-

operated mice, which was consistent with previous studies[21,24,25]. In contrast, LPS did not produce a depression-like phenotype or downregulation of synaptic proteins in the mPFC of SDV-operated mice. Furthermore, we found a notable increase in spleen weight in the sham-operated mice after LPS administration. Interestingly, SDV significantly attenuated the increased spleen weight and plasma expression of IL-6 and TNF-α detected in mice after LPS administration. Collectively, these results suggest that the subdiaphragmatic vagus nerve plays a role in the depression-like phenotype, inflammation, increases in spleen volume, and reduced synaptic proteins in the PFC observed after a single administration of LPS. Interestingly, we found positive correlations between the plasma levels of IL-6 (or TNF-α) and spleen weight, suggesting that LPS-induced inflammatory events play a role in the
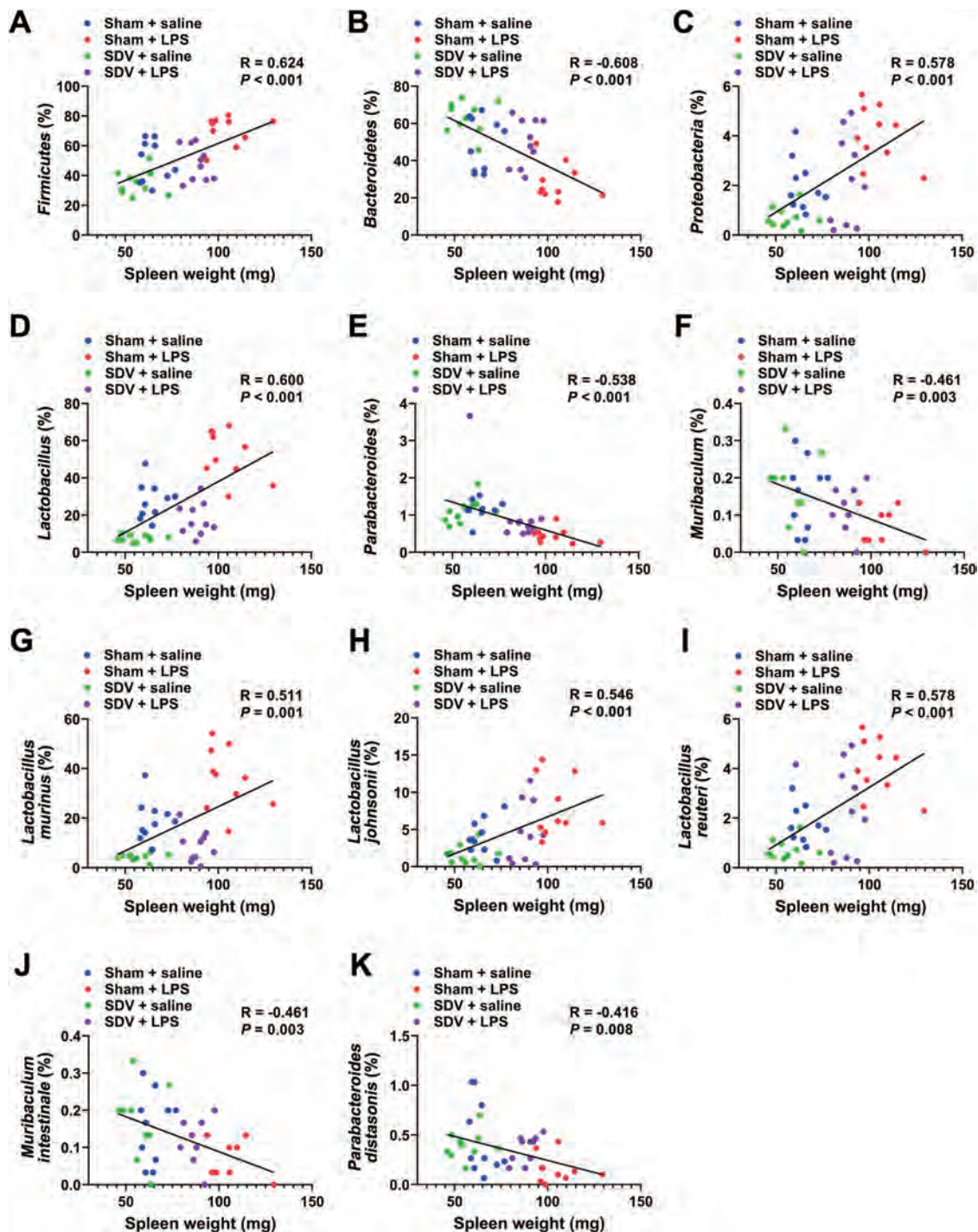
Fig. 7 Pearson correlation analysis of spleen weight and gut microbiota. There was a positive correlation between spleen weight and *Firmicutes* ($r = 0.624$, $P < 0.001$) (**a**), *Proteobacteria* ($r = 0.578$, $P < 0.001$) (**c**), *Lactobacillus* ($r = 0.600$, $P < 0.001$) (**d**), *Lactobacillus murinus* ($r = 0.511$, $P = 0.001$) (**g**), *Lactobacillus johnsonii* ($r = 0.546$, $P < 0.001$) (**h**), *Lactobacillus reuteri* ($r = 0.578$, $P < 0.001$) (**i**). There was a negative correlation between spleen weight and *Bacteroidetes* ($r = -0.608$, $P < 0.001$) (**b**), *Parabacteroides* ($r = -0.538$, $P < 0.001$) (**e**), *Muribaculum* ($r = -0.461$, $P = 0.003$) (**f**), *Muribaculum intestinale* ($r = -0.461$, $P = 0.003$) (**j**), *Parabacteroides distasonis* ($r = -0.416$, $P = 0.008$) (**k**).

increase in spleen weight. The results of the 16S rRNA analysis suggest that LPS caused significant changes in the diversity of the host gut microbiota in sham-operated mice, but not in SDV-operated mice. In an unweighted UniFrac PCoA, the dots representing the sham + LPS group were located far away from the dots representing the other three groups. Moreover, we found correlations between spleen weight and the abundance of the components of the microbiome, suggesting a relationship within the spleen–inflammation–microbiome axis. Taken together, our results indicate that LPS might produce a depression-like phenotype, increase spleen weight, trigger systemic inflammation, downregulate synaptic proteins in the mPFC, and cause abnormal composition of gut microbiota in mice through the brain–gut–microbiota axis and brain–spleen axis via the subdiaphragmatic vagus nerve.

Previous studies demonstrated that the ingestion of beneficial bacteria or selective serotonin reuptake inhibitors alleviated stress-induced anxiety and depression-like behaviors via the subdiaphragmatic vagus nerve, and that these antidepressant-like effects were abolished after SDV[46,50]. It was also reported that SDV blocked the depression-like phenotype after intraperitoneal injection of LPS (0.25 mg/kg) in rats[47], which is consistent with the present results. Here, we found that LPS produced a depression-like phenotype, an increase in plasma IL-6 and TNF-α levels, and downregulation of synaptic proteins in the mPFC in the sham-operated mice, in agreement with previous reports[20,21,23,25]. In contrast, LPS did not cause a depression-like phenotype or reduced synaptic proteins in the mPFC of the SDV-operated mice. Thus, the subdiaphragmatic vagus nerve seems to play a role in the depression-like phenotype and alteration of synaptic protein expression detected in LPS-treated mice. Although the detailed mechanisms underlying the depression-like phenotype of the sham-operated mice caused by LPS are currently unknown, this study suggests that the subdiaphragmatic vagus nerve is necessary for the LPS-induced depression-like phenotype and the downregulation of synaptic proteins in the mPFC. In contrast, it is well known that LPS-induced inflammation is a dynamic process, from induction to recovery[2]. A further detailed study of the effects of the subdiaphragmatic vagus nerve on the different stages of LPS-induced systemic inflammation and neuroinflammation is needed.

Recently, we reported that CSDS significantly increased the expression of IL-6 in the blood of water-treated mice, but not in that of antibiotic-treated mice, suggesting that antibiotic-induced microbiota depletion has anti-inflammatory effects[38]. Furthermore, CSDS significantly reduced the expression of the synaptic proteins in the PFC of the water-treated mice, but not of the antibiotic-treated mice. These data suggest that antibiotic-induced

depletion of gut bacteria leads to stress resilience in CSDS-exposed mice via the brain–gut–microbiota axis[38]. In this study, LPS caused a depression-like phenotype and an abnormality in gut microbiota composition through systemic inflammation in the sham-operated mice, whereas LPS did not cause these changes in SDV-operated mice. These data suggest that the brain–gut–microbiota axis via the subdiaphragmatic vagus nerve exerts effects on the development of the depression-like phenotype in LPS-treated mice, although the precise underlying mechanisms remain unclear. Further detailed studies are required to clarify the relationship between the brain–gut–microbiota axis via the subdiaphragmatic vagus nerve and inflammation-related behavioral abnormalities.

Recently, we observed marked increases in spleen weight in CSDS-susceptible mice compared with non-CSDS control mice and CSDS-resilient mice[26]. In addition, McKim et al.[51] reported that the total increase in the number of splenic erythrocytes, monocytes, and granulocytes derived from splenic progenitors that migrated from the bone marrow is associated with an increase of about twofold in the size and weight of the spleen after chronic stress. In this study, we also found that LPS caused an increase in spleen weight in the sham-operated mice, and that SDV significantly alleviated the LPS-induced increase in spleen weight. In addition, it has been reported that repeated LPS (0.1 mg/kg/day for 10 days) administration increased spleen weight in rats[52]. Interestingly, we found positive correlations between IL-6 (or TNF-α) and spleen weight, indicating a close relationship between peripheral inflammation and spleen weight. It is also known that LPS produces excessive lymphocyte proliferation and induces large-scale pro-inflammatory cytokine production, resulting in spleen enlargement. Given the role of the immune system in the pathogenesis of depression, these data suggest that the brain–spleen axis via the subdiaphragmatic vagus nerve may exert effects on the depression-like phenotype, increase in spleen weight, and inflammation in the periphery observed in the LPS-treated mice. Further detailed studies are required to confirm the relationship between the brain–spleen axis via the subdiaphragmatic vagus nerve and inflammation-related behavioral abnormalities.

Several routes, including the vagus nerve, the immune system, and the enteric nervous system, mediate the bidirectional communication between the brain and the gut microbiota[40–44]. In this study, we found that LPS did not produce a depression-like behavior or reduced synaptic protein expression in the mPFC in the vagotomized mice. We speculate that the dominant specific microorganisms present in the intestinal flora after LPS treatment may lead to the depression-like phenotype through the subdiaphragmatic vagus nerve system,

although further study is needed to confirm this hypothesis. The subdiaphragmatic vagus nerve may mediate the communication between the brain and the gut microbiota to exert beneficial or detrimental effects depending on the predominance of probiotic or pathogenic microorganisms present in the intestinal flora. Interestingly, transcutaneous auricular vagus nerve stimulation therapy is approved for patients with treatment-resistant depression[53–55], suggesting the anti-inflammatory properties of vagus nerve stimulation[56]. Taken together, these findings suggest that the vagus nerve plays a key role in depression, in the antidepressant actions of certain compounds, and in vagus nerve stimulation. Furthermore, it seems that the different branches of the vagus nerve play different roles under pathological conditions.

Recently, we reported that levels of colony stimulating factor 1 receptor (CSF1R) in the spleen, but not postmortem brain, from patients with depression were significantly lower than those of control groups, and that there was a negative correlation between CSF1R and interacting protein SPI1 in the spleen[57], suggesting a brain–spleen axis in psychiatric disorders such as depression[26,57,58]. A recent study demonstrated that neurons in the central nucleus of the amygdala and the paraventricular nucleus that express corticosterone-releasing hormone are connected to the splenic nerve, indicating a key role of brain–spleen communication in antibody production[59]. Collectively, it is likely that brain–spleen axis plays a key role in a number of disorders related with immune system.

In conclusion, the present study showed that LPS produced a depression-like phenotype and caused abnormal composition of gut microbiota in mice via the subdiaphragmatic vagus nerve. It is likely that both the brain–gut–microbiota axis and the brain–spleen axis via the subdiaphragmatic vagus nerve play an important role in the pathogenesis of inflammation-related depression. Future studies of the role of the subdiaphragmatic vagus nerve in the brain–gut–microbiota axis and the brain–spleen axis in other inflammatory-mediator-induced depression models or noninflammatory depression models (i.e., CSDS) are needed.

Conflict of interest
K.H. has received research support from Dainippon-Sumitomo, Otsuka, and Taisho. The other authors report no biomedical financial interests or potential conflicts of interest.

Publisher's note
Springer Nature remains neutral with regard to jurisdictional claims in published maps and institutional affiliations.

References
1. World Health Organization (WHO) Depression (2020). https://www.who.int/health-topics/depression#tab=tab_1
2. Dantzer, R., O'Connor, J. C., Freund, G. G., Johnson, R. W. & Kelly, K. W. From inflammation to sickness and depression: when the immune system subjugates the brain. *Nat. Rev. Neurosci.* **9**, 46–57 (2008).
3. Miller, A. H., Maletic, V. & Raison, C. L. Inflammation and its discontents: The role of cytokines in the pathophysiology of major depression. *Biol. Psychiatry* **65**, 732–741 (2009).
4. Raison, C. L., Lowry, C. A. & Rook, G. A. Inflammation, sanitation, and consternation: loss of contact with coevolved, tolerogenic microorganisms and the pathophysiology and treatment of major depression. *Arch. Gen. Psychiatry* **67**, 1211–1224 (2010).
5. Hashimoto, K. Inflammatory biomarkers as differential predictors of antidepressant response. *Int. J. Mol. Sci.* **16**, 7796–7801 (2015).
6. Mechawar, N. & Savitz, J. Neuropathology of mood disorders: do we see the stigmata of inflammation? *Transl. Psychiatry* **6**, e946 (2016).
7. Miller, A. H. & Raison, C. L. The role of inflammation in depression: from evolutionary imperative to modern treatment target. *Nat. Rev. Immunol.* **16**, 22–34 (2016).
8. Wohleb, E. S., Franklin, T., Iwata, M. & Duman, R. S. Integrating neuroimmune systems in the neurobiology of depression. *Nat. Rev. Neurosci.* **17**, 497–511 (2016).
9. Dowlati, Y. et al. A meta-analysis of cytokines in major depression. *Biol. Psychiatry* **67**, 446–457 (2010).
10. Strawbridge, R. et al. Inflammation and clinical response to treatment in depression: a meta-analysis. *Eur. Neuropsychopharmacol.* **25**, 1532–1543 (2015).
11. Goldsmith, D. R., Rapaport, M. H. & Miller, B. J. A meta-analysis of blood cytokine network alterations in psychiatric patients: comparisons between schizophrenia, bipolar disorder and depression. *Mol. Psychiatry* **21**, 1696–1709 (2016).
12. Köhler, C. A. et al. Peripheral cytokine and chemokine alterations in depression: a meta-analysis of 82 studies. *Acta Psychiatr. Scand.* **135**, 373–387 (2017).
13. Ng, A. et al. IL-1β, IL-6, TNF-α and CRP in elderly patients with depression or Alzheimer's disease: systematic review and meta-analysis. *Sci. Rep.* **8**, 12050 (2018).
14. Yuan, N., Chen, Y., Xia, Y., Dai, J. & Liu, C. Inflammation-related biomarkers in major psychiatric disorders: a cross-disorder assessment of reproducibility and specificity in 43 meta-analyses. *Transl. Psychiatry* **9**, 233 (2019).
15. Wang, L. et al. Effects of SSRIs on peripheral inflammatory markers in patients with major depressive disorder: a systematic review and meta-analysis. *Brain Behav. Immun.* **79**, 24–38 (2019).
16. Liu, J. J. et al. Peripheral cytokine levels and response to antidepressant treatment in depression: a systematic review and meta-analysis. *Mol. Psychiatry* **24**, 339–350 (2020).
17. Yang, C., Shirayama, Y., Zhang, J. C., Ren, Q. & Hashimoto, K. Peripheral interleukin-6 promotes resilience versus susceptibility to inescapable electric stress. *Acta Neuropsychiatr.* **27**, 312–316 (2015).
18. Zhang, J. C. et al. Blockade of interleukin-6 receptor in the periphery promotes rapid and sustained antidepressant actions: a possible role of gut-microbiota-brain axis. *Transl. Psychiatry* **7**, e1138 (2017).
19. O'Connor, J. C. et al. Lipopolysaccharide-induced depressive-like behavior is mediated by indoleamine 2,3-dioxygenase activation in mice. *Mol. Psychiatry* **14**, 511–522 (2009).
20. Ohgi, Y., Futamura, T., Kikuchi, T. & Hashimoto, K. Effects of antidepressants on alterations in serum cytokines and depressive-like behavior in mice after lipopolysaccharide administration. *Pharmacol. Biochem. Behav.* **103**, 856–859 (2013).
21. Zhang, J. C. et al. Antidepressant effects of TrkB ligands on depression-like behavior and dendritic changes in mice after inflammation. *Int. J. Neuropsychopharmacol.* **18**, pyu077 (2015).
22. Parrott, J. M. et al. Neurotoxic kynurenine metabolism is increased in the dorsal hippocampus and drives distinct depressive behaviors during inflammation. *Transl. Psychiatry* **6**, e918 (2016).
23. Zhang, J. C., Yao, W. & Hashimoto, K. Brain-derived neurotrophic factor (BDNF)-TrkB signaling in inflammation-related depression and potential therapeutic targets. *Curr. Neuropharmacol.* **14**, 721–731 (2016).

24. Ma, M. et al. Antidepressant effects of combination of brexpiprazole and fluoxetine on depression-like behavior and dendritic changes in mice after inflammation. *Psychopharmacology* **234**, 525–533 (2017).

25. Zhang, J. C. et al. Prophylactic effects of sulforaphane on depression-like behavior and dendritic changes in mice after inflammation. *J. Nutr. Biochem.* **39**, 134–144 (2017).

26. Zhang, K. et al. Splenic NKJG2D confers resilience versus susceptibility in mice after chronic social defeat stress: beneficial effects of (*R*)-ketamine. *Eur. Arch. Psychiatry Clin. Neurosci.* https://doi.org/10.1007/s00406-019-01092-z (2019).

27. Jiang, H. et al. Altered fecal microbiota composition in patients with major depressive disorder. *Brain Behav. Immun.* **48**, 186–194 (2015).

28. Zheng, P. et al. Gut microbiome remodeling induces depressive-like behaviors through a pathway mediated by the host's metabolism. *Mol. Psychiatry* **21**, 786–796 (2016).

29. Wong, M. L. et al. Inflammasome signaling affects anxiety- and depressive-like behavior and gut microbiome composition. *Mol. Psychiatry* **21**, 797–805 (2016).

30. Burokas, A. et al. Targeting the microbiota-gut-brain axis: prebiotics have anxiolytic and antidepressant-like effects and reverse the impact of chronic stress in mice. *Biol. Psychiatry* **82**, 472–487 (2017).

31. Yang, C. et al. *Bifidobacterium* in the gut microbiota confer resilience to chronic social defeat stress in mice. *Sci. Rep.* **7**, 45942 (2017).

32. Qu, Y. et al. Comparison of (*R*)-ketamine and lanicemine on depression-like phenotype and abnormal composition of gut microbiota in a social defeat stress model. *Sci. Rep.* **7**, 15725 (2017).

33. Yang, C. et al. Possible role of the gut microbiota-brain axis in the anti-depressant effects of (*R*)-ketamine in a social defeat stress model. *Transl. Psychiatry* **7**, 1294 (2017).

34. Luo, Y. et al. Gut microbiota regulates mouse behaviors through glucocorti-coid receptor pathway genes in the hippocampus. *Transl. Psychiatry* **8**, 187 (2018).

35. Huang, N. et al. Role of *Actinobacteria* and *Coriobacteriia* in the antidepressant effects of ketamine in an inflammation model of depression. *Pharmacol. Biochem. Behav.* **176**, 93–100 (2019).

36. Yang, C. et al. Key role of gut microbiota in anhedonia-like phenotype in rodents with neuropathic pain. *Transl. Psychiatry* **9**, 57 (2019).

37. Zhang, K. et al. Abnormal composition of gut microbiota is associated with resilience versus susceptibility to inescapable electric stress. *Transl. Psychiatry* **9**, 231 (2019).

38. Wang, S. et al. Antibiotic-induced microbiome depletion is associated with resilience in mice after chronic social defeat stress. *J. Affect. Disord.* **260**, 448–457 (2020).

39. Capuco, A. et al. Current perspectives on gut microbiome dysbiosis and depression. *Adv. Ther.* **37**, 1328–1346 (2020).

40. Forsythe, P., Bienenstock, J. & Kunze, W. A. Vagal pathway for microbiome-brain-gut axis communication. *Adv. Exp. Med. Biol.* **817**, 115–133 (2014).

41. Bonaz, B., Bazin, T. & Pellissier, S. The vagus nerve at the interface of the microbiota-gut-brain axis. *Front. Neurosci.* **12**, 49 (2018).

42. Cawthon, C. R. & de La Serre, C. B. Gut bacteria interaction with vagal afferents. *Brain Res.* **1693**(Pt B), 134–139 (2018).

43. Cryan, J. F. et al. The microbiota-gut-brain axis. *Physiol. Rev.* **99**, 1877–2013 (2019).

44. Long-Smith, C. et al. Microbiota-gut-brain axis: new therapeutic opportunities. *Annu. Rev. Pharmacol. Toxicol.* **60**, 477–502 (2020).

45. Bharwani, A. et al. The vagus nerve is necessary for the rapid and widespread neuronal activation in the brain following oral administration of psychoactive bacteria. *Neuropharmacology* **170**, 108067 (2020).

46. Bravo, J. A. et al. Ingestion of Lactobacillus strain regulates emotional behavior and central GABA receptor expression in a mouse via the vagus nerve. *Proc. Natl Acad. Sci. USA* **108**, 16050–16055 (2011).

47. Konsman, J. P., Luheshi, G. N., Bluthé, R. M. & Dantzer, R. The vagus nerve mediates behavioural depression, but not fever, in response to peripheral immune signals; a functional anatomical analysis. *Eur. J. Neurosci.* **12**, 4434–4446 (2000).

48. Zhang, J. et al. Beneficial effects of anti-RANKL antibody in depression-like phenotype, inflammatory bone markers, and bone mineral density in male susceptible mice after chronic social defeat stress. *Behav. Brain Res.* **379**, 112397 (2020).

49. Pu, Y. et al. Antibiotic-induced microbiome depletion protects against MPTP-induced dopaminergic neurotoxicity in the brain. *Aging* **11**, 6915–6929 (2019).

50. McVey Neufeld, K. A. et al. Oral selective serotonin reuptake inhibitors activate vagus nerve dependent gut-brain signalling. *Sci. Rep.* **9**, 14290 (2019).

51. McKim, D. B. et al. Social stress mobilizes hematopoietic stem cells to establish persistent splenic myelopoiesis. *Cell Rep.* **25**, 2552–2562 (2018).

52. Zhong, Y., Zhang, X., Hu, X. & Li, Y. Effects of repeated lipopolysaccharide treatment on growth performance, immune organ index, and blood para-meters of Sprague-Dawley rats. *J. Vet. Res.* **62**, 341–346 (2018).

53. Bottomley, J. M., LeReun, C., Diamantopoulous, A., Mitchell, S. & Gaynes, B. N. Vagus nerve stimulation (VNS) therapy in patients with treatment resistant depression: a systematic review and meta-analysis. *Compr. Psychiatry* **98**, 152156 (2019).

54. Lv, H., Zhao, Y. H., Chen, J. G., Wang, D. Y. & Chen, H. Vagus nerve stimulation for depression: a systematic review. *Front. Psychol.* **10**, 64 (2019).

55. Liu, C. H. et al. Neural networks and the anti-inflammatory effect of transcu-taneous auricular vagus nerve stimulation in depression. *J. Neuroinflamm.* **17**, 54 (2020).

56. Bonaz, B., Sinniger, V. & Pellissier, S. Anti-inflammatory properties of the vagus nerve: potential therapeutic implications of vagus nerve stimulation. *J. Physiol.* **594**, 5781–5790 (2016).

57. Zhang, J., Chang, L., Pu, Y. & Hashimoto, K. Abnormal expression of colony stimulating factor 1 receptor (CSF1R) and transcription factor PU.1 (SPI1) in the spleen from patients with major psychiatric disorders: a role of brain-spleen axis. *J. Affect. Disord.* **272**, 110–115 (2020).

58. Yang, B., Ren, Q., Zhang, J. C., Chen, Q. X. & Hashimoto, K. Altered expression of BDNF, BDNF pro-peptide and their precursor proBDNF in brain and liver tissues from psychiatric disorders: rethinking the brain-liver axis. *Transl. Psychiatry* **7**, e1128 (2017).

59. Zhang, X. et al. Brain control of humoral immune responses amenable to behavioral modulation. *Nature* **581**, 204–208 (2020).
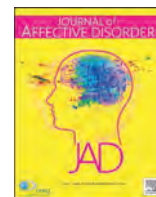
Research paper

Betaine supplementation is associated with the resilience in mice after chronic social defeat stress: a role of brain–gut–microbiota axis

Youge Qu[a], Kai Zhang[a], Yaoyu Pu[a], Lijia Chang[a], Siming Wang[a], Yunfei Tan[a], Xingming Wang[a], Jiancheng Zhang[a], Tetsuo Ohnishi[b], Takeo Yoshikawa[b], Kenji Hashimoto[a],*

[a] *Division of Clinical Neuroscience, Chiba University Center for Forensic Mental Health, Chiba 260-8670, Japan*
[b] *Laboratory for Molecular Psychiatry, RIKEN Center for Brain Science, Saitama 351-0198, Japan*

A R T I C L E   I N F O

A B S T R A C T

Background: The brain–gut–microbiota axis plays a role in the pathogenesis of stress-related psychiatric disorders; however, its role in the resilience versus susceptibility after stress remains unclear. Dietary nutrient betaine is suggested to affect the gut microbiome. Here, we examined whether betaine supplementation can affect anhedonia-like phenotype in mice subjected to chronic social defeat stress (CSDS).

Methods: CSDS was performed during betaine supplementation. Sucrose preference test and 16S rRNA analysis of fecal samples were performed.

Results: CSDS did not produce an anhedonia-like phenotype in the betaine-treated mice, but did induce an anhedonia-like phenotype in water-treated mice. Furthermore, CSDS treatment did not alter the plasma levels of interleukin-6 (IL-6) of betaine-treated mice whereas CSDS caused higher plasma levels of IL-6 in water-treated mice. Betaine supplementation ameliorated the abnormal diversity and composition of the microbiota in the host gut after CSDS. At the genus level, CSDS caused marked increases in the several bacteria of water-treated mice, but not betaine-treated mice. CSDS increased levels of short-chain fatty acids (i.e., succinic acid and acetic acid) in feces from water-treated mice, but not betaine-treated mice. Interestingly, there are positive correlations between short-chain fatty acids (i.e., succinic acid, acetic acid, butyric acid) and several bacteria among the groups.

Limitations: Specific microbiome were not determined.

Conclusions: These findings suggest that betaine supplementation contributed to resilience to anhedonia in mice subjected to CSDS through anti-inflammation action. Therefore, it is likely that betaine could be a prophylactic nutrient to prevent stress-related psychiatric disorders.

1. Introduction

Humans display a wide physiological variability in their response to stressor after exposures to psychological stress (Beery et al., 2015). Resilience is mediated by adaptive changes in several neural circuits, including numerous neurotransmitters and molecular pathways (Franklin et al., 2012; Russo et al., 2012; Russo and Nestler, 2013). However, the precise underlying mechanisms of resilience in stress-related psychiatric disorders remain to be elucidated.

Brain–gut–microbiome axis consists of bidirectional communication between the gut and brain. Accumulating evidence suggests that brain–gut–microbiome axis plays a role in the pathogenesis of a number of stress-related psychiatric disorders (Cussotto et al., 2018; Dinan et al., 2017; Forsythe et al., 2016; Fung et al., 2017; Kelly et al.,

2016; Ma et al., 2019; Mayer et al., 2015; Molina-Torres et al., 2019). Interestingly, gut microbiota may contribute to resilience versus susceptibility to anhedonia in rodents after repeated stress (Bailey et al., 2011; Hao et al., 2019; Szyszkowicz et al., 2017; Yang et al., 2017; Yang et al., 2019). Previously, we reported higher levels of *Bifidobacterium* in resilient mice compared with susceptible mice after chronic social defeat stress (CSDS), and supplementation with *Bifidobacterium* produced resilience in mice after CSDS, suggesting a possible role for *Bifidobacterium* in stress resilience (Yang et al., 2017). It is reported that specific clusters of bacterial communities in the cecum may be linked to vulnerability to CSDS (Szyszkowicz et al., 2017).

Dietary nutrients are essential not only for human health but also for the health and survival of the trillions of microbiomes that reside within the human intestines (Gentile et al., 2018). Betaine

---

(trimethylglycine) is distributed widely in animals, plants, microorganisms, and rich dietary sources (Craig, 2004). The principal physiological role of betaine is as an osmolyte and methyl donor. As an osmolyte, betaine protects cells, proteins, and enzymes from environmental stress. As a methyl donor, betaine plays a role in the methionine cycle. For example, higher intakes of betaine have been shown to be associated with lower plasma levels of homocysteine (the putative risk factor for cardiovascular disease)(Rajaie et al., 2011). Accumulating evidence has shown that betaine has anti-inflammatory functions in numerous diseases (Zhao et al., 2018a), and that betaine is an important nutrient for the prevention of chronic diseases (Cholewa et al., 2014; Craig, 2004; Fillipcev et al., 2018; Rajaie et al., 2011).

Furthermore, Koike et al. (2014) reported decreased plasma levels of betaine in first-episode patients with schizophrenia. Very recently, it is demonstrated that betaine supplementation could block methamphetamine-induced behavioral sensitization, and phencyclidine-induced cognitive deficits in mice (Ohnishi et al., 2019), suggesting the role of betaine in schizophrenia. Clinical trial of betaine in schizophrenia is underway at the University of Tokyo Hospital (UMIN000017295). Collectively, it is likely that betaine supplementation may have prophylactic effects for psychiatric disorders (Ohnishi et al., 2019). However, there are no reports showing the effect of betaine supplementation in resilience versus susceptibility after chronic stress.

Anhedonia (loss of pleasure) is a core symptom of stress-related disorders, although the neurobiological mechanisms of anhedonia remain poorly understood (Pizzagalli, 2014; Treadway et al., 2011). Therefore, we hypothesized that betaine supplementation may affect the resilience of mice with anhedonia-like phenotype after CSDS. The present study was undertaken to examine whether betaine supplementation contributes to resilience and susceptibility in mice after CSDS. Furthermore, we examined the role of brain–gut axis in the stress resilience by betaine supplementation since betaine is shown to alter gut microbiota in rodents (Wang et al., 2018).

2. Materials and methods

2.1. Animals

Male adult C57BL/6 mice, aged 8 weeks (body weight 20–25g, Japan SLC, Inc., Hamamatsu, Japan) and male adult CD1 (ICR) mice, aged 13–15 weeks (body weight >40g, Japan SLC, Inc., Hamamatsu, Japan) were used. Animals were housed under controlled temperatures and 12 hour light/dark cycles (lights on between 07:00–19:00 h), with ad libitum food (CE-2; CLEA Japan, Inc., Tokyo, Japan) and water. The study was approved by the Chiba University Institutional Animal Care and Use Committee (Permission number: 31-141). This study was carried out in strict accordance with the recommendations in the Guide for the Care and Use of Laboratory Animals of the National Institutes of Health. All efforts were made to minimize suffering.

2.2. Betaine supplementation, collection of fecal samples, and CSDS

As previously reported (Ohnishi et al., 2019), betaine (Nacalai Tesque, Inc., Kyoto, Japan. 2.5% as monohydrate in drinking water) or water was given to mice for 24 days from day 1 to day 24 (**Fig. 1**A). CSDS was performed for 10 days from day 15 to day 24 (**Fig. 1**A). The procedure of CSDS was performed as previously reported (Golden et al., 2011; Ren et al., 2016; Yang et al., 2015; Yang et al., 2018; Wang et al., 2020; Zhang et al., 2020). Every day the C57BL/6 mice were exposed to a different CD1 aggressor mouse for 10 min, total for 10 days (day 15 – day 24). When the social defeat session ended, the resident CD1 mouse and the intruder mouse were housed in one half of the cage separated by a perforated Plexiglas divider to allow visual, olfactory, and auditory contact for the remainder of the 24-h period. At 24 h after the last session, all mice were housed individually. On day 25, we collected fecal samples from each mouse at around 10:00 in order to avoid

circadian effects on the microbiome. We also collected fecal samples when each mouse was placed in a new, clean cage. The fecal samples were put into a sterilized screw cap microtube immediately after defecation, and these samples were stored at -80°C until use.

On day 26, sucrose preference test (SPT: one % sucrose and water) was performed from 17:00 to 18:00, to identify anhedonia-like phenotypes. Mice were exposed to water and 1% sucrose solution for 48 h, followed by 4 h of water and food deprivation and a 1-h exposure to two identical bottles containing either water or a 1% sucrose solution. The bottles containing water and sucrose were weighed before and at the end of this period. The sucrose preference was calculated as the ratio of sucrose solution consumption to total liquid consumption.

2.3. ELISA measurement of pro-inflammatory cytokine IL-6

Plasma levels of interleukin-6 (IL-6) were measured, because we previously found an increase in blood IL-6 in the CSDS model (Zhang et al., 2017). The plasma IL-6 levels were measured using the ELISA kit (Invitrogen, cat#: 88-7064-22) according to the manufacturer's instructions.

2.4. 16S rRNA analysis

The 16S rRNA analysis of fecal samples was performed by the TechnoSuruga Laboratory, Co., Ltd. (Shizuoka, Japan). DNA extraction and 16S rRNA analysis were performed as previously described method (Zhang et al., 2019). The fecal samples were suspended in a buffer containing 4M guanidium thiocyanate, 100 mM Tris-HCl (pH 9.0) and 40 mM EDTA and broken up in the presence of zirconia beads using the FastPrep-24 5G homogenizer (MP Biomedicals, Irvine, CA). Thereafter, the DNA was extracted from the bead-treated suspension using GENE PREP STAR PI-480 (KURABO, Japan). The final concentration of the DNA sample was adjusted to 10 ng/μL. Briefly, the V3-V4 hypervariable regions of the 16S rRNA were amplified from microbial genomic DNA using PCR with the bacterial universal primers (341F/R806) and the dual-index method. Bioinformatics analysis was performed according to a previously described method. The overlapping paired-end reads were merged using the fastq-join program with default settings. The reads were processed for quality and chimera filtering as follows. Only reads with quality value scores of 20 for >99% of the sequence were extracted, and chimeric sequences were removed using the program usearch6.1. Non-chimeric reads were submitted for 16S rDNA-based taxonomic analysis using the Ribosomal Database Project (RDP) Multiclassifier tool. Reads obtained in the Multi-FASTA format were assigned to genus or phylum levels with an 80% confidence threshold. Principal component analysis (PCoA) was performed using Metagenome@KIN software (World Fusion Co., Ltd., Tokyo, Japan) based on data obtained from the bacterial family using the RDP taxonomic analysis software.

2.5. Measurement of fecal short-chain fatty acids

Measurement of short-chain fatty acids (acetic acid, propionic acid, butyric acid, lactic acid, and succinic acid) in fecal samples was performed by the TechnoSuruga Laboratory, Co., Ltd. (Shizuoka, Japan), as previously reported (Zhang et al., 2019). For the determination of organic acids, feces were suspended in distilled water, heated at 85°C for 15 minutes to inactivate viruses, and then centrifuged according to previously reported methods. The concentrations of short-chain fatty acids in feces were measured using a high-performance liquid chromatography organic acid analysis system with a Prominence CDD-10A conductivity detector (Shimadzu, Kyoto, Japan), two tandemly arranged Shim-pack SCR-102(H) columns [300 mm × 8 mm inner diameter (ID)], and a Shim-pack SCR-102(H) guard column (50 mm × 6 mm ID). The HPLC calibration curves for the measurement of these acids were created using prepared standard solutions.
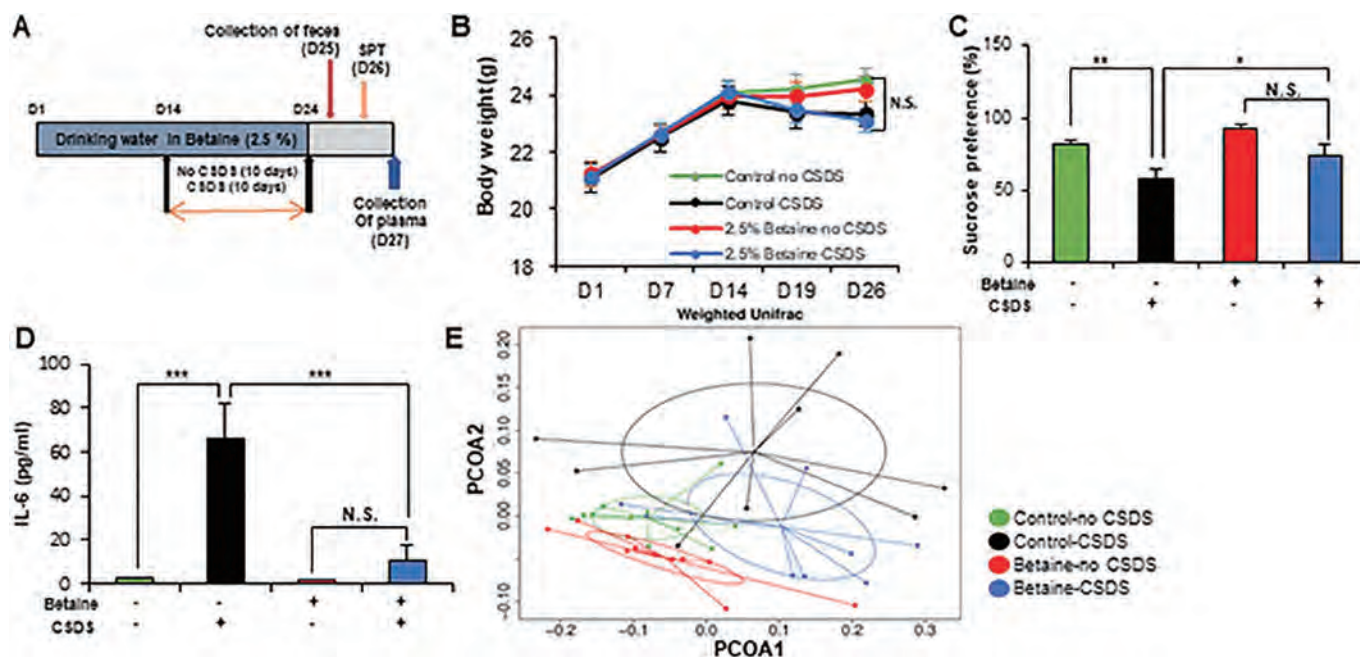
Figure 1. Effects of betaine supplementation. (A): The schedule of drinking water in betaine, feces collection, sucrose preference test, and collection of plasma. Drinking water including betaine or water was given to adult mice from day 1 to day 24. CSDS was performed from day 15 to day 24 for 10 days. On day 25, feces were collected. On day 26, one % SPT was performed, and plasma was collected on day 27. (B): Body weight (repeated two-way ANOVA, betaine: $F_{1,36} = 0.003$, $P = 0.995$, CSDS: $F_{1,36} = 0.953$, $P = 0.335$, interaction: $F_{1,36} = 0.061$, $P = 0.806$). (C): One % SPT (two-way ANOVA, betaine: $F_{1,36} = 4.949$, $P = 0.032$, CSDS: $F_{1,36} = 14.877$, $P < 0.001$, interaction: $F_{1,36} = 2.205$, $P = 0.146$). (D): Plasma IL-6. Data are shown as mean ± S.E.M (two-way ANOVA, betaine: $F_{1,36} = 14.371$, $P < 0.001$, CSDS: $F_{1,36} = 24.084$, $P < 0.001$, interaction: $F_{1,36} = 14.050$, $P < 0.001$). (n = 9-11). *$P < 0.05$, **$P < 0.01$, ***$P < 0.001$. NS: not significant. (E): Principal coordinates analysis (PCA). PCOA1: $P = 0.026$. PCOA2: $P = 0.001$.

2.6. Statistical Analysis

The data are shown as the mean ± standard error of the mean (S.E.M.). Analysis was performed by using PASW Statistics 20 (formerly SPSS statistics; SPSS, Tokyo, Japan). Comparisons between groups were performed by one-way or two-way analysis of variance (ANOVA), followed by *post-hoc* Fisher's Least Significant Difference (LSD) test. The *P* < 0.05 was considered statistically significant.

3. Results

3.1. Effects of CSDS on body weight, anhedonia-like phenotype, and plasma IL-6

There were no changes of body weight among the four groups (**Fig. 1B**). In SPT, CSDS caused significant reduction in sucrose preference in the water-treated group, but not in the betaine-treated group (**Fig. 1C**). There was no significant difference between the betaine-treated non-CSDS group and the betaine-treated CSDS group (**Fig. 1C**). Furthermore, CSDS significantly increased plasma levels of IL-6 in the water-treated group, whereas CSDS did not alter plasma IL-6 levels in the betaine-treated group (**Fig. 1D**). Overall, the betaine-treated group appeared to be protected against the CSDS-induced anhedonia-like phenotype, and inflammation.

3.2. Altered composition in gut bacteria

Analysis of 16S rRNA was used to identify differences in the composition of gut microbiota among the four groups. The UniFrac-based PCoA showed significant differences among the four groups. CSDS caused the abnormality of diversity of microbiota in mice, and betaine supplementation attenuated the abnormal diversity of microbiota after CSDS (**Fig. 1E**).

The phylum level composition of gut bacterium was identified (**Fig. 2A**). *Firmicutes* and *Bacteroidetes* were the most abundant phyla in the water-treated group (**Fig. 2A**). At the phylum level, CSDS significantly increased *Deferribacteres* in the water-treated group, but not the betaine-treated group (**Fig. 2B**).

The class level composition of gut bacterium was identified (**Fig. 3A**). *Bacteroidetes* and *Firmicutes* were the most abundant phyla in the water-treated group (**Fig. 3A**). At the class level, CSDS significantly increased *Clostridia, Erysipelotrichia, Negativicutes, Chloroplast* in the water-treated group, but not the betaine-treated group (**Fig. 3B-3E**).

The order level composition of gut bacterium was identified (**Fig. 4A**). At the order level, CSDS significantly increased *Clostridiales, Erysipelotrichales, Bacillales, Selenomonadales,* and *Chloroplast* in the water-treated group, but not the betaine-treated group (**Fig. 4B-4F**). The family level composition of gut bacterium was identified (**Fig. 5A**). At the family level, CSDS significantly increased *Lachnospiraceae, Erysipelotrichaceae,* and *Clostridiales_Incertae Sedis XIII* in the water-treated group, but not the betaine-treated group (**Fig. 5B, 5E, 5F**). Furthermore, CSDS significantly increased *Ruminococcaceae,* and *Rikenellaceae* in the water-treated group and the betaine-treated group although effect of CSDS in the betaine-treated group was less potent than water-treated group (**Fig. 5B, 5C**).

At the genus level, CSDS significantly increased *Clostridium XIVa, Coprococcus, Clostridium IV, Ruminococcus2, Pseudoflavonifractor,* and *Erysipelotrichaceae_incertae_sedis* in the water-treated group, but not the betaine-treated group (**Fig. 6A,6B,6D,6E,6F,6G,6H**) Furthermore, CSDS significantly increased *Alistipes* in the water-treated group and the betaine-treated group although effect of CSDS in the betaine-treated group was less potent than water-treated group (**Fig. 6C**).

3.3. Short-chain fatty acids in fecal samples

CSDS significantly increased levels of succinic acid and acetic acid in the water-treated group, but not betaine-treated group (**Fig. 7A,7B**). Furthermore, CSDS significantly increased butyric acid in the water-
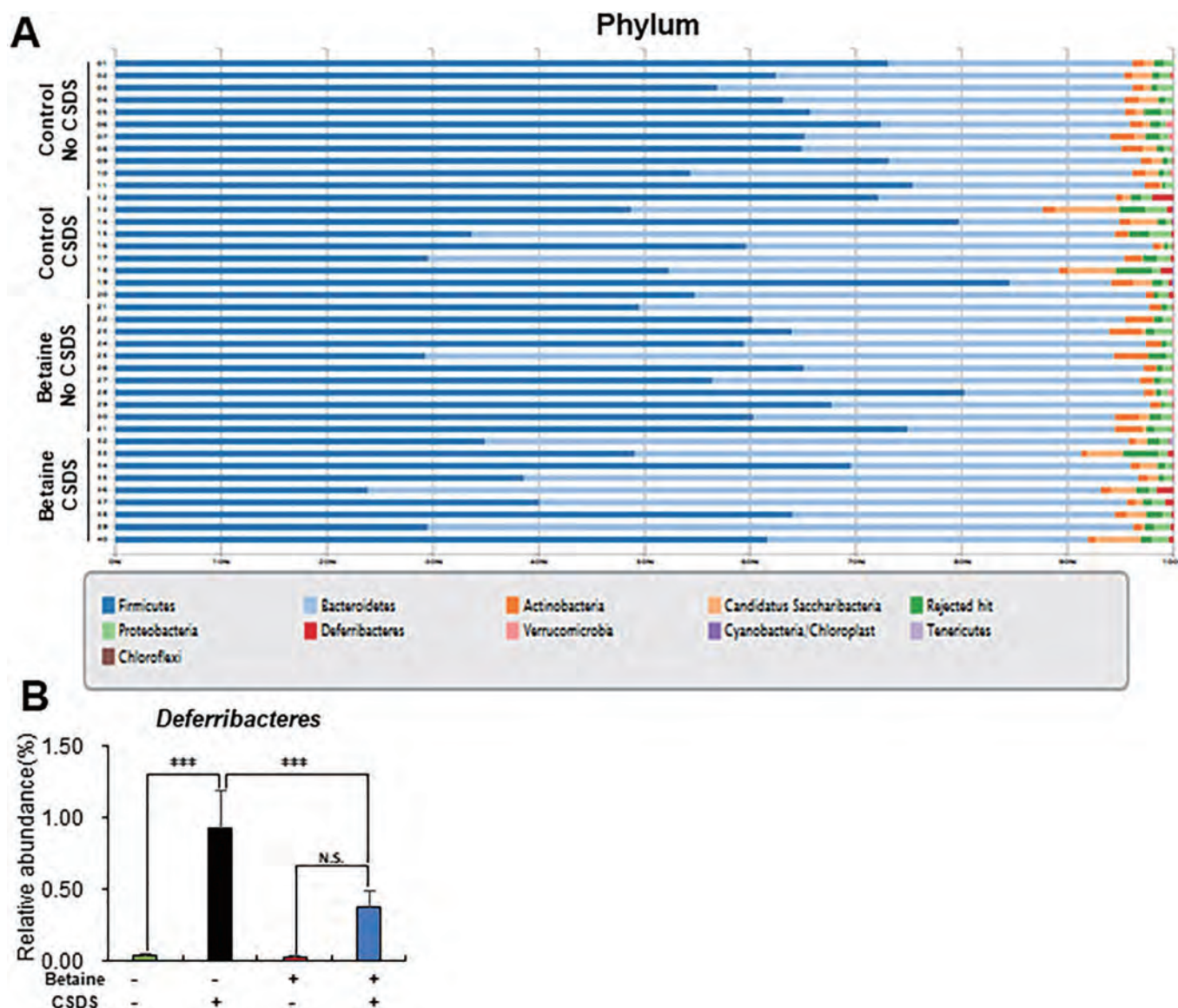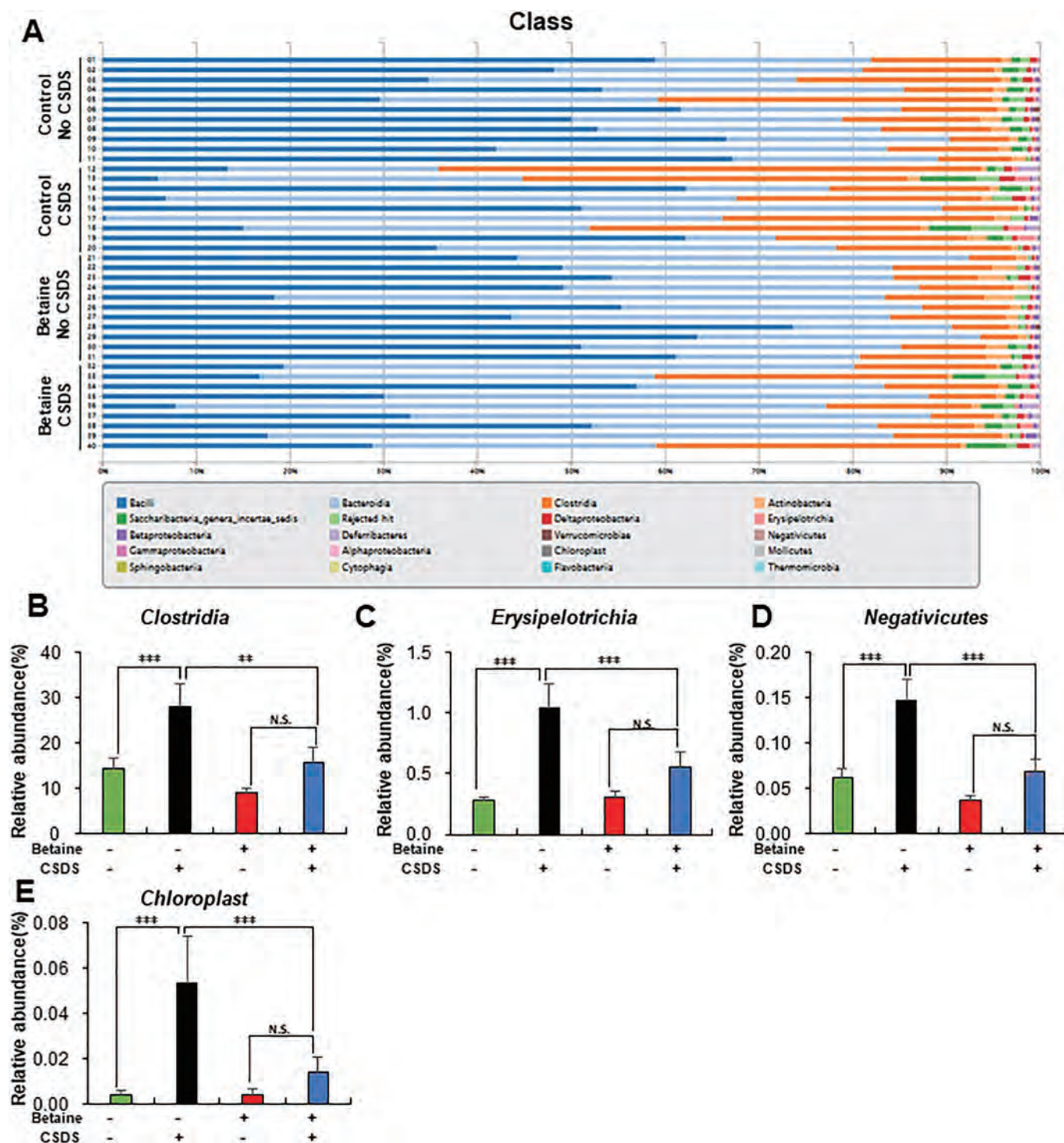
Figure 2. Altered composition in the gut bacteria at the levels of phylum. (A): The relative abundances of microbiome at phylum level in fecal samples of the four groups. (B): *Deferribacteres* (two-way ANOVA, betaine: $F_{1,36} = 0.269$, P = 0.607, CSDS: $F_{1,36} = 13.719$, P < 0.001, interaction: $F_{1,36} = 0.232$, P = 0.633). Data are shown as mean ± S.E.M. (n = 9-11). ***P < 0.001. NS: not significant.

treated group and the betaine-treated group although effect of CSDS in the betaine-treated group was less potent than water-treated group (**Fig. 7**E). Moreover, CSDS significantly decreased levels of propionic acid in the water-treated group, but not betaine-treated group (**Fig. 7**D). There were no changes in lactic acid among the four groups (**Fig. 7**C).

There were positive correlations between succinic acid (or acetic acid) and *Alistipes* levels among four groups (**Fig. 7**F, **7**G). There were also positive correlations between butyric acid and *Clostridium XIVa* (or *Clostridium IV*) levels among four groups (**Fig. 7**H, **7**I). There were no correlations between other short-chain fatty acids and the microbiome composition among the four experimental groups.

4. Discussion

The major findings of this study are as follows. Betaine supplementation did not cause anhedonia-like phenotype and blood inflammation in mice after CSDS although CSDS caused anhedonia-like phenotype and blood inflammation in water-treated group. Betaine supplementation ameliorated the marked alterations in the diversity of

microbiota in the host gut after CSDS. At the several levels, CSDS showed marked alterations in the several bacteria in host gut. At the genus levels, CSDS showed marked increases in several bacteria (*Clostridium XIVa, Alistipes, Coprococcus, Clostridium IV, Ruminococcus2, Pseudoflavonifractor, Erysipelotrichaceae*) in water-treated group, but not betaine-treated group. Interestingly, CSDS caused alterations in fecal levels of short-chain organic acids in water-treated group, but not betaine-treated group. In addition, there were positive correlation between some organic acids and bacteria among the four groups. Overall, betaine supplementation might be associated with the resilience after CSDS through anti-inflammation effects.

In this study, we found that CSDS decreased the sucrose preference of SPT in the water-treated group, although CSDS did not decrease the sucrose preference of SPT in the betaine-treated group. CSDS also significantly increased the plasma levels of IL-6 in the water-treated group, but not in the betaine-treated group, suggesting anti-inflammatory effects in betaine-treated group. It has been reported that CSDS resilient mice had lower blood levels of IL-6 than CSDS susceptible mice in response to acute stress (Hodes et al., 2014). Recently, Zhao et al. (2018b) demonstrated that maternal betaine supplementation attenuated

Figure 3. Altered composition in the gut bacteria at the levels of class. (A): The relative abundances of microbiome at class level in fecal samples of the four groups. (B): *Clostridia* (two-way ANOVA, betaine: $F_{1,36} = 8.505$, $P = 0.006$, CSDS: $F_{1,36} = 11.4417$, $P = 0.002$ interaction: $F_{1,36} = 1.319$, $P = 0.258$). (C): *Erysipelotrichia* (two-way ANOVA, betaine: $F_{1,36} = 4.742$, $P = 0.036$, CSDS: $F_{1,36} = 22.478$, $P < 0.001$, interaction: $F_{1,36} = 5.929$, $P = 0.020$). (D): *Negativicutes* (two-way ANOVA, betaine: $F_{1,36} = 13.474$, $P < 0.001$, CSDS: $F_{1,36} = 17.240$, $P < 0.001$, interaction: $F_{1,36} = 4.057$, $P = 0.052$). (E): *Chloroplast* (two-way ANOVA, betaine: $F_{1,36} = 3.858$, $P = 0.057$, CSDS: $F_{1,36} = 9.338$, $P = 0.004$, interaction: $F_{1,36} = 3.858$, $P = 0.057$). Data are shown as mean ± S.E.M. (n = 9-11). **$P < 0.01$, ***$P < 0.001$. NS: not significant.

glucocorticoid-induced hepatic lipid accumulation through epigenetic modulation in adult offspring. In addition, mechanistically, betaine is shown to ameliorate sulfur amino acid metabolism against oxidative stress. Betaine inhibits nuclear factor–κB activity and NLRP3 in-flammasome activation (Zhao et al., 2018a). It is also suggested that betaine has anti-inflammatory effects in several models such as

oxidative stress, endoplasmic reticulum stress and chronic inflamma-tion (Zhao et al., 2018a). A recent study showed that betaine exerts protective effects on diabetes-induced blood-testis barrier dysfunction by regulating oxidative stress-mediated p38 MAPK pathways (Jiang et al., 2019). Furthermore, it is suggested that betaine/GABA transporter-1 (GAT2/BGT-1) plays a role in the beneficial effects of
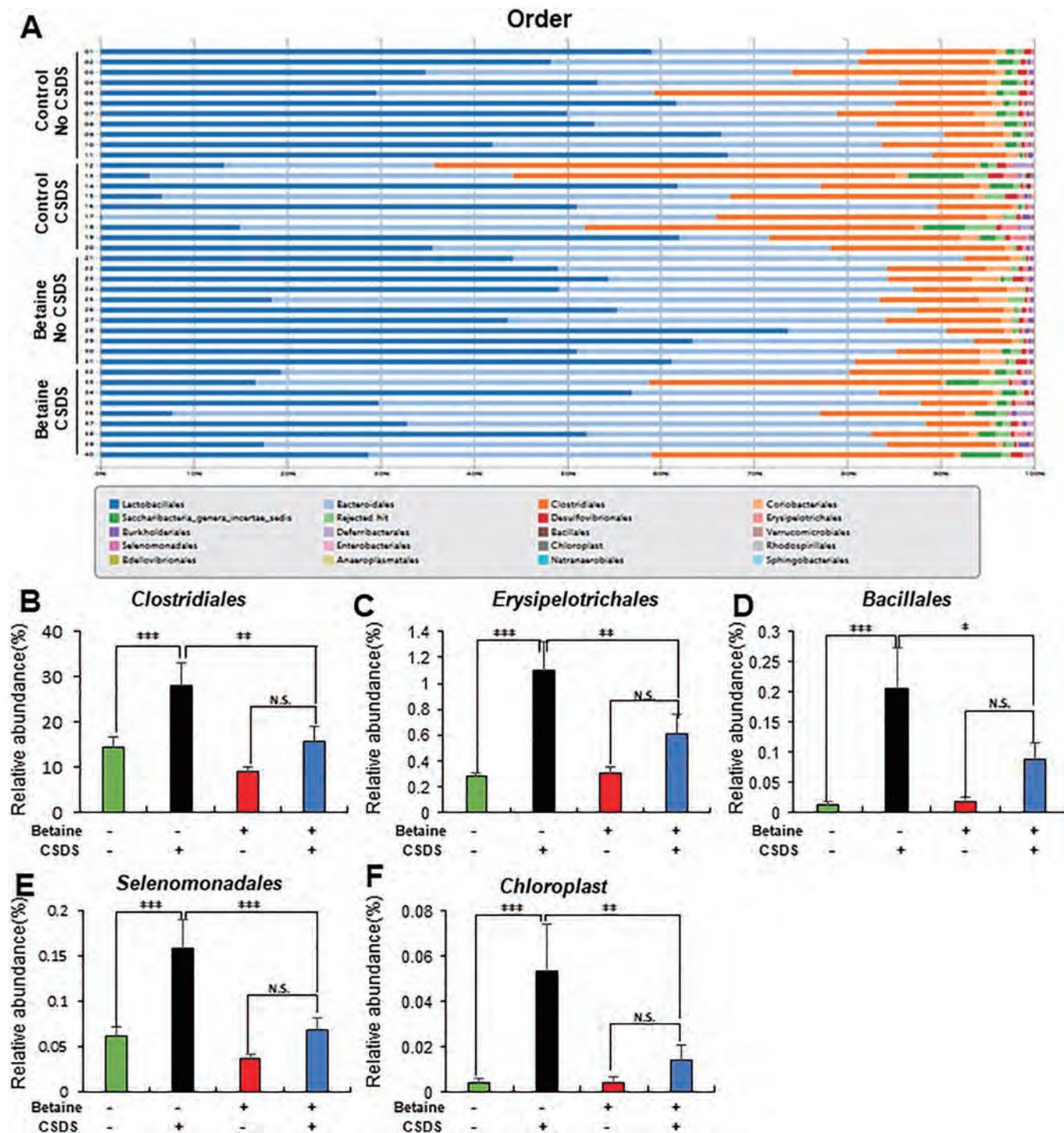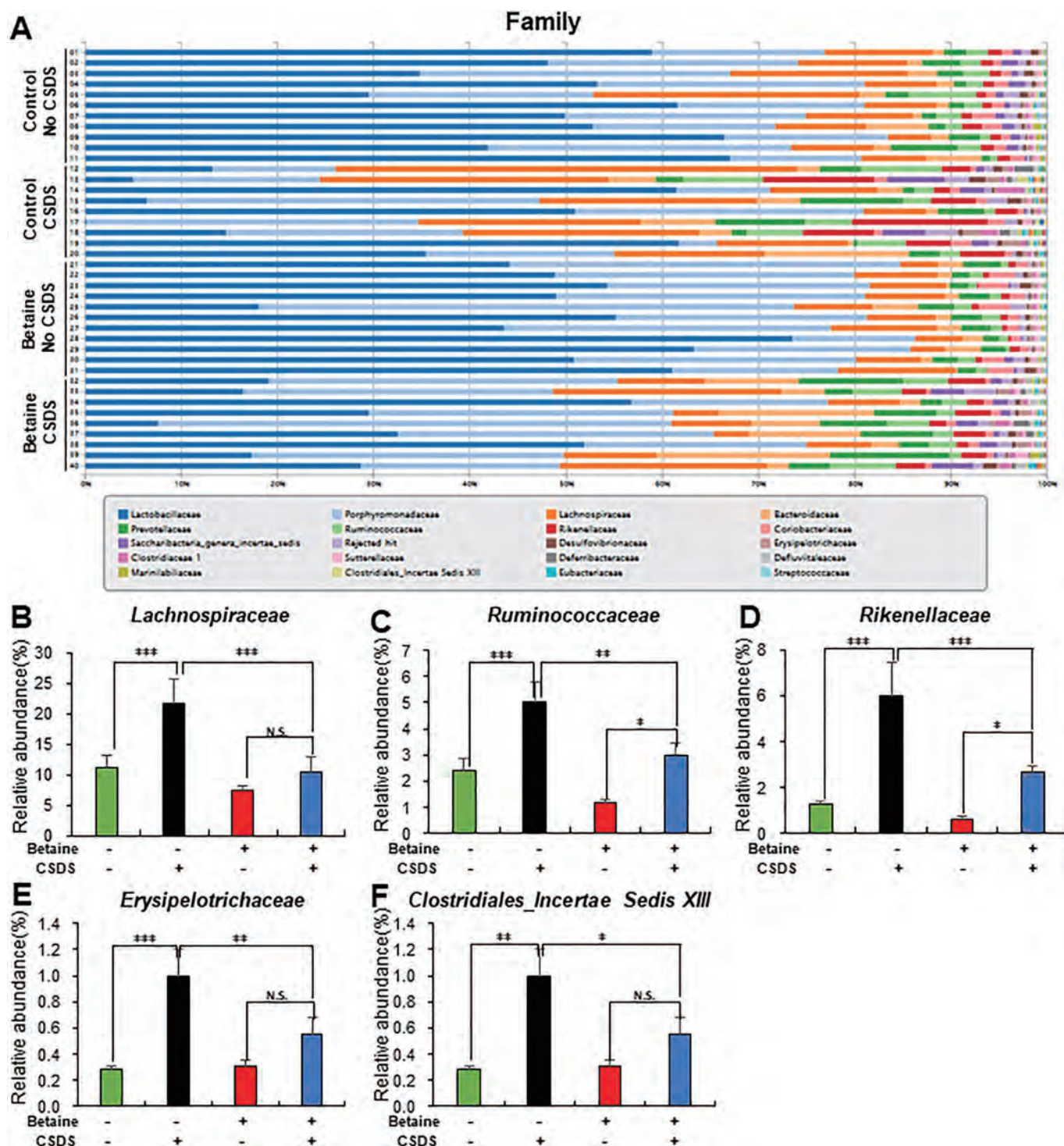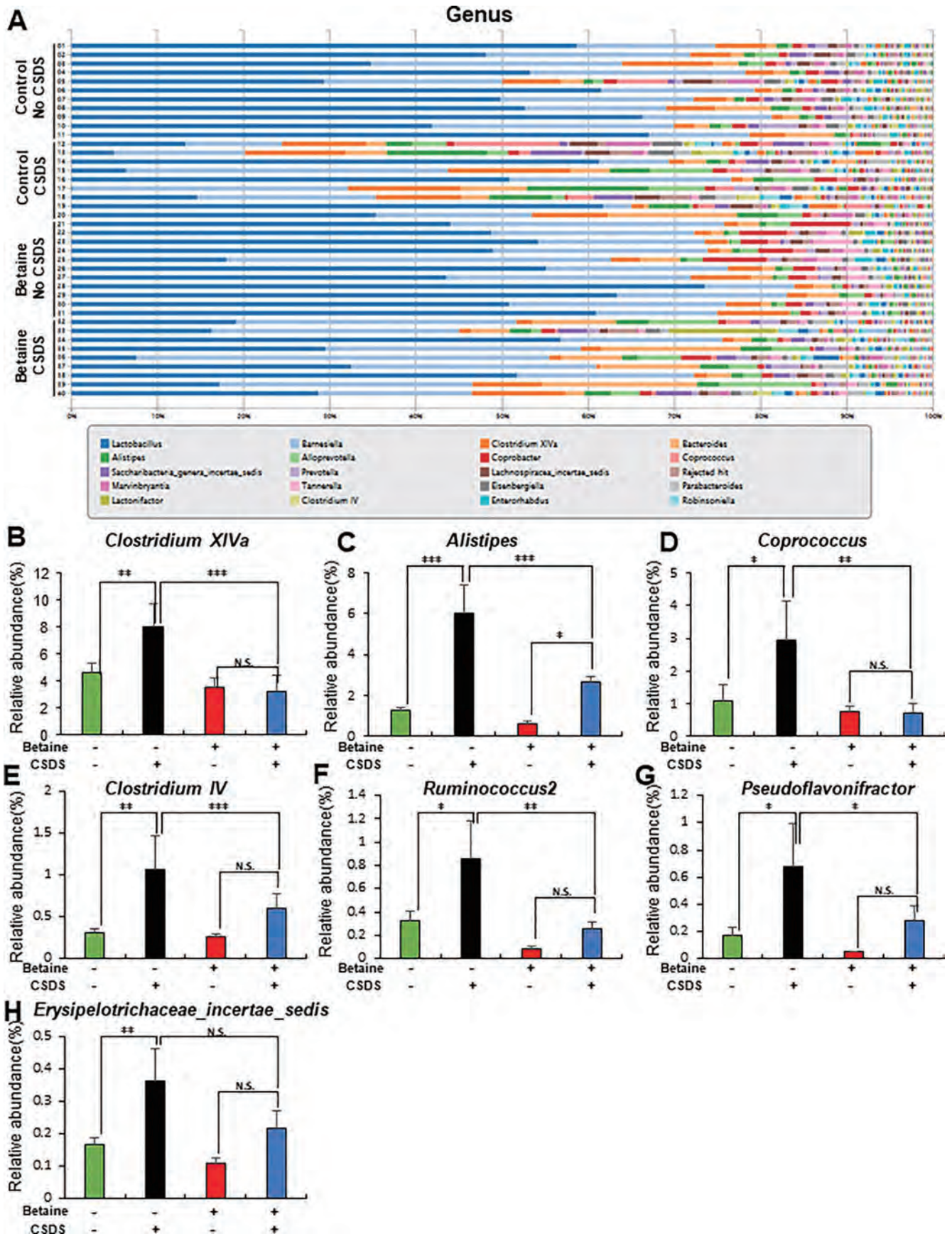
Figure 4. Altered composition in the gut bacteria at the levels of order. (A): The relative abundances of order in fecal samples of the four groups. (B): *Clostridiales* (two-way ANOVA, betaines: $F_{1,36} = 8.474$, P = 0.006, CSDS: $F_{1,36} = 11.667$, P = 0.002, interaction: $F_{1,36} = 1.385$, P = 0.247). (C): *Erysipelotrichales* (two-way ANOVA, betaines: $F_{1,36} = 3.616$, P = 0.065, CSDS: $F_{1,36} = 21.140$, P < 0.001, interaction: $F_{1,36} = 4.521$, P = 0.040). (D): *Bacillales* (two-way ANOVA, betaines: $F_{1,36} = 3.118$, P = 0.086, CSDS: $F_{1,36} = 16.778$, P < 0.001, interaction: $F_{1,36} = 3.615$, P = 0.065). (E): *Selenomonadales* (two-way ANOVA, betaines: $F_{1,36} = 10.612$, P = 0.002, CSDS: $F_{1,36} = 8.050$, P = 0.007, interaction: $F_{1,36} = 1.866$, P = 0.180). (F): *Chloroplast* (two-way ANOVA, betaines: $F_{1,36} = 3.795$, P = 0.059, CSDS: $F_{1,36} = 8.653$, P = 0.006, interaction: $F_{1,36} = 3.914$, P = 0.056). Data are shown as mean ± S.E.M. (n = 9-11). *P< 0.05, **P < 0.01, ***P < 0.001. NS: not significant.

betaine for cognitive deficits in β-amyloid$_{25-35}$ injected mice (Ibi et al., 2019). These findings suggest that betaine supplementation may contribute to stress resilience in mice after CSDS via anti-inflammatory actions. It is also possible that a complex interaction of these manipulations—betaine treatment and CSDS—may contribute to the current data. Further detailed study is needed to confirm the relationship

between stress resilience and anti-inflammatory actions of betaine.

The UniFrac-based PCoA showed significant differences among the four groups. Betaine supplementation ameliorated the abnormal diversity of microbiota in host after CSDS. In this study, we found, that CSDS significantly increased levels of several genus bacteria (*Clostridium XIVa, Alistipes, Coprococcus, Clostridium IV, Ruminococcus2,*

Figure 5. Altered composition in the gut bacteria at the levels of family. (A): The relative abundances of family in fecal samples of the four groups. (B): *Lachnospiraceae* (two-way ANOVA, betaines: $F_{1,36} = 9.323$, $P = 0.004$, CSDS: $F_{1,36} = 7.619$, $P = 0.009$, interaction: $F_{1,36} = 2.289$, $P = 0.139$). (C): *Ruminococcaceae* (two-way ANOVA, betaines: $F_{1,36} = 11.587$, $P = 0.002$, CSDS: $F_{1,36} = 20.599$, $P < 0.001$, interaction: $F_{1,36} = 0.572$, $P = 0.454$). (D): *Rikenellaceae* (two-way ANOVA, betaines: $F_{1,36} = 9.485$, $P = 0.004$, CSDS: $F_{1,36} = 26.763$, $P < 0.001$, interaction: $F_{1,36} = 4.288$, $P = 0.046$). (E): *Erysipelotrichaceae* (two-way ANOVA, betaines: $F_{1,36} = 3.139$, $P = 0.085$, CSDS: $F_{1,36} = 17.165$, $P < 0.001$, interaction: $F_{1,36} = 4.040$, $P = 0.052$). (F): *Clostridiales_Incertae Sedis XIII* (two-way ANOVA, betaines: $F_{1,36} = 5.210$, $P = 0.028$, CSDS: $F_{1,36} = 8.605$, $P = 0.006$, interaction: $F_{1,36} = 1.052$, $P = 0.312$). Data are shown as mean ± S.E.M. (n = 9-11). *$P < 0.05$, **$P < 0.01$, ***$P < 0.001$. NS: not significant.

*Pseudoflavonifractor, Erysipelotrichaceae*) in water-treated group, but not betaine-treated group. The mechanisms underlying betaine-mediated recovery from the altered composition of the microbiota in the host gut mice caused by CSDS are currently unknown. Previously, Bailey et al. (2011) reported that the exposure to a social stressor called

social disruption failed to increase blood IL-6 in antibiotic-treated mice (i.e., microbiome depletion), although the same stress caused increases in levels of IL-6 in the blood of control mice, suggesting that the microbiota are necessary for stress-induced increases in circulating cytokines. Given the role of immune system in resilience (Cathomas et al.,

(caption on next page)

- 214 -

Figure 6. Altered composition in the gut bacteria at the levels of genus. (A): The relative abundances of genus in fecal samples of the four groups. (B): *Clostridium XIVa* (two-way ANOVA, betaines: $F_{1,36} = 6..960$, P = 0.012, CSDS: $F_{1,36} = 1.995$, P = 0.166, interaction: $F_{1,36} = 2.793$, P = 0.103). (C): *Alistipes* (two-way ANOVA, betaines: $F_{1,36} = 9.492$, P = 0.004, CSDS: $F_{1,36} = 26.669$, P < 0.001, interaction: $F_{1,36} = 4.322$, P = 0.045). (D): *Coprococcus* (two-way ANOVA, betaines: $F_{1,36} = 4.392$, P = 0.043, CSDS: $F_{1,36} = 2.189$, P = 0.148, interaction: $F_{1,36} = 2.417$, P = 0.129). (E): *Clostridium IV* (two-way ANOVA, betaines: $F_{1,36} = 1.831$, P = 0.0184, CSDS: $F_{1,36} = 8.449$ P = 0.006, interaction: $F_{1,36} = 1.146$, P = 0.291). (F): *Ruminococcus2* (two-way ANOVA, betaines: $F_{1,36} = 7.491$, P = 0.010, CSDS: $F_{1,36} = 5.176$, P = 0.029, interaction: $F_{1,36} = 1.346$, P = 0.254). (G): *Pseudoflavonifractor* (two-way ANOVA, betaines: $F_{1,36} = 2.861$, P = 0.099, CSDS: $F_{1,36} = 5.713$, P = 0.022, interaction: $F_{1,36} = 0.788$, P = 0.381). (H): *Erysipelotrichaceae_incertae_sedis* (two-way ANOVA, betaines: $F_{1,36} = 3.604$, P = 0.066, CSDS: $F_{1,36} = 8.139$, P = 0.007, interaction: $F_{1,36} = 0.673$, P = 0.417).Data are shown as mean ± S.E.M. (n = 9-11). *P < 0.05, **P < 0.01, ***P < 0.001. NS: not significant.
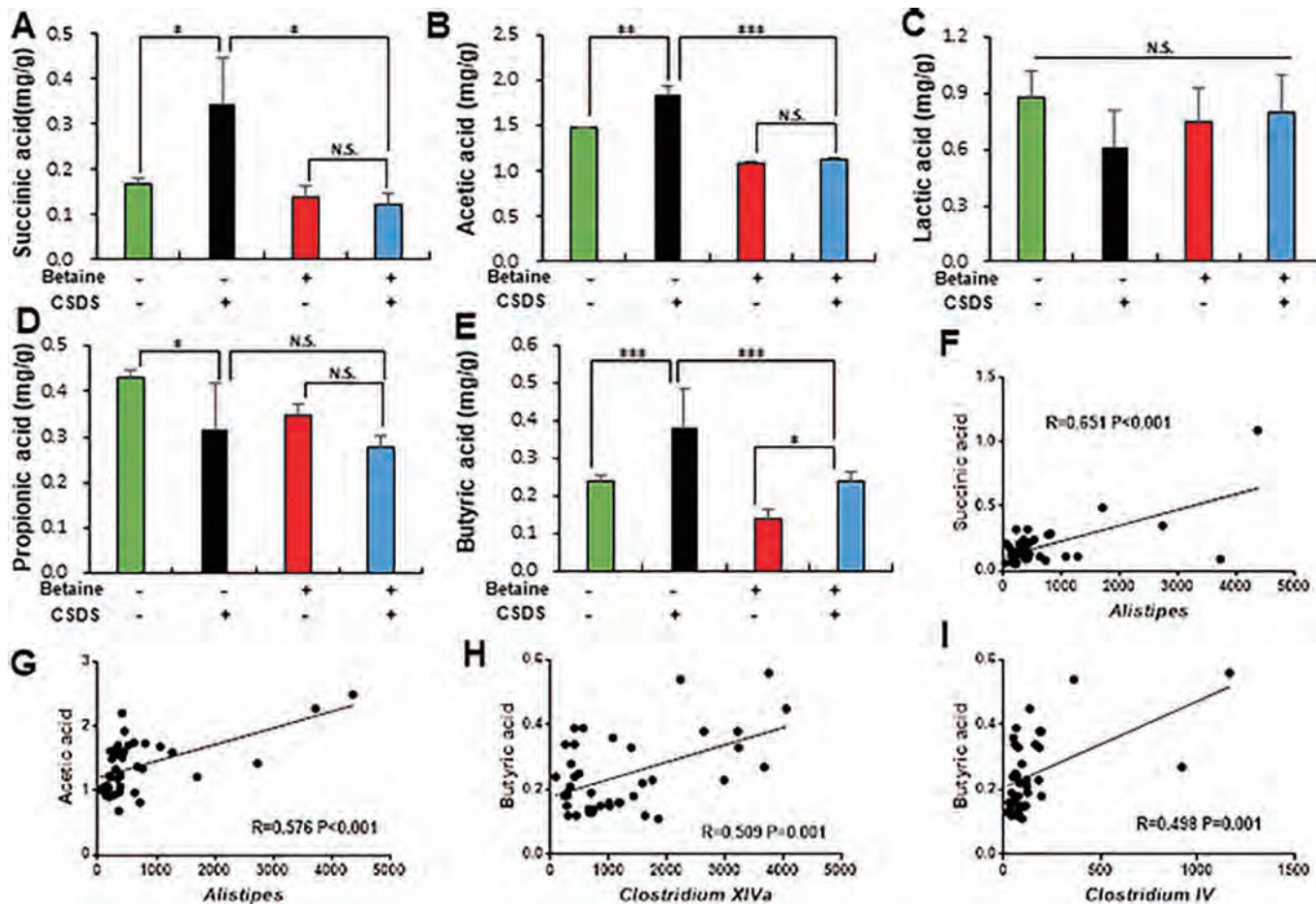
Figure 7. Levels of short-chain organic acids and correlation between bacteria. (A): Succinic acid (two-way ANOVA, betaines: $F_{1,36} = 5.063$, P = 0.031, CSDS: $F_{1,36} = 2.050$, P = 0.162, interaction: $F_{1,36} = 3.068$, P = 0.089). (B): Acetic acid(two-way ANOVA, betaines: $F_{1,36} = 41.856$, P < 0.001, CSDS: $F_{1,36} = 2.665$, P = 0.111, interaction: $F_{1,36} = 1.551$, P = 0.221). (C): Lactic acid (two-way ANOVA, betaines: $F_{1,36} = 0.036$, P = 0.850, CSDS: $F_{1,36} = 0.381$, P = 0.541, interaction: $F_{1,36} = 0.767$, P = 0.387). (D): Propionic acid (two-way ANOVA, betaines: $F_{1,36} = 5.418$, P = 0.026, CSDS: $F_{1,36} = 13.436$, P < 0.001, interaction: $F_{1,36} = 1.043$, P = 0.314). (E): Butyric acid (two-way ANOVA, betaines: $F_{1,36} = 19.813$, P < 0.001, CSDS: $F_{1,36} = 21.262$, P < 0.001, interaction: $F_{1,36} = 0.615$, P = 0.438). (F): Correlation (r = 0.651, P < 0.001) between succinic acid and *Alistipes*. (G): Correlation (r = 0.576, P < 0.001) between acetic acid and *Alistipes*. (H): Correlation (r = 0.509, P = 0.001) between butyric acid and *Clostridium XIVa*. (I): Correlation (r = 0.498, P = 0.001) between butyric acid and *Clostridium IV*. Data are shown as mean ± S.E.M. (n = 9-11). *P < 0.05, **P < 0.01, ***P < 0.001. NS: not significant.

2019; Dantzer et al., 2018; Zhang et al., 2020), it is likely that modulation of the bidirectional relationship between resilience and immunity by the gut microbiota plays a role in the recovery from CSDS. Further detailed study on the relationship between resilience and immunity via the brain–gut–microbiota axis is needed.

In this study, we found marked increases in organisms from the genus bacteria (*Clostridium XIVa, Alistipes, Coprococcus, Clostridium IV, Ruminococcus2, Pseudoflavonifractor, Erysipelotrichaceae*) in water-treated group after CSDS. It is reported that *Alistipes* are associated with gut inflammation and were elevated in chronic fatigue syndrome, irritable bowel syndrome and depression (Fremont et al., 2013; Naseribafrouei et al., 2014). High levels of *Alistipes* might be a potential cause for the hypoxia-induced intestinal disorders (Fremont et al.,

2013). The stressor increased blood levels of IL-6 and *Coprococcus* (Bailey et al., 2011). High levels of *Erysipelotrichaceae* in rats were shown after fast stress (Yoshikawa et al., 2013), suggesting a role of this bacteria in stress response. A recent study showed that dietary betaine supplementation decreased liver lipid accumulation caused by a high-carbohydrate diet through improvement of the gut microbiota composition (Wang et al., 2019). Collectively, these bacteria may contribute to resilience versus susceptibility in mice after CSDS. However, precise mechanisms underlying betaine-induced prophylactic effects for these bacteria are unknown.

In this study, we found positive correlations between succinic acid (or acetic acid) and *Alistipes* levels among four groups. It is shown that *Alistipes* can produce succinic acid and acetic acid (Nagai et al., 2010).

Furthermore, we also found positive correlations between butyric acid and *Clostridium XIVa* (or *Clostridium IV*) levels among four groups. It is reported that highest levels of butyric acid are produced by *Clostridium XIVa* and *Clostridium IV* (Eeckhaut et al., 2011). Collectively, it is possible that increases in these bacteria and subsequent increases in these short-chain fatty acids (succinic acid, acetic acid, butyric acid) after CSDS may confer anhedonia susceptibility to mice after CSDS although further study is needed.

The crosstalk between brain and gut is predominately influenced by the gut bacteria (Kelly et al., 2016). Imbalance of gut microbiota is well established as causing abnormal brain–gut–microbiota axis in several stress-related psychiatric disorders (Fung et al., 2017; Kelly et al., 2016). Accumulating evidence suggests that an abnormal composition of gut microbiota may contribute to resilience versus susceptibility in rodents after repeated stress (Bailey et al., 2011; Hao et al., 2019; Szyszkowicz et al., 2017; Yang et al., 2017; Wang et al., 2020; Zhang et al., 2019). It is likely that an altered composition of gut microbiota may play a role in the susceptibility in stress-induced disorders.

Choline is the precursor of betaine, which can be further metabolized to *N,N*-di-methylglycine. *N,N*-di-methylglycine is oxidatively demethylated to *N*-methylglycine (or sarcosine). Sarcosine has been found to be effective in patients with depression, schizophrenia, obsessive compulsive disorder, or Parkinson's disease (Huang et al., 2013; Lane et al., 2005; 2008; Tsai et al., 2014; Wu et al., 2011). Therefore, it is likely that metabolism of sarcosine from betaine may be one of betaine's beneficial effects although further study is needed.

This study has some limitations. In this study, we did not identify the specific microbiota, which plays a role in betaine-related resilience after CSDS. Additionally, we do not obtain conclusive evidence that the improvement in the abnormal composition of the microbiota is mainly due to CSDS. Further study is needed.

In conclusion, the present study suggests that betaine supplementation may contribute to resilience versus susceptibility in mice subjected to CSDS, and that betaine may have prophylactic effects for abnormal composition of gut microbiota in mice after CSDS. Collectively, the brain–gut–microbiota axis may play a role in susceptibility to stress-related disorders. Therefore, it is likely that betaine supplementation could be prophylactic nutrient to prevent or minimize the relapse by stress in the remission state of depressed patients.

CRediT authorship contribution statement

Youge Qu: Conceptualization, Data curation, Methodology, Formal analysis, Writing - original draft, Writing - review & editing. **Kai Zhang:** Data curation, Methodology, Writing - review & editing. **Yaoyu Pu:** Data curation, Methodology, Writing - review & editing. **Lijia Chang:** Data curation, Methodology, Writing - review & editing. **Siming Wang:** Data curation, Methodology, Writing - review & editing. **Yunfei Tan:** Data curation, Methodology, Writing - review & editing. **Xingming Wang:** Data curation, Methodology, Writing - review & editing. **Jiancheng Zhang:** Data curation, Methodology, Writing - review & editing. **Tetsuo Ohnishi:** Methodology, Writing - review & editing. **Takeo Yoshikawa:** Methodology, Writing - review & editing. **Kenji Hashimoto:** Conceptualization, Funding acquisition, Supervision, Writing - original draft, Writing - review & editing.

Declaration of Competing Interest

All authors report no biomedical financial interests or potential conflicts of interest.

Role of funding source

This study was supported by Smoking Research Foundation, Japan

Supplementary materials

Supplementary material associated with this article can be found, in the online version, at doi:10.1016/j.jad.2020.03.095.

References

Bailey, M.T., Dowd, S.E., Galley, J.D., Hufnagle, A.R., Allen, R.G., Lyte, M., 2011. Exposure to a social stressor alters the structure of the intestinal microbiota: implications for stressor-induced immunomodulation. Brain Behav Immun 25, 397–407.

Beery, A.K., Kaufer, D., 2015. Stress, social behavior, and resilience: insights from rodents. Neurobiol Stress 21, 116–127.

Cathomas, F., Murrough, J.W., Nestler, E.J., Han, M.H., Russo, S.J., 2019. Neurobiology of resilience: interface between mind and body. Biol Psychiatry 86, 410–420.

Cholewa, J.M., Guimarães-Ferreira, L., Zanchi, N.E., 2014. Effects of betaine on performance and body composition: a review of recent findings and potential mechanisms. Amino Acids 46, 1785–1793.

Craig, S.A.S., 2004. Betaine in human nutrition. Am J Clin Nutr 80, 539–549.

Cussotto, S., Sandhu, K.V., Dinan, T.G., Cryan, J.F., 2018. The neuroendocrinology of the microbiota-gut-brain axis: a behavioural perspective. Front Neuroendocrinol 51, 80–101.

Dantzer, R., Cohen, S., Russo, S.J., Dina, T.G., 2018. Resilience and immunity. Brain Behav Immun 74, 28–42.

Dinan, T.G., Cryan, J.F., 2017. Brain-gut-microbiota axis and mental health. Psychosom Med 79, 920–926.

Eeckhaut, V., Van Immerseel, F., Croubels, S., De Baere, S., Haesebrouck, F., Ducatelle, R., Louis, P., Vandamme, P., 2011. Butyrate production in phylogenetically diverse *Firmicutes* isolated from the chicken caecum. Microb Biotechnol 4, 503–512.

Filipčev, B., Kojić, J., Krulj, J., Bodroža-Solarov, M., Ilić, N., 2018. Betaine in cereal grains and grain-based products. Foods 7, 49.

Forsythe, P., Kunze, W., Bienenstock, J., 2016. Moody microbes or fecal phrenology: what do we know about the microbiota-gut-brain axis? BMC Med 14, 58.

Franklin, T.B., Saab, B.J., Mansuy, I.M., 2012. Neural Mechanisms of Stress Resilience and Vulnerability. Neuron 75, 747–761.

Fremont, M., Coomans, D., Massart, S., De Meirleir, K., 2013. High-throughput 16S rRNA gene sequencing reveals alterations of intestinal microbiota in myalgic encephalomyelitis/chronic fatigue syndrome patients. Anaerobe 22, 50–56.

Fung, T.C., Olson, C.A., Hsiao, E.Y., 2017. Interactions between the microbiota, immune and nervous systems in health and disease. Nat Neurosci 20, 145–155.

Gentile, C.L., Weir, T.L., 2018. The gut microbiota at the intersection of diet and human health. Science 362, 776–780.

Golden, S.A., Covington 3rd, H.E., Berton, O., Russo, S.J., 2011. A standardized protocol for repeated social defeat stress in mice. Nat Protoc 6, 1183–1191.

Hao, Z., Wang, W., Guo, R., Liu, H., 2019. *Faecalibacterium prausnitzii* (ATCC 27766) has preventive and therapeutic effects on chronic unpredictable mild stress-induced depression-like and anxiety-like behavior in rats. Psychoneuroendocrinology 104, 132–142.

Hodes, G.E., Pfau, M.L., Leboeuf, M., Golden, S.A., Christoffel, D.J., Bregman, D., Rebusi, N., Heshmati, M., Aleyasin, H., Warren, B.L., Lebonté, B., Horn, S., Lapidus, K., Stelzhammer, V., Wong, E.H.F., Bahn, S., Krishnan, V., Bolaños-Guzman, C., Murrough, J.W., Merad, M., Russo, S.J., 2014. Individual differences in the peripheral immune system promote resilience versus susceptibility to social stress. Proc Natl Acad Sci USA 111, 16136–16141.

Huang, C.C., Wei, I.H., Huang, C.L., Chen, K.T., Tsai, M.H., Tsai, P., Tun, R., Huang, K.H., Chang, Y.C., Lane, H.Y., Tsai, G.E., 2013. Inhibition of glycine transporter-1 as a novel mechanism for the treatment of depression. Biol Psychiatry 74, 734–741.

Ibi, D., Tsuchihashi, A., Nomura, T., Hiramatsu, M., 2019. Involvement of GAT2/BGT-1 in the preventive effects of betaine on cognitive impairment and brain oxidative stress in amyloid-β peptide-injected mice. Eur J Pharmacol 842, 57–63.

Jiang, Y.P., Yang, J.M., Ye, R.J., Liu, N., Zhang, W.J., Ma, L., Zheng, P., Niu, J.G., Liu, P., Yu, J.Q., 2019. Protective effects of betaine on diabetic induced disruption of the male mice blood-testis barrier by regulating oxidative stress-mediated p38 MAPK pathways. Biomed Pharmacother 120, 109474.

Kelly, J.R., Clarke, G., Cryan, J.F., Dinan, T.G., 2016. Brain-gut-microbiota axis: challenges for translation in psychiatry. Ann Epidemiol 26, 366–372.

Koike, S., Bundo, M., Iwamoto, K., Suga, M., Kuwabara, H., Ohashi, Y., Shinoda, K., Takano, Y., Iwashiro, N., Satomura, Y., Nagai, T., Natsubori,, Tada, M., Yamasue, H., Kasai, K., 2014. A snapshot of plasma metabolites in first-episode schizophrenia: a capillary electrophoresis time-of-flight mass spectrometry study. Transl Psychiatry 4, e379.

Lane, H.Y., Chang, Y.C., Liu, Y.C., Chiu, C.C., Tsai, G.E., 2005. Sarcosine or D-serine add-on treatment for acute exacerbation of schizophrenia: a randomized, double-blind,

placebo-controlled study. Arch Gen Psychiatry 62, 1196–1204.

Lane, H.Y., Liu, Y.C., Huang, C.L., Chang, Y.C., Liau, C.H., Perng, C.H., Tsai, G.E., 2008. Sarcosine (*N* -methylglycine) treatment for acute schizophrenia: a randomized, double-blind study. Biol Psychiatry 63, 9–12.

Ma, Q., Xing, C., Long, W., Wang, H.Y., Liu, Q., Wang, R.F., 2019. Impact of microbiota on central nervous system and neurological diseases: the gut-brain axis. J Neuroinflammation 16, 53.

Mayer, E.A., Tillisch, K., Gupta, A., 2015. Gut/brain axis and the microbiota. J Clin Invest 125, 926–938.

Molina-Torres, G., Rodriguez-Arrastia, M., Roman, P., Sanchez-Labraca, N., Cardona, D., 2019. Stress and the gut microbiota-brain axis. Behav Pharmacol 30 (2 and 3 Special Issue), 187–200.

Nagai, F., Morotomi, M., Watanabe, Y., Sakon, H., Tanaka, R., 2010. *Alistipes indistinctus sp. nov.* and *Odoribacter laneus sp. nov.*, common members of the human intestinal microbiota isolated from faeces. Int J Syst Evol Microbiol 60, 1296–1302.

Naseribafrouei, A., Hestad, K., Avershina, E., Sekelja, M., Linlokken, A., Wilson, R., Rudi, K., 2014. Correlation between the human fecal microbiota and depression. Neurogastroenterol Motil 26, 1155–1162.

Ohnishi, T., Balan, S., Toyoshima, M., Maekawa, M., Ohba, H., Watanabe, A., Iwayama, Y., Fujita, Y., Tan, Y., Hisano, Y., Shimamoto-Mitsuyama, C., Nozaki, Y., Esaki, K., Nagaoka, A., Matsumoto, J., Hino, M., Mataga, N., Hayashi-Takagi, A., Hashimoto, K., Kunii, Y., Kakita, A., Yabe, H., Yoshikawa, T., 2019. Investigation of betaine as a novel psychotherapeutics for schizophrenia. EBioMedicine 45, 432–446.

Pizzagalli, D., 2014. Depression, stress, and anhedonia: toward a synthesis and integrated model. Annu Rev Clin Psychol 10, 393–423.

Rajaie, S., Esmaillzadeh, A., 2011. Dietary choline and betaine intakes and risk of cardiovascular diseases: review of epidemiological evidence. ARYA Atheroscler 7, 78–86.

Ren, Q., Ma, M., Ishima, T., Morisseau, C., Yang, J., Wagner, K.M., Zhang, J., Yang, C., Yao, W., Dong, C., Han, M., Hammock, B.D., Hashimoto, K., 2016. Gene deficiency and pharmacological inhibition of soluble epoxide hydrolase confers resilience to repeated social defeat stress. Proc Natl Acad Sci USA 113, E1944–E1952.

Russo, S.J., Nestler, E.J., 2013. The brain reward circuitry in mood disorders. Nat Rev Neurosci 14, 609–625.

Russo, S.J., Murrough, J.W., Han, M.H., Charney, D.S., Nestler, E.J., 2012. Neurobiology of resilience. Nat Neurosci 15, 1475–1484.

Szyszkowicz, J.K., Wong, A., Anisman, H., Merali, Z., Audet, M.C., 2017. Implications of the gut microbiota in vulnerability to the social avoidance effects of chronic social defeat in male mice. Brain Behav Immun 66, 45–55.

Treadway, M.T., Zald, D.H., 2011. Reconsidering anhedonia in depression: Lessons from translational neuroscience. Neurosci Biobehav Rev 35, 537–555.

Tsai, C.H., Huang, H.C., Liu, B.L., Li, C.I., Lu, M.K., Chen, X., Tsai, M.C., Yang, Y.W., lane, H.Y., 2014. Activation of *N* -methyl-D-aspartate receptor glycine site temporally ameliorates neuropsychiatric symptoms of Parkinson's disease with dementia. Psychiatry Clin Neurosci 68, 692–700.

Wang, H., Li, S., Fang, S., Yang, X., Feng, J., 2018. Betaine improves intestinal functions

by enhancing digestive enzymes, ameliorating intestinal morphology, and enriching intestinal microbiota in high-salt stressed rats. Nutrients 10, 907.

Wang, S., Qu, Y., Chang, L., Pu, Y., Zhang, K., Hashimoto, K., 2020. Antibiotic-induced microbiome depletion is associated with resilience in mice after chronic social defeat stress. J Affect Disord 260, 448–457.

Wang, F., Xu, J., Jakovlic, I., Wang, W.M., Zhao, Y.H., 2019. Dietary betaine reduces liver lipid accumulation via improvement of bile acid and trimethylamine- *N* -oxide metabolism in blunt-snout bream. Food Funct 10, 6675–6689.

Wu, P.L., Tang, H.S., Lane, H.Y., Tsai, C.A., Tsai, G.E., 2011. Sarcosine therapy for obsessive compulsive disorder: a prospective, open-label study. J Clin Psychopharmacol 31, 369–374.

Yang, C., Fang, X., Zhan, G., Huang, N., Li, S., Bi, J., Jiang, R., Yang, L., Miao, L., Zhu, B., Luo, A., Hashimoto, K., 2019. Key role of gut microbiota in anhedonia-like phenotype in rodents with neuropathic pain. Transl Psychiatry 9, 57.

Yang, C., Fujita, Y., Ren, Q., Ma, M., Dong, C., Hashimoto, K., 2017. *Bifidobacterium* in the gut microbiota confer resilience to chronic social defeat stress in mice. Sci Rep 7, 45942.

Yang, C., Ren, Q., Qu, Y., Zhang, J.C., Ma, M., Dong, C., Hashimoto, K., 2018. Mechanistic target of rapamycin-independent antidepressant effects of (*R*)-ketamine in a social defeat stress model. Biol Psychiatry 83, 18–28.

Yang, C., Shirayama, Y., Zhang, J.C., Ren, Q., Yao, W., Ma, M., Dong, C., Hashimoto, K., 2015. *R* -ketamine: a rapid-onset and sustained antidepressant without psychotomimetic side effects. Transl Psychiatry 5, e632.

Yoshikawa, K., Shimada, M., Kuwahara, T., Hirakawa, H., Kurita, N., Sato, H., Utsunomiya, T., Iwata, T., Miyatani, T., Higashijima, J., Kashihara, H., Takasu, C., Matsumoto, N., Nakayama-Imaohji, H., 2013. Effect of Kampo medicine "; *Dai-kenchu-to* " on microbiome in the intestine of the rats with fast stress. J Med Invest 60, 221–227.

Zhang, K., Sakamoto, A., Chang, L., Qu, Y., Wang, S., Pu, Y., Tan, Y., Wang, X., Fujita, Y., Ishima, T., Hatano, M., Hashimoto, K., 2020. Splenic NKG2D confers resilience versus susceptibility in mice after chronic social defeat stress: beneficial effects of (*R*)-ketamine. Eur Arch Psychiatry Clin Neurosci. https://doi.org/10.1007/s00406-019-01092-z. 2019 Dec. 24.

Zhang, J.C., Yao, W., Dong, C., Yang, C., Ren, Q., Ma, M., Hashimoto, K., 2017. Blockade of interleukin-6 receptor in the periphery promotes rapid and sustained antidepressant actions: a possible role of gut-microbiota-brain axis. Transl Psychiatry 7, e1138.

Zhang, K., Fujita, Y., Chang, L., Qu, Y., Pu, Y., Wang, S., Shirayama, Y., Hashimoto, K., 2019. Abnormal composition of gut microbiota is associated with resilience versus susceptibility to inescapable electric stress. Transl Psychiatry 9, 231.

Zhao, G., He, F., Wu, C., Li, P., Li, N., Deng, J., Zhu, G., Ren, W., Peng, Y., 2018a. Betaine in inflammation: mechanistic aspects and application. Front Immunol 8, 1070.

Zhao, N., Yang, S., Jia, Y., Sun, B., He, B., Zhao, R., 2018b. Maternal betaine supplementation attenuates glucocorticoid-induced hepatic lipid accumulation through epigenetic modification in adult offspring rats. J Nutr Biochem 54, 105–112.

- 217-

Journal of Neuroinflammation

RESEARCH   **Open Access**

Ingestion of *Lactobacillus intestinalis* and *Lactobacillus reuteri* causes depression- and anhedonia-like phenotypes in antibiotic-treated mice via the vagus nerve

Siming Wang, Tamaki Ishima, Jiancheng Zhang, Youge Qu, Lijia Chang, Yaoyu Pu, Yuko Fujita, Yunfei Tan, Xingming Wang and Kenji Hashimoto[*]

Abstract

Background: The brain–gut–microbiota axis plays a role in the pathogenesis of stress-related disorders such as depression. In this study, we examined the effects of fecal microbiota transplantation (FMT) in mice with antibiotic-treated microbiota depletion.

Methods: The fecal microbiota was obtained from mice subjected to chronic social defeat stress (CSDS) and control (no CSDS) mice. FMT from these two groups was performed to antibiotic-treated mice. 16S rRNA analysis was performed to examine the composition of gut microbiota. Furthermore, the effects of subdiaphragmatic vagotomy in depression-like phenotypes after ingestion of microbes were examined.

Results: The ingestion of fecal microbiota from CSDS-susceptible mice resulted in an anhedonia-like phenotype, higher plasma levels of interleukin-6 (IL-6), and decreased expression of synaptic proteins in the prefrontal cortex (PFC) in antibiotic-treated mice but not in water-treated mice. 16S rRNA analysis suggested that two microbes (*Lactobacillus intestinalis* and *Lactobacillus reuteri*) may be responsible for the anhedonia-like phenotype in antibiotic-treated mice after FMT. Ingestion of these two microbes for 14 days led to depression- and anhedonia-like phenotypes, higher plasma IL-6 levels, and decreased expression of synaptic proteins in the PFC of antibiotic-treated mice. Interestingly, subdiaphragmatic vagotomy significantly blocked the development of behavioral abnormalities, elevation of plasma IL-6 levels, and downregulation of synaptic proteins in the PFC after ingestion of these two microbes.

Conclusions: These findings suggest that microbiota depletion using an antibiotic cocktail is essential for the development of FMT-induced behavioral changes and that the vagus nerve plays a key role in behavioral abnormalities in antibiotic-treated mice after the ingestion of *L. intestinalis* and *L. reuteri*. Therefore, it is likely that the brain–gut–microbiota axis participates in the pathogenesis of depression via the vagus nerve.

Keywords: Anhedonia, Antibiotic, Depression, Gut microbiota, Vagus nerve

* Correspondence: hashimoto@faculty.chiba-u.jp
Division of Clinical Neuroscience, Chiba University Center for Forensic Mental Health, 1-8-1 Inohana, Chiba 260-8670, Japan

Background

The brain–gut–microbiota axis plays a fundamental role in host physiology, homeostasis, development, and metabolism [1–6]. Accumulating evidence has implicated an abnormal microbiota composition in the host gastrointestinal tract in the pathogenesis of stress-related disorders such as depression [7–15], and this abnormality could affect the antidepressant-like effects of certain compounds [16–21].

Instead of germ-free mice, antibiotic cocktail-induced microbiome depletion has been used to investigate the role of the gastrointestinal microbiota in pathological conditions such as Parkinson's disease and depression [13, 15, 22–25]. Recently, we reported that microbiome depletion via antibiotic treatment contributed to resilience to anhedonia in mice subjected to chronic social defeat stress (CSDS) [15], suggesting that the brain–gut–microbiota axis plays a role in resilience versus susceptibility to CSDS. Furthermore, we reported that the transplantation of fecal microbiota from rats with an anhedonia-like phenotype aggravated depression- and anhedonia-like phenotypes in mice treated with an antibiotic cocktail [13]. Interestingly, the transplantation of fecal microbes from mice with depression into germ-free mice resulted in depression-like behaviors compared with the effects of the transplantation of fecal microbes obtained from control animals [9]. Collectively, it appears that the brain–gut–microbiota axis plays a key role in depression- and anhedonia-like phenotypes in rodents. However, the precise mechanisms underlying fecal microbiota transplantation (FMT)-induced behavioral abnormalities in rodents treated with an antibiotic cocktail remain unknown.

This study thus aimed to investigate the role of the brain–gut–microbiota axis in depression- and anhedonia-like phenotypes in mice. First, we examined whether transplantation of the fecal microbiota from CSDS-susceptible mice could induce an anhedonia-like phenotype in mice treated with an antibiotic cocktail. Using 16S rRNA analysis, we analyzed the composition of the gastrointestinal microbiota in fecal samples from these mice. We identified two microbes (*Lactobacillus intestinalis* and *Lactobacillus reuteri*) potentially responsible for the anhedonia-like phenotype in recipient mice. Second, we examined whether ingestion of these two microbes for 14 days produced depression- and anhedonia-like phenotypes in mice treated with an antibiotic cocktail. Furthermore, we measured the plasma levels of the inflammatory cytokine interleukin-6 (IL-6) and synaptic proteins (i.e., α-amino-3-hydroxy-5-methyl-4-isoxazole-propionic acid receptor A1 [GluA1] and postsynaptic density 95 [PSD-95]) in the prefrontal cortex (PFC) since the expression of these synaptic proteins was decreased in the PFC from rodents with depression-like phenotypes [26, 27]. Finally, we investigated whether subdiaphragmatic vagotomy (SDV) affected depression- and anhedonia-like phenotypes in mice treated with an antibiotic cocktail after the ingestion of these two microbes because the microbiota and brain are known to communicate through the vagus nerve [28–32].

Materials and methods

Animals

Male adult C57BL/6 mice (n = 120, 8 weeks old, body weight = 20–25 g, Japan SLC, Inc., Hamamatsu, Japan) and male adult CD1 (ICR) mice (n = 20, 13–15 weeks old, body weight > 40 g, Japan SLC, Inc.) were used. Animals were housed under controlled temperatures and 12-h/12-h light/dark cycles (lights on between 07:00 and 19:00 h) with ad libitum access to food (CE-2; CLEA Japan, Inc., Tokyo, Japan) and water. The protocol was approved by the Chiba University Institutional Animal Care and Use Committee (permission number: 30-399 and 1-456). This study was conducted in strict accordance with the recommendations in the Guide for the Care and Use of Laboratory Animals of the US National Institutes of Health. Animals were deeply anesthetized with isoflurane before being sacrificed via cervical dislocation. All efforts were made to minimize suffering. Transplantation of fecal samples and bacteria was performed from 16:00 to 17:00, and the 1% sucrose preference test (SPT) was performed from 17:00 to 18:00.

CSDS

The CSDS procedure was performed as previously reported [15, 17–19, 33–37]. C57BL/6 mice were exposed to a different CD1 aggressor mouse for 10 min per day for 10 consecutive days (days 1–10). When the social defeat session ended, the resident CD1 mouse and intruder mouse were housed on opposite sides of the cage, separated by a perforated Plexiglass divider to allow visual, olfactory, and auditory contact for the remainder of the 24-h period. At 24 h after the last session, all mice were housed individually. On day 11, a social interaction test was performed to identify subgroups of mice that were susceptible and unsusceptible to CSDS. This was accomplished by placing mice in an interaction test box ($42 \times 42 \, \text{cm}^2$) with an empty wire-mesh cage ($10 \times 4.5 \, \text{cm}^2$) located at one end. The movement of the mice was tracked for 2.5 min, followed by 2.5 min in the presence of an unfamiliar aggressor confined in the wire-mesh cage. The duration of the subject's presence in the "interaction zone" (defined as the 8-cm-wide area surrounding the wire-mesh cage) was recorded using a stopwatch. The interaction ratio was calculated as time spent in the interaction zone with an aggressor divided by the time spent in the interaction zone

without an aggressor. An interaction ratio of 1 was set as the cutoff. Mice with scores < 1 were defined as "susceptible" to social defeat stress, and those with scores ≥ 1 were defined as "resilient." Fresh fecal samples were collected from CSDS-susceptible mice and control (no CSDS) mice on days 12–14 in sterilized screw cap microtubes immediately after defecation and stored at − 80 °C until FMT. The fecal samples were collected from each mouse around 9:00–10:00 on each day to avoid circadian effects on the microbiome. In total, about 30 collected tubes containing approximately 0.5 g of feces per each tube were used for FMT. Before FMT, fecal samples were removed from the freezer every morning, and they were allowed to thaw for 10–15 min at room temperature. Then, drinking water (10 mL/g feces) was added to the tube including the fecal samples. The drinking water including fecal samples (0.2 mL/mouse) was given to the antibiotic-treated mice using gastric gavage for consecutive 14 days.

Antibiotic cocktail treatment, FMT, and behavioral tests

Based on previous reports [13, 15, 24, 25], broad-spectrum antibiotics (ampicillin 1 g/L, neomycin sulfate 1 g/L, metronidazole 1 g/L, Sigma-Aldrich Co. Ltd, St. Louis, MO, USA) dissolved in drinking water were given ad libitum to male C57BL/6 mice for 14 consecutive days (days 1–14). The drinking solution was renewed every 2 days.

Experiment 1 (Fig. 1a): Water alone or water containing the antibiotic cocktail was given to mice on days 1–14. Subsequently, mice were divided into four groups: water + FMT from control (no CSDS-susceptible) mice, water + FMT from CSDS-susceptible mice, antibiotic cocktail + FMT from control (no CSDS-susceptible) mice, and antibiotic cocktail + FMT from CSDS-susceptible mice. The fecal microbiota from CSDS-susceptible or control (no CSDS-susceptible) mice was administered orally from day 15 to day 28. On day 29, fecal samples were collected. The 1% SPT was performed on day 30. Blood samples were collected from the heart under isoflurane anesthesia and placed into a tube containing ethylenediamine-N,N,N',N
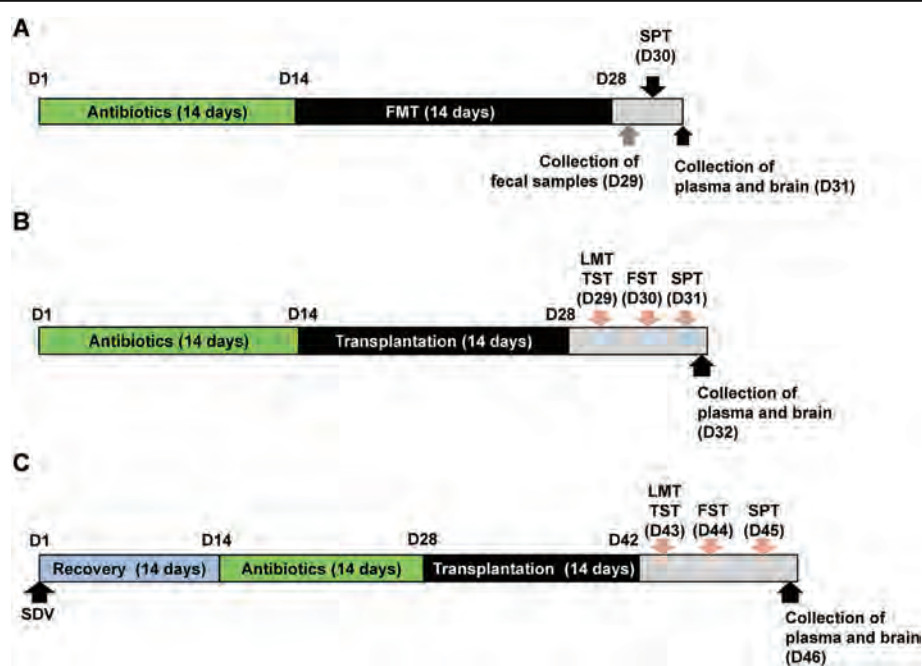

Fig. 1 The schedule of the experiments. **a** The schedule of treatment of antibiotic cocktail, fecal microbiota transplantation (FMT), collection of fecal samples, sucrose preference test (SPT), and collection of the plasma and brain. Antibiotic cocktail or water in drinking water was given to adult male mice for 14 days (day 1–day 14). Subsequently, FMT from CSDS-susceptible mice or control (no CSDS) mice was performed for 14 days (day 15–day 28). On day 29, fecal samples were collected. On day 30, 1% SPT was performed. On day 31, the plasma and brain (i.e., PFC) were collected. **b** The schedule of treatment of antibiotic cocktail, microbiota transplantation, collection of fecal samples, behavioral tests, and collection of the plasma and brain. Antibiotic cocktail or water in drinking water was given to adult male mice for 14 days (day 1–day 14). Subsequently, two bacteria (*L. intestinalis* and *L. reuteri*) were administered orally for 14 days (day 15–day 28) using gastric gavage. On day 29, locomotion test (LMT) and tail suspension test (TST) were performed. Forced swimming test (FST) and 1% SPT were performed on days 30 and 31, respectively. On day 32, the plasma and brain were collected. **c** The schedule of subdiaphragmatic vagotomy (SDV), treatment of antibiotic cocktail, microbiota transplantation, behavioral tests, and collection of the plasma and brain. SDV or sham was performed in adult male mice, and mice were recovered 14 days after surgery (day 1–day 14). Subsequently, an antibiotic cocktail or water in drinking water was given to all mice for 14 days (day 15–day 28). Subsequently, transplantation of two microbiota was performed for 14 days (day 29–day 42). On day 43, LMT and TST were performed. FST and 1% SPT were performed on day 44 and day 45, respectively. On day 46, the plasma and brain were collected

´-tetraacetic acid potassium salt dehydrate as an anti-coagulant. Subsequently, blood samples were centrifuged (3000×*g*, 3 min) to prepare plasma samples. The plasma samples were stored at − 80 °C until assay. The brain region such as PFC was dissected from the brain on ice and stored at − 80 °C until use.

Experiment 2 (Fig. 1b): Mice were given drinking water alone or drinking water containing the antibiotic cocktail on days 1–14. Subsequently, mice were divided into three groups: water + water, antibiotic cocktail + water, and antibiotic cocktail + microbe (*L. intestinalis* and *L. reuteri*) groups. *L. intestinalis* (catalog number: JCM7548) and *L. reuteri* (catalog number: JCM1112) were purchased from RIKEN BioResource Research Center (Tsukuba, Ibaraki, Japan). Mice were orally administered water or water containing the microbes (approximately 1×10^8 CFU/day) for 14 days (days 15–28) using gastric gavage. The locomotion test and tail suspension test (TST) were performed on day 29. The forced swimming test (FST) and 1% SPT were performed on days 30 and 31, respectively. On day 32, plasma samples and PFC samples were collected as described above and stored at − 80 °C until use.

Experiment 3 (Fig. 1c): Sham surgery or subdiaphragmatic vagotomy (SDV) was performed under anesthesia with 5% isoflurane. Mice were put under a microscope (Leica LEICA S9E, Germany), and hair was removed from the abdomen [38]. The esophagus of each mouse was exposed to the full view. The ventral and dorsal vagus nerves of the esophagus were severed. After the muscle and skin were sutured, mice were kept in clean cages until complete recovery from anesthesia. Then, mice were housed in cages for 14 days (days 1–14). The antibiotic cocktail was given to all mice in drinking water for 14 days (from day 15 to day 28). Subsequently, mice were divided into four groups: sham + water, SDV + water, SDV + microbe (*L. intestinalis* and *L. reuteri*), and sham + microbe (*L. intestinalis* and *L. reuteri*) groups. Water alone or water containing the microbes (approximately 1×10^8 CFU/day) was administered orally for 14 days (day 29 to day 42) using gastric gavage. The locomotion test and TST were performed on day 43. The FST and 1% SPT were performed on days 44 and 45, respectively. On day 46, plasma samples and PFC tissues were collected and stored at − 80 °C until use.

Behavioral tests

Behavioral tests, including the locomotion test, TST, FST, and 1% SPT, were performed as previously reported [15, 17–19, 33–37].

Locomotion: Locomotor activity was measured using a SCANETMV-40 animal movement analysis system (MELQUEST Co., Ltd., Toyama, Japan). The animals were placed in experimental cages ($560 \times 560 \times 330$ mm^3).

Cumulative exercise was recorded for 60 min. The cages were cleaned after each testing session.

TST: A small piece of adhesive tape was placed approximately 2 cm from the tip of the tail of each mouse. A single hole was punched in the tape, and mice were hung individually on a hook. The immobility time was recorded for 10 min. Mice were considered immobile only when they hung passively and completely motionless.

FST: The FST was conducted using an automated forced-swim apparatus (SCANET MV-40; MELQUEST Co., Ltd.). Mice were placed individually in a cylinder (23×31 cm^2) containing 15 cm of water maintained at a temperature of 23 ± 1 °C. The immobility time was calculated using the activity time as total time − active time by the apparatus analysis software. The immobility time of each mouse was recorded for a period of 6 min.

SPT: Mice were exposed to water and 1% sucrose solution for 48 h, followed by 4 h of water and food deprivation and a 1-h exposure to two identical bottles (water and 1% sucrose solution). The bottles containing water and sucrose were weighed before and at the end of this period. The sucrose preference was calculated as a percentage of sucrose solution consumption to the total liquid consumption.

Measurement of the inflammatory cytokine IL-6

Plasma levels of IL-6 were measured because we previously identified an increase in blood IL-6 levels in the CSDS model [15, 18]. Plasma IL-6 levels were measured using an ELISA kit (cat#: 88-7064-22 Invitrogen, Carlsbad, CA, USA) according to the manufacturer's instructions.

Western blot analysis

PFC tissues were homogenized in the Laemmli lysis buffer. Aliquots (60 µg) of protein were measured using a DC protein assay kit (Bio-Rad, Hercules, CA, USA); incubated for 5 min at 95 °C with a quarter volume of 125 mM Tris-HCl, pH 6.8, 20% glycerol, 0.1% bromophenol blue, 10% β-mercaptoethanol, and 4% sodium dodecyl sulfate; and subjected to sodium dodecyl sulfate-polyacrylamide gel electrophoresis using mini-gels (catalog #: 4568126, Mini-PROTEAN TGX™ Stain-Free Gel; Bio-Rad). Proteins were transferred onto polyvinylidene difluoride membranes using a Trans-Blot Mini Cell (Bio-Rad). For immunodetection, the blots were blocked with 2% bovine serum albumin in TBS + 0.1% Tween-20 (TBST) for 1 h at room temperature and incubated with a primary antibody against GluA1 (catalog number: ab31232, 1 µg/mL, Abcam, Cambridge, MA, USA) and β-actin (catalog number: A5441 1:10,000; Sigma-Aldrich) overnight at 4 °C. The next day, blots were washed three times in TBST and incubated with horseradish peroxidase-conjugated anti-rabbit antibody (catalog number: NA934, GE Healthcare) and anti-mouse

Wang *et al. Journal of Neuroinflammation*   (2020) 17:241

Page 5 of 12

antibody (catalog number: NA931, GE Healthcare) for 1 h at room temperature. After three final washes with TBST, bands were detected using enhanced chemiluminescence plus a Western Blotting Detection system (GE Healthcare Bioscience). The blots then were incubated in stripping buffer (2% sodium dodecyl sulfate, 100 mM β-mercaptoethanol, and 62.5 mM Tris-HCl, pH 6.8) for 30 min at 60 °C and then washed three times with TBST. The stripped blots were kept in the blocking solution for 1 h and incubated with primary antibody directed against PSD-95 (catalog number: 51-6900, 1 μg/mL, Invitrogen). Images were captured using a ChemiDoc™ Touch Imaging System (170-01401; Bio-Rad Laboratories, Hercules, CA), and immunoreactive bands were quantified.

16S rRNA analysis and short-chain fatty acids
16S rRNA analysis of fecal samples was performed by MyMetagenome Co., Ltd. (Tokyo, Japan) as previously reported [15]. Measurement of short-chain fatty acids (i.e., acetic acid, propionic acid, butyric acid, lactic acid, and succinic acid) in fecal samples was performed at TechnoSuruga Laboratory, Co., Ltd. (Shizuoka, Japan) as previously reported [14, 15].

Statistical analysis
The data are presented as the mean ± standard error of the mean (S.E.M.). Analysis was performed using PASW Statistics 20 (formerly SPSS statistics; SPSS, Tokyo, Japan). Comparisons between groups were performed via two-way analysis of variance (ANOVA) or one-way ANOVA, followed by post hoc Fisher's least significant difference (LSD) test. The data for body weight were analyzed using repeated-measures two-way ANOVA, followed by post hoc Fisher LSD test. $P < 0.05$ was considered statistically significant.

Results
FMT from CSDS-susceptible mice and control (no CSDS) mice
The first experiment examined the effects of FMT from CSDS-susceptible mice (Fig. 1a). Treatment with an antibiotic cocktail significantly decreased the body weight of the mice (Fig. 2a). Meanwhile, FMT did not result in body weight changes in CSDS-susceptible mice (Fig. 2a). In the 1% SPT, FMT from CSDS-susceptible mice caused significant reductions in sucrose preference in antibiotic-treated mice but not in water-treated mice
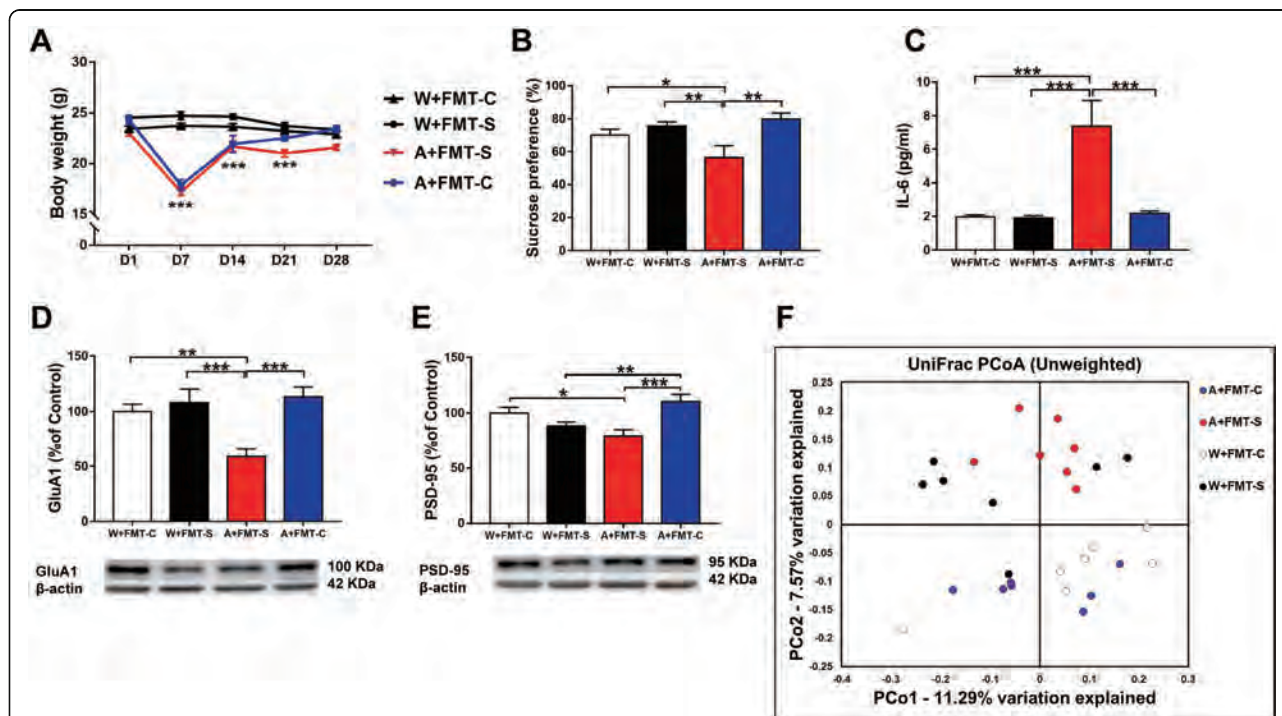

Fig. 2 Effects of FMT in antibiotic-treated and water-treated mice. **a** Body weight (repeated measure two-way ANOVA, antibiotic: $F_{1,24} = 38.007$, $P < 0.001$; FMT: $F_{1,24} = 0.667$, $P = 0.422$; interaction: $F_{1,24} = 2.282$, $P = 0.144$). **b** SPT (two-way ANOVA, antibiotic: $F_{1,24} = 1.021$, $P = 0.322$; FMT: $F_{1,24} = 3.722$, $P = 0.066$; interaction: $F_{1,24} = 9.757$, $P = 0.005$). **c** Plasma IL-6 (two-way ANOVA, antibiotic: $F_{1,24} = 13.300$, $P = 0.001$; FMT: $F_{1,24} = 10.919$, $P = 0.003$; interaction: $F_{1,24} = 11.393$, $P = 0.003$). **d** GluA1 (two-way ANOVA, antibiotic: $F_{1,24} = 3.833$, $P = 0.062$; FMT: $F_{1,24} = 6.437$, $P = 0.018$; interaction: $F_{1,24} = 11.657$, $P = 0.002$). **e** PSD-95 (two-way ANOVA, antibiotics: $F_{1,24} = 0.014$, $P = 0.908$; FMT: $F_{1,24} = 15.604$, $P = 0.001$; interaction: $F_{1,24} = 3.284$, $P = 0.082$). **f** PCoA analysis of gut microbiota data. Data are shown as mean ± S.E.M. ($n = 7$). *$P < 0.05$, **$P < 0.01$, ***$P < 0.001$. FMT fecal microbiota transplantation, NS not significant, W + FMT-C water + FMT from control (no CSDS) mice, W + FMT-S water + FMT from CSDS-susceptible mice, A + FMT-S antibiotic + FMT from CSDS-susceptible mice, A + FMT-C antibiotic + FMT from control (no CSDS) mice

Wang *et al. Journal of Neuroinflammation* (2020) 17:241

Page 6 of 12

(Fig. 2b). In contrast, FMT from control (no CSDS) mice did not cause significant reductions in sucrose preference in antibiotic-treated and water-treated mice (Fig. 2b). Among CSDS-susceptible mice, FMT resulted in significant increases in plasma IL-6 levels in the antibiotic-treated group but not in the water-treated group (Fig. 2c). Furthermore, FMT from CSDS-susceptible mice significantly decreased PSD-95 and GluA1 expression in the PFC in the antibiotic-treated group but not in the water-treated group (Fig. 2d, e).

Analysis of 16S rRNA was used to identify differences in the composition of the gastrointestinal microbiota among the four groups. Unweighted UniFrac-based principal coordinate analysis (PCoA) revealed significant differences among the four groups (Fig. 2f). *Firmicutes* and *Bacteroidetes* were the most abundant phyla in all groups (Figure S1A). At the phylum level, *Verrucomicrobia* was present at significantly high levels in the antibiotic + FMT group than in the water-treated groups (Figure S1B). Four genera of bacteria (*Akkermansia*, *Alistipes*, *Candidatus Arthromitus*, and *Parabacteroides*) were present at different levels among the four groups (Figure S2). At the species level, five bacteria (*Clostridium cocleatum*, *Akkermansia muciniphila*, *Lactobacillus intestinalis*, *Candidatus Arthromitus* sp. SFB-mouse, and *Lactobacillus reuteri*) were present at different levels among the four groups (Fig. 3). There were no differences in short-chain fatty acid levels

(i.e., acetic acid, butyric acid, lactic acid, succinic acid, propionic acid) among the four groups (Figure S3). However, there was a positive correlation ($r = 0.397$, $P = 0.045$) between the presence of *L. intestinalis* and succinic acid levels in all groups (Figure S3).

Overall, FMT from CSDS-susceptible mice induced an anhedonia-like phenotype, inflammation, and downregulation of synaptic proteins in the PFC in the antibiotic-treated group. Among these bacteria, *L. intestinalis* and *L. reuteri* may be involved in the anhedonia-like phenotype, upregulation of IL-6, and downregulation of synaptic proteins in the PFC after FMT from CSDS-susceptible mice.

Oral administration of *L. intestinalis* and *L. reuteri* in antibiotic-treated mice

Next, we investigated whether two microbes (*L. intestinalis* and *L. reuteri*) could induce depression-like and anhedonia-like phenotypes in mice treated with an antibiotic cocktail (Fig. 1b). Treatment with an antibiotic cocktail significantly decreased the body weight of mice (Fig. 4a). Ingestion of the two microbes did not alter body weight in antibiotic-treated mice (Fig. 4a). There were no changes in locomotion among the three groups (Fig. 4b). The immobility times in the antibiotic + microbe group as determined using the TST and FST were significantly higher than those in the control and


Fig. 3 Altered composition in the gut microbiota at the species level. **a** The relative abundances of species in fecal samples of the four groups 24 h after the final FMT. **b** *Akkermansia muciniphila* (two-way ANOVA, antibiotic: $F_{1,24} = 6.721$, $P = 0.016$; FMT: $F_{1,24} = 0.107$, $P = 0.746$; interaction: $F_{1,24} = 0.963$, $P = 0.336$). **c** *[Clostridium] cocleatum* (two-way ANOVA, antibiotic: $F_{1,24} = 6.153$, $P = 0.021$; FMT: $F_{1,24} = 2.733$, $P = 0.111$; interaction: $F_{1,24} = 16.133$, $P = 0.001$). **d** *Lactobacillus intestinalis* (two-way ANOVA, antibiotic: $F_{1,24} = 1.753$, $P = 0.198$; FMT: $F_{1,24} = 1.830$, $P = 0.189$; interaction: $F_{1,24} = 13.700$, $P = 0.001$). **e** *Lactobacillus reuteri* (two-way ANOVA, antibiotic: $F_{1,24} = 0.298$, $P = 0.590$; FMT: $F_{1,24} = 1.154$, $P = 0.293$; interaction: $F_{1,24} = 6.966$, $P = 0.014$). Data are shown as mean ± S.E.M. ($n = 7$). *$P < 0.05$, **$P < 0.01$, ***$P < 0.001$. FMT fecal microbiota transplantation, NS not significant, W + FMT-C water + FMT from control (no CSDS) mice, W + FMT-S water + FMT from CSDS-susceptible mice, A + FMT-S antibiotic + FMT from CSDS-susceptible mice, A + FMT-C antibiotic + FMT from control (no CSDS) mice

Fig. 4 Effects of *L. intestinalis* and *L. reuteri* in the antibiotic-treated mice. **a** Body weight (repeated measure two-way ANOVA, antibiotic: $F_{1,27}$ = 9.281, P = 0.005; transplantation: $F_{1,27}$ = 1.284, P = 0.267). **b** Locomotion (LMT) (one-way ANOVA, $F_{2,27}$ = 0.533, P = 0.593). **c** TST (one-way ANOVA, $F_{2,27}$ = 9.695, P = 0.001). **d** FST (one-way ANOVA, $F_{2,27}$ = 10.749, P < 0.001). **e** SPT (one-way ANOVA, $F_{2,27}$ = 8.214, P = 0.002). **f** Plasma IL-6 (one-way ANOVA, $F_{2,27}$ = 2.775, P = 0.080). **g** GluA1 (one-way ANOVA, $F_{2,27}$ = 15.481, P < 0.001). **h** PSD-95 (one-way ANOVA, $F_{2,27}$ = 9.185, P = 0.001). Data are shown as mean ± S.E.M. (n = 10). *P < 0.05, **P < 0.01, ***P < 0.001. NS not significant, W + W water + water-treated mice, A + W antibiotic + water-treated mice, A + M antibiotic + microbiota transplantation

antibiotic + water groups (Fig. 4c, d). Furthermore, the sucrose preference in the antibiotic + microbe group was significantly lower than that in the control and antibiotic + water groups (Fig. 4e). Moreover, the expression of synaptic proteins (i.e., GluA1 and PSD-95) in the PFC was significantly lower in the antibiotic + microbe group than in the control and antibiotic + water groups (Fig. 4g, h). In addition, the blood levels of IL-6 were significantly higher in the antibiotic + microbe group than in the control and antibiotic + water groups (Fig. 4f).

Next, we performed 16S rRNA analysis of fecal samples after transplantation of the two microbes. There were significant differences in the examined species indices among the three groups (Fig. 5a). The Chao1 and abundance-based coverage estimator (ACE) indices are used to evaluate the α-diversity of the gastrointestinal microbiota. These indices were significantly different among the three groups (Fig. 5b, c). Interestingly, the transplantation of the two microbes decreased the Chao1 and ACE indices. In unweighted UniFrac-based PCoA, dots representing the antibiotic + microbe group were far from those representing the other two groups (Fig. 5d).

These data suggest that oral administration of these two bacteria for 14 days induced depression- and anhedonia-like phenotypes, inflammation, and synaptic protein downregulation in the PFC in mice treated with an antibiotic cocktail.

Effects of SDV on behavioral abnormalities, inflammation, and decreased expression of synaptic proteins in the PFC of antibiotic-treated mice after ingestion of *L. intestinalis* and *L. reuteri*

We investigated the effects of SDV on abnormal behaviors and inflammation in antibiotic-treated mice after the ingestion of *L. intestinalis* and *L. reuteri* (Fig. 1c). Body weight was not significantly different between before and 14 days after SDV (Fig. 6a). Treatment with an antibiotic cocktail significantly decreased body weight in the sham-treated groups (sham + water and sham + microbes) but not in SDV-treated groups (SDV + water and SDV + microbes) on day 21 (Fig. 6a). There were no changes in body weight from day 28 to day 42 (Fig. 6a). There were no changes in locomotion among the four groups (Fig. 6b). The immobility times in the SDV + microbe group as
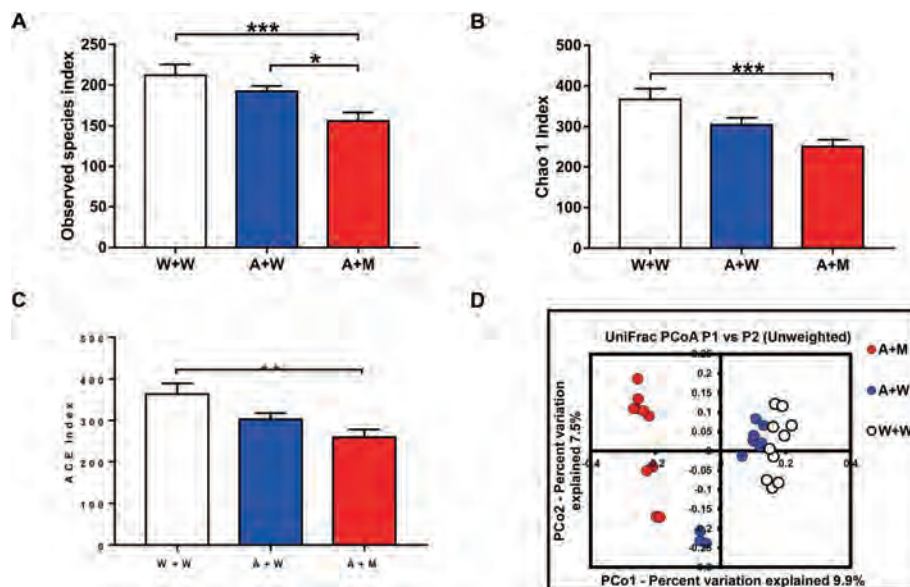
Fig. 5 Effects of transplantation of *L. intestinalis* and *L. reuteri* in the antibiotic-treated mice. **a** Observed species index (one-way ANOVA, $F_{2,27} = 7.381$, $P = 0.003$). **b** Chao 1 index (one-way ANOVA, $F_{2,27} = 7.811$, $P = 0.002$). **c** ACE index (one-way ANOVA, $F_{2,27} = 6.642$, $P = 0.005$). **d** PCoA analysis of gut bacteria data. Data are shown as mean ± S.E.M. ($n = 10$). *$P < 0.05$, ***$P < 0.001$. NS not significant

determined using the TST and FST were significantly lower than those in the sham + microbe group (Fig. 6c, d). Furthermore, the sucrose preference was significantly higher in the SDV + microbe group than in the sham + microbe group (Fig. 6e). Moreover, GluA1 and PSD-95 expression in the PFC was significantly higher in the SDV + microbe group than in the sham + microbe group (Fig. 6g, h). Conversely, IL-6 blood levels were significantly lower in the SDV + microbe group than in the sham + microbe group (Fig. 6f).

These data suggest that SDV blocked the development of depression- and anhedonia-like phenotypes, inflammation, and synaptic protein downregulation in the PFC in antibiotic-treated mice after the ingestion of *L. intestinalis* and *L. reuteri*.

Discussion

The major findings of this study were as follows. First, FMT from CSDS-susceptible mice caused an anhedonia-like phenotype, inflammation, and synaptic protein downregulation in the PFC among those treated with antibiotics but not those treated with water. Thus, antibiotic-induced microbiota depletion in the host is essential for the development of FMT-induced behavioral and biochemical changes in recipient mice. 16S rRNA analysis suggested that among antibiotic-treated mice, *L. intestinalis* and *L. reuteri* counts were higher in the FMT group from CSDS-susceptible mice than in the FMT group from control mice, suggesting that these two bacteria may play a role in the anhedonia-like phenotype, inflammation, and reduction of

synaptic protein expression in the PFC. Second, ingestion of *L. intestinalis* and *L. reuteri* for 14 days induced depression- and anhedonia-like phenotypes, inflammation, and synaptic protein downregulation in the PFC among antibiotic-treated mice. In unweighted UniFrac PCoA, dots representing the antibiotic + microbe group were distantly separated from dots representing the two water groups. Transplantation of the two microbes caused significant changes in the diversity and composition of the host gastrointestinal microbiota. Third, SDV significantly attenuated the depression- and anhedonia-like phenotypes, inflammation, and downregulation of synaptic proteins in the PFC in antibiotic-treated mice after the repeated ingestion of *L. intestinalis* and *L. reuteri*, suggesting a key role of the vagus nerve in the behavioral abnormalities and inflammation induced by oral administration of these two bacteria. Collectively, it is likely that *L. intestinalis* and *L. reuteri* produces depression-like and anhedonia-like phenotypes in antibiotic-treated mice through the brain–gut–microbiota axis via the vagus nerve.

In this study, we found that fecal microbes isolated from CSDS-susceptible mice did not induce anhedonia-like phenotypes, increased plasma IL-6 production, and reduced synaptic protein expression in the PFC in water-treated mice, whereas such changes were induced by these microbes in antibiotic-treated mice. Thus, antibiotic-induced microbiome depletion is necessary for the anhedonia-like phenotype and biochemical changes in recipient mice after FMT.

Fig. 6 Effects of SDV on behavioral abnormalities after transplantation of *L. intestinalis* and *L. reuteri* in the antibiotic-treated mice. **a** Body weight (repeated measure two-way ANOVA, SDV: $F_{1,28} = 8.910$, $P = 0.006$; microbiota transplantation: $F_{1,28} = 0.317$, $P = 0.578$; interaction: $F_{1,28} = 1.713$, $P = 0.201$). **b** Locomotion (two-way ANOVA, SDV: $F_{1,28} = 1.716$, $P = 0.201$; microbiota transplantation: $F_{1,28} = 0.015$, $P = 0.905$; interaction: $F_{1,28} = 1.649$, $P = 0.210$). **c** TST (two-way ANOVA, SDV: $F_{1,28} = 9.916$, $P = 0.004$; microbiota transplantation: $F_{1,28} = 25.222$, $P < 0.001$; interaction: $F_{1,28} = 10.069$, $P = 0.004$). **d** FST (two-way ANOVA, SDV: $F_{1,28} = 10.181$, $P = 0.003$; microbiota transplantation: $F_{1,28} = 4.893$, $P = 0.035$; interaction: $F_{1,28} = 6.957$, $P = 0.013$). **e** SPT (two-way ANOVA, SDV: $F_{1,28} = 4.820$, $P = 0.037$; microbiota transplantation: $F_{1,28} = 19.414$, $P < 0.001$; interaction: $F_{1,28} = 5.943$, $P = 0.021$). **f** Plasma IL-6 (two-way ANOVA, SDV: $F_{1,28} = 64.671$, $P < 0.001$; microbiota transplantation: $F_{1,28} = 92.048$, $P < 0.001$; interaction: $F_{1,28} = 57.921$, $P < 0.001$). **g** GluA1 (two-way ANOVA, SDV: $F_{1,28} = 43.231$, $P < 0.001$; microbiota transplantation: $F_{1,28} = 24.521$, $P < 0.001$; interaction: $F_{1,28} = 2.093$, $P = 0.159$). **h** PSD-95 (two-way ANOVA, SDV: $F_{1,28} = 4.376$, $P = 0.046$; microbiota transplantation: $F_{1,28} = 4.560$, $P = 0.042$; interaction: $F_{1,28} = 1.945$, $P = 0.174$). Data are shown as mean ± S.E.M. ($n = 8$). *$P < 0.05$, **$P < 0.01$, ***$P < 0.001$. NS not significant, sham + W sham + water-treated mice, SDV + W SDV + water-treated mice, SDV + M SDV + microbiota transplantation, sham + M sham + microbiota transplantation

Collectively, FMT in antibiotic-treated mice using "depression-related microbes" obtained from CSDS-susceptible mice resulted in anhedonia-like behaviors and reduced synaptic protein expression in the PFC through systemic inflammation. It is likely that the microbiota in the host gastrointestinal tract of water-treated mice could protect against the effects of FMT using "depression-related microbes" isolated from CSDS-susceptible mice. The mechanisms underlying anhedonia-like phenotypes in antibiotic-treated mice caused by FMT using depression-related microbes are currently unknown. Previously, we reported that CSDS failed to increase plasma IL-6 levels and the expression of synaptic proteins, such as GluA1 and PSD-95, in antibiotic-treated mice, although the same stress increased plasma IL-6 levels and reduced synaptic protein expression in water-treated mice [15]. This study suggests that the host gastrointestinal microbes are necessary for CSDS-induced increases in circulating cytokines and decreased expression of synaptic proteins in the PFC.

In this study, we found that *L. intestinalis* and *L. reuteri* counts were higher in the FMT group from CSDS-susceptible mice than in the FMT group from control (no CSDS) mice, suggesting that these two bacteria play a role in the anhedonia-like phenotype, inflammation, and reduced synaptic protein expression in the PFC. Ingestion of these two microbes for 14 days induced depression- and anhedonia-like phenotypes, increased blood IL-6 levels, and reduced synaptic protein expression in the PFC in antibiotic-treated mice. These data suggest that these two microbes induce depression- and anhedonia-like phenotypes and reduce synaptic protein expression in the PFC of antibiotic-treated mice through systemic inflammation even though these mice were not exposed to stress.

Treatment with a broad-spectrum antibiotic cocktail is known to cause a dramatic loss in the diversity and representation of specific taxa, increase the prevalence of antibiotic-resistant strains, and upregulate antibiotic resistance genes [39, 40]. Furthermore, Yang et al. [13] reported that FMT from anhedonia-susceptible rats into antibiotic-treated mice significantly exaggerated depression-like phenotypes including anhedonia and that FMT from resilient rats into antibiotic-treated mice significantly improved depression-like phenotype including anhedonia. Although the precise mechanisms underlying the abnormal composition of the gastrointestinal microbiota after treatment with an antibiotic cocktail are currently unknown, antibiotic-induced microbiome depletion is essential for behavioral abnormalities in recipients after FMT using microbes from CSDS-susceptible mice.

Previously, we reported that CSDS significantly increased the blood levels of IL-6 in water-treated mice but not in antibiotic-treated mice, suggesting that antibiotic-induced microbiota depletion has anti-inflammatory effects in mice [15]. Furthermore, CSDS significantly decreased the expression of synaptic proteins such as PSD-95 and GluA1 in the PFC in the water-treated group but not in the antibiotic-treated group. These findings suggest that antibiotic-induced microbiome depletion may contribute to stress resilience in mice after CSDS via the brain–gut–microbiome axis [15]. In this study, transplantation of two microbes caused depression- and anhedonia-like phenotypes in antibiotic-treated mice through systemic inflammation. These data suggest that these two microbes facilitate the development of behavioral abnormalities in antibiotic-treated mice, although the precise mechanisms remain unclear. Further detailed study is required to confirm the relationship between these two microbes and antibiotic-induced microbiota depletion in the host gastrointestinal tract.

The crosstalk between the brain and the gastrointestinal microbiota is predominately influenced through various routes including the vagus nerve, immune system, and enteric nervous system [28–32]. It has been demonstrated that the ingestion of *Lactobacillus rhamnosus* reduced stress-induced corticosterone levels and anxiety- and depression-related behaviors in mice and that these neurochemical and behavioral effects were not found in vagotomized mice, suggesting a role of the vagus nerve in the communication between the gastrointestinal microbiome and the brain [41]. The subdiaphragmatic vagus nerve serves as a major modulatory pathway between the brain and gut microbiota. Very recently, we demonstrated that

lipopolysaccharide produces a depression-like phenotype and abnormal composition of gut microbiota via the subdiaphragmatic vagus nerve [38]. In this study, we found that the ingestion of *L. intestinalis* and *L. reuteri* did not induce depression- and anhedonia-like behaviors, increase plasma IL-6 levels, or reduce synaptic protein expression in the PFC in vagotomized mice. Taken all together, it is likely that the subdiaphragmatic vagus nerve plays a key role in behavioral abnormalities in rodents after the transplantation of these two microbes.

L. reuteri is a well-studied probiotic bacterium that can colonize a large number of mammals. It is well recognized that *L. reuteri* has several beneficial effects on anti-microbial activity, the host immune system, and microbial translocation [42]. It is reported that *L. reuteri* can rescue social dysfunction in a mouse model of autism in a vagus nerve-dependent manner [43]. Conversely, we found that ingestion of *L. reuteri* and *L. intestinalis* into antibiotic-treated mice caused depression-like behaviors via systemic inflammation. Thus, *L. reuteri* may have detrimental effects in the host gastrointestinal tract after antibiotic-induced microbiota depletion. Nonetheless, further study is needed to investigate the beneficial and detrimental effects of *L. reuteri* in mammals.

Conclusions

The present study suggests that FMT using microbes from CSDS-susceptible mice induced depression- and anhedonia-like phenotypes in antibiotic-treated mice and that ingestion of *L. intestinalis* and *L. reuteri* caused behavioral and biochemical abnormalities in antibiotic-treated mice via the subdiaphragmatic vagus nerve. It is likely that the brain–gut–microbiota axis plays a role in the pathology of depression via the subdiaphragmatic vagus nerve.

Supplementary information

Supplementary information accompanies this paper at https://doi.org/10.1186/s12974-020-01916-z.

Additional file 1: Figure S1. Altered composition in the gut microbiota at the phylum level. (A): The relative abundances of phylum in fecal samples of the four groups 24 hrs after the final FMT. (B): *Verrucomicrobi* (two-way ANOVA, antibiotic: $F_{1,24} = 6.769$, $P = 0.016$, FMT: $F_{1,24} = 0.128$, $P = 0.724$, interaction: $F_{1,24} = 1.053$, $P = 0.315$). Data are shown as mean ± S.E.M. (n = 7). *$P < 0.05$. FMT: fecal microbiota transplantation. NS: not significant. W + FMT-C: water + FMT from control (no CSDS) mice. W + FMT-S: water + FMT from CSDS susceptible mice. A + FMT-S: antibiotic + FMT from CSDS susceptible mice. A + FMT-C: antibiotic + FMT from control (no CSDS) mice. **Figure S2.** Altered composition in the gut microbiota at the genus level. (A): The relative abundances of genus in fecal samples of the four groups 24 hrs after the final FMT. (B): *Akkermansia* (two-way ANOVA, antibiotic: $F_{1,24} = 6.721$, $P = 0.016$, FMT: $F_{1,24} = 0.107$, $P = 0.746$, interaction: $F_{1,24} = 0.963$, $P = 0.336$). (C): *Alistipes* (two-way ANOVA, antibiotic: $F_{1,24} = 11.641$, $P = 0.002$, FMT: $F_{1,24} = 9.142$, $P = 0.006$,

interaction: $F_{1,24}$ = 3.879, P = 0.061). (D): *Candidatus Arthromitus* (two-way ANOVA, antibiotic: $F_{1,24}$ = 1.064, P =0.313, FMT: $F_{1,24}$ = 5.899, P = 0.023, interaction: $F_{1,24}$ = 1.356, P = 0.256). (E): *Parabacteroides* (two-way ANOVA, antibiotic: $F_{1,24}$ = 0.665, P =0.423, FMT: $F_{1,24}$ = 9.407, P = 0.005, interaction: $F_{1,24}$ = 3.961, P = 0.058). Data are shown as mean ± S.E.M. (n = 7). *P< 0.05, **P < 0.01. FMT: fecal microbiota transplantation. NS: not significant. W + FMT-C: water + FMT from control (no CSDS) mice. W + FMT-S: water + FMT from CSDS susceptible mice. A + FMT-S: antibiotic + FMT from CSDS susceptible mice. A + FMT-C: antibiotic + FMT from control (no CSDS) mice. **Figure S3.** Levels of short-chain fatty acids in fecal samples and correlation with microbiota. (A): Acetic acid (two-way ANOVA, antibiotics: $F_{1,24}$ = 0.170, P =0.684, FMT: $F_{1,24}$ =1.028, P =0.321, interaction: $F_{1,24}$ =0.170, P =0.683) among the four groups. (B): Butyric acid (two-way ANOVA, antibiotics: $F_{1,23}$ = 0.831, P =0.372, FMT: $F_{1,23}$ =0.497, P =0.488, interaction: $F_{1,23}$=0.122, P =0.730) among the four groups. (C): Lactic acid (two-way ANOVA, antibiotics: $F_{1,23}$ = 0.248, P =0.623, FMT: $F_{1,23}$ =0.038, P =0.847, interaction: $F_{1,23}$=0.782, P =0.386) among the four groups. (D): Succinic acid (two-way ANOVA, antibiotics: $F_{1,23}$ = 0.511, P =0.482, FMT: $F_{1,23}$ = 0.970, P =0.355, interaction: $F_{1,23}$=2.053, P =0.165) among the four groups. (E): Propionic acid (two-way ANOVA, antibiotics: $F_{1,24}$ = 0.095, P =0.761, FMT: $F_{1,24}$ =0.003, P =0.959, interaction: $F_{1,24}$ =1.325, P =0.261) among the four groups. (F): There is a positive correlation (r = 0.397, P = 0.045) between succinic acid and *L. intestinalis* in fecal samples. The data are shown as mean ± S.E.M. (n = 7). FMT: fecal microbiota transplantation. NS: not significant.

Abbreviations
ACE: Abundance-based coverage estimator; ANOVA: Analysis of variance; CSDS: Chronic social defeat stress; FMT: Fecal microbiome transplantation; FST: Forced swimming test; GluA1: α-Amino-3-hydroxy-5-methyl-4-isoxazolepropionic acid receptor A1; IL-6: Interleukin-6; PCoA: Principal coordinate analysis; PFC: Prefrontal cortex; PSD-95: Postsynaptic density 95; SDV: Subdiaphragmatic vagotomy; SPT: Sucrose preference test; TBST: Tris buffer saline with 0.1% Tween-20; TST: Tail suspension test

Authors' contributions
KH conceived and designed the study. SW, TI, JZ, YQ, LC, YP, YF, YT, and XW performed the experiments. SW analyzed the data. SW and KH drafted a significant portion of the manuscript. All authors read and approved the final manuscript.

Availability of data and materials
The data during the current study are available from the corresponding author upon reasonable request.

Ethics approval
The protocol of this study was approved by the Chiba University Institutional Animal Care and Use Committee (permission number: 30-399 and 1-456).

Consent for publication
Not applicable

Competing interests
Dr. Hashimoto has received research support from Dainippon-Sumitomo, Otsuka, and Taisho. The other authors report no biomedical financial interests or potential conflicts of interest.

References
1. Dinan TG, Cryan JF. Brain-gut-microbiota axis and mental health. Psychosom Med. 2017;79:920–6.
2. Kelly JR, Clarke G, Cryan JF, Dinan TG. Brain-gut-microbiota axis: challenges for translation in psychiatry. Ann Epidemiol. 2016;26:366–72.
3. Fung TC, Olson CA, Hsiao EY. Interactions between the microbiota, immune and nervous systems in health and disease. Nat Neurosci. 2017;20:145–55.
4. Cussotto S, Clarke G, Dinan TG, Cryan JF. Psychotropics and the microbiome: a chamber of secrets. Psychopharmacology. 2019;236:1411–32.
5. Dinan TG, Cryan JF. Gut microbes and depression: still waiting for godot. Brain Behav Immun. 2019;79:1–2.
6. Ma QQ, Xing CS, Long WY, Wang HY, Liu Q, Wang RF. Impact of microbiota on central nervous system and neurological diseases: the gut-brain axis. J Neuroinflammation. 2019;16.
7. Jiang HY, Ling ZX, Zhang YH, Mao HJ, Ma ZP, Yin Y, Wang WH, Tang WX, Tan ZL, Shi JF, et al. Altered fecal microbiota composition in patients with major depressive disorder. Brain Behav Immun. 2015;48:186–94.
8. Wong ML, Inserra A, Lewis MD, Mastronardi CA, Leong L, Choo J, Kentish S, Xie P, Morrison M, Wesselingh SL, et al. Inflammasome signaling affects anxiety- and depressive-like behavior and gut microbiome composition. Mol Psychiatry. 2016;21:797–805.
9. Zheng P, Zeng B, Zhou C, Liu M, Fang Z, Xu X, Zeng L, Chen J, Fan S, Du X, et al. Gut microbiome remodeling induces depressive-like behaviors through a pathway mediated by the host's metabolism. Mol Psychiatry. 2016;21:786–96.
10. Yang C, Fujita Y, Ren Q, Ma M, Dong C, Hashimoto K. *Bifidobacterium* in the gut microbiota confer resilience to chronic social defeat stress in mice. Sci Rep. 2017;7.
11. Huang TT, Lai JB, Du YL, Xu Y, Ruan LM, Hu SH. Current understanding of gut microbiota in mood disorders: an update of human studies. Front Genet. 2019;10.
12. Jianguo L, Xueyang J, Cui W, Changxin W, Xuemei Q. Altered gut metabolome contributes to depression-like behaviors in rats exposed to chronic unpredictable mild stress. Transl Psychiatry. 2019;9:40.
13. Yang C, Fang X, Zhan GF, Huang NN, Li S, Bi JJ, Jiang RY, Yang L, Miao LY, Zhu B, et al. Key role of gut microbiota in anhedonia-like phenotype in rodents with neuropathic pain. Transl Psychiatry. 2019;9:57.
14. Zhang K, Fujita Y, Chang L, Qu Y, Pu Y, Wang S, Shirayama Y, Hashimoto K. Abnormal composition of gut microbiota is associated with resilience versus susceptibility to inescapable electric stress. Transl Psychiatry. 2019;9:231.
15. Wang S, Qu Y, Chang L, Pu Y, Zhang K, Hashimoto K. Antibiotic-induced microbiome depletion is associated with resilience in mice after chronic social defeat stress. J Affect Disord. 2020;260:448–57.
16. Burokas A, Arboleya S, Moloney RD, Peterson VL, Murphy K, Clarke G, Stanton C, Dinan TG, Cryan JF. Targeting the microbiota-gut-brain axis: prebiotics have anxiolytic and antidepressant-like effects and reverse the impact of chronic stress in mice. Biol Psychiatry. 2017;82:472–87.
17. Qu YG, Yang C, Ren Q, Ma M, Dong C, Hashimoto K. Comparison of (R)-ketamine and lanicemine on depression-like phenotype and abnormal composition of gut microbiota in a social defeat stress model. Sci Rep. 2017;7.
18. Zhang JC, Yao W, Dong C, Yang C, Ren Q, Ma M, Hashimoto K. Blockade of interleukin-6 receptor in the periphery promotes rapid and sustained antidepressant actions: a possible role of gut-microbiota-brain axis. Transl Psychiatry. 2017;7.
19. Yang C, Qu YG, Fujita Y, Ren Q, Ma M, Dong C, Hashimoto K. Possible role of the gut microbiota-brain axis in the antidepressant effects of (R)-ketamine in a social defeat stress model. Transl Psychiatry. 2017;7.
20. Huang NN, Hua DY, Zhan GF, Li S, Zhu B, Jiang RY, Yang L, Bi JJ, Xu H, Hashimoto K, et al. Role of *Actinobacteria* and *Coriobacteriia* in the antidepressant effects of ketamine in an inflammation model of depression. Pharmacol Biochem Behav. 2019;176:93–100.
21. Lukic I, Getselter D, Ziv O, Oron O, Reuveni E, Koren O, Elliott E. Antidepressants affect gut microbiota and *Ruminococcus flavefaciens* is able to abolish their effects on depressive-like behavior. Transl Psychiatry. 2019;9.
22. Sampson TR, Debelius JW, Thron T, Janssen S, Shastri GG, Ilhan ZE, Challis C, Schretter CE, Rocha S, Gradinaru V, et al. Gut microbiota regulate motor

deficits and neuroinflammation in a model of Parkinson's disease. Cell. 2016; 167:1469.

23. Zarrinpar A, Chaix A, Xu ZJZ, Chang MW, Marotz CA, Saghatelian A, Knight R, Panda S. Antibiotic-induced microbiome depletion alters metabolic homeostasis by affecting gut signaling and colonic metabolism. Nat Commun. 2018;9.

24. Pu Y, Chang L, Qu Y, Wang S, Zhang K, Hashimoto K. Antibiotic-induced microbiome depletion protects against MPTP-induced dopaminergic neurotoxicity in the brain. Aging (Albany NY). 2019;11:6915–29.

25. Zhan GF, Yang N, Li S, Huang NN, Fang X, Zhang J, Zhu B, Yang L, Yang C, Luo AL. Abnormal gut microbiota composition contributes to cognitive dysfunction in SAMP8 mice. Aging-Us. 2018;10:1257–67.

26. Li N, Lee B, Liu RJ, Banasr M, Dwyer JM, Iwata M, Li XY, Aghajanian G, Duman RS. mTOR-dependent synapse formation underlies the rapid antidepressant effects of NMDA antagonists. Science. 2010;329:959–64.

27. Duman RS, Aghajanian GK. Synaptic dysfunction in depression: potential therapeutic targets. Science. 2012;338:68–72.

28. Forsythe P, Bienenstock J, Kunze WA. Vagal pathways for microbiome-brain-gut axis communication. Microbial Endocrinol. 2014;817:115–33.

29. Bonaz B, Bazin T, Pellissier S. The vagus nerve at the interface of the microbiota-gut-brain axis. Front Neurosci. 2018;12:49.

30. Cawthon CR, de La Serre CB. Gut bacteria interaction with vagal afferents. Brain Res. 2018;1693:134–9.

31. Cryan JF, O'Riordan KJ, Cowan CSM, Sandhu KV, Bastiaanssen TFS, Boehme M, Codagnone MG, Cussotto S, Fulling C, Golubeva AV, et al. The microbiota-gut-brain axis. Physiol Rev. 2019;99:1877–2013.

32. Long-Smith C, O'Riordan KJ, Clarke G, Stanton C, Dinan TG, Cryan JF. Microbiota-gut-brain axis: new therapeutic opportunities. Annu Rev Pharmacol Toxicol. 2020;60:477–502.

33. Yang C, Shirayama Y, Zhang JC, Ren Q, Yao W, Ma M, Dong C, Hashimoto K. R-ketamine: a rapid-onset and sustained antidepressant without psychotomimetic side effects. Transl Psychiatry. 2015;5.

34. Ren Q, Ma M, Ishima T, Morisseau C, Yang J, Wagner KM, Zhang JC, Yang C, Yao W, Dong C, et al. Gene deficiency and pharmacological inhibition of soluble epoxide hydrolase confers resilience to repeated social defeat stress. Proc Natl Acad Sci U S A. 2016;113:E1944–52.

35. Yang C, Ren Q, Qu Y, Zhang JC, Ma M, Dong C, Hashimoto K. Mechanistic target of rapamycin-independent antidepressant effects of (R)-ketamine in a social defeat stress model. Biol Psychiatry. 2018;83:18–28.

36. Yang C, Kobayashi S, Nakao K, Dong C, Han M, Qu Y, Ren Q, Zhang JC, Ma M, Toki H, et al. AMPA receptor activation-independent antidepressant actions of ketamine metabolite (S)-norketamine. Biol Psychiatry. 2018;84: 591–600.

37. Zhang K, Yang C, Chang L, Sakamoto A, Suzuki T, Fujita Y, Qu Y, Wang S, Pu Y, Tan Y, et al. Essential role of microglial transforming growth factor-β1 in antidepressant actions of (*R*)-ketamine and the novel antidepressant TGF-β1. Transl Psychiatry. 2020;10:32.

38. Zhang J, Ma L, Chang L, Pu Y, Qu Y, Hashimoto K, et al. A key role of the subdiaphragmatic vagus nerve in the depression-like phenotype and abnormal composition of gut microbiota in mice after lipopolysaccharide administration. Transl Psychiatry. 2020;10:186.

39. Becattini S, Taur Y, Pamer EG. Antibiotic-induced changes in the intestinal microbiota and disease. Trends Mol Med. 2016;22:458–78.

40. Jernberg C, Lofmark S, Edlund C, Jansson JK. Long-term ecological impacts of antibiotic administration on the human intestinal microbiota. ISME J. 2007;1:56–66.

41. Bravo JA, Forsythe P, Chew MV, Escaravage E, Savignac HM, Dinan TG, Bienenstock J, Cryan JF. Ingestion of *Lactobacillus* strain regulates emotional behavior and central GABA receptor expression in a mouse via the vagus nerve. Proc Natl Acad Sci U S A. 2011;108:16050–5.

42. Mu Q, Tavella VJ, Luo XM. Role of *Lactobacillus reuteri* in human health and diseases. Front Microbiol. 2018;9:757.

43. Sgritta M, Dooling SW, Buffington SA, Momin EN, Francis MB, Britton RA, Costa-Mattioli M. Mechanisms underlying microbial-mediated changes in social behavior in mouse models of autism spectrum disorder. Neuron. 2019;101:246–59 e246.

Publisher's Note

ORIGINAL PAPER

Rapid-acting and long-lasting antidepressant-like action of (*R*)-ketamine in *Nrf2* knock-out mice: a role of TrkB signaling

Youge Qu[1] · Jiajing Shan[1] · Siming Wang[1] · Lijia Chang[1] · Yaoyu Pu[1] · Xingming Wang[1] · Yunfei Tan[1] ·
Masayuki Yamamoto[2] · Kenji Hashimoto[1]

Abstract

The transcription nuclear factor-erythroid factor 2-related factor 2 (*Nrf2*) plays a key role in inflammation that is involved in depression. We previously reported that *Nrf2* knock-out (KO) mice exhibit depression-like phenotypes through systemic inflammation. (*R*)-ketamine, an enantiomer of ketamine, has rapid-acting and long-lasting antidepressant-like effects in rodents. We investigated whether (*R*)-ketamine can produce antidepressant-like effects in *Nrf2* KO mice. Effects of (*R*)-ketamine on the depression-like phenotypes in *Nrf2* KO mice were examined. Furthermore, the role of TrkB in the antidepressant-like actions of (*R*)-ketamine was also examined. In the tail-suspension test (TST) and forced swimming test (FST), (*R*)-ketamine (10 mg/kg) significantly attenuated the increased immobility times of TST and FST in the *Nrf2* KO mice. In the sucrose preference test (SPT), (*R*)-ketamine significantly ameliorated the reduced preference of SPT in *Nrf2* KO mice. Decreased expression of synaptic proteins (i.e., GluA1 and PSD-95) in the medial prefrontal cortex (mPFC) of *Nrf2* KO mice was significantly ameliorated after a single injection of (*R*)-ketamine. Furthermore, the pre-treatment with the TrkB antagonist ANA-12 (0.5 mg/kg) significantly blocked the rapid and long-lasting antidepressant-like effects of (*R*)-ketamine in *Nrf2* KO mice. Furthermore, ANA-12 significantly antagonized the beneficial effects of (*R*)-ketamine on decreased expression of synaptic proteins in the mPFC of *Nrf2* KO mice. These findings suggest that (*R*)-ketamine can produce rapid and long-lasting antidepressant-like actions in *Nrf2* KO mice via TrkB signaling.

Keywords Brain-derived neurotrophic factor · *Nrf2*: (*R*)-ketamine · TrkB

Introduction

Depression, one of the most common mental disorders, has high incidence and prevalence worldwide. Although the precise molecular mechanisms underlying the patho-physiology of depression remain unidentified, accumulating evidence supports inflammatory processes [1–7]. Meta-analysis showed increased blood levels of pro-inflammatory cytokines in depressed patients compared with healthy control subjects [8–10]. Collectively, it seems that inflammation

may play a crucial role in the development of depression [6, 11].

The transcription factor nuclear factor-erythroid 2-derived-like 2 (*Nrf2*) plays a key role in cellular defense against inflammatory events. In addition, it is known that the Keap1-Nrf2 system plays a role in attenuating inflammation-associated events [12–17]. We previously reported that pre-treatment with a potent Nrf2 activator sulforaphane has prophylactic effects in rodent models of depression [18, 19], and that *Nrf2* knock-out (KO) mice have depression-like phenotypes through systemic inflammation [18]. Furthermore, the expressions of the proteins Keap1 and Nrf2 in the parietal cortex from patients with depression were lower than controls [20]. Collectively, abnormalities in the Keap1–Nrf2 system may be involved in the development of depression.

(*R*,*S*)-ketamine has rapid-acting and sustained antidepressant actions in treatment-resistant patients with depression [21–24]. In preclinical studies, (*R*)-ketamine produced

✉ Kenji Hashimoto
hashimoto@faculty.chiba-u.jp

1 Division of Clinical Neuroscience, Chiba University Center for Forensic Mental Health, Chiba 260-8670, Japan

2 Departments of Medical Biochemistry and Respiratory Medicine, Tohoku University Graduate School of Medicine, SendaiMiyagi, Miyagi 980-8575, Japan

 Springer

greater potency and longer-lasting antidepressant-like effects than (*S*)-ketamine [25–29]. Importantly, side effects of (*R*)-ketamine in rodents and monkeys are lower than those of (*R, S*)-ketamine and (*S*)-ketamine [26, 29–33]. In addition, (*R*)-ketamine did not produce psychotomimetic effects in healthy subjects, whereas the same dose of (*S*)-ketamine caused psychotomimetic side effects in healthy control subjects [34]. A recent previous study reported that (*R*)-ketamine produced rapid-acting and sustained antidepressant effects in treatment-resistant patients with depression, and that side effects (i.e., dissociation) after a single infusion of (*R*)-ketamine were very low [35]. Taken together, (*R*)-ketamine would be a safer antidepressant than (*R,S*)-ketamine and (*S*)-ketamine [36–39]. However, there is no report that shows whether (*R*)-ketamine can produce antidepressant-like actions in depression-like phenotypes in *Nrf2* KO mice.

The purpose of this study was to examine whether (*R*)-ketamine can produce antidepressant-like actions in *Nrf2* KO mice. Furthermore, we examined the role of tropomyosin-receptor-kinase B (TrkB) in the antidepressant-like effects of (*R*)-ketamine given that brain-derived neurotrophic factor (BDNF) and its receptor TrkB system play a role in the antidepressant-like actions of ketamine and its enantiomers [26, 36–45].

Methods and materials

Animals

Male adult C57BL/6 mice and male adult *Nrf2* KO mice (*Nrf2*$^{-/-}$) mice [46] were used as reported previously [18]. Mice were housed under controlled temperature conditions in 12 h light/dark cycles (lights on between 07:00 and 19:00), with food and water provided ad libitum. The protocol was approved by the Chiba University Institutional Animal Care and Use Committee (Permission number: 29–316, 30–310, 1–147, and 2–138).

Drugs and treatment

(*R*)-ketamine hydrochloride was prepared as reported previously [25]. ANA-12, N2-(2-{[(2-oxoazepan-3-yl) amino]carbonyl}phenyl)benzo[b] thiophene-2-carboxamide (0.5 mg/kg, Sigma-Aldrich Co., Ltd., Tokyo, Japan), was dissolved in 17% dimethylsulfoxide (DMSO) in physiological saline [47]. The dose of (*R*)-ketamine (10 mg/kg) and ANA-12 (0.5 mg/kg) was selected as previously reported [26, 48–50].

Behavioral tests

Behavioral tests including locomotion test (LMT), tail-suspension test (TST), forced swimming test (FST), and

1% sucrose preference test (SPT) were performed as previously reported [26, 51]. For LMT, the animals were placed individually in the cages (length × width × height: 560 × 560 × 330 mm). Locomotor activities of animals were recorded for 60 min by the SCANETMV-40 (MELQUEST Co., Ltd., Toyama, Japan). Cages were cleaned between test sessions.

A small piece of adhesive tape of TST was placed at approximately 2 cm from the tip of the mouse tail. A single hole was punched in the tape and mice were hung individually on a hook. The immobility time of each mouse was recorded over a period of 10 min. Immobility time will be counted only when the mice hung passively and completely motionless.

For FST, the animals were placed individually in a cylinder (diameter: 23 cm; height: 31 cm) which contained 15 cm of water, and the temperature was kept at 23 ± 1 °C. Animals were tested in an automated forced-swim apparatus with SCANETMV-40 (MELQUEST Co., Ltd., Toyama, Japan). Cumulative immobility time was measured for 6 min from the activity time as the (total − active) time with the apparatus analysis software.

For SPT, before confirming the change in the sucrose solution intake, the mice were allowed to ingest the sucrose solution 48 h before the test to adapt the mice to the 1% sucrose solution. Subsequently, food, water and sucrose were removed for 4 h, followed by a preference test that lasted 1 h with 1% sucrose and water delivered from identical bottles. The bottles contained water and sucrose and were weighed prior to and immediately following the test, and determined the preference for sucrose.

Western blot analysis

The brain samples of medial prefrontal cortex (mPFC) from mice were dissected on ice, as previously reported [26, 51]. The tissue was homogenized in Laemmli lysis buffer. Equal amounts of protein (30 μg) were calculated with a DC protein assay kit (Bio-Rad, Hercules, CA, USA), heated for 5 min at 95 °C with a quarter volume of 10% β-mercaptoethanol, 125 mM Tris/HCl, pH of 6.8, 20% glycerol, 4% sodium dodecyl sulfate, and 0.1% bromophenol blue, and were subjected to sodium dodecyl sulfate–polyacrylamide gel electrophoresis using mini-gels (catalog #: 4568126, Mini-PROTEAN TGX™ Stain-Free Gel, Bio-Rad), as previously reported [52]. Proteins were transferred onto polyvinylidene difluoride membranes using a Trans-Blot Mini Cell (Bio-Rad). For immunodetection, the blot was blocked with 2% TBS + 0.1% Tween-20 (TBST) bovine serum albumin for 1 h at room temperature, and then in β-actin (catalog number: A5441 1:10,000, Sigma-Aldrich) overnight, and then it was combined with the anti-GluA1 primary antibody (catalog number: ab31232, 1 μg/ml, at

4 °C overnight. The next day, the blots were washed three times in TBST and incubated with a horseradish oxidase-conjugated anti-mouse antibody (catalog number: NA931, GE Healthcare) and anti-rabbit antibody (catalog number: NA934, GE Healthcare) for 1 h at room temperature. After three final washes with TBST, the bands were detected by the chemiluminescence and Western Blotting detection system (GE Healthcare Biosciences). Then, the blots were incubated in stripping buffer (62.5 mM Tris–HCl, pH 6.8, 100 mM β-mercaptoethanol, and 2% sodium dodecyl sulfate) for 30 min at 60 °C, and then washed three times with TBST. The stripped blots were stored in blocking solution for 1 h and combined with the primary antibody against PSD-95 (catalog number: 51-6900, 1 μg/ml, Invitrogen). A Chemi-Doc TM touch imaging system (170-01401, Bio-Rad Laboratories, Hercules, CA, USA) was used to collect images and quantify immunoreactive bands.

Statistical analysis

The data were shown as the mean ± standard error of the mean (SEM). One-way analysis of variance to analyze

followed the post hoc Fisher's least significant difference (LSD) test was used to analyze the data. P-values less than 0.05 were considered statistically significant.

Results

(*R*)-ketamine showed antidepressant-like effects in Nrf2 KO mice

We previously reported that *Nrf2* KO mice show depression-like phenotypes attributed to systemic inflammation [18]. First, we investigated whether (*R*)-ketamine (10 mg/kg) could cause rapid and long-lasting antidepressant-like effects in *Nrf2* KO mice (Fig. 1a). There were no changes in locomotion among the three groups (Fig. 1b). In the TST and FST, (*R*)-ketamine significantly attenuated the increased immobility times of TST and FST in *Nrf2* KO mice (Fig. 1c, d). In the SPT, (*R*)-ketamine significantly ameliorated the decreased sucrose preference of *Nrf2* KO mice 2, 4, and 6 days after a single injection (Fig. 1e–g). These findings
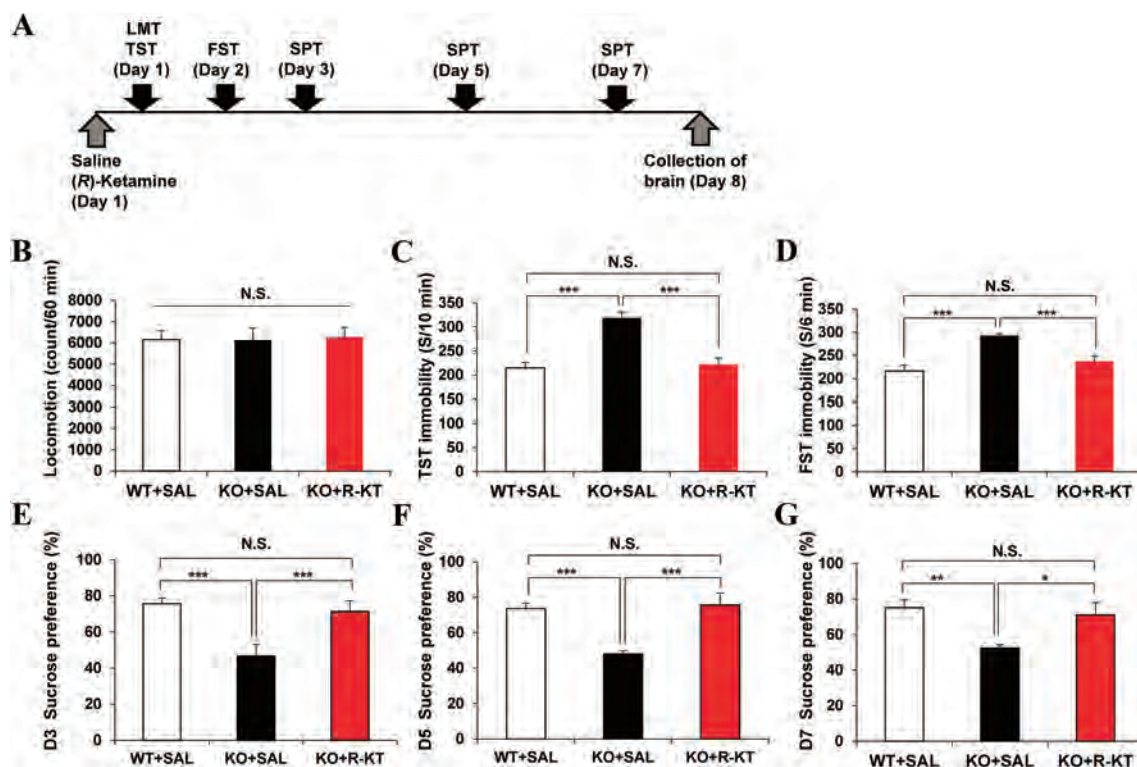
Fig. 1 Effects of (*R*)-ketamine on depression-like phenotypes of *Nrf2* KO mice. **a** Schedule of treatment, behavioral tests, and brain collection. Saline (10 ml/kg) or (*R*)-ketamine (10 mg/kg) was administered i.p. to mice on day 1. Locomotion and TST were performed 1 and 3 h after injection. FST was performed 1 day after injection. 1% SPT was performed 2, 4, and 6 days after injection. **b** Locomotion (LMT): (one-way ANOVA: $F_{2,25} = 0.025$, $P = 0.975$). **c** Tail-suspension test

(TST): (one-way ANOVA: $F_{2,25} = 23.666$, $P < 0.001$). **d** Forced swimming test (FST): (one-way ANOVA: $F_{2,25} = 16.391$, $P < 0.001$). **e** 1% sucrose preference test (SPT): (one-way ANOVA: $F_{2,25} = 12.461$, $P < 0.001$). **f** 1% SPT: (one-way ANOVA: $F_{2,25} = 13.752$, $P < 0.001$). **g** 1% SPT: (one-way ANOVA: $F_{2,25} = 5.503$, $P = 0.010$). Data represent the mean ± S.E.M ($n = 8$–12). *$P < 0.05$, **$P < 0.01$, ***$P < 0.001$ compared with the saline-treated KO group

Springer

show that (*R*)-ketamine produced rapid and long-lasting antidepressant-like effects in *Nrf2* KO mice.

(*R*)-ketamine ameliorated the reduced expression of synaptic proteins in the mPFC from Nrf2 KO mice

We measured the synaptic proteins (GluA1 and PSD-95) in the mouse brain using Western blot analysis. We previously reported that protein levels of GluA1 and PSD-95 in the mPFC of *Nrf2* KO mice were significantly lower than those of WT mice [18]. A single injection of (*R*)-ketamine significantly ameliorated the reduced expressions of GluA1 and PSD-95 in the mPFC from *Nrf2* KO mice (Fig. 2a, b).

ANA-12 blocked antidepressant-like effects of (*R*)-ketamine in Nrf2 KO mice

We previously reported that *Nrf2* KO mice had decreased the BDNF-TrkB signaling in the PFC, and that the TrkB agonist 7,8-dihydroxyfravone yielded antidepressant-like effects in *Nrf2* KO mice [18]. In addition, BDNF-TrkB signaling plays a role in the antidepressant-like effects of ketamine and its enantiomers [26, 40]. Herein, we investigated whether the TrkB antagonist ANA-12 could antagonize the antidepressant-like effects of (*R*)-ketamine in *Nrf2* KO mice (Fig. 3a). There were no changes in locomotion among the five groups (Fig. 3b). In the TST and FST, pre-treatment with ANA-12 significantly antagonized the antidepressant-like effects of (*R*)-ketamine (10 mg/kg) in the *Nrf2* KO mice (Fig. 3c, d). In the SPT, ANA-12 significantly antagonized the anti-anhedonia-like effects of (*R*)-ketamine (10 mg/kg) in *Nrf2* KO mice (Fig. 3e–g). In contrast, a single administration of ANA-12 alone did not affect the depression-like phenotypes in *Nrf2* KO mice (Fig. 3c–g). These findings are consistent with those of a previous report [18]. These findings suggest that the TrkB system plays a role in the rapid-acting and long-lasting antidepressant-like effects of (*R*)-ketamine in *Nrf2* KO mice.

ANA-12 blocked beneficial effects of (*R*)-ketamine on the reduced expression of synaptic proteins in the mPFC from Nrf2 KO mice

Pre-treatment with ANA-12 significantly blocked the beneficial effects of (*R*)-ketamine on reduced expression of GluA1 and PSD-95 in the mPFC of *Nrf2* KO mice (Fig. 4a, b). In contrast, a single injection of ANA-12 alone did not affect the reduced expression of GluA1 and PSD-95 in the mPFC from *Nrf2* KO mice (Fig. 4a, b).

Discussion

Here, we found that (*R*)-ketamine could produce rapid-acting and long-lasting antidepressant-like effects in *Nrf2* KO mice, and that the TrkB antagonist ANA-12 blocked the antidepressant-like effects of (*R*)-ketamine in KO mice. Furthermore, ANA-12 alone did not affect the increased immobility times of TST and FST, and the reduced sucrose preference of SPT in *Nrf2* KO mice, consistent with a previous report [18]. Moreover, we found that (*R*)-ketamine significantly ameliorated the reduced expressions of GluA1 and PSD-95 in the mPFC of *Nrf2* KO mice, and that ANA-12 blocked the beneficial effects of (*R*)-ketamine on the decreased expressions of synaptic proteins in the mPFC of *Nrf2* KO mice. Collectively, the current data suggest that (*R*)-ketamine could produce the rapid action and long-lasting antidepressant effects in *Nrf2* KO mice via TrkB activation.

We previously reported decreased BDNF-TrkB signaling and decreased expressions of synaptic proteins in the mPFC of *Nrf2* KO mice, resulting in the depression-like phenotype of *Nrf2* KO mice [18]. In addition, 7,8-dihydroxyflavone (a TrkB agonist) yielded an antidepressant-like effect in *Nrf2* KO mice [18]. Here, we showed that (*R*)-ketamine significantly ameliorated the reduced expressions of synaptic proteins in the mPFC of *Nrf2* KO mice. Given the role of synaptogenesis in the antidepressant-like actions of ketamine [26, 53–56], it is likely that improvement of synaptic

Fig. 2 Western blot of GluA1 and PSD-95 in the mPFC from WT and *Nrf2* KO mice. **a** GluA1: (one-way ANOVA, $F_{2,23} = 5.329$, $P = 0.013$). **b** PSD-95: (one-way ANOVA, $F_{2,23} = 4.823$, $P = 0.018$). Data represent the mean ± S.E.M ($n = 8$–10). *$P < 0.05$, **$P < 0.01$ compared with the saline-treated KO group
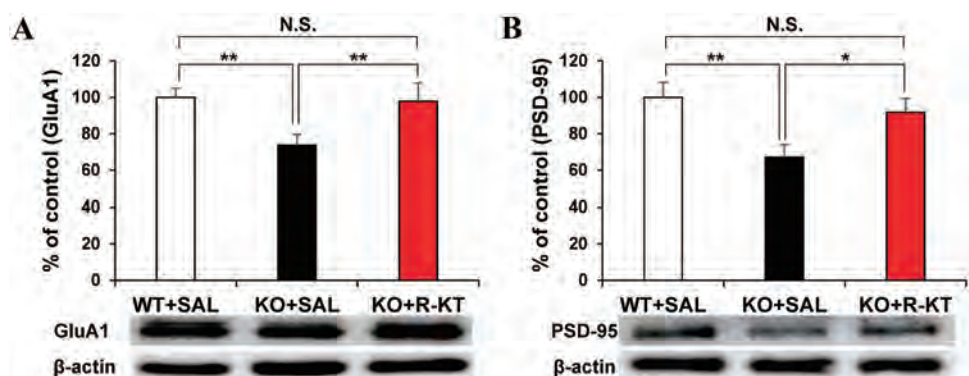
Fig. 3 Effects of ANA-12 on antidepressant-like effect of (*R*)-ketamine in *Nrf2* KO mice. **a** Schedule of treatment, behavioral tests, and brain collection. Vehicle or ANA-12 (0.5 mg/kg) was administered i.p. to mice (day 1). Saline (10 ml/kg) or (*R*)-ketamine (10 mg/kg) was administered i.p. to mice 30 min after injection of vehicle or ANA-12 (day 1). Locomotion and TST were performed 1 and 3 h after injection. FST was performed 1 day after injection. 1% SPT was performed 2, 4, and 6 days after injection. **b** Locomotion (LMT): (one-way ANOVA: $F_{4,53} = 0.148$, $P = 0.963$). **c** Tail-suspension test (TST): (one-way ANOVA: $F_{4,53} = 7.640$, $P < 0.001$). **d** Forced swimming test (FST): (one-way ANOVA: $F_{4,53} = 9.284$, $P < 0.001$). **e** 1% SPT: (one-way ANOVA: $F_{4,53} = 6.838$, $P = 0.001$). **f** 1% SPT: (one-way ANOVA: $F_{4,53} = 17.716$, $P < 0.001$). **g** 1% SPT: (one-way ANOVA: $F_{4,53} = 11.894$, $P < 0.001$). Data represent the mean ± S.E.M ($n = 11$–13). **$P < 0.01$, ***$P < 0.001$. *N.S.* not significance
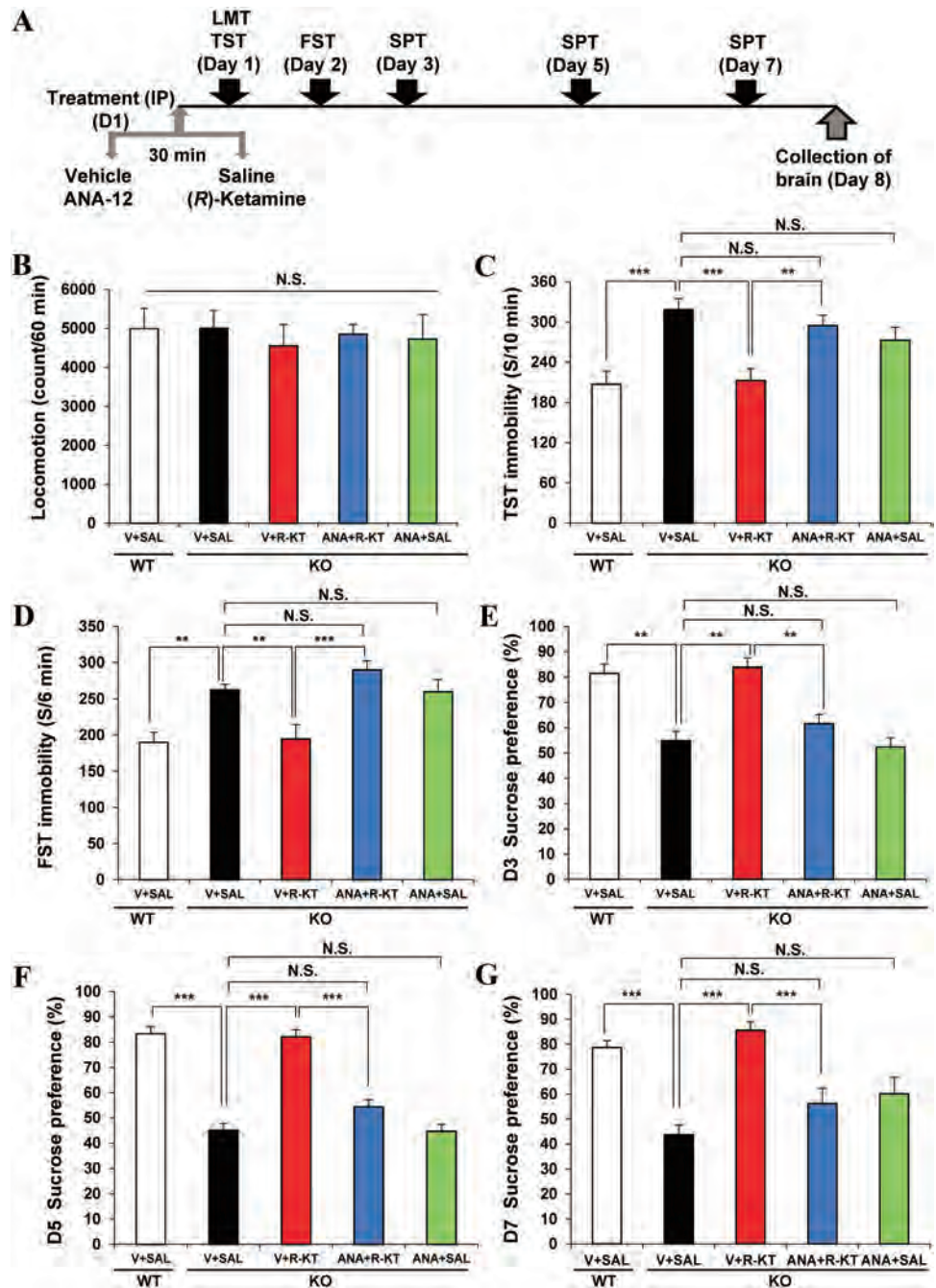
proteins by (*R*)-ketamine may be associated with its rapid and long-lasting antidepressant actions.

The expressions of BDNF in the PFC of rodents with depression-like behaviors were lower than control rodents [26, 48, 50, 55]. Interestingly, a single bilateral infusion of 7,8-dihydroxyflavone into the infralimbic region of mPFC could produce antidepressant-like effects in the learned helplessness model of depression [57], suggesting that decreased expression of BDNF in the mPFC may contribute to the depression-like phenotypes. Thus, it is likely that decreased BDNF-TrkB signaling in the mPFC,

precipitated by a deletion of the *Nrf2* gene may mediate depression behaviors in *Nrf2* KO mice [18]. However, the exact molecular mechanisms underlying reduced BDNF-TrkB signaling in mPFC of *Nrf2* KO mice are unclear. Future study on the role of Nrf2 in BDNF-TrkB signaling in the brain is needed. Here, we also found that (*R*)-ketamine significantly ameliorated the decreased expressions of synaptic proteins in the mPFC of *Nrf2* KO mice through the activation of TrkB. However, the precise mechanisms underlying the activation of BDNF-TrkB signaling in the mPFC of *Nrf2* KO mice by (*R*)-ketamine are unclear.

Fig. 4 Effects of ANA-12 and (*R*)-ketamine on the expression of GluA1 and PSD-95 in the mPFC from WT and *Nrf2* KO mice. **a** GluA1: (one-way ANOVA, $F_{4,52} = 8.500$, $P < 0.001$). **b** PSD-95: (one-way ANOVA, $F_{4,52} = 4.131$, $P = 0.006$). Data represent the mean $\pm$ S.E.M ($n = 10–13$). $*P < 0.05$, $**P < 0.01$, $***P < 0.001$. *N.S.* not significance
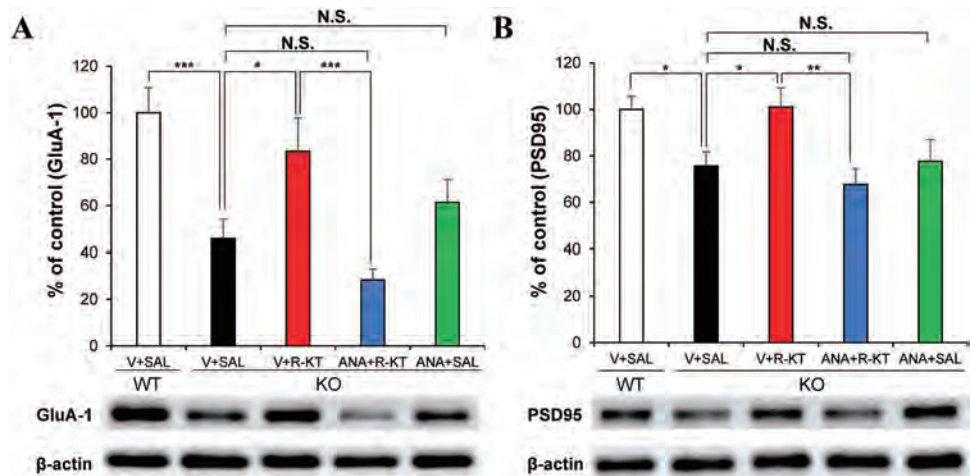
Additional precise studies underlying the crosstalk of *Nrf2* and BDNF-TrkB signaling are also needed.

It is known that the stress or inflammation causes decreased Nrf2 expressions in brain regions, including mPFC [18–20]. Interestingly, the Nrf2 expressions in the postmortem brain from depressed patients were decreased compared with control subjects [20, 58]. Furthermore, a previous report showed alterations in the levels of Nrf2 and Keap1 of peripheral blood mononuclear cells of patients with major depression compared to healthy controls [59]. Therefore, it is possible that (*R*)-ketamine could produce rapid-acting and sustained antidepressant actions in depressed patients with decreased Nrf2 expressions.

Lin et al. [60] demonstrated alterations in the mRNA expression of NMDAR-related genes in patients with major depression, supporting the NMDAR hypothesis in depression. Furthermore, dysregulation of BDNF-TrkB signaling mediated by NMDAR might contribute to postoperative cognitive impairments in aged mice [61]. Collectively, it seems that the regulation of BDNF-TrkB signaling by NMDAR signaling might play a role in the antidepressant-like effects of (*R*)-ketamine in *Nrf2* KO mice.

In conclusion, the study demonstrated that (*R*)-ketamine could produce rapid-acting and long-lasting antidepressant-like effects in *Nrf2* KO mice via the BDNF-TrkB signaling pathway. Therefore, it is possible that (*R*)-ketamine could potentially serve as a potential antidepressant for MDD patients with decreased Nrf2 expressions.

Compliance with ethical standards

Conflict of interest Dr. Hashimoto is an inventor on a filed patent application on "The use of *R*-ketamine in the treatment of psychiatric diseases" by Chiba University. Other authors have no conflicts of interest.

References

1. Dantzer R, O'Connor C, Freund GG, Johnson RW, Kelley KW (2008) From inflammation to sickness and depression: when the immune system subjugates the brain. Nat Rev Neurosci 9:46–56
2. Hashimoto K (2009) Emerging role of glutamate in the pathophysiology of major depressive disorder. Brain Res Rev 61:105–123
3. Raison CL, Lowry CA, Rook GA (2010) Inflammation, sanitation, and consternation: loss of contact with coevolved, tolerogenic microorganisms and the pathophysiology and treatment of major depression. Arch Gen Psychiatry 67:1211–1224
4. Hashimoto K (2015) Inflammatory biomarkers as differential predictors of antidepressant response. Int J Mol Sci 16:7796–7801
5. Miller AH, Raison CL (2016) The role of inflammation in depression: from evolutionary imperative to modern treatment target. Nat Rev Immunol 16:22–34
6. Zhang JC, Yao W, Hashimoto K (2016) Brain-derived neurotrophic factor (BDNF) – TrkB signaling in inflammation-related depression and potential therapeutic targets. Curr Neuropharmacol 14:721–731
7. Beurel E, Toups M, Nemeroff CB (2020) The bidirectional relationship of depression and inflammation: double trouble. Neuron 107:234–256
8. Dowlati Y, Hermann N, Swardfager W, Liu H, Sham L, Reim EK, Lanctôt KL (2010) A meta-analysis of cytokines in major depression. Biol Psychiatry 67:446–457
9. Young JJ, Bruno D, Pomara N (2014) A review of the relationship between pro-inflammatory cytokines and major depressive disorder. J Affect Disord 169:15–20
10. Haapakoski R, Mathieu J, Ebmeiner KP, Alenius H, Kivimäki M (2015) Cumulative meta-analysis of interleukins 6 and 1β, tumour necrosis factor α and C-reactive protein in patients with major depressive disorder. Brain Behav Immun 49:206–215
11. Nettis MA, Pariante CM (2020) Is there neuroinflammation in depression? Understanding the link between the brain and the peripheral immune system in depression. Int Rev Neurobiol 152:23–40
12. O'Connell MA, Hayes JD (2015) The Keap1/Nrf2 pathway in health and disease: from the bench to the clinic. Biochem Soc Trans 43:687–689
13. Suzuki T, Yamamoto M (2015) Molecular basis of the Keap1-Nrf2 system. Free Radic Biol Med 88:93–100
14. Wardyn JD, Ponsford AH, Sanderson CM (2015) Dissecting molecular cross-talk between Nrf2 and NF-κB response pathways. Biochem Soc Trans 43:621–626

15. Hashimoto K (2018) Essential role of Keap1-Nrf2 signaling in mood disorders: overview and future perspective. Front Pharmacol 9:1182

16. Yamamoto M, Kensler TW, Motohashi H (2018) The Keap1-Nrf2 system: a thiol-based sensor-effector apparatus for maintaining redox homeostasis. Physiol Rev 98:1169–1203

17. Baird L, Yamamoto M (2020) The molecular mechanisms regulating the Keap1-Nrf2 pathway. Mol Cell Biol 40:e00099-e120

18. Yao W, Zhang JC, Ishima T, Dong C, Yang C, Ren Q, Ma M, Han M, Wu J, Suganuma H, Ushida Y, Yamamoto M, Hashimoto K (2016) Role of Keap1-Nrf2 signaling in depression and dietary intake of glucoraphanin confers stress resilience in mice. Sci Rep 6:30659

19. Zhang JC, Yao W, Dong C, Yang C, Ren Q, Ma M, Han M, Wu J, Ushida Y, Suganuma H, Hashimoto K (2017) Prophylactic effects of sulforaphane on depression-like behavior and dendritic changes in mice after inflammation. J Nutr Biochem 39:134–144

20. Zhang JC, Yao W, Dong C, Han M, Shirayama Y, Hashimoto K (2018) Keap1-Nrf2 signaling pathway confers resilience versus susceptibility to inescapable electric stress. Eur Arch Psychiatry Clin Neurosci 268:865–870

21. Krystal JH, Abdallah CG, Sanacora G, Charney DS, Duman RS (2019) Ketamine: a paradigm shift for depression research and treatment. Neuron 101:774–778

22. Abdallah CG, Krystal JH (2020) Ketamine and rapid acting antidepressants: are we ready to cure, rather than treat depression? Behav Brain Res 390:112628

23. Lavender E, Hirasawa-Fujita M, Domino EF (2020) Ketamine's dose related multiple mechanisms of actions: dissociative anesthetic to rapid-antidepressant. Behav Brain Res 390:112631

24. Zhang K, Hashimoto K (2019) An update on ketamine and its two enantiomers as rapid-acting antidepressants. Expert Rev Neurother 19:83–92

25. Zhang JC, Li SX, Hashimoto K (2014) R (−)-ketamine shows greater potency and longer lasting antidepressant effects than S (+)-ketamine. Pharmacol Biochem Behav 116:137–141

26. Yang C, Shirayama Y, Zhang JC, Ren Q, Yao W, Ma M, Dong C, Hashimoto K (2015) R-ketamine: a rapid-onset and sustained antidepressant without psychotomimetic side effects. Transl Psychiatry 5:e632

27. Fukumoto K, Toki H, Iijima M, Hashihayata T, Yamaguchi J, Hashimoto K, Chaki S (2017) Antidepressant potential of (R)-ketamine in rodent models: comparison with (S)-ketamine. J Pharmacol Exp Ther 361:9–16

28. Yang C, Ren Q, Qu Y, Zhang JC, Ma M, Dong C, Hashimoto K (2018) Mechanistic target of rapamycin-independent antidepressant effects of (R)-ketamine in a social defeat stress model. Biol Psychiatry 83:18–28

29. Chang L, Zhang K, Pu Y, Qu Y, Wang SM, Xiong Z, Ren Q, Dong C, Fujita Y, Hashimoto K (2019) Comparison of antidepressant and side effects in mice after intranasal administration of (R, S)-ketamine, (R)-ketamine, and (S)-ketamine. Pharmacol Biochem Behav 181:53–59

30. Yang C, Han M, Zhang JC, Ren Q, Hashimoto K (2016) Loss of parvalbumin-immunoreactivity in mouse brain regions after repeated intermittent administration of esketamine, but not R-ketamine. Psychiatry Res 239:281–283

31. Hashimoto K, Kakiuchi T, Ohba H, Nishiyama S, Tsukada H (2017) Reduction of dopamine $D_{2/3}$ receptor binding in the striatum after a single administration of esketamine, but not R-ketamine: a PET study in conscious monkeys. Eur Arch Psychiatry Clin Neurosci 267:173–176

32. Tian Z, Dong C, Fujita A, Fujita Y, Hashimoto K (2018) Expression of heat shock protein HSP-70 in the retrosplenial cortex of rat brain after administration of (R, S)-ketamine and (S)-ketamine, but not (R)-ketamine. Pharmacol Biochem Behav 172:17–21

33. Tan Y, Hashimoto K (2020) Risk of psychosis after repeated intermittent administration of (S)-ketamine, but not (R)-ketamine, in mice. J Affect Disord 269:198–200

34. Vollenweider FX, Leenders KL, Oye I, Hell D, Angst J (1997) Differential psychopathology and patterns of cerebral glucose utilisation produced by (S)- and (R)-ketamine in healthy volunteers using positron emission tomography (PET). Eur Neuropsychopharmacol 7:25–38

35. Leal GC, Bandeira ID, Correia-Melo FS, Telles M, Mello RP, Vieira F, Lima CS, Jesus-Nunes AP, Guerreiro-Costa LNF, Marback RF, Caliman-Fontes AT, Marques BLS, Bezerra MLO, Dias-Neto AL, Silva SS, Sampaio AS, Sanacora G, Turecki G, Loo C, Lacerda ALT, Quarantini LC (2020) Intravenous arketamine for treatment-resistant depression: open-label pilot study. Eur Arch Psych Clin Neurosci. https://doi.org/10.1007/s00406-020-01110-5

36. Hashimoto K (2019) Rapid-acting antidepressant ketamine, its metabolites and other candidates: a historical overview and future perspective. Psychiatry Clin Neurosci 73:613–627

37. Yang C, Yang J, Luo A, Hashimoto K (2019) Molecular and cellular mechanisms underlying the antidepressant effects of ketamine enantiomers and its metabolites. Transl Psychiatry 9:280

38. Wei Y, Chang L, Hashimoto K (2020) A historical review of antidepressant effects of ketamine and its enantiomers. Pharmacol Biochem Behav 190:172870

39. Hashimoto K (2020a) Molecular mechanisms of the rapid-acting and long-lasting antidepressant actions of (R)-ketamine. Biochem Pharmacol 177:113935

40. Autry AE, Adachi M, Nosyreva E, Na ES, Los MF, Cheng PF, Kavalali ET, Monteggia LM (2011) NMDA receptor blockade at rest triggers rapid behavioral antidepressant responses. Nature 475:91–95

41. Björkholm C, Monteggia LM (2015) BDNF- a key transducer of antidepressant effects. Neuropharmacology 102:72–79

42. Liu WX, Wang J, Xie ZM, Xu N, Zhang GF, Jia M, Zhou ZQ, Hashimoto K, Yang JJ (2016) Regulation of glutamate transporter 1 via BDNF-TrkB signaling plays a role in the anti-apoptotic and antidepressant effects of ketamine in chronic unpredictable mild stress model of depression. Psychopharmacology 233:405–415

43. Sun HL, Zhou ZQ, Zhang GF, Yang C, Wang XM, Shen JC, Hashimoto K, Yang JJ (2016) Role of hippocampal p11 in the sustained antidepressant effect of ketamine in the chronic unpredictable mild stress model. Transl Psychiatry 6:e741

44. Li S, Luo X, Hua D, Wang Y, Zhan G, Huang N, Jiang R, Yang L, Zhu B, Yuan X, Luo A, Yang C (2020) Ketamine alleviates postoperative depression-like symptoms in susceptible mice: the role of BDNF-TrkB signaling. Front Pharmacol 10:1702

45. Hashimoto K (2020b) Brain-derived neurotrophic factor -TrkB signaling and the mechanism of antidepressant activity by ketamine in mood disorders. Eur Arch Psychiatry Clin Neurosci 270:137–138

46. Itoh K, Chiba T, Takahashi S, Ishii T, Igarashi K, Katoh Y, Oyake T, Hayashi N, Satoh K, Hatayama I, Yamamoto M, Nabeshima Y (1997) An Nrf2/small Maf heterodimer mediates the induction of phase II detoxifying enzyme genes through antioxidant response elements. Biochem Biphys Res Commun 236:313–322

47. Cazorla M, Prémont J, Mann A, Girad N, Kellendonk C, Rognan D (2011) Identification of a low-molecular weight TrkB antagonist with anxiolytic and antidepressant activity in mice. J Clin Invest 121:1846–1857

48. Zhang JC, Wu J, Fujita Y, Yao W, Ren Q, Yang C, Li SX, Shirayama Y, Hashimoto K (2014) Antidepressant effects of TrkB ligands on depression-like behavior and dendritic changes in mice after inflammation. Int J Neuropsychopharmacol 18:pyu077

49. Ren Q, Ma M, Yang C, Zhang JC, Yao W, Hashimoto K (2015) BDNF-TrkB signaling in the nucleus accumbens shell of mice

has key role in methamphetamine withdrawal symptoms. Transl Psychiatry 5:e666

50. Zhang JC, Yao W, Dong C, Yang C, Ren Q, Ma M, Han M, Hashimoto K (2015) Comparison of ketamine, 7,8-dihydroxyflavone, and ANA-12 antidepressant effects in the social defeat stress model of depression. Psychopharmacology 232:4325–4335

51. Qu Y, Yang C, Ren Q, Ma M, Dong C, Hashimoto K (2017) Comparison of (*R*)-ketamine and lanicemine on depression-like phenotype and abnormal composition of gut microbiota in a social defeat stress model. Sci Rep 7:15725

52. Wang S, Ishima T, Zhang J, Qu Y, Chang L, Pu Y, Fujita Y, Tan Y, Wang X, Hashimoto K (2020) Ingestion of *Lactobacillus intestinalis* and *Lactobacillus reuteri* causes depression- and anhedonia-like phenotypes in antibiotic-treated mice via the vagus nerve. J Neuroinflammation 17:241

53. Duman RS, Aghajanian GK (2011) Synaptic dysfunction in depression: potential therapeutic targets. Science 338:68–72

54. Ohgi Y, Futamura T, Hashimoto K (2015) Glutamate signaling in synaptogenesis and NMDA receptors as potential therapeutic targets for psychiatric disorders. Curr Mol Med 15:206–221

55. Yang C, Shirayama Y, Zhang JC, Ren Q, Hashimoto K (2015) Regional differences in brain-derived neurotrophic factor levels and dendritic spine density confer resilience to inescapable stress. Int J Neuropsychopharmacol 18:pyu121

56. Zhang J, Qu Y, Chang L, Pu Y, Hashimoto K (2019) (*R*)-ketamine rapidly ameliorates the decreased spine density in the medial prefrontal cortex and hippocampus of susceptible mice after chronic social defeat stress. Int J Neuropsychopharmacol 22:675–679

57. Shirayama Y, Yang C, Zhang JC, Ren Q, Yao W, Hashimoto K (2015) Alterations in brain-derived neurotrophic factor (BDNF) and its precursor proBDNF in the brain regions of a learned helplessness rat model and the antidepressant effects of a TrkB agonist and antagonist. Eur Neuropsychopharmacol 25:2449–2458

58. Martín-Hernández D, Caso JR, Javier Meana J, Callado LF, Madrigal JLM, García-Bueno B, Leza JC (2018) Intracellular inflammatory and antioxidant pathways in postmortem frontal cortex of subjects with major depression: effect of antidepressants. J Neuroinflammation 15:251

59. Lukic I, Mitic M, Djordjevic J, Tatalovic N, Bozovic N, Soldatovic I, Mihaljevic M, Pavlovic Z, Radojcic MB, Maric NP, Adzic M (2014) Lymphocyte levels of redox-sensitive transcription factors and antioxidative enzymes as indicators of pro-oxidative state in depressive patients. Neuropsychobiology 70:1–9

60. Lin CH, Huang MW, Lin CH, Huang CH, Lane HY (2019) Altered mRNA expressions for *N*-methyl-D-aspartate receptor-related genes in WBC of patients with major depressive disorder. J Affect Disord 245:1119–1125

61. Qiu LL, Pan W, Luo D, Zhang GF, Zhou ZQ, Sun XY, Yang JJ, Ji MH (2020) Dysregulation of BDNF/TrkB signaling mediated by NMDAR/Ca^{2+}/calpain might contribute to postoperative cognitive dysfunction in aging mice. J Neuroinflammation 17:23
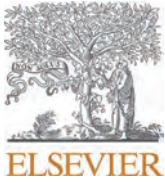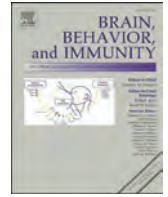
A role of the subdiaphragmatic vagus nerve in depression-like phenotypes in mice after fecal microbiota transplantation from *Chrna7* knock-out mice with depression-like phenotypes

Yaoyu Pu [1,2], Yunfei Tan [1], Youge Qu, Lijia Chang, Siming Wang, Yan Wei, Xingming Wang, Kenji Hashimoto [*]

Division of Clinical Neuroscience, Chiba University Center for Forensic Mental Health, Chiba 260-8670, Japan

ARTICLE INFO

ABSTRACT

The α7 subtype of the nicotinic acetylcholine receptor (α7 nAChR: coded by *Chrna7*) regulates the cholinergic ascending anti-inflammatory pathway involved in depression. We previously reported that *Chrna7* knock-out (KO) mice show depression-like phenotypes through systemic inflammation. In this study, we investigated whether fecal microbiota transplantation (FMT) from *Chrna7* KO mice causes depression-like phenotypes in mice treated with an antibiotic cocktail (ABX). *Chrna7* KO mice with depression-like phenotypes show an abnormal gut microbiota composition, although the alpha diversity and beta diversity were not altered. FMT from *Chrna7* KO mice caused depression-like phenotypes, systemic inflammation, and downregulation of synaptic proteins in the prefrontal cortex (PFC) in the ABX-treated mice compared to FMT from the control mice. The Principal component analysis based on the OTU level showed that the FMT group from the KO mice were different from the FMT group from the control mice. We found differences in abundance for several bacteria in the FMT group from the KO mice at the taxonomic level when compared with the other group. Interestingly, subdiaphragmatic vagotomy significantly blocked the development of depression-like phenotypes in the ABX-treated mice after FMT from *Chrna7* KO mice. These data suggest that FMT from *Chrna7* KO mice produce depression-like phenotypes in ABX-treated mice via the subdiaphragmatic vagus nerve. The brain–gut–microbiota axis association with the subdiaphragmatic vagus nerve plays an important role in the development of depression.

1. Introduction

The α7 subtype of nicotinic acetylcholine receptors (α7 nAChRs, coded by the *Chrna7* gene) plays a prominent role in inflammation implicated in depression (Kalkman and Feuerbach, 2016). It is well known that α7 nAChR regulates the so-called cholinergic ascending anti-inflammatory pathway, mediated by the vagus nerve modulation of the immune system (Hoover, 2017; Lei and Duan, 2019; Lu et al., 2014; Martelli et al., 2014; Suzuki et al., 2006; Thomsen and Mikkelsen, 2012; Ulloa, 2005; Wang et al., 2003). Therefore, activation of α7 nAChR would be a potential therapeutic approach for inflammation-related psychiatric and neurological disorders (Corsi-Zuelli et al., 2017; Hashimoto, 2015a, 2015b; Ishikawa and Hashimoto, 2011; Toyohara and Hashimoto, 2010). We previously reported that *Chrna7* KO mice exhibit

depression-like phenotypes through systemic inflammation (Zhang et al., 2016). Furthermore, pharmacological activation of α7 nAChR produced antidepressant-like effects in inflammation-presenting mice (Alzarea and Rahman, 2019) and mice exposed to chronic stress (Zhao et al., 2017). Moreover, nicotine attenuated the depression-like behaviors in CaMKIV KO mice via α7 nAChR activation (Moriguchi et al., 2020). Collectively, α7 nAChR possibly plays a crucial role in depression.

The brain–gut–microbiota axis has a central function in depression (Cryan et al., 2019; Dinan and Cryan, 2017), as demonstrated by the abnormal composition of gut microbiota in patients with depression (Jiang et al., 2015; Liu et al., 2020a, 2020b; Wong et al., 2016; Zheng et al., 2016). Preclinical findings have shown that the abnormal composition of gut microbiota may contribute to depression-like

* Corresponding author.
  E-mail address: hashimoto@faculty.chiba-u.jp (K. Hashimoto).
[1] Dr. Pu and Dr. Tan contributed equally to this work.
[2] Present address: West China Hospital, Sichuan University, Chengdu, China.

behaviors in rodents (Huang et al., 2019; Luo et al., 2018; Qu et al., 2017; Wang et al., 2020a, 2020b; Wu et al., 2020; Yang et al., 2017, 2019; Zhang et al., 2017, 2019). Interestingly, the vagus nerve system regulates communication between the brain and the microbiota in the gastrointestinal tract (Bonaz et al., 2018; 2019; Cawthon and de La Serre, 2018; Forsythe et al., 2014). The ingestion of *Lactobacillus rhamnosus (JB-1)* ameliorated stress-induced depression-like behaviors via the subdiaphragmatic vagus nerve, and subdiaphragmatic vagotomy (SDV) blocked the beneficial effects of the microbe (Bravo et al., 2011). Furthermore, SDV blocked the depression-like behaviors after systemic administration of recombinant interleukin-1β (IL-1β) or lipopolysaccharide (LPS) (Konsman et al., 2000; Zhang et al., 2020). Moreover, SDV blocked depression-like phenotypes in antibiotic-treated mice after repeated ingestion of *Lactobacillus intestinalis* and *Lactobacillus reuteri* (Wang et al., 2020a). Taken together, it seems that the brain–gut–microbiota axis via the subdiaphragmatic vagus nerve participates in depression.

The present study was undertaken to investigate whether fecal microbiota transplantation (FMT) from *Chrna7* KO mice with depression-like phenotypes can induce depression-like phenotypes and abnormal composition of the gut microbiota in mice treated with an antibiotic cocktail (ABX). Furthermore, we measured the expression of synaptic proteins [e.g., α-amino-3-hydroxy-5-methyl-4-isoxazole propionic acid receptor A1 (GluA1) and the postsynaptic density 95 (PSD-95) protein] in the prefrontal cortex (PFC) because the expression of synaptic proteins in the PFC of rodents with depression-like phenotypes has been found to be lower than that of control mice (Duman and Aghajanian, 2012; Yang et al., 2015; Zhang et al., 2014). Finally, we examined whether SDV blocks depression-like phenotypes in ABX-treated mice after FMT from *Chrna7* KO mice.

2. Materials and methods

2.1. Animals

Mice deficient in α7 nAChR (coded by *Chrna7* gene, C57BL/6 background) were purchased from The Jackson Laboratory (Bar Harbor, ME, USA). Male C57BL/6 mice (aged 8 weeks, bodyweight 20–25 g) were purchased from Japan SLC Inc. (Hamamatsu, Shizuoka, Japan). The mice were housed in clear polycarbonate cages (21 × 30 × 22.5 cm) in groups of 4 or 5 per cage under a controlled 12/12-h light/dark cycle (lights on from 7:00 a.m. to 7:00p.m.), with a room temperature of 23 ± 1 °C and humidity of 55 ± 5%. The experimental protocol of this study was approved by the Chiba University Institutional Animal Care and Use Committee (Permission number 1–146 and 2–154). The animals were deeply anesthetized with inhaled isoflurane and rapidly killed by cervical dislocation. All efforts were made to minimize animal suffering.

2.2. Behavioral tests

Adult male littermate wild-type (WT) and *Chrna7* KO mice were used for the behavioral tests and 16S ribosome RNA sequencing of the fecal samples. The behavioral tests included a locomotion test (LMT), tail suspension test (TST), forced swimming test (FST), and 1% sucrose preference test (SPT) and were performed as described previously and in brief below (Wang et al., 2020a; 2020b; Zhang et al., 2017).

An automated animal movement analysis system (SCANET MV-40; MELQUEST Co., Ltd., Toyama, Japan) was used to measure the locomotor activity of the mice. The cumulative ambulatory activity counts were recorded continuously over a period of 60 min after the mice were placed in the experimental cages (56 cm (length) × 56 cm (width) × 33 cm (height)). The cages were cleaned between the testing sessions.

The TST was performed using a small piece of adhesive tape placed approximately 2 cm from the tip of the tail of the mouse. A single hole was punched in the tape, and the mice were hung individually from a hook. The immobility time was recorded over a 10 min period. A mouse was considered immobile only when it had hung passively and remained completely motionless.

The FST was performed using an automated forced-swim apparatus (SCANET MV-40; MELQUEST Co., Ltd., Toyama, Japan). The mice were placed individually into a cylinder (23 cm (diameter) × 31 cm (height)) with a water depth of 15 cm (water temperature, 23 °C ± 1 °C). The immobility time was recorded and calculated using the analytical software of the apparatus over a 6 min observation time period.

For the SPT, the mice were provided with both water and a 1% sucrose solution for 48 h, followed by 4-h period of water and food deprivation and a 1-h exposure to two identical bottles (water and 1% sucrose solution), which were weighed before and after the exposure period. The sucrose preference was calculated as the percent sucrose solution consumption relative to the total liquid consumption.

2.3. Collection of fecal samples from WT mice and KO mice

We collected fresh fecal samples from each mouse at around 10:00 in order to avoid any circadian effects on the microbiome. The fecal samples were individually placed into sterilized screw cap microtubes immediately after defecation, and these samples were stored at −80 °C prior to 16S ribosome RNA sequencing or FMT.

2.4. Treatment with antibiotic cocktail, FMT, and behavioral testing

Broad-spectrum antibiotics (ABX: ampicillin 1 g/L, FUJIFILM Wako Pure Chemical Corporation, Tokyo, Japan; neomycin sulfate 1 g/L, Sigma-Aldrich Co. Ltd, MO, USA; metronidazole 1 g/L, FUJIFILM Wako Pure Chemical Corporation, Tokyo, Japan) dissolved in drinking water were provided *ad libitum* to the male C57BL/6 mice for 14 consecutive days (day 1–day 14), as previously reported (Pu et al., 2019; Wang et al., 2020a, 2020b; Yang et al., 2019). >90% of the gut microbiota are known to be killed by ABX (Hernández-Chirlaque et al., 2016; Zhan et al., 2018). The drinking solution was renewed every 2 or 3 days. Subsequently, the FMT from the control mice or KO mice was performed for 14 days (day 15–day 28). The locomotion test and TST were performed on day 29; the TST was performed 2 hr after the locomotion test. The FST and SPT were performed on days 30 and day 31, respectively. Plasma and PFC were collected on day 32.

2.5. Subdiaphragmatic vagotomy, treatment with antibiotic cocktail, FMT, and behavioral testing

Bilateral SDV was performed under anesthesia with 5% isoflurane, as previously described (Wang et al., 2020a; Zhang et al., 2020). Briefly, a 1-cm right transverse abdominal incision was made 0.5 cm below the xiphisternum, starting from the *linea alba*. The liver was carefully retracted with a small cotton pellet dampened with sterile normal saline, and the costal arc was repositioned using a vascular clamp to expose the esophagus. The dorsal and ventral branches of the vagus nerve were exposed along the subdiaphragmatic esophagus, visualized using a surgical microscope (Leica, Heidelberg, Germany). Fourteen days after the operation (designated as day 14), the observation of an increased stomach size was considered indicative of a successful SDV. For the surgery control, the trunk of the vagus nerve was gently exposed but not cut. In all mice that were subjected to SDV, particular care was taken to avoid any injuries to the subdiaphragmatic esophagus. The mice that underwent bilateral SDV were allowed to recover for 14 days.

Subsequently, the antibiotic cocktail (ABX) dissolved in drinking water was provided *ad libitum* to male C57BL/6 mice for 14 consecutive days (day 15–day 28), as described above. The drinking solution was renewed every 2 or 3 days. Subsequently, the FMT from the control mice or the KO mice was performed for 14 days (day 29–day 42). The LMT and TST were performed on day 43; the TST was performed 2 hr after the LMT. The FST and SPT were performed on day 44 and day 45, respectively. On day 46, plasma and PFC samples were collected.

2

2.6. Western blotting

Western blotting of synaptic proteins (i.e., PSD-95 and GluA1) in the PFC was performed as reported previously (Wang et al., 2020a, 2020b; Zhang et al., 2020). We used primary antibodies against PSD-95 (1:1000, Cat Number: 51-6900, Invitrogen, Camarillo, CA, USA), GluA1 (1:1000, Cat Number: ab31232, Abcam, Cambridge, MA, USA), and β-actin (1:10,000, Sigma-Aldrich Co., Ltd., St Louis, MO, USA). The bands were visualized using enhanced chemiluminescence (ECL) along with a Western Blotting Detection System (GE Healthcare Bioscience), and images were captured using a ChemiDoc™ Touch Imaging System (170–01401; Bio-Rad Laboratories, Hercules, CA). The images were subjected to gray-scale analysis using the Image Lab™ 3.0 software (Bio-Rad Laboratories).

2.7. Collection of fecal samples and 16S ribosome RNA sequencing

Fresh fecal samples from mice were collected before the LMT. The fecal samples were each placed into individual sterilized screw cap microtubes immediately after defecation and were stored at –80℃ prior to use. The DNA extractions from the fecal samples and 16S ribosome RNA sequencing analyses were performed by MyMetagenome Co., Ltd. (Tokyo, Japan), as reported previously (Wang et al., 2020a, 2020b; Zhang et al., 2020).

The alpha diversity was used to analyze the complexity of species diversity for each sample using four indices: Observed_OTUs, Chao1, ACE, and Shannon. Differences in the bacterial taxa between groups at the species level or higher (depending on the taxon annotation) were calculated using linear discriminant analysis (LDA) effect size (LEfSe) with LEfSe software (LDA score >2.0, P < 0.05) (Segata et al., 2011).

For beta diversity of the gut microbiota, principal component analysis of the OTU level was performed using analysis of similarities (ANOSIM) in R package vegan (2.5.4) (Xin and Sun, 2017).

2.8. Measurement of short-chain fatty acid (SCFA) levels in fecal samples

Short-chain fatty acids (SCFAs) produced by microbiome play a role in brain- gut communication (Dalile et al., 2019; Silva et al., 2020; Wu et al., 2020). Characterization of SCFAs (e.g., acetic acid, propionic acid, butyric acid, lactic acid, succinic acid) in the fecal samples was performed by TechnoSuruga Laboratory, Co., Ltd. (Shizuoka, Japan), as reported previously (Wang et al., 2020a, 2020b; Zhang et al., 2019, 2020). The concentrations of the SCFAs were measured using gas chromatography with a flame ionization detector. The SCFA data were expressed as milligrams per gram of feces.

2.9. Statistical analysis

The data are expressed as the mean ± standard error of the mean. The data for the behavioral tests, Western blot analyses, and gut microbiota findings were analyzed using Student's *t*-test, Mann Whitney *U* test, or one-way analysis of variance followed by a *post hoc* Fisher's Least Significant Difference test. The significance was set at *P* < 0.05.

3. Results

3.1. Depression-like phenotypes and abnormal composition of gut microbiota in Chrna7 KO mice

First, we performed the behavioral tests for depression-like phenotypes. There were no changes in locomotion between the WT mice and the KO mice (Fig. 1A). The immobility time of the TST and FST in the KO mice were significantly higher than those of the WT mice (Fig. 1B and 1C). Furthermore, the sucrose preference determined from the SPT in the KO mice was significantly lower than that of the WT mice (Fig. 1D). The data show that *Chrna7* KO mice show depression-like phenotypes,

consistent with the previous results (Zhang et al., 2016).

3.2. Abnormal composition of gut microbiota and SCFAs in Chrna7 KO mice

We performed 16S ribosome RNA sequencing analysis of the fecal samples. There were no changes in alpha diversity (i.e., Observed_OTUs, Chao1, ACE, Shannon) between the two groups (Fig. S1A). The PCA between the two groups showed that there were no changes (R = 0.0199, P = 0.306) in beta diversity (Fig. S1B).

The gut microbiota changes of the abundant taxa between the two groups were analyzed using the LEfSe algorithm, which permits the identification of microbial markers that are more important in one group than in another (Fig. 1E). We identified the different distributions of two bacteria (e.g., *Pontibacter, Cytophagaceae*) for the KO mice (Fig. 1E). Four mixed-level phylotypes, including *Prevotellasp_R79, Pontibacter, Cytophagaceae,* and *Clostridiumpolynesiense,* were identified as potential microbial markers for the KO group (Fig. 1F).

At the genus level, the abundances of *Dorea* and *Blautia* in the KO group were lower than the WT group (Fig. 2A). In contrast, the abundance of *Candidatus Arthromitus* was more pronounced in the KO group than the WT group (Fig. 2A). At the species level, the abundance of *Candidatus Arthromitus* sp. *SFB-mouse* was more pronounced in the KO group than the WT group (Fig. 2B).

There were no changes in SCFAs (e.g., succinic acid, lactic acid, acetic acid, propionic acid, butyric acid) between the WT group and the KO group (Fig. S2).

3.3. Effects of FMT from WT mice and KO mice

Next, we investigated whether FMT from the WT mice or *Chrna7* KO mice with depression-like phenotypes caused depression-like phenotypes in the control mice treated with ABX (Fig. 3A). No difference was found in locomotor activity between the two groups (Fig. 3B). FMT from KO mice significantly increased the immobility time of the TST and the FST in the ABX-treated mice compared to FMT from the WT mice (Fig. 3C and 3D). Furthermore, FMT from the KO mice significantly decreased the sucrose preference measured using the SPT in the ABX-treated mice compared to FMT from the WT mice (Fig. 3E). The plasma levels of IL-6 in the mice after FMT from the KO mice were significantly higher than those of FMT from the WT mice (Fig. 3F). Western blot analysis showed the decreased expression of synaptic proteins (e.g., PSD-95 and GluA1) in the PFC from mice after FMT from the KO mice compared to FMT from the WT mice (Fig. 3G and 3H).

Regarding alpha diversity, there was a significant change in ACE between the two groups (Fig. S3). However, there were no changes in other indices for alpha diversity (i.e., Observed_OTUs, Chao1, Shannon) between the two groups, although these indices in the FMT group from the KO mice were slightly higher than the other group (Fig. S3). The PCA revealed significant change in the community composition evaluated by ANOSIM (R = 0.1662, P = 0.013) (Fig. 3I).

3.4. Effects of FMT from KO mice on the LEfSe algorithm of gut microbiota

The gut microbiota changes of the abundant taxa among the two groups were analyzed using the LEfSe algorithm. The color differences were indicative of differences in the abundant taxa between the two groups. As presented in Fig. 4A, a distribution for potential microbial markers was found between the two groups. Seventeen mixed-level phylotypes, including *Clostridiumpolynesiense, Parabacteroides, Ruminococcaceae, Clostridiaceae, Clostridium, Thiotrichales, Methylophaga, Piscirickettsiaceae, Erysipelothrixinopinata, Methylophagathalassica, Erysipelothrix, Gammaproteobacteria, Helicobacteeganmani, Helicobacteraceae, Helicobacter, Epsilonproteobacteria,* and *Campylobacterales* were identified as potential microbial markers in the FMT group from the KO
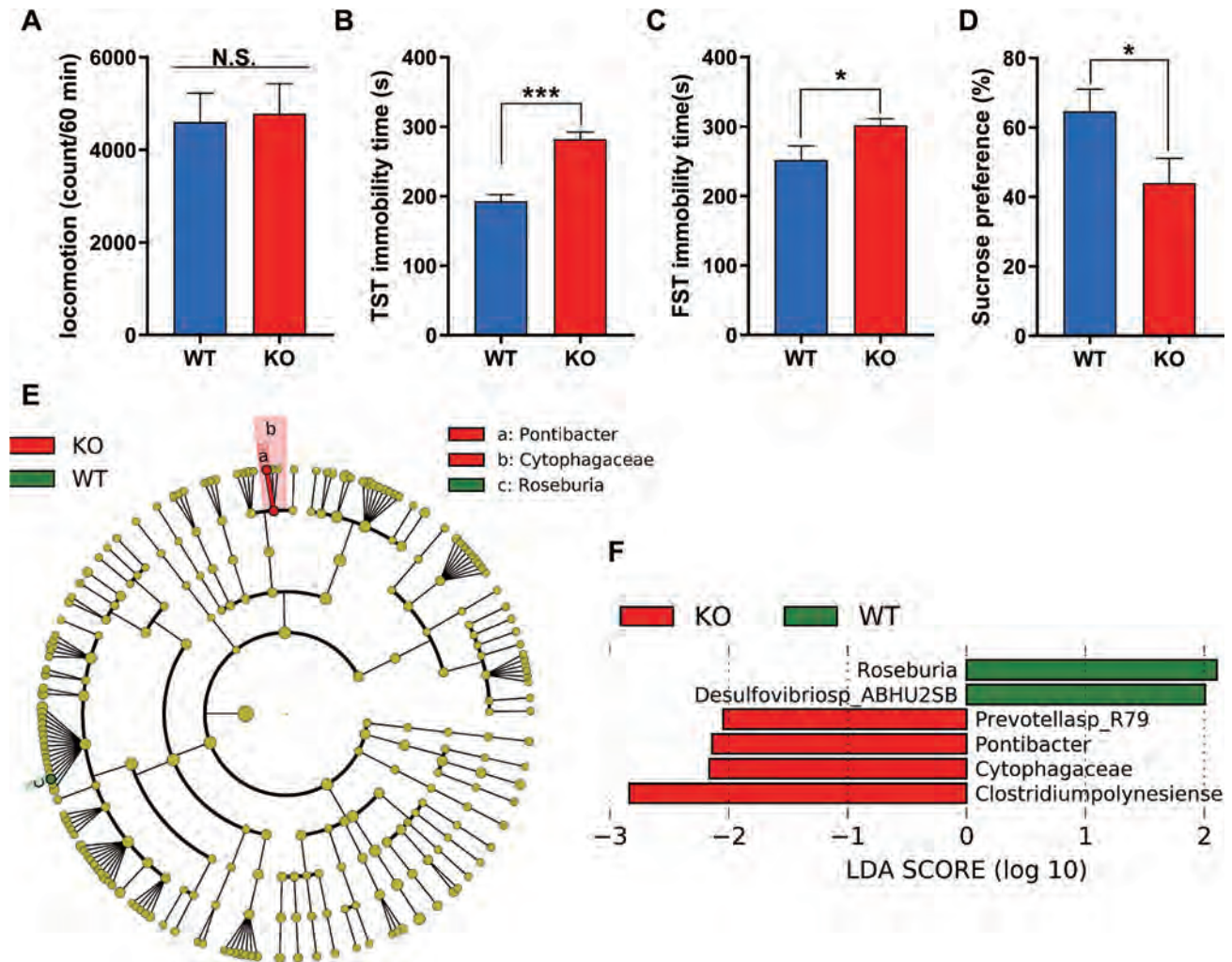
3

Fig. 1. Depression-like phenotypes and abnormal composition of gut microbiota of *Chrna7* KO mice (A): Locomotion test (LMT). (Student *t*-test: t = −0.201, P = 0.843). (B): TST (Student *t*-test: t = −6.217, P < 0.001). (C): FST (Student *t*-test: t = −2.246, P = 0.040). (D): SPT (Student *t*-test: t = 2.171, P = 0.049). (E): Cladogram (LDA score > 2.0, P < 0.05) showed the taxonomic distribution difference between the two groups, indicating with different color region. Each successive circle represents a differentially abundant taxonomic clades at phylum, class, order, family, genus and species level from the inner to outer rings. (F): Histograms of the different abundant taxa based on the cutoff value of LDA score (log10) > 2.0 and P < 0.05 between the two groups. The LDA scores of the KO group was negative, while those of the WT group was positive. The data represent mean ± S.E.M. (n = 8). *P < 0.05, **P < 0.01. N.S.: not significant.

mice compared with the findings in the FMT group from the WT mice (Fig. 4B).

3.5. Effects of FMT on composition of gut microbiota

At the phylum level, *Firmicutes* were the most abundant for the two groups (Fig. S4). The abundance of *Proteobacteria* was more pronounced in the FMT group from the KO mice than the FMT group from the WT mice (Fig. S4). At the genus level, the abundances of *Helicobacter* and *Butyricimonas* were more pronounced in the FMT group from the KO mice than the other group (Fig. S5). In contrast, the abundances of *Muribaculum* and *Faecalimonas* in the FMT group from the KO mice were lower than the other group (Fig. S5). At the species level, the abundances of *Lactobacillus animalis* and *Helicobacter ganmani* were more pronounced in the FMT group from the KO mice than the other group (Fig. 5A). In contrast, the abundance of *Muribaculum intestinale* in the FMT group from the KO mice was lower than the other group (Fig. 5A).

3.6. Effects of SDV on depression-like phenotypes in mice after FMT from Chrna7 KO mice

To examine the role of the subdiaphragmatic vagus nerve in

depression-like phenotypes after FMT from *Chrna7* KO mice, we performed SDV (Fig. 6A). No difference was found in locomotor activity between the three groups (Fig. 6B). SDV significantly blocked the increased immobility time of the TST and FST in the ABX-treated mice after FMT from the KO mice (Fig. 6C and 6D). Furthermore, SDV significantly inhibited the decreased sucrose preference of SPT in the ABX-treated mice after FMT from the KO mice (Fig. 6E).

4. Discussion

The major findings of this study were as follows. First, FMT from *Chrna7* KO mice produced depression-like phenotypes, systemic inflammation, and downregulation of synaptic proteins (e.g., PSD-95 and GluA1) in the PFC of the ABX-treated mice. In contrast, FMT from the WT mice without depression-like phenotypes did not produce depression-like phenotypes or downregulation of synaptic proteins in the PFC of the ABX-treated mice. Second, the PCA showed that the FMT group from the KO mice were distanced from the FMT group from the WT mice. Analysis using the LEfSe algorithm showed that seventeen mixed-level phylotypes were identified as potential microbial markers for the FMT group from the KO mice. Third, SDV significantly inhibited the development of depression-like phenotypes in the ABX-treated mice

4
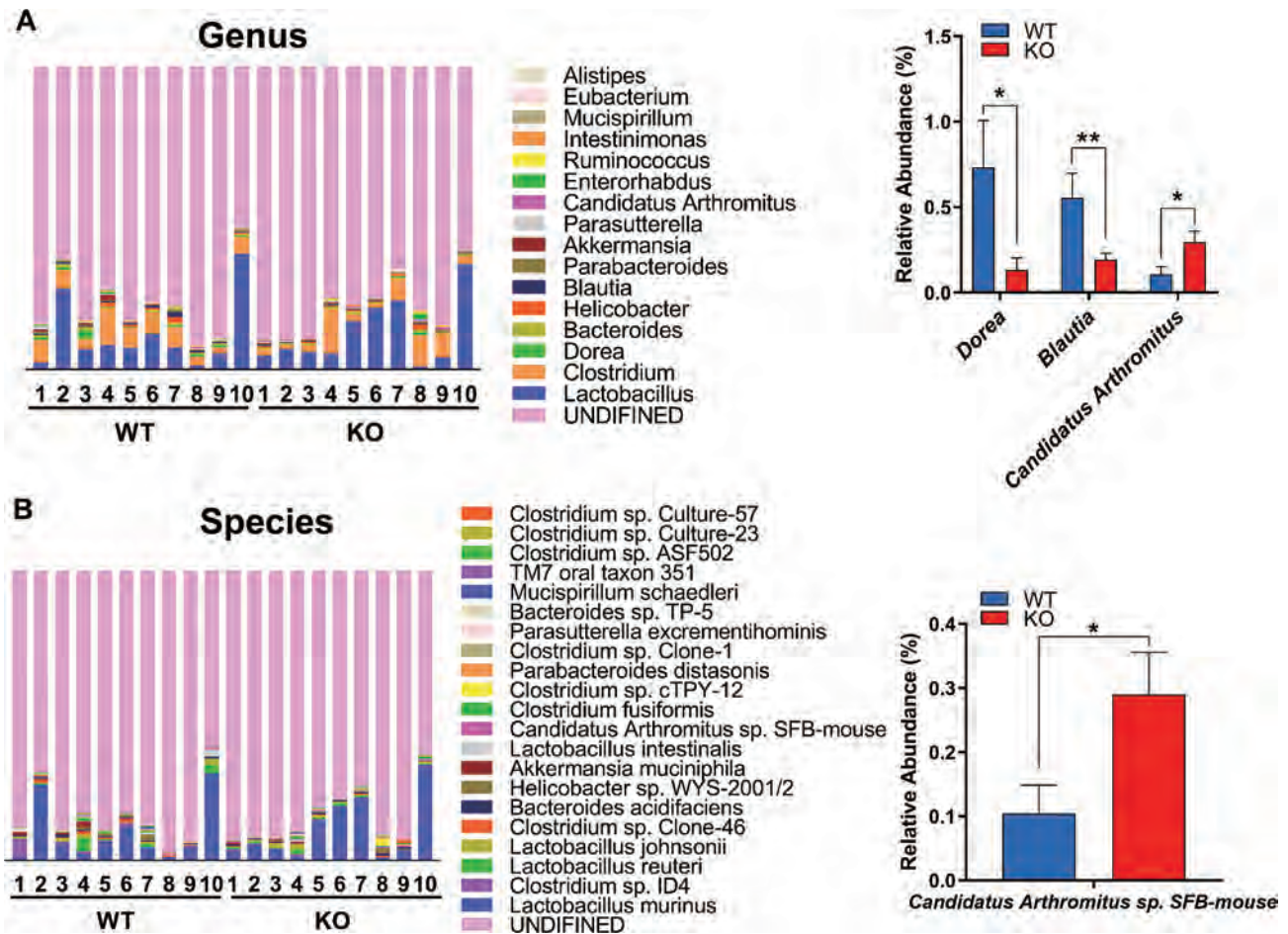
Fig. 2. Altered gut bacteria composition at the genus level and species level (A): Relative abundance at the genus level in the two groups. *Dorea* (Mann-Whitney *U* test: U = 20, P = 0.020). *Blautia* (Mann-Whitney *U* test: U = 15, P = 0.008). *Candidatus Arthromitus* (Mann-Whitney *U* test: U = 24, P = 0.047). (B): Relative abundance at the species level in the two groups. *Candidatus Arthromitus* sp. *SFB-mouse* (Mann-Whitney *U* test: U = 24, P = 0.047). The data represent mean ± S.E.M. (n = 10). *P < 0.05, **P < 0.01.

after FMT from the KO mice, suggesting the role of the sub-diaphragmatic vagus nerve in the depression-like phenotypes in mice after FMT from the KO mice. Collectively, the present data indicate that FMT from *Chrna7* KO mice with depression-like phenotypes could produce depression-like phenotypes in the ABX-treated mice through the brain–gut–microbiota axis via the subdiaphragmatic vagus nerve.

ABX is known to induce dramatic alterations in the diversity and composition of the gut microbiota in the host intestine (Becattini et al., 2016; Kennedy et al., 2018). Previously, we reported that FMT from mice with depression-like phenotypes caused depression-like phenotypes, higher blood levels of IL-6, and downregulation of synaptic proteins in the PFC in ABX-treated mice but not in control mice (Wang et al., 2020b). Thus, it seems that ABX-induced microbiome depletion is necessary for these behavioral and biochemical changes to occur in recipient mice after administration of "depression-related microbes" obtained from mice with a depression-like phenotype (Wang et al., 2020a, 2020b). In this study, we found that FMT from *Chrna7* KO mice resulted in depression-like behaviors and systemic inflammation and reduced the expression of synaptic proteins in the PFC of ABX-treated mice. Thus, FMT using "depression-related microbes" obtained from *Chrna7* KO mice causes depression-like behaviors through systemic inflammation. The precise mechanisms underlying the depression-like phenotypes in ABX-treated mice caused by FMT of "depression-related microbes" from *Chrna7* KO mice remain unknown, but it seems that systemic inflammation may be induced in the recipient mice, resulting in depression-like phenotypes.

In this study, we found that at the species level, the abundances of *L. animalis* and *H. ganmani* were more pronounced in the FMT group from the KO mice than the other group. It is shown that *L. animalis* contributes to the immune response by regulating pro- and anti-inflammatory pathways (Karunasena et al., 2013, 2014). *H. ganmani* is a urease-negative enterohepatic anaerobe species of *Helicobacter* isolated from the intestine and liver from mice (Robertson et al., 2001). Furthermore, colonization of *H. ganmani* to interleukin-10 KO mice increased the rate of typhlocolitis development (Zhang et al., 2005). In contrast, the abundance of *M. intestinale* in the FMT group from the KO mice was lower than the other group. *M. intestinale* is a dominant member of the mouse gut microbiota community (Dowden et al., 2020; Shin et al., 2016). It is also reported that *M. intestinale* is a strictly anaerobic bacteria that contributes to galactose degradation (Lagkouvardos et al., 2016) and homoserine and serine metabolism (Snijders et al., 2016). Abnormalities in these bacteria may contribute to depression-like phenotypes after FMT from *Chrna7* KO mice, although the precise role of these bacteria in depression-like phenotypes after FMT from the KO mice remains unclear.

The vagus nerve is the longest of the cranial nerves and links the brain and the peripheral organs. The vagus nerve plays an important role in the anti-inflammatory system and can modulate the immune system (Ulloa, 2005). In this study, we found that SDV blocked depression-like phenotypes in ABX-treated mice after FMT of "depression-related microbes" from *Chrna7* KO mice. Thus, it seems that the subdiaphragmatic vagus nerve plays a role in the depression-like
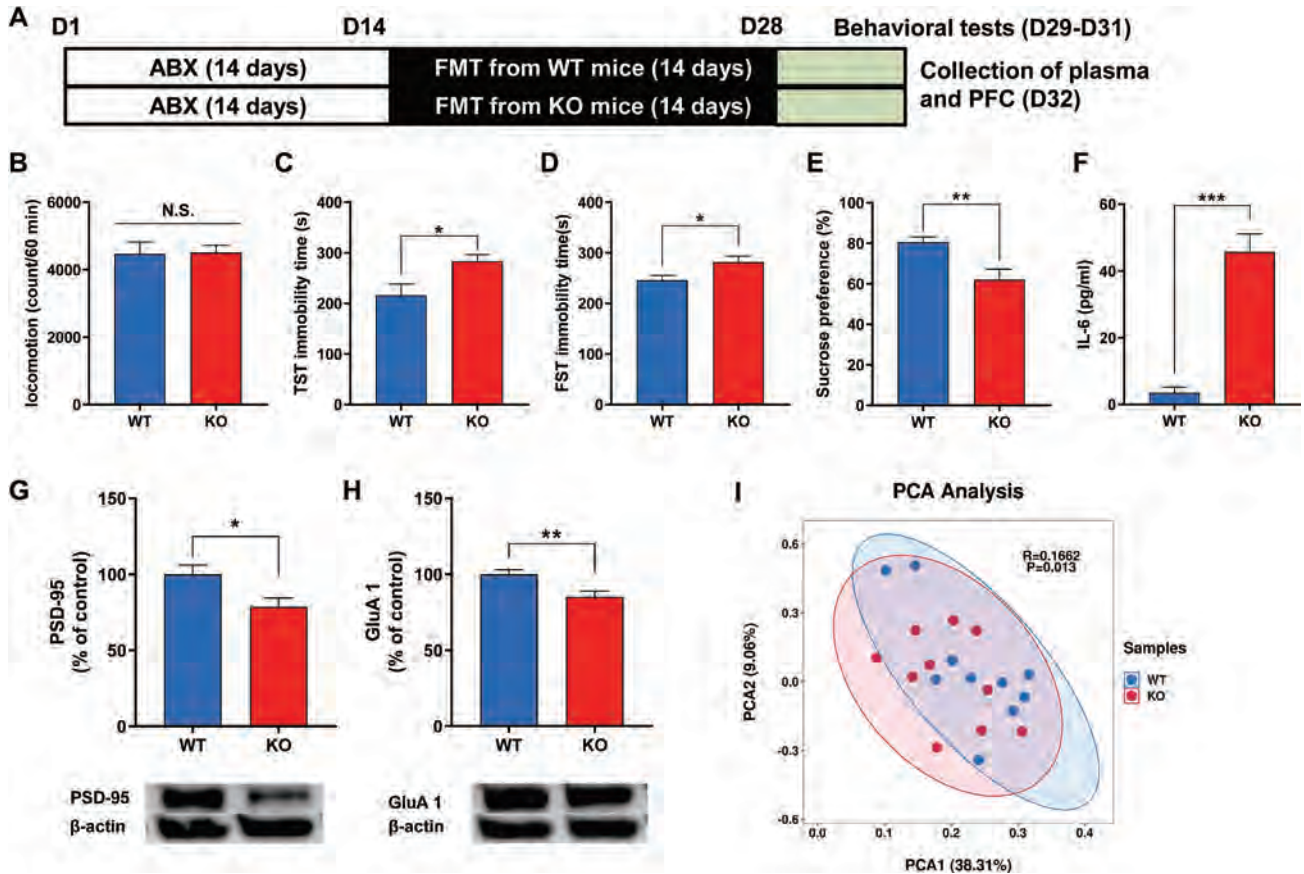
Fig. 3. Effects of FMT on depression-like phenotypes in mice treated with antibiotic cocktail (A): Schedule of treatment with antibiotic cocktail (ABX), FMT, behavioral tests, and sample collection. (B): Locomotion test (LMT) (Student *t*-test: t = −0.090, P = 0.929). (C): TST (Student *t*-test: t = −2.409, P = 0.027). (D): FST (Student *t*-test: t = 2.578, P = 0.019). (E): SPT (Student *t*-test: t = 3.203, P = 0.005). (F): Plasma IL-6 levels (Student *t*-test: t = −7.393, P < 0.001). (G): PSD-95 (Student *t*-test: t = 2.521, P = 0.021). (H): GluA1 (Student *t*-test: t = 3.091, P = 0.006). (I): Principal component analysis (PCA) of beta-diversity based on the OTU level, where each point represents a single sample colored by group circle, indicated by the second principal component of 9.06% on the Y- axis and the first principal component of 38.31% on the X- axis (ANOSIM) (R = 0.1662, P = 0.013).
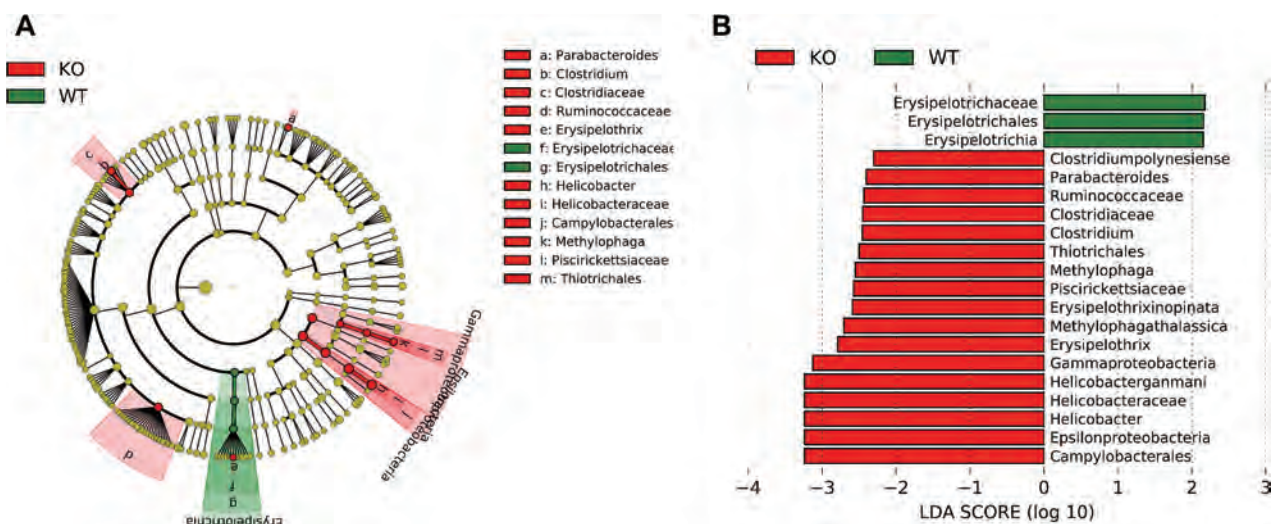
Fig. 4. LEfSe algorithm of gut microbiota Linear discriminant analysis Effect Size (LEfSe) algorithm of gut microbiota changes in abundant taxa between the two groups. The colors showed that the group of abundant taxa was different with the other groups. (A): Cladogram (LDA score > 2.0, P < 0.05) showed the taxonomic distribution difference between the FMT group from control mice and the FMT group from KO mice, indicating with different color region. Each successive circle represents a differentially abundant taxonomic clades at phylum, class, order, family, genus and species level from the inner to outer rings. (B): Histograms of the different abundant taxa based on the cutoff value of LDA score (log10) > 2.0 and P < 0.05 between the FMT group from control mice and the FMT group from KO mice. The LDA scores of the FMT group from KO mice was negative, while those of the FMT group from control mice was positive.
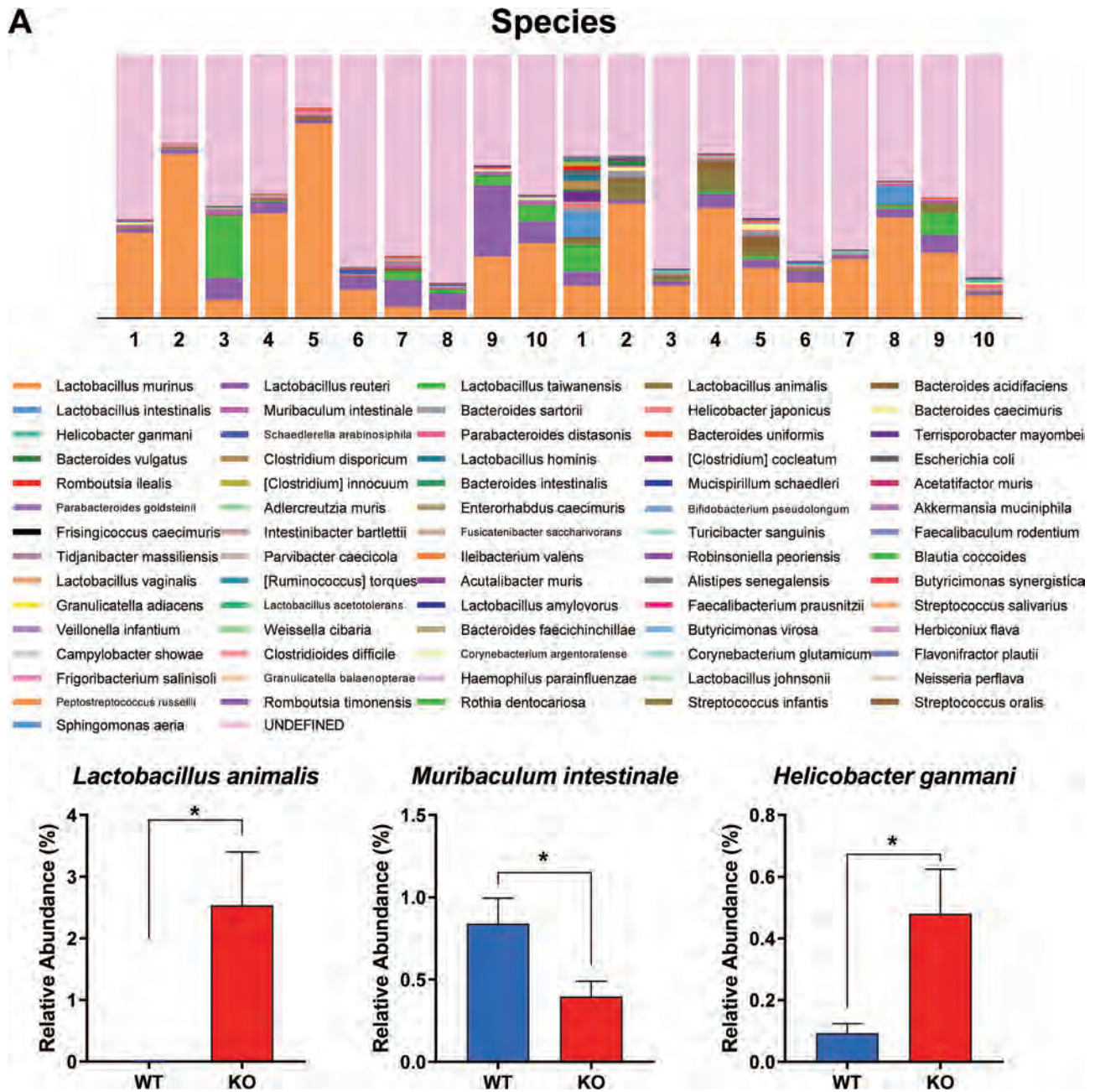
Fig. 5. Altered gut bacteria composition at the species level (A): Relative abundance at the phylum level in the FMT group from control mice and the FMT group from KO mice. *Lactobasillus animals* (Mann-Whitney U test: U = 21, P = 0.026). *Muribaculum intestinale* (Mann-Whitney U test: U = 22, P = 0.034). *Helicobacter ganmani* (Mann-Whitney U test: U = 23.5, P = 0.045). The data represent mean ± S.E.M. (n = 10). *P < 0.05.

phenotypes in the ABX-treated mice after FMT of "depression-related microbes" from the KO mice. In contrast, vagotomy significantly enhanced the serum levels of C-reactive protein (CRP) and tissue levels of IL-6 and IL-1β in the colon of WT mice treated with dextran sulfate sodium (DSS), whereas vagotomy did not affect serum CRP levels of DSS-treated *Chrna7* KO mice (Ghia et al., 2009), suggesting that vagotomy had no effect on the DSS-induced colitis in *Chrna7* KO mice. Although the precise mechanisms underlying the depression-like phenotypes of the ABX-treated mice after FMT from the KO mice are currently unknown, this study shows that the subdiaphragmatic vagus nerve is necessary for depression-like phenotypes in mice after FMT of "depression-related microbes" from *Chrna7* KO mice. Interestingly, accumulating evidence suggests that vagus nerve stimulation might produce anti-inflammatory actions within the central nervous system

(CNS), as it has been used for the treatment of depression (Bonaz et al., 2019; Liu et al., 2020a, 2020b; Pope and Wood, 2020). It is also known that vagus nerve stimulation affects the activity of the hypothalamic-pituitary axis in humans (Agorastos et al., 2019; O'Keane et al., 2005). A subsequent detailed study of the role of the subdiaphragmatic vagus nerve on the cross-talk between the brain and the gut microbiota is needed.

This study has two limitations. First, we did not identify the specific microbes which contribute to depression-like phenotypes in ABX-treated mice after FMT from *Chrna7* KO mice. Further study is needed to characterize these microbes. Second, we did not investigate the inflammatory state (i.e., microglial activation) in the CNS of ABX-treated mice after FMT from *Chrna7* KO. Further study is also needed to investigate the inflammatory state of the CNS.
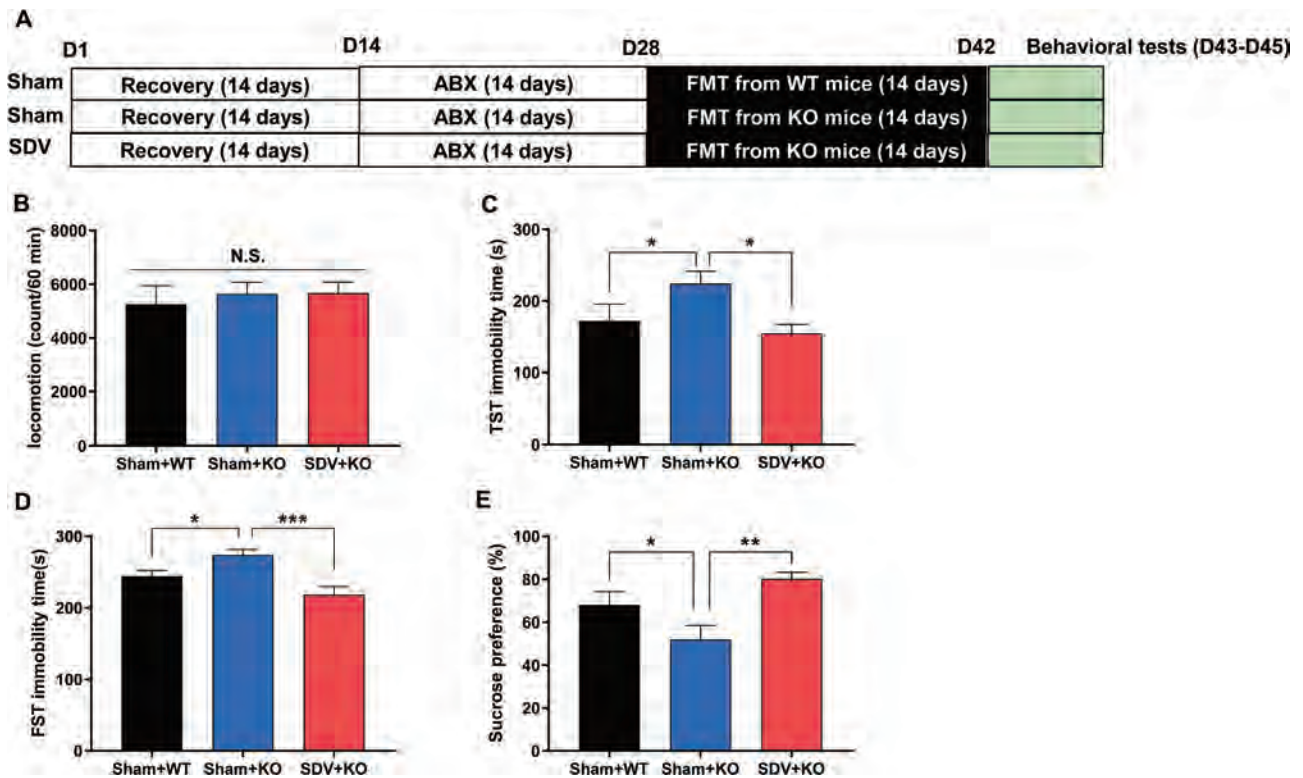
Fig. 6. Effects of SDV on depression-like phenotypes after FMT from KO mice (A): Schedule of SDV, treatment with antibiotic cocktail (ABX), FMT, behavioral tests, and sample collection. (B): Locomotion test (LMT) (one-way ANOVA: $F_{2,31} = 0.695$, $P = 0.507$). (C): TST (one-way ANOVA: $F_{2,31} = 3.974$, $P = 0.029$). (D): FST (one-way ANOVA: $F_{2,31} = 9.087$, $P < 0.001$). (E): SPT (one-way ANOVA: $F_{2,31} = 6.911$, $P = 0.003$). *$P < 0.05$, **$P < 0.01$, ***$P < 0.001$.

In conclusion, this study showed that FMT of "depression-related microbes" from *Chrna7* KO mice caused depression-like phenotypes in ABX-treated mice via the subdiaphragmatic vagus nerve. Further studies of the role of the brain–gut–microbiota axis via the subdiaphragmatic vagus nerve in depression are needed.

Statement of interest

Dr. Hashimoto has received research support from Dainippon-Sumitomo, Otsuka, and Taisho. The other authors report no biomedical financial interests or potential conflicts of interest.

Appendix A. Supplementary data

Supplementary data to this article can be found online at https://doi.org/10.1016/j.bbi.2020.12.032.

References

Agorastos, A., Heinig, A., Stiedl, O., Hager, T., Sommer, A., Müller, J.C., Schruers, K.R., Wiedemann, K., Demiralay, C., 2019. Vagal effects of endocrine HPA axis challenges on resting autonomic activity assessed by heart rate variability measures in healthy humans. Psychoneuroendocrinology 102, 196–203.

Alzarea, S., Rahman, S., 2019. α7 nicotinic receptor allosteric modulator PNU120596 prevents lipopolysaccharide-induced anxiety, cognitive deficit and depression-like behaviors in mice. Behav. Brain Res. 366, 19–28.

Becattini, S., Taur, Y., Pamer, E.G., 2016. Antibiotic-induced changes in the intestinal microbiota and disease. Trends Mol. Med. 22, 458–478.

Bonaz, B., Bazin, T., Pellissier, S., 2018. The vagus nerve at the interface of the microbiota-gut-brain axis. Front. Neurosci. 12, 49.

Bonaz, B., Sinniger, V., Pellissier, S., 2019. Vagus nerve stimulation at the interface of brain – gut interactions. Cold Spring Harb. Perspect. Med. 9, a034199.

Bravo, J.A., Forsythe, P., Chew, M.V., Escaravage, E., Savignac, H.M., Dinan, T.G., Bienenstock, J., Cryan, J.F., 2011. Ingestion of *Lactobacillus* strain regulates emotional behavior and central GABA receptor expression in a mouse via the vagus nerve. Proc. Natl Acad. Sci. U S A 108, 16050–16055.

Cawthon, C.R., de La Serre, C.B., 2018. Gut bacteria interaction with vagal afferents. Brain Res. 1693 (Pt B), 134–139.

Corsi-Zuelli, F.M.D.G., Brognara, F., Quirino, G.F.D.S., Hiroki, C.H., Fais, R.S., Del-Ben, C.M., Ulloa, L., Salgado, H.C., Kanashiro, A., Loureiro, C.M., 2017. Neuroimmune interactions in schizophrenia: focus on vagus nerve stimulation and activation of the alpha-7 nicotinic acetylcholine receptor. Front. Immunol. 8, 618.

Cryan, J.F., O'Riordan, K.J., Cowan, C.S.M., Sandhu, K.V., Bastiaanssen, T.F.S., Boehme, M., Codagnone, M.G., Cussotto, S., Fulling, C., Golubeva, A.V., Guzzetta, K. E., Jaggar, M., Long-Smith, C.M., Lyte, J.M., Martin, J.A., Molinero-Perez, A., Moloney, G., Morelli, E., Morillas, E., O'Connor, R., Cruz-Pereira, J.S., Peterson, V.L., Rea, K., Ritz, N.L., Sherwin, E., Spichak, S., Teichman, E.M., van de Wouw, M., Ventura-Silva, A.P., Wallace-Fitzsimons, S.E., Hyland, N., Clarke, G., Dinan, T.G., 2019. The microbiota-gut-brain axis. Physiol. Rev. 99, 1877–2013.

Dalile, B., Van Oudenhove, L., Vervliet, B., Verbeke, K., 2019. The role of short-chain fatty acids in microbiota-gut-brain communication. Nat. Rev. Gastroenterol. Hepatol. 16, 461–478.

Dinan, T.G., Cryan, J.F., 2017. Brain-gut-microbiota axis and mental health. Psychosom. Med. 79, 920–926.

Dowden, R.A., McGuinness, L.R., Wisniewski, P.J., Campbell, S.C., Guers, J.J., Oydanich, M., Vatner, S.F., Häggblom, M.M., Kerkhof, L.J., 2020. Host genotype and exercise exhibit species-level selection for members of the gut bacterial communities in the mouse digestive system. Sci. Rep. 10, 8984.

Duman, R.S., Aghajanian, G.K., 2012. Synaptic dysfunction in depression: potential therapeutic targets. Science 338, 68–72.

Forsythe, P., Bienenstock, J., Kunze, W.A., 2014. Vagal pathway for microbiome-brain-gut axis communication. Adv. Exp. Med. Biol. 817, 115–133.

Ghia, J.E., Blennerhassett, P., Deng, Y., Verdu, E.F., Khan, W.I., Collins, S.M., 2009. Reactivation of inflammatory bowel disease in a mouse model of depression. Gastroenterology 136, 2280–2288.

Hashimoto, K., 2015a. Tropisetron and its targets in Alzheimer's disease. Expert Opin. Ther. Targets 19, 1–5.

Hashimoto, K., 2015b. Targeting of α7 nicotinic acetylcholine receptors in the treatment of schizophrenia and the use of auditory sensory gating as a translational biomarker. Curr. Pharm. Des. 21, 3797–3806.

8

Hernández-Chirlaque, C., Aranda, C.J., Ocón, B., Capitán-Cañadas, F., Ortega-González, M., Carrero, J.J., Suárez, M.D., Zarzuelo, A., Sánchez de Medina, F., Martínez-Augustín, O., 2016. Germ-free and antibiotic-treated mice are highly susceptible to epithelial injury in DSS colitis. J Crohn's Colitis. 10, 1324–1335.

Hoover, D.B., 2017. Cholinergic modulation of the immune system presents new approaches for treating inflammation. Pharmacol. Ther. 179, 1–16.

Huang, N., Hua, D., Zhan, G., Li, S., Zhu, B., Jiang, R., Yang, L., Bi, J., Xu, H., Hashimoto, K., Luo, A., Yang, C., 2019. Role of *Actinobacteria* and *Coriobacteriia* in the antidepressant effects of ketamine in an inflammation model of depression. Pharmacol. Biochem. Behav. 176, 93–100.

Ishikawa, M., Hashimoto, K., 2011. α7 nicotinic acetylcholine receptor as a potential therapeutic target for schizophrenia. Curr. Pharm. Des. 17, 121–129.

Jiang, H., Ling, Z., Zhang, Y., Mao, H., Ma, Z., Yin, Y., Wang, W., Tang, W., Tan, Z., Shi, J., Li, L., Ruan, B., 2015. Altered fecal microbiota composition in patients with major depressive disorder. Brain Behav. Immun. 48, 186–194.

Kalkman, H.O., Feuerbach, D., 2016. Modulatory effects of α7 nAChRs on the immune system and its relevance for CNS disorders. Cell Mol. Life Sci. 73, 2511–2530.

Karunasena, E., Kurkure, P.C., Lackey, R.D., McMahon, K.W., Kiernan, E.P., Graham, S., Alabady, M.S., Campos, D.L., Tatum, O.L., Brashears, M.M., 2013. Effects of the probiotic *Lactobacillus animalis* in murine *Mycobacterium avium* subspecies paratuberculosis infection. BMC Microbiol. 13, 8.

Karunasena, E., McMahon, K.W., Kurkure, P.C., Brashears, M.M., 2014. A comparison of cell mediators and serum cytokines transcript expression between male and female mice infected with *Mycobacterium avium* subspecies paratuberculosis and/or consuming probiotics. Pathog. Dis. 72, 104–110.

Kennedy, E.A., King, K.Y., Baldridge, M.T., 2018. Mouse microbiota models: comparing germ-free mice and antibiotics treatment as tools for modifying gut bacteria. Front. Physiol. 9, 1534.

Konsman, J.P., Luheshi, G.N., Bluthé, R.M., Dantzer, R., 2000. The vagus nerve mediates behavioural depression, but not fever, in response to peripheral immune signals; a functional anatomical analysis. Eur. J. Neurosci. 12, 4434–4446.

Lagkouvardos, I., Pukall, R., Abt, B., Foesel, B.U., Meier-Kolthoff, J.P., Kumar, N., Bresciani, A., Martínez, I., Just, S., Ziegler, C., Brugiroux, S., Garzetti, D., Wenning, M., Bui, T.P., Wang, J., Hugenholtz, F., Plugge, C.M., Peterson, D.A., Hornef, M.W., Baines, J.F., Smidt, H., Walter, J., Kristiansen, K., Nielsen, H.B., Haller, D., Overmann, J., Stecher, B., Clavel, T., 2016. The Mouse Intestinal Bacterial Collection (miBC) provides host-specific insight into cultured diversity and functional potential of the gut microbiota. Nat. Microbiol. 1, 16131.

Lei, W., Duan, Z., 2019. Advances in the treatment of cholinergic anti-inflammatory pathways in gastrointestinal diseases by electrical stimulation of vagus nerve. Digestion 2019 Nov 29;1–11. doi: 10.1159/000504474.

Liu, R.T., Rowan-Nash, A.D., Sheehan, A.E., Walsh, R.F.L., Sanzari, C.M., Korry, B.J., Belenky, P., 2020a. Reductions in anti-inflammatory gut bacteria are associated with depression in a sample of young adults. Brain Behav. Immun. 88, 308–324.

Liu, C.H., Yang, M.H., Zhang, G.Z., Wang, X.X., Li, B., Li, M., Woelfer, M., Walter, M., Wang, L., 2020b. J. Neuroinflammation 17, 54.

Lu, B., Kwan, K., Levine, Y.A., Olofsson, P.S., Yang, H., Li, J., Joshi, S., Wang, H., Andersson, U., Chavan, S.S., Tracey, K.J., 2014. α7 nicotinic acetylcholine receptor signaling inhibits inflammasome activation by preventing mitochondrial DNA release. Mol. Med. 14, 350–358.

Luo, Y., Zeng, B., Zeng, L., Du, X., Li, B., Huo, R., Liu, L., Wang, H., Dong, M., Pan, J., Zheng, P., Zhou, C., Wei, H., Xie, P., 2018. Gut microbiota regulates mouse behaviors through glucocorticoid receptor pathway genes in the hippocampus. Transl. Psychiatry 8, 187.

Martelli, D., McKinley, M.J., McAllen, R.M., 2014. The cholinergic anti-inflammatory pathway: a critical review. Auton. Neurosci. 182, 65–69.

Moriguchi, S., Inagaki, R., Yi, L., Shibata, M., Sakagami, H., Fukunaga, K., 2020. Nicotine rescues depressive-like behaviors via α7-type nicotinic acetylcholine receptor activation in CaMKIV null mice. Mol. Neurobiol. 57, 4929–4940.

O'Keane, V., Dinan, T.G., Scott, L., Corcoran, C., 2005. Changes in hypothalamic-pituitary-adrenal axis measures after vagus nerve stimulation therapy in chronic depression. Biol. Psychiatry 58, 963–968.

Pope, B.S., Wood, S.K., 2020. Advances in understanding mechanisms and therapeutic targets to treat comorbid depression and cardiovascular disease. Neurosci. Biobehav. Rev. 116, 337–349.

Pu, Y., Chang, L., Qu, Y., Wang, S., Zhang, K., Hashimoto, K., 2019. Antibiotic-induced microbiome depletion protects against MPTP-induced dopaminergic neurotoxicity in the brain. Aging (Albany NY) 11, 6915–6929.

Qu, Y., Yang, C., Ren, Q., Ma, M., Dong, C., Hashimoto, K., 2017. Comparison of (*R*)-ketamine and lanicemine on depression-like phenotype and abnormal composition of gut microbiota in a social defeat stress model. Sci. Rep. 7, 15725.

Robertson, B.R., O'Rourke, J.L., Vandamme, P., On, S.L., Lee, A., 2001. *Helicobacter ganmani sp. nov.*, a urease-negative anaerobe isolated from the intestines of laboratory mice. Int. J. Syst. Evol. Microbiol. 51 (Pt 5), 1881–1889.

Segata, N., Izard, J., Waldron, L., Gevers, D., Miropolsky, L., Garrett, W.S., Huttenhower, C., 2011. Metagenomic biomarker discovery and explanation. Genome Biol. 12, R60.

Shin, J., Lee, S., Go, M.J., Lee, S.Y., Kim, S.C., Lee, C.H., Cho, B.K., 2016. Analysis of the mouse gut microbiome using full-length 16S rRNA amplicon sequencing. Sci. Rep. 6, 29681.

Silva, Y.P., Bernardi, A., Frozza, R.L., 2020. The role of short-chain fatty acids from gut microbiota in gut-brain communication. Front. Endocrinol. 11, 25.

Snijders, A.M., Langley, S.A., Kim, Y.M., Brislawn, C.J., Noecker, C., Zink, E.M., Fansler, S.J., Casey, C.P., Miller, D.R., Huang, Y., Karpen, G.H., Celniker, S.E., Brown, J.B., Borenstein, E., Jansson, J.K., Metz, T.O., Mao, J.H., 2016. Influence of early life exposure, host genetics and diet on the mouse gut microbiome and metabolome. Nat. Microbiol. 2, 16221.

Suzuki, T., Hide, I., Matsubara, A., Hama, C., Harada, K., Miyano, K., Andrä, M., Matsubayashi, H., Sakai, N., Kohsaka, S., Inoue, K., Nakata, Y., 2006. Microglial α7 nicotinic acetylcholine receptors drive a phospholipase C/IP3 pathway and modulate the cell activation toward a neuroprotective role. J. Neurosci. Res. 83, 1461–1470.

Thomsen, M.S., Mikkelsen, J.D., 2012. The α7 nicotinic acetylcholine receptor ligands methyllycaconitine, NS6740 and GTS-21 reduce lipopolysaccharide-induced TNF-α release from microglia. J. Neuroimmunol. 251, 65–72.

Toyohara, J., Hashimoto, K., 2010. Alpha-7 nicotinic receptor agonists: Potential therapeutic drugs for treatment of cognitive impairments in schizophrenia and Alzheimer's disease. Open Med. Chem. J. 4, 37–56.

Ulloa, L., 2005. The vagus nerve and the nicotinic anti-inflammatory pathway. Nat. Rev. Drug Discov. 4, 673–684.

Xin, Y., Sun, J., 2017. Hypothesis testing and statistical analysis of microbiome. Genes Diseases 4, 138–148.

Wang, S., Ishima, T., Zhang, J., Qu, Y., Chang, L., Pu, Y., Fujita, Y., Tan, Y., Wang, X., Hashimoto, K., 2020a. Ingestion of *Lactobacillus intestinalis* and *Lactobacillus reuteri* causes depression- and anhedonia-like phenotypes in antibiotic-treated mice via the vagus nerve. J. Neuroinflammation. 17, 241.

Wang, S., Qu, Y., Chang, L., Pu, Y., Zhang, K., Hashimoto, K., 2020b. Antibiotic-induced microbiome depletion is associated with resilience in mice after chronic social defeat stress. J. Affect. Disord. 260, 448–457.

Wang, H., Yu, M., Ochani, M., Amella, C.A., Tanovic, M., Susarla, S., Li, J.H., Wang, H., Yang, H., Ulloa, L., Al-Abed, Y., Czura, C.J., Tracey, K.J., 2003. Nicotinic acetylcholine receptor α7 subunit is an essential regulator of inflammation. Nature 421, 384–388 (2003).

Wong, M.L., Inserra, A., Lewis, M.D., Mastronardi, C.A., Leong, L., Choo, J., Kentish, S., Xie, P., Morrison, M., Wesselingh, S.L., Rogers, G.B., Licinio, J., 2016. Inflammasome signaling affects anxiety- and depressive-like behavior and gut microbiome composition. Mol. Psychiatry 21, 797–805.

Wu, M., Tian, T., Mao, Q., Zou, T., Zhou, C.J., Xie, J., Chen, J.J., 2020. Associations between disordered gut microbiota and changes of neurotransmitters and short-chain fatty acids in depressed mice. Transl. Psychiatry 10, 350.

Yang, C., Fang, X., Zhan, G., Huang, N., Li, S., Bi, J., Jiang, R., Yang, L., Miao, L., Zhu, B., Luo, A., Hashimoto, K., 2019. Key role of gut microbiota in anhedonia-like phenotype in rodents with neuropathic pain. Transl. Psychiatry 9, 57.

Yang, C., Qu, Y., Fujita, Y., Ren, Q., Ma, M., Dong, C., Hashimoto, K., 2017. Possible role of the gut microbiota-brain axis in the antidepressant effects of (*R*)-ketamine in a social defeat stress model. Transl. Psychiatry 7, 1294.

Yang, C., Shirayama, Y., Zhang, J.C., Ren, Q., Yao, W., Ma, M., Dong, C., Hashimoto, K., 2015. *R*-ketamine: a rapid-onset and sustained antidepressant without psychotomimetic side effects. Transl. Psychiatry 5, e632.

Zhan, G., Yang, N., Li, S., Huang, N., Fang, X., Zhang, J., Zhu, B., Yang, C., Luo, A., 2018. Abnormal gut microbiota composition contributes to cognitive dysfunction in SAMP8 mice. Aging (Albany NY) 10, 1257–1267.

Zhang, L., Danon, S.J., Grehan, M., Chan, V., Lee, A., Mitchell, H., 2005. Natural colonization with *Helicobacter* species and the development of inflammatory bowel disease in interleukin-10-deficient mice. Helicobacter 10, 223–230.

Zhang, K., Fujita, Y., Chang, L., Qu, Y., Pu, Y., Wang, S., Shirayama, Y., Hashimoto, K., 2019. Abnormal composition of gut microbiota is associated with resilience versus susceptibility to inescapable electric stress. Transl. Psychiatry 9, 231.

Zhang, J., Ma, L., Chang, L., Pu, Y., Qu, Y., Hashimoto, K., 2020. A key role of the subdiaphragmatic vagus nerve in the depression-like phenotype and abnormal composition of gut microbiota in mice after lipopolysaccharide administration. Transl. Psychiatry 10, 186.

Zhang, J.C., Wu, J., Fujita, Y., Yao, W., Ren, Q., Yang, C., Li, S.X., Shirayama, Y., Hashimoto, K., 2014. Antidepressant effects of TrkB ligands on depression-like behavior and dendritic changes in mice after inflammation. Int. J. Neuropsychopharmacol. 18, pyuu077.

Zhang, J.C., Yao, W., Dong, C., Yang, C., Ren, Q., Ma, M., Hashimoto, K., 2017. Blockade of interleukin-6 receptor in the periphery promotes rapid and sustained antidepressant actions: a possible role of gut-microbiota-brain axis. Transl. Psychiatry 7, e1138.

Zhang, J.C., Yao, W., Ren, Q., Yang, C., Dong, C., Ma, M., Wu, J., Hashimoto, K., 2016. Depression-like phenotype by deletion of α7 nicotinic acetylcholine receptor: Role of BDNF-TrkB in nucleus accumbens. Sci. Rep. 6, 36705.

Zhao, D., Xu, X., Pan, L., Zhu, W., Fu, X., Guo, L., Lu, Q., Wang, J., 2017. Pharmacologic activation of cholinergic α7 nicotinic receptors mitigates depressive-like behavior in a mouse model of chronic stress. J. Neuroinflammation 14, 234.

Zheng, P., Zeng, B., Zhou, C., Liu, M., Fang, Z., Xu, X., Zeng, L., Chen, J., Fan, S., Du, X., Zhang, X., Yang, D., Yang, Y., Meng, H., Li, W., Melgiri, N.D., Licinio, J., Wei, H., Xie, P., 2016. Gut microbiome remodeling induces depressive-like behaviors through a pathway mediated by the host's metabolism. Mol. Psychiatry 21, 786–796.

Dextran sulfate sodium-induced inflammation and colitis in mice are ameliorated by (R)-ketamine, but not (S)-ketamine: A role of TrkB signaling

Yuko Fujita [a], Yaeko Hashimoto [a,b], Hiroyo Hashimoto [a,c], Lijia Chang [a], Kenji Hashimoto [a,*]

[a] *Division of Clinical Neuroscience, Chiba University Center for Forensic Mental Health, Chiba, 260-8670, Japan*
[b] *Department of Respirology, Chiba University Graduate School of Medicine, Chiba, 260-8670, Japan*
[c] *Department of Dermatology, Chiba University Graduate School of Medicine, Chiba, 260-8670, Japan*

ABSTRACT

Ulcerative colitis (UC) is a chronic inflammatory bowel disease that causes long-lasting inflammation and colitis in the gastrointestinal tract. Depression is a common symptom in patients with UC. (R)-ketamine is a new safer antidepressant than (R,S)-ketamine and (S)-ketamine. Here, we examined the effects of two ketamine enantiomers on the dextran sulfate sodium (DSS)-induced colitis model of UC. Ingestion of 3% DSS in drinking water for 14 days increased the scores of Disease Activity Index (DAI) in mice. Repeated administration of (R)-ketamine (10 mg/kg/day, 14 days or last 7 days), but not (S)-ketamine (10 mg/kg/day, 14 days or last 7 days), significantly ameliorated the increased DAI score and increased blood levels of interleukin-6 (IL-6) in DSS-treated mice. In addition, (R)-ketamine, but not (S)-ketamine, attenuated the reduced colonic length in DSS-treated mice. Furthermore, DSS-induced increased DAI score and blood IL-6 levels were significantly ameliorated after subsequent repeated administration of (R)-ketamine (10 mg/kg/day for last 7 days), but not 5-aminosalicyclic acid (50 mg/kg/day for last 7 days). Moreover, the pretreatment with a tropomyosin-receptor-kinase B (TrkB) antagonist ANA-12 (0.5 mg/kg) significantly blocked the beneficial effects of (R)-ketamine in DSS-induced UC model. The study shows that (R)-ketamine can produce beneficial effects in DSS-induced colitis model through TrkB stimulation. Therefore, (R)-ketamine may be a novel therapeutic drug for inflammatory bowel diseases such as UC.

1. Introduction

Ulcerative colitis (UC) is a chronic inflammatory bowel disease that causes long-lasting inflammation, ulcers and colitis in the gastrointestinal tract. Several lines of evidence show that UC patients have a high incidence of depression, and that depression worsens the prognosis of UC (Bernstein et al., 2019; Marrie et al., 2016; Mikocka-Walus et al., 2016; Mittermaier et al., 2004; Neuendorf et al., 2016; Walker et al., 2008). A cohort study demonstrated that individuals with depression had a greater risk (hazard risk = 2.23) of developing UC after controlling for demographic and clinical covariates, and that the use of antidepressants can attenuate the risk for UC (Frolkis et al., 2019). Therefore, the treatment for depression in UC patients is of great important (Mikocka-Walus et al., 2020).

The *N*-methyl-D-aspartate (NMDA) receptor antagonist (R,S)-ketamine produces rapid-onset antidepressant actions in treatment-resistant patients with major depressive disorder (MDD) (Kishimoto et al., 2016;

Krystal et al., 2019; Newport et al., 2015; Zhang and Hashimoto, 2019). (R,S)-ketamine (Ki = 0.53 μM for NMDA receptor) is a mixture containing equal amount of (R)-ketamine (Ki = 1.4 μM for NMDA receptor) and (S)-ketamine (Ki = 0.30 μM for NMDA receptor) (Ebert et al., 1997). It is reported that (R)-ketamine could produce greater potency and longer-lasting antidepressant-like effects than (S)-ketamine in several rodent models of depression (Chang et al., 2019; Fukumoto et al., 2017; Yang et al., 2015, 2018; Zhang et al., 2014). Importantly, the side effects of (R)-ketamine in rodents, monkeys, and humans were lower than those of (R,S)-ketamine and (S)-ketamine (Chang et al., 2019; Hashimoto et al., 2017; Tan and Hashimoto, 2020; Vollenweider et al., 1997; Yang et al., 2015). An open-label study in Brazil demonstrated that (R)-ketamine produced rapid-acting and sustained antidepressant effects in treatment-resistant patients with MDD (Leal et al., 2020). Taken together, (R)-ketamine would be a safer antidepressant than (R,S)-ketamine and (S)-ketamine (Hashimoto, 2019, 2020; Wei et al., 2020; Yang et al., 2019). Considering the comorbidity of depression in peoples

---

* Corresponding author.
 E-mail address: hashimoto@faculty.chiba-u.jp (K. Hashimoto).

with UC, it is of great interest to study whether (*R*)-ketamine could produce rapid-acting antidepressant actions in UC patients with depression. At present, there is no report investigating the effects of ketamine enantiomers in rodent models of UC.

Dextran sulfate sodium (DSS)-induced colitis model of mouse has been widely used because of its simplicity and many similarities with UC in humans (Chassaing et al., 2014; Perše and Cerar, 2012). In this study, we investigated the effects of (*R*)-ketamine and (*S*)-ketamine in DSS-induced colitis model of mice. Previously, we demonstrated that tropomyosin-receptor-kinase B (TrkB) plays a role in the beneficial effects of (*R*)-ketamine since TrkB antagonist ANA-12 blocked the beneficial effects of (*R*)-ketamine in several animal models (Fujita et al., 2019; Tan et al., 2020; Yang et al., 2015). Therefore, we examined the role of TrkB in the beneficial effects of (*R*)-ketamine in DSS-induced model since the expression of TrkB in the colon of mouse (Wang et al., 2016) and human (Xu et al., 2020b) was reported.

2. Materials and methods

2.1. Animals

Male Balb/C mice (aged 6 weeks, body weight 25–30 g) were purchased from Japan SLC, Inc (Hamamatsu, Shizuoka, Japan). Mice were housed under controlled conditions ($23 \pm 1\,^{\circ}$C; $55 \pm 5\%$ humidity; a 12-

h light–dark cycle, lights on 7:00 a.m.; food and water *ad libitum*). Chiba University Institutional Animal Care and Use Committee approved the experimental protocol of this study (Permission number: 30–321 and 1–134). Mice were deeply anaesthetized with isoflurane before sacrifice. All efforts were made to minimize suffering.

2.2. Materials

Dextran sulfate sodium (DSS) salt colitis grade (Cat No. 160110. M. W. 36,000–50,000, MP Biomedicals, Inc., Canada) was dissolved in water. (*R*)-ketamine hydrochloride [or (*S*)-ketamine hydrochloride] was prepared by recrystallization of (*R,S*)-ketamine (Ketalar®, Daiichi Sankyo Pharmaceutical Ltd., Tokyo, Japan) and D-(−)-tartaric acid [or (L-(+)-tartaric acid), as previously reported (Zhang et al., 2014). The dose (10 mg/kg as hydrochloride) of ketamine enantiomers dissolved in saline was used since the dose (10 mg/kg) of (*R*)-ketamine was effective in mouse models of other diseases such as depression, schizophrenia and Parkinson's disease (Fujita et al., 2019; Tan et al., 2020; Yang et al., 2015, 2018). 5-Aminosalicyclic acid (5-ASA: 50 mg/kg, Catalog number: A0317, Tokyo Chemical Industry Co., Ltd, Tokyo, Japan) was dissolved in the saline. ANA-12, N2-(2-{[(2-oxoazepan-3-yl) amino] carbonyl}phenyl)benzo[b] thiophene-2-carboxamide (0.5 mg/kg, Sigma–Aldrich Co., Ltd., Tokyo, Japan), was dissolved in 17% dimethylsulfoxide (DMSO) in saline (Fujita et al., 2019; Ren et al., 2015; Tan
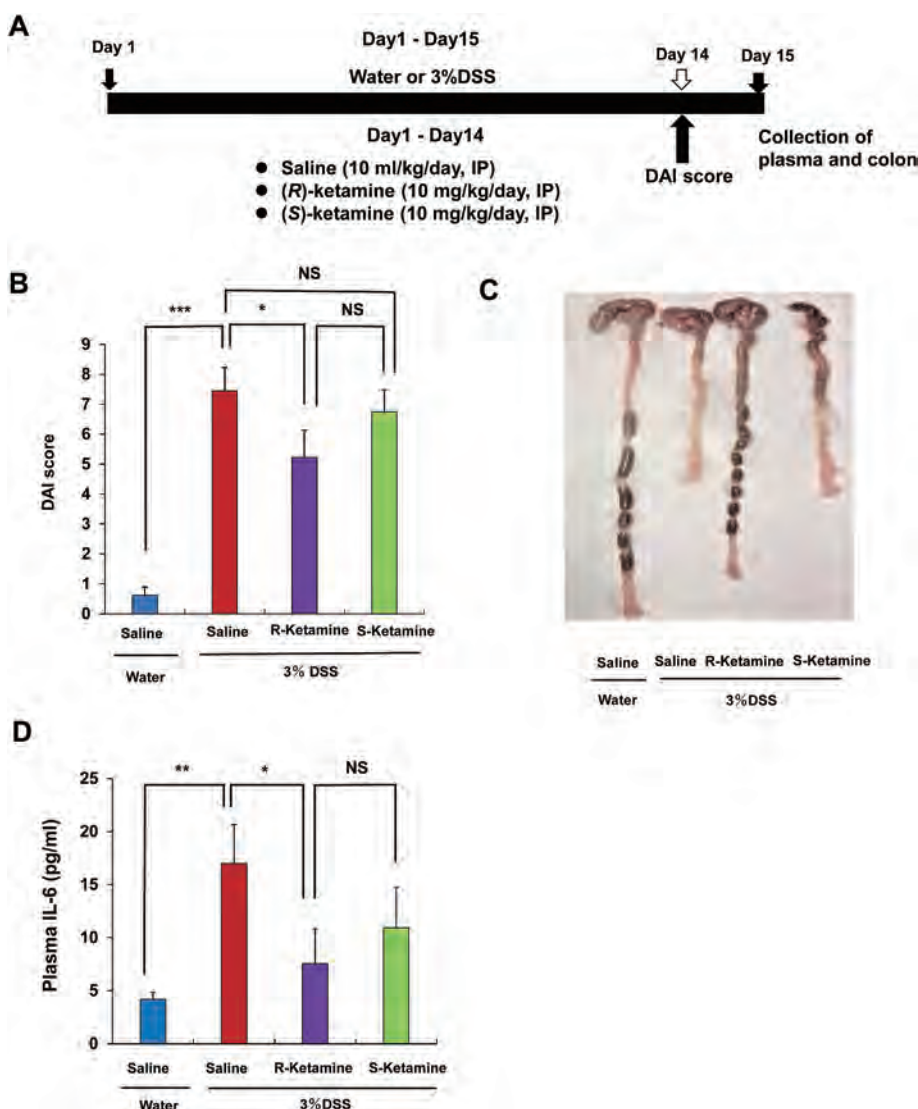

Fig. 1. Effects of (*R*)-ketamine and (*S*)-ketamine in the DSS-induced model (exp-1)(
A): The schedule of DSS-induced model, treatment, and collection of tissues. Water or 3% DSS in drinking water was given to mice for 15 days to induce colitis in mice. Subsequently, saline (10 ml/kg/day), (*R*)-ketamine (10 mg/kg/day) or (*S*)-ketamine (10 mg/kg/day) was administered i.p. to mice for 14 days (day 1 – day 14). On day 14, DAI score was determined. On day 15, blood and colon samples of mice were collected. The length of colon was evaluated. (B): DAI score (one-way ANOVA: $F_{3,30} = 16.885$, P < 0.001). (C): Representative photos of colonic length in each group. (D): Plasma IL-6 levels (one-way ANOVA: $F_{3,29} = 2.948$, P = 0.049). One mouse in the saline-treated DSS group was dead on day 15. *P < 0.05, **P < 0.01, ***P < 0.001. The values represent the mean $\pm$ S.E.M. (n = 8 or 9). N.S.: not significance.

et al., 2020; Zhang et al., 2015). Other reagents were purchased commercially.

2.3. Effects of ketamine enantiomers on DSS-induced colitis

In the experiment 1, the schedule of DSS-induced model, treatment, and collection of tissues was shown in the Fig. 1A. Water or 3% DSS in drinking water was given to mice for 15 days (day 1 – day 15) to induce colitis in mice. Subsequently, saline (10 ml/kg/day), (*R*)-ketamine (10 mg/kg/day) or (*S*)-ketamine (10 mg/kg/day) was administered intraperitoneally (i.p.) to mice for 14 days (day 1 – day 14) (Fig. 1A). On day 14, Disease Activity Index (DAI) scores for the severity of colitis were evaluated by body weight loss, stool consistency and blood in the fresh stool, where which parameter varied from a score of 0–4 (the maximum score is 12 for severe colitis), as previously reported (Nunes et al., 2019). On day 15, blood samples of mice were collected, and then mice were killed. The length of colon was carefully evaluated.

In the experiment 2, the schedule of DSS-induced model, treatment, and collection of tissues was shown in the Fig. 2A. Water or 3% DSS in drinking water was given to mice for 14 days (day 1 – day 14) to induce colitis in mice. Subsequently, saline (10 ml/kg/day), (*R*)-ketamine (10 mg/kg/day) or (*S*)-ketamine (10 mg/kg/day) was administered i.p. to mice 7 days from day 8 to day 14 (Fig. 2A). On day 14, scores of DAI were measured as describe above. On day 15, blood and colon samples of mice were collected. The length of colon was carefully evaluated.

2.4. Effects of (R)-ketamine and 5-ASA on DSS-induced colitis

The schedule of DSS-induced model, treatment, and collection of tissues was shown in the Fig. 3A. Water or 3% DSS in drinking water was given to mice for 14 days (day 1 – day 14) to induce colitis in mice. Subsequently, saline (10 ml/kg/day), (*R*)-ketamine (10 mg/kg/day) or 5-ASA (50 mg/kg/day) was administered i.p. to mice 7 days from day 8 to day 14 (Fig. 3A). On day 14, scores of DAI were measured as describe above. On day 15, blood samples of mice were collected.

2.5. Effects of ANA-12 on the beneficial effects of (R)-ketamine in DSS-induced colitis model

The schedule of DSS-induced model, treatment, and collection of tissues was shown in the Fig. 4A. Water or 3% DSS in drinking water was given to mice for 14 days (day 1 – day 14) to induce colitis in mice. Subsequently, vehicle (17% DMSO: 10 ml/kg/day) + saline (10 ml/kg/day), vehicle (17% DMSO: 10 ml/kg/day) + (*R*)-ketamine (10 mg/kg/day), ANA-12 (0.5 mg/kg/day) + (*R*)-ketamine (10 mg/kg/day) or vehicle (17% DMSO: 10 ml/kg/day) + saline (10 ml/kg/day) was administered i.p. to mice 7 days from day 8 to day 14 (Fig. 4A). Vehicle or ANA-12 was administered i.p. 30 min before injection of saline or (*R*)-ketamine. On day 14, scores of DAI were measured as describe above.

2.6. Measurement of pro-inflammatory cytokines

On day 15, the mice were anesthetized deeply with isoflurane, and blood was placed into a tube containing ethylenediamine-*N,N,N′,N′*-tetraacetic acid dipotassium salt dihydrate as an anticoagulant. Blood samples were immediately centrifuged ($3,000 \times g$, 3 min) to collect plasma samples, and then plasma samples were stored at $-80\ °C$ until ELISA assay (Zhang et al., 2018b). Plasma levels of interluikin-6 (IL-6) and tumor necrosis factor-α (TNF-α) were determined using an ELISA kit (IL-6: cat#: 88–7064. TNF-α: cat#: 88–7324, Invitrogen, Carlsbad, CA, USA) (Zhang et al., 2020), according to the manufacturer's instructions.

2.7. Histology

In the experiment 2, colon samples from the four groups were collected and fixed in 10% formalin (FUJIFILM Wako Chemical

Corporation, Tokyo, Japan). Staining with hematoxylin and eosin (HE) of sections of 3 μm was performed at Biopathology Institute Co., Ltd (Kunisaki, Oita, Japan). Representative images of HE staining were obtained using a Keyence BZ-9000 Generation II microscope (Osaka, Japan). The histological score of colon samples was determined by the method (Xu et al., 2020a). The evaluation of histological score (score = 0: most healthy, score = 8: least healthy) included: 1) Crypt architecture damage score (0–2 points); 2) edema in submucosa score (0–3 points); and 3) inflammatory cell infiltration score (0–3 points) (Xu et al., 2020a).

2.8. Statistical analysis

The data show as the mean ± standard error of the mean (S.E.M.). The data were analyzed using one-way analysis of variance (ANOVA), followed by *post-hoc* Fisher's Least Significant Difference (LSD) test. The P-values of less than 0.05 were considered statistically significant.

3. Results

3.1. Effects of ketamine enantiomers in DSS-induced colitis model

DSS-induced increases in DAI score were significantly attenuated after repeated administration of (*R*)-ketamine (10 mg/kg/day), but not (*S*)-ketamine (10 mg/kg/day) (Fig. 1B). Furthermore, DSS markedly decreased the colonic length in mice. Furthermore, (*R*)-ketamine, but not (*S*)-ketamine, attenuated DSS-induced reduction of colonic length (Fig. 1C). Repeated administration of (*R*)-ketamine, but not (*S*)-ketamine, significantly attenuated the increased plasma levels of IL-6 in the DSS-treated mice (Fig. 1D).

DSS-induced increases in DAI score were significantly improved after subsequent repeated administration of (*R*)-ketamine (10 mg/kg/day for the last 7 days), but not (*S*)-ketamine (10 mg/kg/day for the last 7 days) (Fig. 2B). Furthermore, (*R*)-ketamine, but not (*S*)-ketamine, attenuated DSS-induced reduction of colonic length (Fig. 2C). Moreover, repeated administration of (*R*)-ketamine, but not (*S*)-ketamine, significantly attenuated the increased plasma levels of IL-6 in the DSS-treated mice (Fig. 2D). Both (*R*)-ketamine and (*S*)-ketamine significantly attenuated the increased plasma levels of TNF-α in the DSS-treated mice (Fig. 2E). The colonic epithelium of control mice was intact, and no ulcer or hyperplasia was shown on the mucosal surface (Fig. 2G). DSS-treated mice showed destruction of the crypts, loss of the epithelial barrier, loss of goblet cells and severe inflammation with interstitial lymphocytic infiltration (Fig. 2G). Furthermore, (*R*)-ketamine, but not (*S*)-ketamine, ameliorated DSS-induced increases of these histological changes in the colon of DSS-treated mice (Fig. 2G). Moreover, (*R*)-ketamine, but not (*S*)-ketamine, significantly ameliorated DSS-induced increases of histological score in the colon of DSS-treated mice (Fig. 2F).

3.2. Effects of (R)-ketamine and 5-ASA in DSS-induced colitis model

DSS-induced increases in DAI score were significantly improved after subsequent repeated administration of (*R*)-ketamine (10 mg/kg/day for the last 7 days), but not 5-ASA (50 mg/kg/day for the last 7 days) (Fig. 3B). Repeated administration of (*R*)-ketamine, but not 5-ASA, significantly attenuated the increased plasma levels of IL-6 in the DSS-treated mice (Fig. 3C).

3.3. Effects of ANA-12 in the beneficial effects of (R)-ketamine in DSS-induced colitis model

We previously reported that ANA-12 blocked the beneficial effects of (*R*)-ketamine in several mouse models (Fujita et al., 2019; Tan et al., 2020; Yang et al., 2015), suggesting a role of TrkB signaling in the action of (*R*)-ketamine. In order to the role of TrkB signaling in the effects of (*R*)-ketamine in DSS-induced colitis model, we examined the effects of
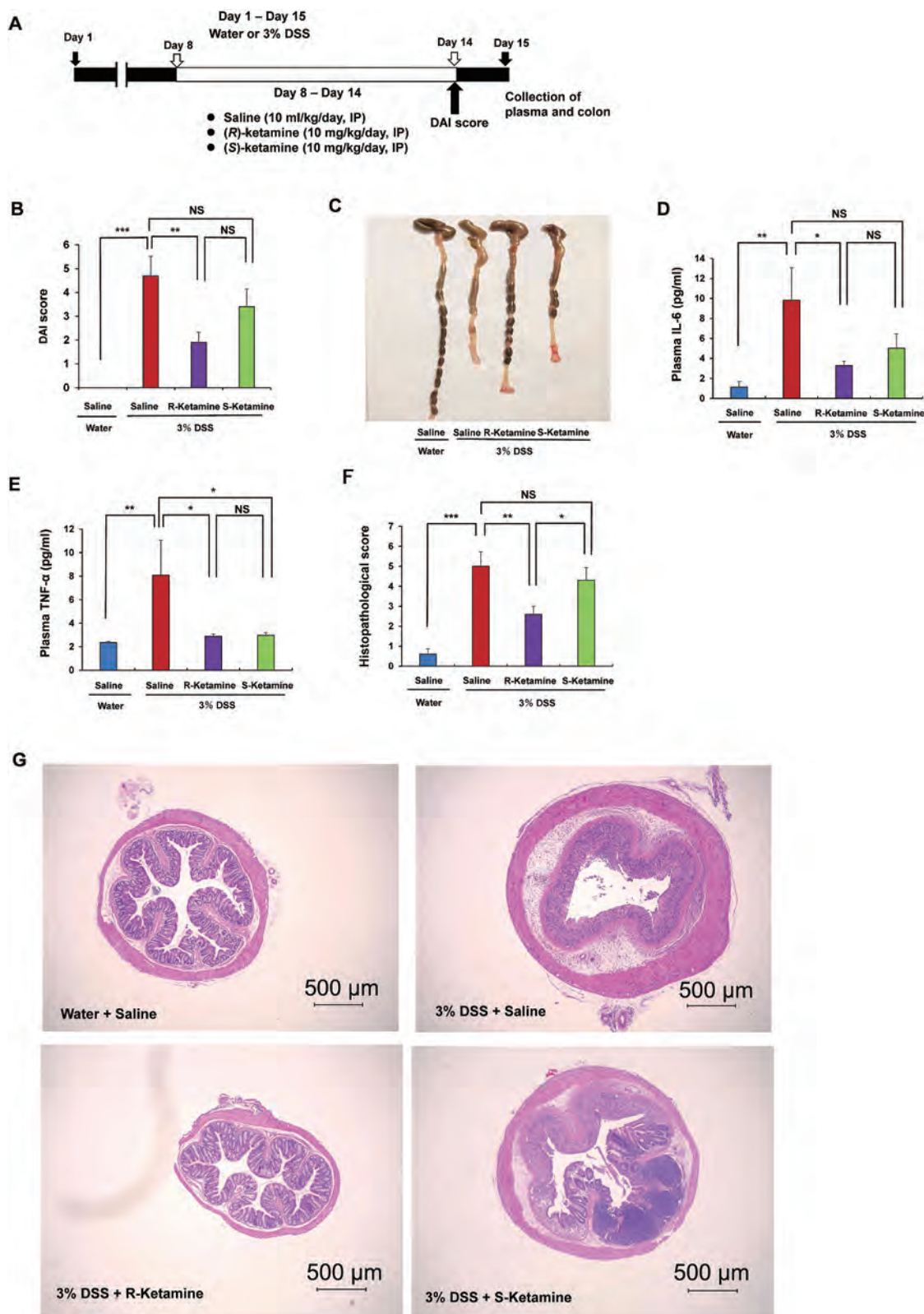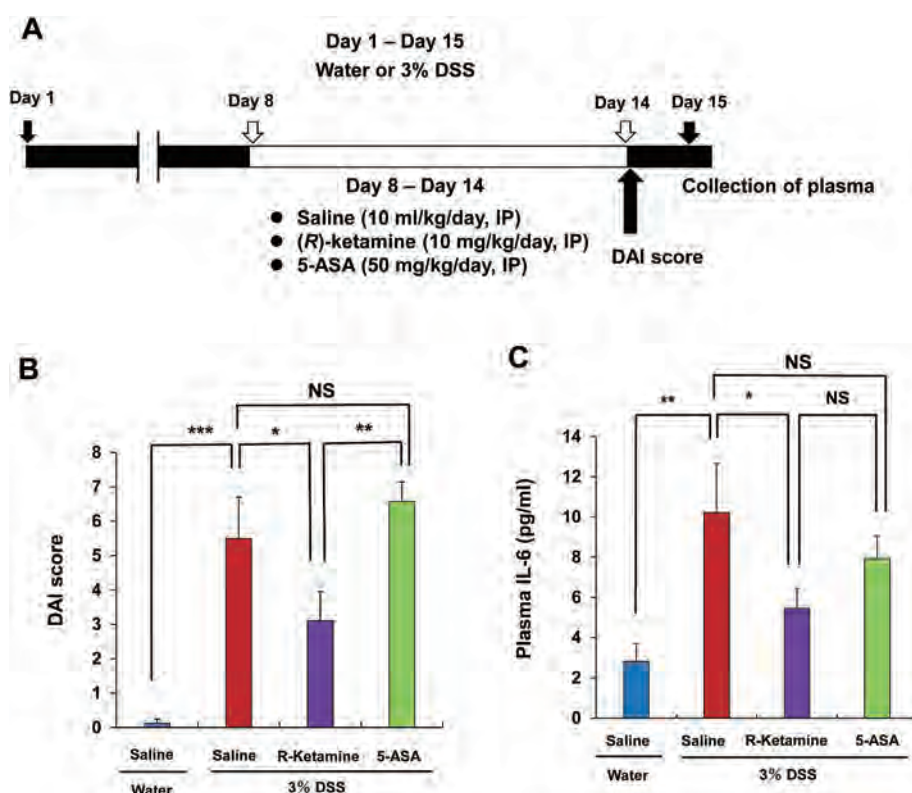
3

Fig. 2. Effects of (*R*)-ketamine and (*S*)-ketamine in the DSS-induced model (exp-2)(
A): The schedule of DSS-induced model, treatment, and collection of tissues. Water or 3% DSS in drinking water was given to mice for 15 days to induce colitis in mice. Subsequently, saline (10 ml/kg/day), (*R*)-ketamine (10 mg/kg/day) or (*S*)-ketamine (10 mg/kg/day) was administered i.p. to mice for 7 days (day 8 – day 14). On day 14, DAI score was determined. On day 15, blood and colon samples of mice were collected. (B): DAI score (one-way ANOVA: $F_{3,36} = 11.548$, $P < 0.001$). (C): Representative photos of colonic length in each group. (D): Plasma IL-6 levels (one-way ANOVA: $F_{3,36} = 4.152$, $P = 0.013$). (E): Plasma TNF-α levels (one-way ANOVA: $F_{3,36} = 3.220$, $P = 0.034$). (F): Histological score of colon samples (one-way ANOVA: $F_{3,36} = 13.210$, $P < 0.001$). (G): Representative sections of HE staining of colon samples. Scale bar = 500 μm. *$P < 0.05$, **$P < 0.01$, ***$P < 0.001$. The values represent the mean ± S.E.M. (n = 10). N.S.: not significance.

4

Fig. 3. Effects of (*R*)-ketamine and 5-ASA in the DSS-induced model
(A): The schedule of DSS-induced model, treatment, and collection of tissues. Water or 3% DSS in drinking water was given to mice for 15 days to induce colitis in mice. Subsequently, saline (10 ml/kg/day), (*R*)-ketamine (10 mg/kg/day) or 5-ASA (50 mg/kg/day) was administered i.p. to mice for 7 days (day 8 – day 14). On day 14, DAI score was determined. On day 15, blood samples of mice were collected. (B): DAI score (one-way ANOVA: $F_{3,29} = 11.484$, $P < 0.001$). (C): Plasma IL-6 levels (one-way ANOVA: $F_{3,29} = 4.528$, $P = 0.01$). *$P < 0.05$, **$P < 0.01$, ***$P < 0.001$. The values represent the mean ± S.E.M. (n = 7–10). N.S.: not significance.

ANA-12 in this model (Fig. 4A). Beneficial effects of (*R*)-ketamine for DSS-induced increases in DAI score were significantly attenuated after ANA-12 (Fig. 4B).

4. Discussion

In this study, we found that the repeated administration of (*R*)-ketamine, but not (*S*)-ketamine or 5-ASA, ameliorated an increase in DAI scores of DSS-treated mice. Furthermore, ANA-12 significantly blocked the beneficial effects of (*R*)-ketamine in DSS-induced colitis model, suggesting a role of TrkB signaling in the action of (*R*)-ketamine. Collectively, it is likely that (*R*)-ketamine could ameliorate inflammation and colitis in UC patients.

Pharmacokinetic profiles of (*R*)-ketamine and (*S*)-ketamine in rodents were similar (Fukumoto et al., 2017), indicating that the differential effects between these two enantiomers on DSS-induced colitis model are not due to differences in their pharmacokinetic profiles. Thus, it is unlikely that NMDA receptor inhibition might play a major role in the beneficial actions of (*R*)-ketamine in DSS-induced colitis model. In this study, ANA-12 blocked the beneficial effects of (*R*)-ketamine in DSS-induced colitis model. A recent study showed that TrkB antagonist K252s aggravated by inhibiting the TrkB system in the intestinal inflammation and apoptosis in mice with colitis (Xu et al., 2020a,b). Collectively, it seems that TrkB signaling plays a crucial role in the beneficial effects of (*R*)-ketamine in DSS-induced colitis model. Nonetheless, further study on the role of TrkB signaling in DSS-induced colitis model is needed.

5-ASA is a first-line drug for inducing and maintaining remission of mild to moderately active UC. At present, several types of 5-ASA formulations with different delivery systems are available for treatment of UC patients. In this study, we found the beneficial effects of (*R*)-ketamine in DSS-induced colitis model although 5-ASA was ineffective in the same model since we did not use 5-ASA formulation which can deliver to the colonic mucosa efficiently.

It was reported that (*R*)-ketamine did not cause side effects (i.e.,

psychosis and dissociation) in healthy control subjects whereas the same dose of (*S*)-ketamine caused these side effects in the same subjects (Vollenweider et al., 1997). In addition, an open-label pilot study in Brazil showed that (*R*)-ketamine showed first-acting antidepressant effects in treatment-resistant MDD patients, and that side effects in these patients was very low (Leal et al., 2020). It is recognized that the detrimental side effects of (*R*,*S*)-ketamine are associated with (*S*)-ketamine, but not (*R*)-ketamine (Zanos et al., 2018). Thus, (*R*)-ketamine could be a safer drug than (*R*,*S*)-ketamine and (*S*)-ketamine in humans. Taken all together, (*R*)-ketamine would be a potential therapeutic drug for colitis as well as depression in UC patients. It is, therefore, of great interest to perform a randomized, placebo-controlled study of (*R*)-ketamine in UC patients with or without depression.

Brain-derived neurotrophic factor (BDNF) and its receptor TrkB plays a crucial role in depression and in the antidepressant action of certain compounds such as antidepressants and ketamine enantiomers (Castrén, 2014; Hashimoto et al., 2004; Hashimoto, 2010; Nestler et al., 2002; Yang et al., 2015; Zhang et al., 2016). It is well recognized that serum BDNF levels in patients with MDD are lower than those of healthy controls (Shimizu et al., 2003; Yoshida et al., 2012), suggesting a blood biomarker for depression (Çakici et al., 2020; Hashimoto, 2010; Shi et al., 2020). However, a study showed no differences in depression scores, blood BDNF levels between UC patients and controls (Fujiwara et al., 2018). Further study using UC patients with depression is needed to confirm the role of BDNF in UC patients with depression.

From the present data, it is unclear if the beneficial effects of (*R*)-ketamine are mediated through central mechanisms. Previously we detected the levels of (*R*)-ketamine and its metabolite (2*R*,6*R*)-hydroxynorketamine (HNK) in the blood and liver of mice after intracerebroventricular administration of (*R*)-ketamine, suggesting that (*R*)-ketamine in the periphery after washout from the brain is metabolized to (2*R*,6*R*)-HNK in the liver (Zhang et al., 2018a). Thus, it is not easy to investigate the role of central mechanisms in the beneficial effects of (*R*)-ketamine in the DSS-induced model. Antidepressants have been proposed to treat IBD patients through the brain–gut axis
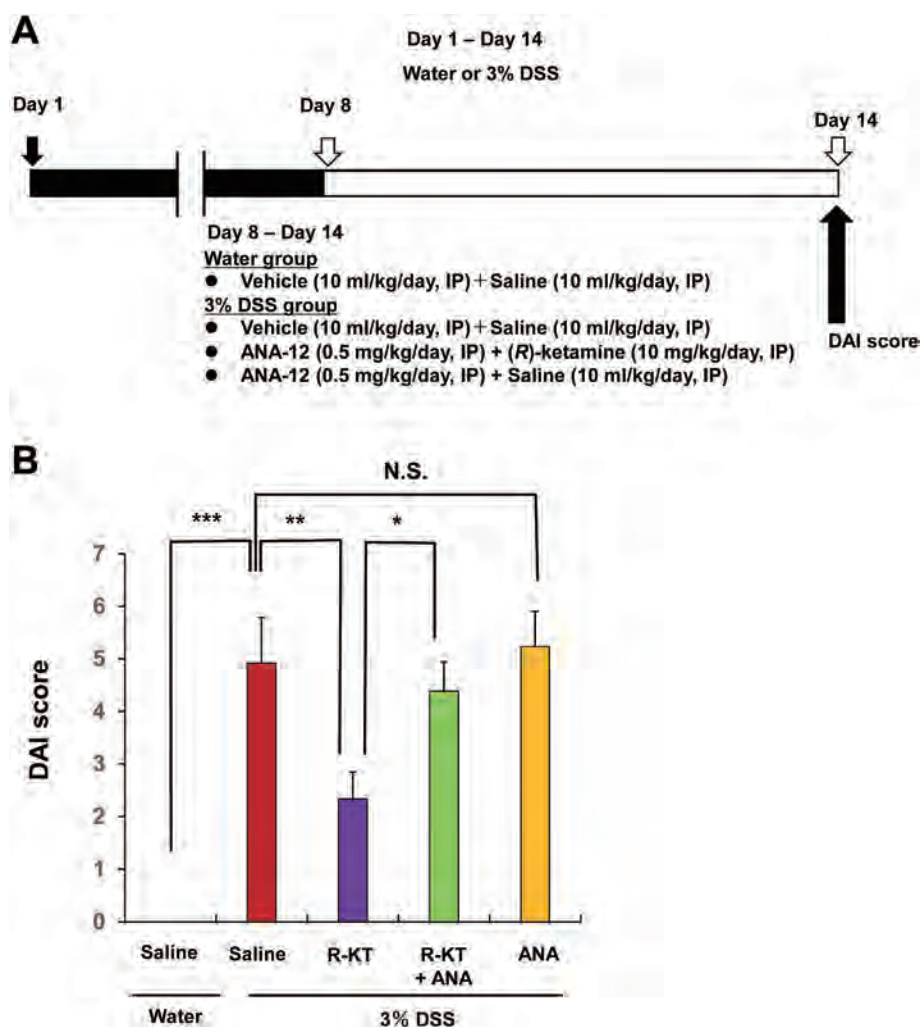
5

Fig. 4. Effects of ANA-12 on the beneficial effects of (R)-ketamine in the DSS-induced model
(A): The schedule of DSS-induced model, treatment, and collection of tissues. Water or 3% DSS in drinking water was given to mice for 14 days to induce colitis in mice. Subsequently, vehicle (10 ml/kg/day, 30 min before) + saline (10 ml/kg/day), vehicle (10 ml/kg/day, 30 min before) + (R)-ketamine (10 mg/kg/day), ANA-12 (0.5 mg/kg/day, 30 min before) + (R)-ketamine (10 mg/kg/day) or ANA-12 (0.5 mg/kg/day, 30 min before) + saline (10 ml/kg/day) was administered i.p. to mice for 7 days (day 8 – day 14). On day 14, DAI score was determined. (B): DAI score (one-way ANOVA: $F_{4,55} = 11.521$, $P < 0.001$). *$P < 0.05$, **$P < 0.01$, ***$P < 0.001$. The values represent the mean ± S.E.M. (n = 10–13). N.S.: not significance.

(Mikocka-Walus et al., 2020). It seems that brain–gut axis may play a role in the beneficial effects of (R)-ketamine in DSS-induced model although further study is needed.

5. Conclusions

The data of this study suggest that (R)-ketamine, but not (S)-ketamine, could ameliorate DSS-induced inflammation and colitis in mice through TrkB stimulation. Therefore, (R)-ketamine would be a new potential therapeutic drug for inflammatory bowel disease such as UC.

CRediT authorship contribution statement

Yuko Fujita: carried out the experiments and data analysis. **Yaeko Hashimoto:** carried out the experiments and data analysis. **Hiroyo Hashimoto:** carried out the experiments and data analysis. **Lijia Chang:** carried out the experiments and data analysis. **Kenji Hashimoto:** designed the experiments, and wrote the manuscript, All authors have read and approved the final manuscript..

Declaration of competing interest

Dr. K. Hashimoto is the inventor of filed patent applications on "The use of *R*-ketamine in the treatment of psychiatric diseases", and "Preventive or therapeutic agent and pharmaceutical composition for inflammatory diseases or bone diseases" by the Chiba University. Dr. K. Hashimoto also declares that he has received research support and

consultant from Dainippon Sumitomo, Otsuka, and Taisho. Other authors had no conflict of interest.

References

Bernstein, C.N., Hitchon, C.A., Walld, R., Bolton, J.M., Sareen, J., Walker, J.R., Graff, L. A., Patten, S.B., Singer, A., Lix, L.M., El-Gabalawy, R., Katz, A., Fisk, J.D., Marrie, R. A., Cihr Team in Defining the Burden and Managing the Effects of Psychiatric Comorbidity in Chronic Immunoinflammatory Disease, 2019. Increased burden of psychiatric disorders in inflammatory bowel disease. Inflamm. Bowel Dis. 25, 360–368.
Çakici, N., Sutterland, A.L., Penninx, B.W.J.H., Dalm, V.A., de Haan, L., van Beveren, N.J. M., 2020. Altered peripheral blood compounds in drug-naïve first-episode patients with either schizophrenia or major depressive disorder: a meta-analysis. Brain Behav. Immun. 88, 547–558.
Castrén, E., 2014. Neurotrophins and psychiatric disorders. Handb. Exp. Pharmacol. 220, 461–479.
Chang, L., Zhang, K., Pu, Y., Qu, Y., Wang, S.M., Xiong, Z., Ren, Q., Dong, C., Fujita, Y., Hashimoto, K., 2019. Comparison of antidepressant and side effects in mice after intranasal administration of (R,S)-ketamine, (R)-ketamine, and (S)-ketamine. Pharmacol. Biochem. Behav. 181, 53–59.
Chassaing, B., Aitken, J.D., Malleshappa, M., Vijay-Kumar, M., 2014. Dextran sulfate sodium (DSS)-induced colitis in mice. Curr. Protoc. Im. 104, 15.25.1-15.25.14.
Ebert, B., Mikkelsen, S., Thorkildsen, C., Borgbjerg, F.M., 1997. Norketamine, the main metabolites of ketamine, is a non-competitive NMDA receptor antagonist in the rat cortex and spinal cord. Eur. J. Pharmacol. 333, 99–104.

6

Frolkis, A.D., Vallerand, I.A., Shaheen, A.A., Lowerison, M.W., Swain, M.G., Barnabe, C., Patten, S.B., Kaplan, G.G., 2019. Depression increases the risk of inflammatory bowel disease, which may be mitigated by the use of antidepressants in the treatment of depression. Gut 68, 1606–1612.

Fujita, A., Fujita, Y., Pu, Y., Chang, L., Hashimoto, K., 2019. MPTP-induced dopaminergic neurotoxicity in mouse brain is attenuated after subsequent intranasal administration of (R)-ketamine: a role of TrkB signaling. Psychopharmacoly (Berl) 237, 83–92.

Fujiwara, T., Kono, S., Katakura, K., Abe, K., Takahashi, A., Gunji, N., Yokokawa, A., Kawashima, K., Suzuki, R., Wada, A., Miura, I., Yabe, H., Ohira, H., 2018. Evaluation of brain activity using near-infrared spectroscopy in inflammatory bowel disease patients. Sci. Rep. 8, 402.

Fukumoto, K., Toki, H., Iijima, M., Hashihayata, T., Yamaguchi, J., Hashimoto, K., Chaki, S., 2017. Antidepressant potential of (R)-ketamine in rodents models: comparison with (S)-ketamine. J. Pharmacol. Exp. Therapeut. 361, 9–16.

Hashimoto, K., 2010. Brain-derived neurotrophic factor as a biomarker for mood disorders: a historical overview and future directions. Psychiatr. Clin. Neurosci. 64, 641–357.

Hashimoto, K., 2019. Rapid-acting antidepressant ketamine, its metabolites and other candidates: a historical overview and future perspective. Psychiatr. Clin. Neurosci. 73, 613–627.

Hashimoto, K., 2020. Molecular mechanisms of the rapid-acting and long-lasting antidepressant actions of (R)-ketamine. Biochem. Pharmacol. 177, 113935.

Hashimoto, K., Kakiuchi, T., Ohba, H., Nishiyama, S., Tsukada, H., 2017. Reduction of dopamine D$_{2/3}$ receptor binding in the striatum after a single administration of esketamine, but not R-ketamine: a PET study in conscious monkeys. Eur. Arch. Psychiatr. Clin. Neurosci. 267, 173–176.

Hashimoto, K., Shimizu, E., Iyo, M., 2004. Critical role of brain-derived neurotrophic factor in mood disorders. Brain Res. Rev. 45, 104–114.

Kishimoto, T., Chawla, J.M., Hagi, K., Zarate, C.A., Kane, J.M., Bauer, M., Correll, C.U., 2016. Single-dose infusion ketamine and non-ketamine N-methyl-D-aspartate receptor antagonists for unipolar and bipolar depression: a meta-analysis of efficacy, safety and time trajectories. Psychol. Med. 46, 1459–1472.

Krystal, J.H., Abdallah, C.G., Sanacora, G., Charney, D.S., Duman, R.S., 2019. Ketamine: a paradigm shift for depression research and treatment. Neuron 101, 774–778.

Leal, G.C., Bandeira, I.D., Correia-Melo, F.S., Telles, M., Mello, R.P., Vieira, F., Lima, C.S., Jesus-Nunes, A.P., Guerreiro-Costa, L.N.F., Marback, R.F., Caliman-Fontes, A.T., Marques, B.L.S., Bezerra, M.L.O., Dias-Neto, A.L., Silva, S.S., Sampaio, A.S., Sanacora, G., Turecki, G., Loo, C., Lacerda, A.L.T., Quarantini, L.C., 2020. Intravenous arketamine for treatment-resistant depression: open-label pilot study. Eur. Arch. Psychiatr. Clin. Neurosci. https://doi.org/10.1007/s00406-020-01110-5, 2020 Feb. 20.

Marrie, R.A., Walker, J.R., Graff, L.A., Lix, L.M., Bolton, J.M., Nugent, Z., Targownik, L. E., Bernstein, C.N., 2016. CIHR Team "Defining the burden and managing the effects of psychiatric comorbidity in chronic immunoinflammatory disease". J. Psychosom. Res. 89, 107–113. Performance of administrative case definitions for depression and anxiety in inflammatory bowel disease.

Mikocka-Walus, A., Ford, A.C., Drossman, D.A., 2020. Antidepressants in inflammatory bowel disease. Nat. Rev. Gastroenterol. Hepatol. 17, 184–192.

Mikocka-Walus, A., Knowles, S.R., Keefer, L., Graff, L., 2016. Controversies revisited: a systematic review of the comorbidity of depression and anxiety with inflammatory bowel diseases. Inflamm. Bowel Dis. 22, 752–762.

Mittermaier, C., Dejaco, C., Waldhoer, T., Oefferlbauer-Ernst, A., Miehsler, W., Beier, M., Tillinger, W., Gangl, A., Moser, G., 2004. Impact of depressive mood on relapse in patients with inflammatory bowel disease: a prospective 18-month follow-up study. Psychosom. Med. 66, 79–84.

Neuendorf, R., Harding, A., Stello, N., Hanes, D., Wahbeh, H., 2016. Depression and anxiety in patients with inflammatory bowel disease: a systematic review. J. Psychosom. Res. 87, 70–80.

Nestler, E.J., Barrot, M., DiLeone, R.J., Eisch, A.J., Gold, S.J., Monteggia, L.M., 2002. Neuron 34, 13–25.

Newport, D.J., Carpenter, L.L., McDonald, W.M., Potash, J.B., Tohen, M., Nemeroff, C.B., Apa Council of Research Task Force on Novel Biomarkers and Treatments, 2015. Ketamine and other NMDA antagonists: early clinical trials and possible mechanisms in depression. Am. J. Psychiatr. 172, 950–966.

Nunes, N.S., Chandran, P., Sundby, M., Visioli, F., da Costa Gonçalves, F., Burks, S.R., Paz, A.H., Frank, J.A., 2019. Therapeutic ultrasound attenuates DSS-induced colitis through the cholinergic anti-inflammatory pathway. EBioMedicine 45, 495–510.

Perše, M., Cerar, A., 2012. Dextran sodium sulfate colitis mouse model: traps and tricks. J. Biomed. Biotechnol. 718617, 2012.

Ren, Q., Ma, M., Yang, C., Zhang, J.C., Yao, W., Hashimoto, K., 2015. BDNF-TrkB signaling in the nucleus accumbens shell of mice has key role in methamphetamine withdrawal symptoms. Transl. Psychiatry 5, e666.

Shi, Y., Luan, D., Song, R., Zhang, Z., 2020. Value of peripheral neurotrophin levels for the diagnosis of depression and response to treatment: a systematic review and meta-analysis. Eur. Neuropsychopharmacol. https://doi.org/10.1016/j.euroneuro.2020.09.633, 2020 Sep. 23.

Shimizu, E., Hashimoto, K., Okamura, N., Koike, K., Komatsu, N., Kumakiri, C., Nakazato, M., Watanabe, H., Shinoda, N., Okada, S., Iyo, M., 2003. Alterations of serum levels of brain-derived neurotrophic factor (BDNF) in depressed patients with or without antidepressants. Biol. Psychiatr. 54, 70–75.

Tan, Y., Fujita, Y., Qu, Y., Chang, L., Pu, Y., Wang, S., Wang, X., Hashimoto, K., 2020. Phencyclidine-induced cognitive deficits in mice are ameliorated by subsequent repeated intermittent administration of (R)-ketamine, but not (S)-ketamine: role of BDNF-TrkB signaling. Pharmacol. Biochem. Behav. 188, 172839.

Tan, Y., Hashimoto, K., 2020. Risk of psychosis after repeated intermittent administration of (S)-ketamine, but not (R)-ketamine, in mice. J. Affect. Disord. 269, 198–200.

Vollenweider, F.X., Leenders, K.L., Oye, I., Hell, D., Angst, J., 1997. Differential psychopathology and patterns of cerebral glucose utilisation produced by (S)- and (R)-ketamine in healthy volunteers using positron emission tomography (PET). Eur. Neuropsychopharmacol 7, 25–38.

Walker, J.R., Ediger, J.P., Graff, L.A., Greenfeld, J.M., Clara, I., Lix, L., Rawsthorne, P., Miller, N., Rogala, L., McPhail, C.M., Bernstein, C.N., 2008. The Manitoba IBD cohort study: a population-based study of the prevalence of lifetime and 12-month anxiety and mood disorders. Am. J. Gastroenterol. 103, 1989–1997.

Wang, P., Du, C., Chen, F.X., Li, C.Q., Yu, Y.B., Han, T., Akhtar, S., Zuo, X.L., Tan, X.D., Li, Y.Q., 2016. BDNF contributes to IBS-like colonic hypersensitivity via activating the enteroglia-nerve unit. Sci. Rep. 6, 20320.

Wei, Y., Chang, L., Hashimoto, K., 2020. A historical review of antidepressant effects of ketamine and its enantiomers. Pharmacol. Biochem. Behav. 190, 172870.

Xu, X., Lin, S., Yang, Y., Gong, X., Tong, J., Li, K., Li, Y., 2020a. Histological and ultrastructural changes of the colon in dextran sodium sulfate-induced mouse colitis. Exp. Ther. Med. 20, 1987–1994.

Xu, G., Sun, Y., He, H., Xue, Q., Liu, Y., Dong, L., 2020b. Effect of TrkB-PLC/IP3 pathway on intestinal inflammatory factors and enterocyte apoptosis in mice with colitis. Acta Biochim. Biophys. Sin. 52, 675–682.

Yang, C., Ren, Q., Qu, Y., Zhang, J.C., Ma, M., Dong, C., Hashimoto, K., 2018. Mechanistic target of rapamycin-independent antidepressant effects of (R)-ketamine in a social defeat stress model. Biol. Psychiatry 83, 18–28.

Yang, C., Shirayama, Y., Zhang, J.C., Ren, Q., Yao, W., Ma, M., Dong, C., Hashimoto, K., 2015. R-ketamine: a rapid-onset and sustained antidepressant without psychotomimetic side effects. Transl. Psychiatry 5, e632.

Yang, C., Yang, J., Luo, A., Hashimoto, K., 2019. Molecular and cellular mechanisms underlying the antidepressant effects of ketamine enantiomers and its metabolites. Transl. Psychiatry 9, 280.

Yoshida, T., Ishikawa, M., Niitsu, T., Nakazato, M., Watanabe, H., Shiraishi, T., Shiina, A., Hashimoto, T., Kanahara, N., Hasegawa, T., Enohara, M., Kimura, A., Iyo, M., Hashimoto, K., 2012. Decreased serum levels of mature brain-derived neurotrophic factor (BDNF), but not its precursor proBDNF, in patients with major depressive disorder. PloS One 7, e42676.

Zanos, P., Moaddel, R., Morris, P.J., Riggs, L.M., Highland, J.N., Georgiou, P., Pereira, E. F.R., Albuquerque, E.X., Thomas, C.J., Zarate, C.A., Gould, T.D., 2018. Ketamine and ketamine metabolite pharmacology: insights into therapeutic mechanisms. Pharmacol. Rev. 70, 621–660.

Zhang, K., Fujita, Y., Hashimoto, K., 2018a. Lack of metabolism in (R)-ketamine 's antidepressant actions in a chronic social defeat stress model. Sci. Rep. 8, 4007.

Zhang, K., Hashimoto, K., 2019. An update on ketamine and its two enantiomers as rapid-acting antidepressants. Expert Rev. Neurother. 19, 83–92.

Zhang, J.C., Li, S.X., Hashimoto, K., 2014. R(-)-ketamine shows greater potency and longer lasting antidepressant effects than S(+)-ketamine. Pharmacol. Biochem. Behav. 116, 137–141.

Zhang, K., Ma, M., Dong, C., Hashimoto, K., 2018b. Role of inflammatory bone markers in the antidepressant actions of (R)-ketamine in a chronic social defeat stress model. Int. J. Neuropsychopharmacol. 21, 1025–1030.

Zhang, J., Ma, L., Chang, L., Pu, Y., Qu, Y., Hashimoto, K., 2020. A key role of the subdiaphragmatic vagus nerve in the depression-like phenotype and abnormal composition of gut microbiota in mice after lipopolysaccharide administration. Transl. Psychiatry 10, 186.

Zhang, J.C., Yao, W., Dong, C., Yang, C., Ren, Q., Ma, M., Han, M., Hashimoto, K., 2015. Comparison of ketamine, 7,8-dihydroxyflavone, and ANA-12 antidepressant effects in the social defeat stress model of depression. Psychopharmacology 232, 4325–4335.

Zhang, J.C., Yao, W., Hashimoto, K., 2016. Brain-derived neurotrophic factor (BDNF)-TrkB signaling in inflammation-related depression and potential therapeutic targets. Curr. Neuropharmacol. 14, 721–731.

Comparison of antidepressant and side effects in mice after intranasal administration of (*R*,*S*)-ketamine, (*R*)-ketamine, and (*S*)-ketamine

（RS–ケタミン、R－ケタミンおよびS－ケタミンの鼻腔内投与後の抗うつ作用
および副作用の比較）

千葉大学大学院医学薬学府

先端医学薬学専攻

（主任：橋本謙二教授）

常 立甲

TABLE OF CONTENTS

ABSTRACT

The *N*-methyl-D-aspartate receptor (NMDAR) antagonist (*R,S*)-ketamine produces rapid and sustained antidepressant effects in treatment-resistant patients with depression although intranasal use of (*R,S*)-ketamine in ketamine abusers is popular. In March 5, 2019, nasal spray of (*S*)-ketamine for treatment-resistant depression was approved as a new antidepressant by the US Food Drug Administration. Clinical study of (*R*)-ketamine is underway. In a chronic social defeat stress (CSDS) model, we compared the antidepressant effects of (*R,S*)-ketamine, (*R*)-ketamine, and (*S*)-ketamine after a single intranasal administration. Furthermore, we also compared the side effects (i.e., locomotion, prepulse inhibition (PPI), abuse liability) of these three compounds in mice. The order of potency of antidepressant effects after a single intranasal administration was (*R*)-ketamine > (*R,S*)-ketamine > (*S*)-ketamine. In contrast, the order of locomotor activity and prepulse inhibition (PPI) deficits after a single intranasal administration was (*S*)-ketamine > (*R,S*)-ketamine > (*R*)-ketamine. In the conditioned place preference (CPP) test, both (*S*)-ketamine and (*R,S*)-ketamine increased CPP scores in mice after repeated intranasal administration, in a dose dependent manner. In contrast, (*R*)-ketamine did not increase CPP scores in mice. These findings suggest that intranasal administration of (*R*)-ketamine would be a safer antidepressant than (*R,S*)-ketamine and (*S*)-ketamine.

Introduction

In 2010, Berman et al. (2000) reported a first double-blind, placebo-controlled study of the N-methyl-D-aspartate receptor (NMDAR) antagonist (*R,S*)-ketamine, demonstrating that (*R,S*)-ketamine exhibits rapid antidepressant effects in treatment-resistant patients with major depressive disorder (MDD). Subsequently, a number of groups replicated robust antidepressant effects of (*R,S*)-ketamine in treatment-resistant patients with MDD (Murrough et al., 2013; Su et al., 2017; Zarate et al., 2006;). Interestingly, (*R,S*)-ketamine could produce anti-suicidal effects in treatment-resistant patients with MDD (Grunebaum et al., 2018; Larkin et al., 2011; Murrough et al., 2015; Price et al., 2009). Several meta-analyses showed that (*R,S*)-ketamine exhibits rapid antidepressant and anti-suicidal ideation effects in treatment-resistant patients with MDD or bipolar disorder (Kishimoto et al., 2016; Newport et al., 2015; Wilkinson et al., 2018; Xu et al., 2016). Off-label use of (*R,S*)-ketamine (i.e., intravenous and intranasal administration) for antidepressant effects is increasing in the United State of America (USA) although the common adverse effects (e.g., psychotomimetic effects and dissociative effects) of (*R,S*)-ketamine are not resolved (Singh et al., 2017; Wilkinson et al., 2017; Zhu et al., 2017). Thus, although (*R,S*)-ketamine is the most attractive antidepressant in the treatment of severe depression, the precise mechanisms underlying its antidepressant actions remain elusive (Abdallah et al., 2018; Chaki, 2017a; 2017b; Duman, 2018; Gould et al., 2019; Hashimoto, 2016a; 2016b; Krystal et al., 2019; Monteggia and Zarate, 2015; Murrough et al., 2017; Zanos et al., 2018; Zhang and Hashimoto, 2019a).

(*R,S*)-ketamine (Ki = 0.53 μM for NMDAR) is a racemic mixture containing equal parts of (*R*)-ketamine (or arketamine) (Ki = 1.4 μM for NMDAR) and (*S*)-ketamine (or esketamine) (Ki = 0.30 μM for NMDAR) (Ebert et al., 1997). (*R*)-ketamine is reported to show greater potency and longer-lasting antidepressant effects than (*S*)-ketamine in several animal models of depression (Fukumoto et al., 2017; Yang et al., 2015; 2017a; 2017b; 2018a;

Zanos et al., 2016; Zhang et al., 2014). Unlike (*S*)-ketamine, (*R*)-ketamine might not induce psychotomimetic side effects or exhibit abuse potential in rodents (Yang et al., 2015; 2016). In addition, unlike (*R,S*)-ketamine and (*S*)-ketamine, (*R*)-ketamine did not cause the expression of heat shock protein HSP-70 (a marker for neuronal injury) in the rat retrosplenial cortex after a single intraperitoneal (i.p.) administration (Tian et al., 2018). A positron emission tomography (PET) study showed a marked reduction of dopamine D2/3 receptor binding in conscious monkey striatum after a single intravenous (i.v.) infusion of (*S*)-ketamine but not that of (*R*)-ketamine, suggesting that (*S*)-ketamine-induced dopamine release might be associated with acute psychotomimetic and dissociative side effects in humans (Hashimoto et al., 2017). Therefore, it seems that (*R*)-ketamine could be a safer antidepressant in humans than (*R,S*)-ketamine and (*S*)-ketamine (Hashimoto, 2014; 2016a; 2016b; 2016c).

Fukumoto et al. (2017) reported that (*R,S*)-ketamine (10 mg/kg) and (*R*)-ketamine (10 mg/kg), but not (*S*)-ketamine (3 and 10 mg/kg), significantly reversed the depressive-like behavior induced by repeated treatments with corticosterone in rats at 24 hours after a single i.p. administration, indicating that (*S*)-ketamine's antidepressant effects are less potent than (*R,S*)-ketamine and (*R*)-ketamine. On March 5, 2019, the US Food Drug Administration (FDA) approved Janssen Pharmaceutical Inc.'s (*S*)-ketamine nasal spray for treatment-resistant depression (FDA 2019). It is well known that bioavailability (17 – 29%) of intranasal administration of (*R,S*)-ketamine in humans is markedly lower than i.v. (100%) and intramuscular (i.m.) administration (93%) (Li et al., 2016; Pelltoniemi et al., 2016; Zhang and Hashimoto, 2019a), suggesting lower efficacy and higher individual difference of intranasal administration compared to i.v. and i.m. administration. However, there are no reports showing the direct comparison of intranasal administration of (*R,S*)-ketamine and its two enantiomers for antidepressant and side effects in rodents.

The purpose of this study is to compare the antidepressant and side effects of intranasal administration of (R,S)-ketamine and its two enantiomers (R)-ketamine and (S)-ketamine. First, we compared the antidepressant effects of a single intranasal administration of (R,S)-ketamine, (R)-ketamine and (S)-ketamine in susceptible mice after chronic social defeat stress (CSDS). Second, we compared the side effects [i.e., locomotion, prepulse inhibition (PPI), conditioned place preference (CPP)] of intranasal administration of (R,S)-ketamine, (R)-ketamine and (S)-ketamine in mice.

Material and methods

Animals

Male adult C57BL/6 mice (n = 400), aged 8 weeks (body weight 20-25g, Japan SLC, Inc., Hamamatsu, Japan) and male adult CD1 (ICR) mice (n = 40), aged 13-15 weeks (body weight >40g, Japan SLC, Inc., Hamamatsu, Japan) were used. Animals were housed under controlled temperatures and 12-hour light/dark cycles (lights on between 07:00-19:00 h), with ad libitum food (CE-2; CLEA Japan, Inc., Tokyo, Japan) and water. The protocol was approved by the Chiba University Institutional Animal Care and Use Committee (Permission number: 29-420). This study was carried out in strict accordance with the recommendations in the Guide for the Care and Use of Laboratory Animals of the National Institutes of Health, USA. Animals were deeply anaesthetized with isoflurane before being killed by cervical dislocation. All efforts were made to minimize suffering.

Materials

(*R*)-ketamine hydrochloride and (*S*)-ketamine hydrochloride were prepared by recrystallization of (*R*,*S*)-ketamine (Ketalar®, ketamine hydrochloride, Daiichi Sankyo Pharmaceutical Ltd., Tokyo, Japan) and D-(-)-tartaric acid and L-(+)-tartaric acid, respectively (Zhang et al., 2014). The dose (10, 20 or 40 mg/kg as hydrochloride) of (*R*,*S*)-ketamine and its enantiomers dissolved in the physiological saline was used as previously reported (Chang et al., 2019; Yang et al., 2015; 2017a; 2017b; 2018a; Zhang et al., 2018). Other reagents were purchased commercially.

Chronic social defeat stress (CSDS) model

The procedure of CSDS was performed as previously reported (Chang et al., 2019; Dong et al., 2017; Golden et al., 2011; Yang et al., 2015; 2017a; 2017b; 2018a; Xiong et al., 2018a; 2018b; Zhang et al., 2018). The C57BL/6 mice were exposed to a different CD1 aggressor mouse for 10 min per day for consecutive 10 days. When the social defeat session ended, the

resident CD1 mouse and the intruder mouse were housed in one half of the cage separated by a perforated Plexiglas divider to allow visual, olfactory, and auditory contact for the remainder of the 24-h period. At 24 h after the last session, all mice were housed individually. On day 11, a social interaction test (SIT) was performed to identify subgroups of mice that were susceptible and unsusceptible to social defeat stress. This was accomplished by placing mice in an interaction test box (42×42 cm) with an empty wire-mesh cage (10×4.5 cm) located at one end. The movement of the mice was tracked for 2.5 min, followed by 2.5 min in the presence of an unfamiliar aggressor confined in the wire-mesh cage. The duration of the subject's presence in the "interaction zone" (defined as the 8-cm-wide area surrounding the wiremesh cage) was recorded by a stopwatch. The interaction ratio was calculated as time spent in an interaction zone with an aggressor/time spent in an interaction zone without an aggressor. An interaction ratio of 1 was set as the cutoff: mice with scores < 1 were defined as "susceptible" to social defeat stress and those with scores $\geqslant$ 1 were defined as "resilient".

Approximately 70-80 % of mice were susceptible after CSDS. Susceptible mice were randomly divided in the subsequent experiments. Control C57BL/6 mice without CSDS were housed in the cage before the behavioral tests.

Treatment and behavioral tests

The CSDS susceptible mice were divided to four groups. Subsequently, saline (0.5 ml/kg), (*R,S*)-ketamine (10 mg/kg), (*R*)-ketamine (10 mg/kg), or (*S*)-ketamine (10 mg/kg) was administered intranasally into CSDS susceptible mice (Figure 1A). Mice were restrained by hand, and saline or ketamine was administered intranasally into awake mice using Eppendorf micropipette (Eppendorf Japan, Tokyo, Japan). Behavioral tests, including locomotion test (LMT), tail suspension test (TST), forced swimming test (FST) and 1% sucrose preference test (SPT), were performed as reported previously (Dong et al., 2017; Yang et al., 2015; 2017a; 2017b; 2018a; Xiong et al., 2018a; 2018b; Zhang et al., 2018). LMT and TST were

performed 2 and 4 hours after a single injection, respectively. FST was performed 1 day after injection. SPT was performed 2, and 7 days after a single injection (Figure 1A).

Locomotion

The locomotor activity was measured by an animal movement analysis system SCANETMV-40 (MELQUEST Co., Ltd., Toyama, Japan). The mice were placed in experimental cages (length× width × height: 560 × 560 × 330 mm). The cumulative locomotor activity counts were recorded for 60 minutes. Cages were cleaned between testing session.

Tail suspension test (TST)

A small piece of adhesive tape placed approximately 2 cm from the tip of the tail for mouse. A single hole was punched in the tape and mice were hung individually, on a hook. The immobility time was recorded for 10 minutes. Mice were considered immobile only when they hung passively and completely motionless.

Forced swimming test (FST)

The FST was conducted using an automated forced-swim apparatus (SCANET MV-40; MELQUEST Co., Ltd., Toyama, Japan). Mice were placed individually in a cylinder (diameter: 23 cm; height: 31 cm) containing 15 cm of water maintained at a temperature of $23ºC \pm 1ºC$. The immobility time was calculated using the activity time as (total) – (active) time by the apparatus analysis software. The immobility time of each mouse was recorded for a period of 6 min.

Sucrose preference test (SPT)

Mice were exposed to water and 1% sucrose solution for 48 h, followed by 4 hours of water and food deprivation and a 1- hour exposure to two identical bottles (water and 1% sucrose solution). The bottles containing water and sucrose were weighed before and at the end of this period. The sucrose preference was calculated as a percentage of sucrose solution consumption to the total liquid consumption.

Side effects

Locomotion

After habituation (60 min) in the cage, saline (0.5 ml/kg), (*R,S*)-ketamine (10, 20 or 40 mg/kg), (*R*)-ketamine (10, 20 or 40 mg/kg), or (*S*)-ketamine (10, 20 or 40 mg/kg) was injected intranasally into male C57BL/6 mice. Locomotor activity was measured using an animal movement analysis system (SCANET MV-40, Melquest, Toyama, Japan). The system consisted of a rectangular enclosure (560 x 560 mm). The side walls (height, 60 mm) of the enclosure were equipped with 144 pairs of photosensors located at 6-mm intervals at a height of 30 mm from the bottom edge. An animal was placed in the observation cage 60 minutes from a single dose of saline or compounds. A pair of photosensors was scanned every 0.1 second to detect the animal's movements. The intersection of paired photosensors (10 mm apart) in the enclosure was counted as one unit of locomotor activity. Data collected for 60 minutes after a single injection were used in this study.

Pupulse inhibition (PPI) test

Male C57BL/6 mice were tested for their acoustic startle reactivity (ASR) in a startle chamber (SR-LAB; San Diego Instruments, San Diego, CA, USA) using the standard methods described previously (Matsuura et al., 2015; Yang et al., 2015; Yang et al., 2018b). The test sessions were begun after an initial 10-min acclimation period in the chamber. The mice were subjected to one of six trials: (1) pulse alone, as a 40 ms broadband burst; a pulse (40 ms broadband burst) preceded by 100 ms with a 20 ms prepulse that was (2) 4 dB, (3) 8 dB, (4) 12 dB, or (5) 16 dB over background (65 dB); and (6) background only (no stimulus). The amount of PPI was expressed as the percentage decrease in the amplitude of the startle reactivity caused by presentation of the prepulse (% PPI). Saline (0.5 ml/kg), or (*R,S*)-ketamine (10, 20 or 40 mg/kg) [or (*R*)-ketamine (10, 20 or 40 mg/kg), (*S*)-ketamine (10, 20 or

40 mg/kg)] was administered intranasally 20 min (including the 10-min acclimation period) before the machine records. The PPI test lasted 20 min in total.

Conditioned place preference (CPP) test

The place conditioning paradigm (Brain Science Idea Inc., Osaka, Japan) was used for studying ketamine-induced rewarding effects, as reported previously (Yang et al., 2015; Yang et al., 2018b). Male C57BL/6 mouse was allowed to move freely between transparent and black boxes for a 15 min session once a day, for 3 days (days 1-3) as preconditioning. On day 3, the time spent in each box was measured. There was no significant difference between time spent in the black compartment with a smooth floor and the white compartment with a textured floor, indicating that there was no place preference before conditioning. On days 4, 6, and 8, saline (0.5 ml/kg), or (R,S)-ketamine (10, 20 or 40 mg/kg) [or (R)-ketamine (10, 20 or 40 mg/kg), (S)-ketamine (10, 20 or 40 mg/kg)] was intranasally administered, and then mice were confined to either the transparent or black box for 30 min. On days 5, 7, and 9, mice were given saline and placed in the opposite ketamine-conditioning box for 30 min. On day 10, the post-conditioning test was performed without drug treatment, and the time spent in each box was measured for 15 min. A counterbalanced protocol was used in order to nullify any initial preference by the mouse. The CPP score was designated as the time spent in the drug-conditioning sites, minus the time spent in the saline-conditioning sites.

Statistical analysis

The data show as the mean ± standard error of the mean (S.E.M.). Analysis was performed using PASW Statistics 20 (formerly SPSS Statistics; SPSS, Tokyo, Japan). The data were analyzed using the one-way analysis of variance (ANOVA), followed by post-hoc Fisher's Least Significant Difference (LSD) test. The PPI data were also analyzed using multivariate analysis of variance, followed by post-hoc Fisher's LSD test. The P-values of less than 0.05 were considered statistically significant.

Results

Antidepressant effects of (*R,S*)-ketamine, (*R*)-ketamine and (*S*)-ketamine in CSDS susceptible mice

Locomotion showed no difference ($F_{4,72} = 0.735$, $P = 0.571$) among the five groups (Figure 1B). One-way ANOVA of TST data showed a statistical significance ($F_{4,72} = 15.23$, $P < 0.001$) among the five groups (Figure 1C). Post-hoc tests showed that (*R,S*)-ketamine (10 mg/kg) and (*R*)-ketamine (10 mg/kg) significantly attenuated the increased immobility times of TST in CSDS susceptible mice (Figure 1C). However, (*S*)-ketamine (10 mg/kg) did not attenuate the increased immobility time of TST in CSDS susceptible mice although (*S*)-ketamine slightly decreased the increased immobility time (Figure 1C). One-way ANOVA of FST data showed a statistical significance ($F_{4,72} = 13.77$, $P < 0.001$) among the five groups (Figure 1D). Post-hoc tests showed that three compounds (10 mg/kg) significantly attenuated the increased immobility times of FST in CSDS susceptible mice (Figure 1D). One-way ANOVA of SPT data showed statistical significance (2 days after a single injection: $F_{4,72} = 20.78$, $P < 0.001$) among the five groups (Figure 1E). Post-hoc tests showed that three compounds (10 mg/kg) significantly attenuated the decreased sucrose preference of SPT in CSDS susceptible mice (Figure 1E). One-way ANOVA of SPT data showed statistical significance (7 days after a single injection: $F_{4,72} = 9.311$, $P < 0.001$,) among the five groups (Figure 1F). Post-hoc tests showed that sucrose preference of (*R*)-ketamine-treated group was significantly higher from saline-treated group. However, sucrose preference of (*R,S*)-ketamine-treated group and (*S*)-ketamine -treated group was not different from saline-treated group (Figure 1E and 1F). Collectively, the order of potency of antidepressant effects in a CSDS model was (*R*)-ketamine > (*R,S*)-ketamine > (*S*)-ketamine.
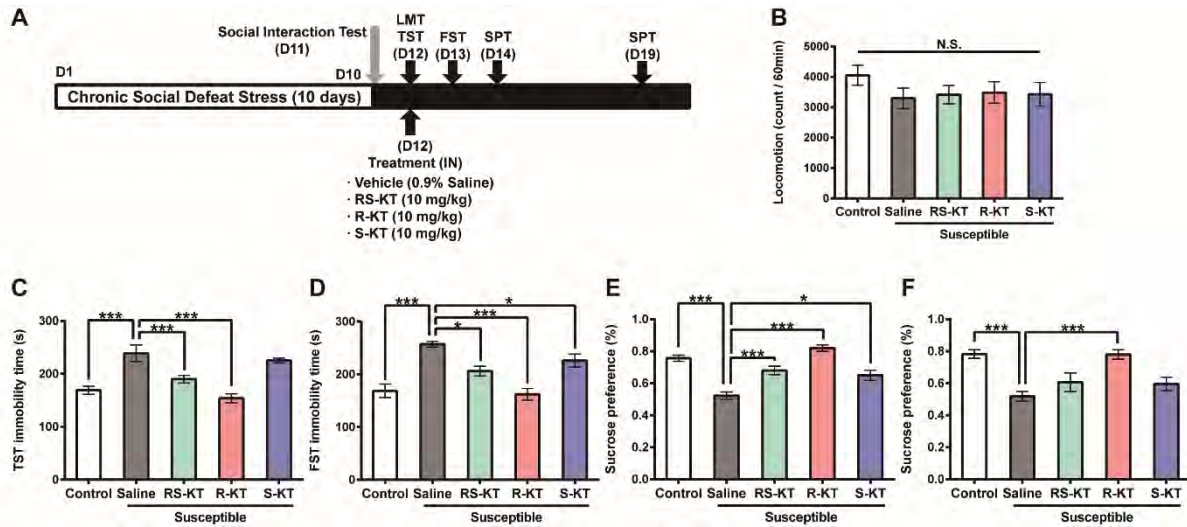
Figure 1. Schedule of a CSDS model, treatment, and behavioral tests
(A): CSDS was performed from day 1 to day 10, and the social interaction test (SIT) was performed on day 11. Saline (0.5 ml/kg), (*R,S*)-ketamine (10 mg/kg), (*R*)-ketamine (10 mg/kg), or (*S*)-ketamine (10 mg/kg) was administered intranasally into the susceptible mice on day 12. LMT and TST were performed 2 and 4 hours after a single injection, respectively. SPT was performed 2, and 7 days after a single injection. (B): LMT. (day 12). (C): TST (day 12). (D): FST (day 13). (E): SPT (day 14). (F): SPT (day 19). The values represent the mean ± S.E.M. (n = 15 or 16). *$P < 0.05$, **$P < 0.01$, ***$P < 0.001$ compared with saline-treated susceptible mice. N.S.: not significant. LMT: locomotion test. TST: tail suspension test. FST: forced swimming test. SPT: 1% sucrose preference test. R-KT: (*R*)-ketamine. RS-KT: (*R*,**S**)-ketamine. S-KT: (*S*)-ketamine.

Effects of (*R,S*)-ketamine, (*R*)-ketamine, and (*S*)-ketamine on locomotion in mice after a single intranasal administration.

Effects of three compounds on locomotion of male mice were examined after a single intranasal administration. One-way ANOVA of the data showed statistical significances ($F_{9,70}$ = 8.931, $P < 0.001$) among the ten groups (Figure 2). Post-hoc tests showed that a single intranasal administration of (*R,S*)-ketamine (20 and 40 mg/kg) or (*S*)-ketamine (10, 20 and 40 mg/kg) significantly increased locomotion compared to saline-treated group (Figure 2). Furthermore, locomotion of (*S*)-ketamine (40 mg/kg) treated mice was significantly higher than that of (*R,S*)-ketamine (40 mg/kg) or (*R*)-ketamine (40 mg/kg) treated mice. In contrast, all doses (10, 20 or 40 mg/kg) of (*R*)-ketamine did not alter locomotion in mice (Figure 2).
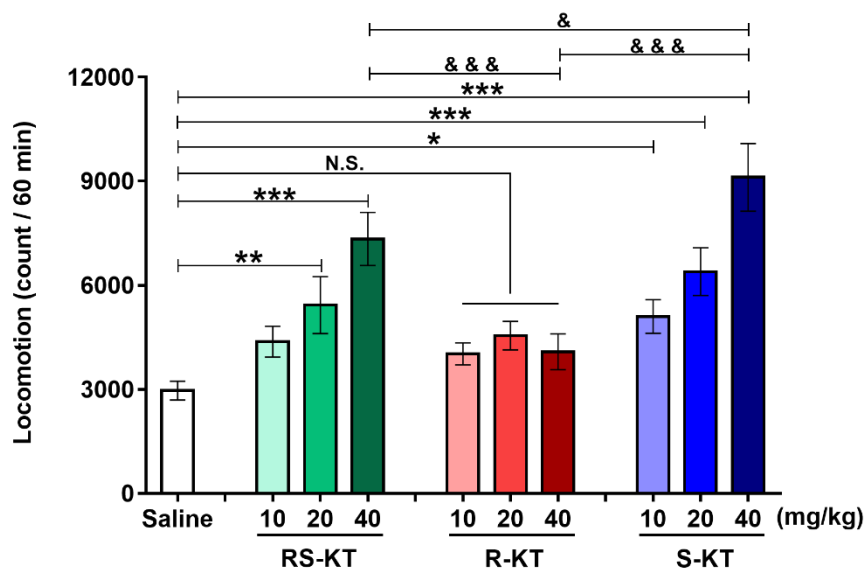
Figure 2. Effects of (*R,S*)-ketamine, (*R*)-ketamine, and (*S*)-ketamine on locomotion after a single intranasal administration
Saline (0.5 ml/kg), (*R,S*)-ketamine (10, 20, or 40 mg/kg), (*R*)-ketamine (10, 20, or 40 mg/kg), or (*S*)-ketamine (10, 20, or 40 mg/kg) was administered intranasally into male mice. Locomotor activity was measured 60 min after a single injection of the compounds. The values represent the mean ± S.E.M. (n = 8). *$P < 0.05$, **$P < 0.01$, ***$P < 0.001$ compared with saline-treated mice. &$P < 0.05$ compared to RS-KT (40 mg/kg). &&&$P < 0.001$ compared to R-KT (40 mg/kg). N.S.: not significant. R-KT: (*R*)-ketamine. RS-KT: (*R,S*)-ketamine. S-KT: (*S*)-ketamine.

Effects of (*R*,*S*)-ketamine, (*R*)-ketamine, and (S)-ketamine on PPI in mice after a single intranasal administration

PPI test was performed to examine the effects of three compounds in mice. There were no changes in the acoustic startle response among the four groups for (*R*,*S*)-ketamine [Wilks lambda = 0.717, *P* = 0.589], (*R*)-ketamine [Wilks lambda = 0.629, *P* = 0.226], and (*S*)-ketamine [Wilks lambda = 0.588, *P* = 0.405] (Figure 3A-3C).

The MANOVA analysis of all PPI data of (*R*,*S*)-ketamine revealed that there was a significant effect [Wilks lambda = 0.497, *P* = 0.042]. Treatment with (*R*,*S*)-ketamine (10, 20 or 40 mg/kg) decreased PPI at all dB groups, in a dose dependent manner. Subsequent post-hoc tests indicated significant differences in PPI between the saline group and (*R*,*S*)-ketamine (40 mg/kg) group at all dB groups (Figure 3A). In contrast, the MANOVA analysis of all PPI data of (*R*)-ketamine revealed that there was not a significant effect [Wilks lambda = 0.625, *P* = 0.216] (Figure 3B). The MANOVA analysis of all PPI data of (*S*)-ketamine revealed that there was a significant effect [Wilks lambda = 0.299, *P* < 0.001]. Treatment with (*S*)-ketamine (10, 20 or 40 mg/kg) decreased PPI at all dB groups, in a dose dependent manner. Subsequent post-hoc tests indicated significant differences in PPI deficits between the saline group and (*S*)-ketamine (20 and 40 mg/kg) group at all dB groups. Furthermore, (*S*)-ketamine (10 mg/kg) significantly decreased PPI at 73 dB (Figure 3C).

Figure 3. Effects of (*R,S*)-ketamine, (*R*)-ketamine, and (*S*)-ketamine on PPI after a single intranasal administration

(A): Saline (0.5 ml/kg), or (*R,S*)-ketamine (10, 20, or 40 mg/kg) was administered intranasally into male mice. (B): Saline (0.5 ml/kg), or (*R*)-ketamine (10, 20, or 40 mg/kg) was administered intranasally into male mice. (C): Saline (0.5 ml/kg), or (*S*)-ketamine (10, 20, or 40 mg/kg) was administered intranasally into male mice. Startle response amplitude and PPI were measured as described in the method section. The values represent the mean ± S.E.M. (n = 9 or 10). *$P < 0.05$, **$P < 0.01$, ***$P < 0.001$ compared with saline-treated mice. N.S.: not significant. R-KT: (*R*)-ketamine. RS-KT: (*R,S*)-ketamine. S-KT: (*S*)-ketamine.

Effects of (*R*,*S*)-ketamine, (*R*)-ketamine, and (*S*)-ketamine on CPP scores in mice after repeated intranasal administration

In the conditioned place preference (CPP) test (Figure 4A), both (*R*,*S*)-ketamine and (*S*)-ketamine, but not (*R*)-ketamine, increased CPP scores, in a dose dependent manner (Figure 4). Repeated intranasal administration of (*R*,*S*)-ketamine (40 mg/kg), but not the low doses (10 and 20 mg/kg), significantly increased CPP scores ($F_{3,34} = 3.054$, $P = 0.042$) (Figure 4B). In contrast, repeated intranasal administration of (*R*)-ketamine (10, 20 or 40 mg/kg) did not increase CPP scores ($F_{3,36} = 0.072$, $P = 0.974$) (Figure 4C). Repeated intranasal administration of (*S*)-ketamine (20 and 40 mg/kg), but not the low dose (10 mg/kg), significantly increased CPP scores ($F_{3,36} = 14.0$, $P < 0.001$) (Figure 4D).

Collectively, the order of potencies of side effects (i.e., psychosis, abuse liability) in mice after intranasal administration was (*S*)-ketamine > (*R*,*S*)-ketamine > (*R*)-ketamine.
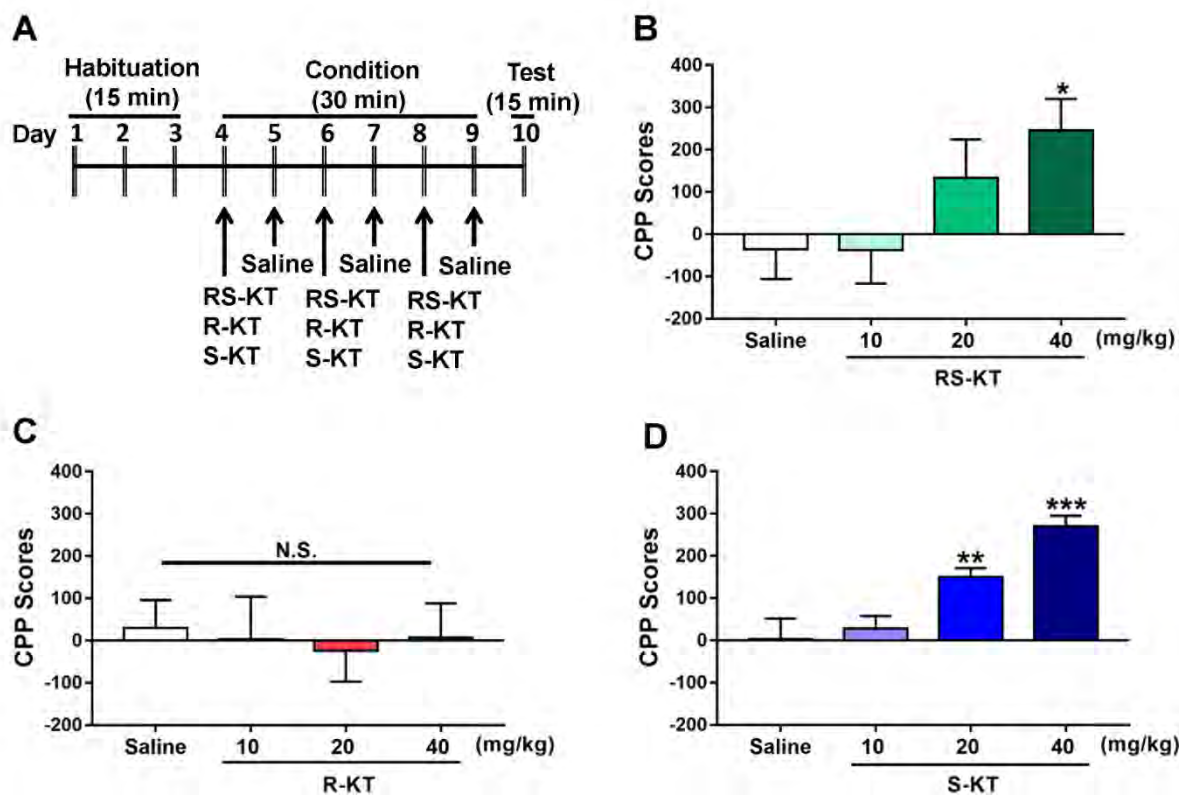
Figure 4. Effects of (*R,S*)-ketamine, (*R*)-ketamine, and (*S*)-ketamine on CPP score after repeated intranasal administration

(A): Schedule of habituation, treatment, and behavioral test. (B): Saline (0.5 ml/kg), or (*R,S*)-ketamine (10, 20, or 40 mg/kg) was administered intranasally into male mice. (C): Saline (0.5 ml/kg), or (*R*)-ketamine (10, 20, or 40 mg/kg) was administered intranasally into male mice. (D): Saline (0.5 ml/kg), or (*S*)-ketamine (10, 20, or 40 mg/kg) was administered intranasally into male mice. CPP score was measured as described in the method section. The values represent the mean ± S.E.M. (n = 8 - 10). *$P < 0.05$, **$P < 0.01$, ***$P < 0.001$ compared with saline-treated mice. N.S.: not significant. R-KT: (*R*)-ketamine. RS-KT: (*R,S*)-ketamine. S-KT: (*S*)-ketamine.

Discussion

In the present study, we compared (*R,S*)-ketamine, and its two enantiomers, in CSDS susceptible mice (for antidepressant effects) and control mice (for side effects). The order of potency of antidepressant effects after a single intranasal administration to CSDS susceptible mice is (*R*)-ketamine > (*R,S*)-ketamine > (*S*)-ketamine. Furthermore, the order of potency of side effects (i.e., psychosis and abuse liability) after intranasal administration is (*S*)-ketamine > (*R,S*)-ketamine > (*R*)-ketamine. Collectively, it is likely that (*R*)-ketamine would be a rapid-acting and sustained antidepressant without side effects compared to (*R,S*)-ketamine and (*S*)-ketamine.

In this study, we found that antidepressant effects of (*R,S*)-ketamine and its two enantiomers in CSDS susceptible mice after a single intranasal administration may be less potent that those of a single i.p. administration (Dong et al., 2017; Yang et al., 2015; 2017a; 2017b; 2018a; Zhang et al., 2015; Zhang and Hashimoto, 2019b). Lower bioavailability of intranasal administration of (*R,S*)-ketamine and its two enantiomers may contribute to lower efficacy of intranasal administration compared to i.p. administration. Interestingly, the potency of antidepressant effects of (*R,S*)-ketamine and its two enantiomers was not correlated with the potencies of these compounds at the NMDAR (Ebert et al., 1997), suggesting that NMDAR inhibition may not play a key role in the antidepressant effects of (*R,S*)-ketamine and its enantiomers. Previously, Fukumoto et al. (2017) reported that (*R,S*)-ketamine and (*R*)-ketamine, but not (*S*)-ketamine, show antidepressant effects in rats with repeated corticosterone treatments after a single i.p. administration, consistent with our current data.

Due to its serious side effects, clinical use of ketamine has remained limited (Domino, 2010; Sanacora et al., 2017; Singh et al., 2017; Zhu et al., 2016), although it has been used as an off-label antidepressant in the USA (Reardon, 2018; Wilkinson et al., 2017). In this study,

we found that locomotion after a single intranasal administration of (*R*)-ketamine is lower than those of (*R,S*)-ketamine and (*S*)-ketamine, consistent with the previous reports (Ryder et al., 1978; Yang et al., 2015) of subcutaneous or i.p. administration. Furthermore, we found that a single intranasal administration of (*R*)-ketamine did not cause PPI deficits in mice compared to (*R,S*)-ketamine and (*S*)-ketamine, consistent with the previous reports of i.p. administration (Yang et al., 2015). Interestingly, it was reported that the ED50 of (*R*)-ketamine (6.33 mg/kg) for PPI deficits in rats was higher than that of (*S*)-ketamine (2.86 mg/kg), indicating that (*S*)-ketamine disrupts PPI with 2.5-fold higher potency than (*R*)-ketamine (Halberstadt et al., 2016). Finally, we found that repeated intranasal administration of (*R*)-ketamine did not increase CPP scores in mice although (*R,S*)-ketamine and (*S*)-ketamine increased CPP scores, in a dose dependent manner, consistent with the previous reports of i.p. administration (Yang et al., 2015; 2018b). A PET study showed that a single i.v. infusion of (*S*)-ketamine (0.5 mg/kg for 40-min), but not (*R*)-ketamine (0.5 mg/kg for 40-min), produced a marked reduction of dopamine D2/3 receptor binding in conscious monkey striatum, suggesting that (*S*)-ketamine-induced dopamine release might be associated with acute psychotomimetic and dissociative side effects in humans (Hashimoto et al., 2017). Unlike (*R,S*)-ketamine and (*S*)-ketamine, it seems that intranasal infusion of (*R*)-ketamine does not appear to cause psychotomimetic effects or have abuse potential in humans, based on the lack of behavioral abnormalities (e.g., PPI deficits, CPP) observed in mice after single or repeated intranasal administration (Hashimoto, 2016a; 2016b; 2016c).

Mathisen et al. (1995) reported that the incidence of side effects (i.e., blurred vision, altered hearing, dizziness, proprioceptive disturbances, illusions) of (*S*)-ketamine (0.45 mg/kg, i.m.) treated group in patients with oral pain was higher than (*R*)-ketamine (1.8 mg/kg, i.m.) treated group, although the dose of (*S*)-ketamine (0.45 mg/kg) is lower than (*R*)-ketamine (1.8 mg/kg). Furthermore, it is also reported that experiencing illusion and alterations in

hearing, vision, and proprioception is attributable to (*S*)-ketamine's actions (Oye et al., 1992; Vollenweider et al., 1997), whereas the feelings of relaxation are associated with (*R*)-ketamine's actions (Vollenweider et al., 1997; Zanos et al., 2018). Taken all together, it seems likely that (*S*)-ketamine contributes to the acute psychotomimetic and dissociative effects of (*R,S*)-ketamine, whereas (*R*)-ketamine may not be associated with these side effects (Zanos et al., 2018).

On March 5, 2019, the US FDA approved nasal spray of (*S*)-ketamine for treatment-resistant depression (FDA 2019). Due to the risk of serious adverse outcomes from sedation and dissociation caused by administration of (*S*)-ketamine, as well as the potential for abuse and misuse of the drug, FDA said that the drug will only be available through a restricted distribution system, under a Risk Evaluation and Mitigation Strategy (REMS). Patients will self-administer (*S*)-ketamine under the supervision of a health care provider in a certified doctor's office or clinic; the nasal spray cannot be taken home (FDA 2019). Given the lack of adverse side effects of (*R*)-ketamine, it is possible that patients may take (*R*)-ketamine to their home.

In conclusion, this study suggests that the order of potency for antidepressant effects in a CSDS model after a single intranasal administration is (*R*)-ketamine > (*R,S*)-ketamine > (*S*)-ketamine. In contrast, the order of potency for side effects in mice after intranasal administration is (*S*)-ketamine > (*R,S*)-ketamine > (*R*)-ketamine. Therefore, it is likely that (*R*)-ketamine could be a safer antidepressant without side effects than (*R,S*)-ketamine and (*S*)-ketamine.

Acknowledgements

References

Abdallah, C.G., Sanacora, G., Duman, R.S., Krystal, J.H., (2018). The neurobiology of depression, ketamine and rapid-acting antidepressants: Is it glutamate inhibition or activation? Pharmacol. Ther. 190, 148-158.

Berman, R.M., Cappiello, A., Anand, A., Oren, D.A., Heninger, G.R., Charney, D.S., Krystal, J.H., (2000). Antidepressant effects of ketamine in depressed patients. Biol. Psychiatry 47, 351–354.

Chaki, S., (2017a). Beyond ketamine: new approaches to the development of safer antidepressants. Curr. Neuropharmacol. 15, 963–976.

Chaki, S., (2017b). mGlu2/3 receptor antagonists as novel antidepressants. Trends Pharmacol. Sci. 38, 569–580.

Chang, L., Zhang, K., Pu, Y., Qu, Y., Wang, S.M., Xiong, Z., Shirayama, Y., Hashimoto, K., (2019). Lack of dopamine D1 receptors in the antidepressant actions of (*R*)-ketamine in a chronic social defeat stress model. Eur. Arch. Psychiatry Clin. Neurosci. 2019 Mar 29. doi: 10.1007/s00406-019-01012-1.

Domino, E.F., (2010). Taming the ketamine tiger. 1965. Anesthesiology 113, 678–684.

Dong, C., Zhang, J.C., Yao, W., Ren, Q., Ma, M., Yang, C., Chaki, S., Hashimoto, K., (2017). Rapid and sustained antidepressant action of the mGlu2/3 receptor antagonist MGS0039 in the social defeat stress model: Comparison with ketamine. Int. J. Neuropsychopharmacol. 20, 228–236.

Duman, R.S., (2018). Ketamine and rapid-acting antidepressants: a new era in the battle against depression and suicide. F1000Res. 7.pii: F1000 Faculty Rev-659.

Ebert, B., Mikkelsen, S., Thorkildsen, C., Borgbjerg, F.M., (1997). Norketamine, the main metabolite of ketamine, is a non-competitive NMDA receptor antagonist in the rat cortex and spinal cord. Eur. J. Pharmacol. 333, 99–104.

FDA News Release on March 5, (2019). FDA approves new nasal spray medication for treatment-resistant depression; available only at a certified doctor's office or clinic. https://www.fda.gov/NewsEvents/Newsroom/PressAnnouncements/ucm632761.htm

Fukumoto, K., Toki, H., Iijima, M., Hashihayata, T., Yamaguchi, J.I., Hashimoto, K., Chaki, S., (2017). Antidepressant Potential of (*R*)-Ketamine in Rodent Models: Comparison with (S)-Ketamine. J. Pharmacol. Exp. Ther. 361, 9–16.

Golden, S.A., Covington III, H.E., Berton, O., Russo, S.J., (2011). A standardized protocol for repeated social defeat stress in mice. Nat. Protoc. 6,1183–1191.

Gould, T.D., Zarate, C.A. Jr., Thompson, S.M., (2019). Molecular Pharmacology and Neurobiology of Rapid-Acting Antidepressants. Annu. Rev. Pharmacol. Toxicol. 59, 213–236.

Grunebaum, M.F., Galfalvy, H.C., Choo, T.H., Keilp, J.G., Moitra, V.K., Parris, M.S., Marver, J.E., Burke, A.K., Milak, M.S., Sublette, M.E., Oquendo, M.A., Mann, J.J., (2018). Ketamine for rapid reduction of suicidal thoughts in major depression: a midazolam-controlled randomized clinical trial. Am. J. Psychiatry 175, 327–335.

Halberstadt, A.L., Slepak, N., Hyun, J., Buell, M.R., Powell, S.B., (2016). The novel ketamine analog methoxetamine produces dissociative-like behavioral effects in rodents. Psychopharmacology (Berl) 233, 1215–1225.

Hashimoto, K., (2014). The R-stereoisomer of ketamine as an alternative for ketamine for treatment-resistant major depression. Clin. Psychopharmacol. Neurosci. 12, 72–73.

Hashimoto, K., (2016a). R-ketamine: a rapid-onset and sustained antidepressant without risk of brain toxicity. Psychol. Med. 46, 2449–2451.

Hashimoto, K., (2016b). Ketamine's antidepressant action: beyond NMDA receptor inhibition. Expert. Opin. Ther. Targets. 20, 1389–1392.

Hashimoto, K., (2016c). Detrimental side effects of repeated ketamine infusions in the brain. Am. J. Psychiatry 173, 1044–1045.

Hashimoto, K., Kakiuchi, T., Ohba, H., Nishiyama, S., Tsukada, H., (2017). Reduction of dopamine D2/3 receptor binding in the striatum after a single administration of esketamine, but not R-ketamine: A PET study in conscious monkeys. Eur. Arch. Psychiatry Clin. Neurosci. 267, 173–176.

Kishimoto, T., Chawla, J.M., Hagi, K., Zarate, C.A., Kane, J.M., Bauer, M., Correll, C.U., (2016). Single-dose infusion ketamine and non-ketamine N-methyl-d-aspartate receptor antagonists for unipolar and bipolar depression: a meta-analysis of efficacy, safety and time trajectories. Psychol. Med. 46, 1459-1472.

Krystal, J.H., Abdallah, C.G., Sanacora, G., Charney, D.S., Duman, R.S., (2019). Ketamine: A paradigm shift for depression research and treatment. Neuron 101, 774-778.

Larkin, G.L., Beautrais, A.L., (2011). A preliminary naturalistic study of low-dose ketamine for depression and suicide ideation in the emergency department. Int. J. Neuropsychopharmacol. 14, 1127–1131.

Li, L., Vlisides, P.E., (2016). Ketamine: 50 years of modulating the mind. Front. Hum. Neurosci. 10, 612.

Mathisen, L.C., Skjelbred, P., Skoglund, L.A., Oye, I., (1995). Effect of ketamine, an NMDA receptor inhibitor, in acute and chronic orofacial pain. Pain 61, 215–220.

Matsuura, A., Fujita, Y., Iyo, M., Hashimoto, K., (2015). Effects of sodium benzoate on pre-pulse inhibition deficits and hyperlocomotion in mice after administration of phencyclidine. Acta. Neuropsychiatr. 27, 159–167.

Monteggia, L.M., Zarate Jr, C., (2015). Antidepressant actions of ketamine: from molecular mechanisms to clinical practice. Curr. Opin. Neurobiol. 30, 139–143.

Murrough, J.W., Abdallah, C.G., Mathew, S.J., (2017). Targeting glutamate signalling in depression: progress and prospects. Nat. Rev. Drug Discov. 16, 472–486.

Murrough, J.W., Iosifescu, D.V., Chang, L.C., Al Jurdi, R.K., Green, C.E., Perez, A.M., Iqbal, S., Pillemer, S., Foulkes, A., Shah, A., Charney, D.S., Mathew, S.J., (2013). Antidepressant efficacy of ketamine in treatment-resistant major depression: a two-site randomized controlled trial. Am. J. Psychiatry 170, 1134–1142.

Murrough, J.W., Soleimani, L., DeWilde, K.E., Collins, K.A., Lapidus, K.A., Iacoviello, B.M., Lener, M., Kautz, M., Kim, J., Stern, J.B., Price, R.B., Perez, A.M., Brallier, J.W., Rodriguez, G.J., Goodman, W.K., Iosifescu, D.V., Charney, D.S., (2015). Ketamine for rapid reduction of suicidal ideation: a randomized controlled trial. Psychol. Med. 45, 3571–3580.

Newport, D.J., Carpenter, L.L., McDonald, W.M., Potash, J.B., Tohen, M., Nemeroff, C.B., (2015). APA Council of Research Task Force on Novel Biomarkers and Treatments. Ketamine and other NMDA antagonists: early clinical trials and possible mechanisms in depression. Am. J. Psychiatry 172, 950–966.

Oye, I., Paulsen, O., Maurset, A., (1992). Effects of ketamine on sensory perception: evidence for a role of N-methyl-D-aspartate receptors. J. Pharmacol. Exp. Ther. 260, 1209–1213.

Peltoniemi, M.A., Hagelberg, N.M., Olkkola, K.T., Saari, T., (2016). Ketamine: a review of clinical pharmacokinetics and pharmacodynamics in anesthesia and pain therapy. Clin. Pharmacokinet. 55, 1059–1077.

Price, R.B., Nock, M.K., Charney, D.S., Mathew, S.J., (2009). Effects of intravenous ketamine on explicit and implicit measures of suicidality in treatment-resistant depression. Biol. Psychiatry 66, 522–526.

Reardon, S., (2018). 'Party drug' turned antidepressant approaches approval. Nat. Rev. Drug Discov. 17, 773–775.

Ryder, S., Way, W.L., Trevor, A.J., (1978). Comparative pharmacology of the optical isomers of ketamine in mice. Eur. J. Pharmacol. 49, 15–23.

Sanacora, G., Frye, M.A., McDonald, W., Mathew, S.J., Turner, M.S., Schatzberg, A.F., Summergrad, P., Nemeroff, C.B.; American Psychiatric Association (APA) Council of Research Task Force on Novel Biomarkers and Treatments, (2017). A consensus statement on the use of ketamine in the treatment of mood disorders. JAMA Psychiatry 74, 399–405.

Singh, I., Morgan, C., Curran, V., Nutt, D., Schlag, A., McShane, R., (2017). Ketamine treatment for depression: opportunities for clinical innovation and ethica foresight. Lancet Psychiatry 4, 419–426.

Su, T.P., Chen, M.H., Li, C.T., Lin, W.C., Hong, C.J., Gueorguieva, R., Tu, P.C., Bai, Y.M., Cheng, C.M., Krystal, J.H., (2017). Dose-related effects of adjunctive ketamine in Taiwanese patients with treatment-resistant depression. Neuropsychopharmacology 42, 2482–2492.

Tian, Z., Dong, C., Fujita, A., Fujita, Y., Hashimoto, K., (2018). Expression of heat shock protein HSP-70 in the retrosplenial cortex of rat brain after administration of (*R,S*)-ketamine and (*S*)-ketamine, but not (*R*)-ketamine. Pharmacol. Biochem. Behav. 172, 17–21.

Vollenweider, F.X., Leenders, K.L., Oye, I., Hell, D., Angst, J., (1997). Differential psychopathology and patterns of cerebral glucose utilisation produced by (*S*)- and (*R*)-ketamine in healthy volunteers using positron emission tomography (PET). Eur. Neuropsychopharmacol. 7, 25–38.

Wilkinson, S.T., Ballard, E.D., Bloch, M.H., Mathew, S.J., Murrough, J.W., Feder, A., Sos, P., Wang, G., Zarate Jr, C.A., Sanacora, G., (2018). The effect of a single dose of intravenous ketamine on suicidal ideation: A systematic review and individual participant data meta-analysis. Am. J. Psychiatry 175, 150–158.

Wilkinson, S.T., Toprak, M., Turner, M.S., Levine, S.P., Katz, R.B., Sanacora, G., (2017). A survey of the clinical, off-label use of ketamine as a treatment for psychiatric disorders. Am. J. Psychiatry 174, 695–696.

Xiong, Z., Zhang, K., Ishima, T., Ren, Q., Chang, L., Chen, J., Hashimoto, K., (2018a). Comparison of rapid and long-lasting antidepressant effects of negative modulators of α5-containing GABAA receptors and (*R*) ketamine in a chronic social defeat stress model. Pharmacol. Biochem. Behav. 175, 139–145.

Xiong, Z., Zhang, K., Ishima, T., Ren, Q., Ma, M., Pu, Y., Chang, L., Chen, J., Hashimoto, K., (2018b). Lack of rapid antidepressant effects of Kir4.1 channel inhibitors in a chronic social defeat stress model: Comparison with (*R*)-ketamine. Pharmacol. Biochem. Behav. 176, 57–62.

Xu, Y., Hackett, M., Carter, G., Loo, C., Gálvez, V., Glozier, N., Glue, P., Lapidus, K., McGirr, A., Somogyi, A.A., Mitchell, P.B., Rodgers, A., (2016). Effects of low-dose and very low-dose ketamine among patients with major depression: a systematic review and meta-analysis. Int. J. Neuropsychopharmacol. 19, pii: pyv124

Yang, C., Han, M., Zhang, J.C., Ren, Q., Hashimoto, K., (2016). Loss of parvalbumin-immunoreactivity in mouse brain regions after repeated intermittent administration of esketamine, but not R-ketamine. Psychiatric. Res. 239, 281–283.

Yang, C., Kobayashi, S., Nakao, K., Dong, C., Han, M., Qu, Y., Ren, Q., Zhang, J.C., Ma, M., Toki, H., Yamaguchi, J.I., Chaki, S., Shirayama, Y., Nakazawa, K., Manabe, T.,

Hashimoto, K., (2018b). AMPA receptor activation-independent antidepressant actions of ketamine metabolite (S)-norketamine. Biol. Psychiatry 84, 591–600.

Yang, C., Qu, Y., Abe, M., Nozawa, D., Chaki, S., Hashimoto, K., (2017a). (*R*)-ketamine shows greater potency and longer lasting antidepressant effects than its metabolite (2R,6R)-hydroxynorketamine. Biol. Psychiatry 82, e43–e44.

Yang, C., Qu, Y., Fujita, Y., Ren, Q., Ma, M., Dong, C., Hashimoto, K., (2017b). Possible role of the gut microbiota-brain axis in the antidepressant effects of (*R*)-ketamine in a social defeat stress model. Transl. Psychiatry 7, 1294.

Yang, C., Ren, Q., Qu, Y., Zhang, J.C., Ma, M., Dong, C., Hashimoto, K., (2018a). Mechanistic target of rapamycin-independent antidepressant effects of (*R*)-ketamine in a social defeat stress model. Biol. Psychiatry 83, 18–28.

Yang, C., Shirayama, Y., Zhang, J.C., Ren, Q., Yao, W., Ma, M., Dong, C., Hashimoto, K., (2015). R-ketamine: a rapid-onset and sustained antidepressant without psychotomimetic side effects. Transl. Psychiatry 5, e632.

Zanos, P., Moaddel, R., Morris, P.J., Georgiou, P., Fischell, J., Elmer, G.I., Alkondon, M., Yuan, P., Pribut, H.J., Singh, N.S., Dossou, K.S., Fang, Y., Huang, X.P., Mayo, C.L., Wainer, I.W., Albuquerque, E.X., Thompson, S.M., Thomas, C.J., Zarate Jr, C.A., Gould, T.D., (2016). NMDAR inhibition-independent antidepressant actions of ketamine metabolites. Nature 533, 481–486.

Zanos, P., Moaddel, R., Morris, P.J., Riggs, L.M., Highland, J.N., Georgiou, P., Pereira, E.F.R., Albuquerque, E.X., Thomas, C.J., Zarate Jr, C.A., Gould, T.D., (2018). Ketamine and ketamine metabolite pharmacology: insights into therapeutic mechanisms. Pharmacol. Rev. 70, 621–660.

Zarate, C.A., Singh, J.B., Carlson, P.J., Brutsche, N.E., Ameli, R., Luckenbaugh, D.A., Charney, D.S., Manji, H.K., (2006). A randomized trial of an N-methyl-D-aspartate antagonist in treatment-resistant major depression. Arch. Gen. Psychiatry 63, 856–864.

Zhang, K., Hashimoto, K., (2019a). An update on ketamine and its two enantiomers as rapid-acting antidepressants. Expert Rev. Neurother. 19, 83–92.

Zhang, K., Hashimoto, K., (2019b). Lack of opioid system in the antidepressant actions of ketamine. Biol. Psychiatry 85, e25–e27.

Zhang, J.C., Li, S.X., Hashimoto, K., (2014). *R*(-)-ketamine shows greater potency and longer lasting antidepressant effects than S(+)-ketamine. Pharmacol. Biochem. Behav. 116, 137–141.

Zhang, K., Toki, H., Fujita, Y., Ma, M., Chang, L., Qu, Y., Harada, S., Nemoto, T., Mizuno-Yasuhira, A., Yamaguchi, J.I., Chaki, S., Hashimoto, K., (2018). Lack of deuterium isotope effects in the antidepressant effects of (R)-ketamine in a chronic social defeat stress model. Psychopharmacology (Berl) 235, 3177–3185.

Zhang, J.C., Yao, W., Dong, C., Yang, C., Ren, Q., Ma, M., Han, M., Hashimoto, K., (2015). Comparison of ketamine, 7,8-dihydroxyflavone, and ANA-12 antidepressant effects in the social defeat stress model of depression. Psychopharmacology (Berl) 232, 4325–4335.

Zhu, W., Ding, Z., Zhang, Y., Shi, J., Hashimoto, K., Lu, L., (2016). Risks associated with misuse of ketamine as a rapid-acting antidepressant. Neurosci. Bull. 32, 557–564.

日中笹川医学奨学金制度（学位取得コース）評価書
論文博士：指導教官用

第 41 期	研究者番号： G4103		作成日 ： 2021 年 3 月 3 日	

氏　名	朱　俊	ZHU JUN	性別	M	生年月日	1980.09.18
所属機関（役職）	江蘇省蘇北人民医院眼科（主治医師）					
研究先（指導教官）	順天堂大学大学院医学研究科 眼科学（村上 晶教 授）					
研究テーマ	体外培養骨髄由来免疫抑制細胞のマウス角膜移植の拒絶反応に及ぼす影響 *Ex vivo*-induced bone marrow-derived myeloid suppressor cells prevent corneal allograft rejection in mice					
専攻種別	☑論文博士			□課程博士		

研究者評価（指導教官記入欄）

成績状況	ⓥ 良 可 不可	取得単位数
		取得単位数／取得すべき単位総数

学生本人が行った 研究の概要	2019 年度は順天堂大学アトピー疾患研究センターと眼科学に在籍し、免疫学に関する実験手技を習得した。2020 年は順天堂大学医学部眼科学猪俣武範准教授の指導の元、「体外培養骨髄由来免疫抑制細胞のマウス角膜移植に及ぼす影響」と「抗 CD80/86 抗体を用いた誘導性制御性 T 細胞による角膜移植における免疫抑制能の解明」に取り組んだ。マウス角膜移植モデルにおいて体外培養骨髄由来免疫抑制細胞を局所に投与することで免疫抑制が誘導され、角膜移植グラフトへの血管新生とリンパ管新生が抑制されることを確認した。
総合評価	【良かった点】 免疫学に関する基礎実験手技を習得し、研究を主導した。角膜カンファランス 2021 ならびに第 40 回眼薬理学会での口演で研究の成果を発表した。また、研究成果は Investigative Ophthalmology & Visual Science 誌に投稿を行った。研究室では、他の研究のサポートに尽力した。 【改善すべき点】 英語でのコミュニケーションがよくとれ、日本語でも十分な会話はできたが、我々のほうでより積極的に日本語能力アップの機会を多くもつとよかった。 【今後の展望】 本研究を発展させ、中国に帰国後も自施設における研究の立ち上げと発展に貢献することが期待できる 1
学位取得見込	現在学位取得に向けた論文を眼科基礎研究領域のトップジャーナルである Investigative Ophthalmology & Visual Science に筆頭著者として投稿し、リバイスをうけ実験を追加実施している。2021 年度中に論文の掲載が得られ 2022 年には学位取得は可能と考える。

評価者（指導教官名）　村上　晶 ㊞

第41期		研究者番号： G4103		作成日：2021年3月＿＿日			
氏名	Zhu Jun		朱 俊	性別	M	生年月日	1980 . 09 . 18

所属機関(役職)	江蘇省蘇北人民医院眼科（主治医師）
研究先（指導教官）	順天堂大学大学院医学研究科 眼科学（村上 晶教授）
研究テーマ	骨髄由来免疫抑制細胞のマウス角膜移植に及ぼす影響 Effect of ex vivo-induced myeloid-derived suppressor cells from bone marrow in a mouse corneal transplantation model

専攻種別	論文博士	☑	課程博士	

１．研究概要（１）

１）目的（Goal）

　To investigate the effects of ex vivo-induced bone marrow myeloid-derived suppressor cells (BM-MDSCs) on allogeneic immune responses in corneal transplantation.

２）戦略（Approach）

　Myeloid-derived suppressor cells (MDSCs) are progenitors of granulocytic cells and are induced under pathological conditions, such as cancer, and in conditions associated with chronic inflammation. In mice, MDSCs express the myeloid lineage marker CD11b and the granulocytic marker Gr1 on their surface [1]. Importantly, MDSCs can induce Tregs and inhibit the proliferation of effector T cells [2]; although its underlying process remains poorly　known. Notably, recent studies have shown that MDSCs can be induced in vitro by culturing bone marrow cells in the presence of signaling factors from the microenvironment of cancer and inflammatory diseases [3]. Therefore, the application of ex vivo-induced bone marrow MDSCs (BM-MDSC) is promising for high-risk corneal transplantation in a local inflammatory environment as a potential approach for preventing graft rejection.

３）材料と方法（Materials and methods）

　Bone marrow cells from C57BL/6J (B6) mice were cultured with interleukin (IL)-6 and granulocyte macrophage-colony stimulating factor (GM-CSF) for 4 days. The ex vivo-induced BM-MDSCs were assessed using flow cytometry, and inducible nitric oxide synthase (iNOS) mRNA expression was determined using reverse transcription quantitative polymerase chain reaction. T cell proliferation and regulatory T cell (Treg) induction were investigated upon allogeneic stimulation in the presence of ex vivo-induced BM-MDSCs. IFN-γ, IL-2, IL-10, and TGF-β1 were measured using enzyme-linked immunosorbent assay. The allogeneic corneal graft survival, neovascularization, and lymphangiogenesis were assessed using slit-lamp microscopy and immunohistochemistry upon subconjunctival injection　of ex vivo-induced BM-MDSCs.

４）実験結果（Results）

　BM-MDSCs were significantly induced by GM-CSF and IL-6 stimulus and presented increased iNOS expression. The ex vivo-induced BM-MDSCs inhibited T cell proliferation, promoted Treg expansion, and decreased IFN-γ production but promoted the secretion of IL-2, IL-10, and TGF-β1. Further, ex vivo-induced BM-MDSC injection prolonged corneal graft survival and prevented angiogenesis and lymphangiogenesis.

５）考察（Discussion）

　Immune reaction control in the local environment is a key mechanism for prolonging corneal grafts survival. In this study, the suppressive function of ex vivo-induced BM-MDSCs was investigated. Our results demonstrated that ex vivo-induced BM-MDSCs had immune suppressive function via the iNOS pathway and expanded Tregs in vitro, indicating that ex vivo-induced BM-MDSCs could prolong corneal grafts survival in an inflamed microenvironment; therefore representing a potentially effective immunosuppressive therapy for corneal transplantation.

We found that IL-6 and GM-CSF cocultures induced functional BM-MDSCs with iNOS upregulation. A previous study reported that MDSCs were induced at a higher frequency with high GM-CSF levels in the tumor microenvironment [4], and IL-6 has been reported to stimulate MDSCs in multiple cancers [5]. However, these observations were made under tumor immunopathological conditions, mostly in the systemic environment, whereas the generation of MDSCs and their influences on the local corneal environment remain poorly know. This study showed that BM-MDSCs expanded in the presence of GM-CSF, which agrees with Park et al. report that described a similar expansion and differentiation of MDSCs from umbilical cord blood with GM-CSF [6]. Interestingly, the relative mRNA expression of iNOS increased significantly in the presence of GM-CSF and IL-6 together. In many tumor microenvironments, iNOS is overexpressed and is known as a tumor-mediated immunosuppression factor. It breaks down L-arginine and generates significant amounts of NO, which in turn prevents effector T-cell activation through the Jak3/STAT5 signaling pathway that is critical for inflammatory and immune responses during the process of transplant rejection. Herein it was demonstrated that the higher BM-MDSCs number and their iNOS expression were the result of GM-CSF and IL-6 combined signals.

The inhibition of T cell proliferation by ex vivo-induced BM-MDSCs was shown to be reversed by an iNOS inhibitor, demonstrating that the suppression effect of BM-MDSCs is strongly related to the iNOS pathway. Previous studies showed that ARG1 expressed by MDSCs could also regulate T lymphocyte responses by impairing their proliferation and cytokine production [7].

1．研究概要（2）

However, in this study, no such effects were observed using an ARG1 inhibitor during the MLR assay. This agrees with the findings of Bian et al., who demonstrated that ARG1 is not required for MDSC-mediated inhibition of T-cell proliferation [8]. Thus, the iNOS pathway should be considered as a major mechanism for the suppressive effect observed in the allogeneic immune microenvironment.Further, this study showed that ex vivo-induced BM-MDSCs suppressed T cell proliferation between donor and recipient allogeneic lymphocyte reactions.

Our results show a notable expansion of Tregs in the presence of ex vivo-induced BM-MDSCs. Tregs are immunosuppressors of the adaptive system, playing a critical role in modulating and maintaining immune tolerance. However, the amplification and induction of Tregs in an inflammatory environment were difficult due to their plasticity [11]. It has been suggested that Tregs might become unstable under certain inflammatory conditions and their phenotype could change. In tumor-bearing hosts, it has been reported that MDSCs mediate the development of Tregs and T cell anergy [12]. In this study, we showed an increased Tregs frequency with allogeneic stimulation via ex vivo-induced BM-MDSCs intervention. This suggests that Tregs expansion is applicable in an ex vivo inflammatory microenvironment. In consideration of immunosuppression function of Tregs, expanding their number via ex vivo-induced BM-MDSCs should be a feasible approach for regulating effector T cell responses. However, the implementation of Treg suppressive function in corneal grafts requires further investigation.

With the presence of ex vivo-induced BM-MDSCs in the inflammatory microenvironment, the production of immunosuppressive cytokines, such as IL-2, IL-10 and TGF-β1, increased. IL-10 and TGF-β were shown to be important in tolerance induction and immune regulation, and IL-2 for the development of Tregs [13]. IL-2 mediates its effects by binding to an IL-2 receptor that is highly expressed on Tregs and activated T cells, subsequently promoting Treg expansion [14,15]. These increased immunosuppressive cytokines may promote Tregs expansion and maintenance in the inflammatory microenvironment, which may help corneal graft survival in vivo.

Furthermore, this study showed that ex vivo-induced BM-MDSCs injection prevent local neovascularization and prolonged grafted cornea survival in vivo in high-risk corneal transplantation conditions. Typically, MDSCs are applied in in vivo models via local and intravenous injections; however, in our high-risk corneal graft models, we applied ex vivo-induced BM-MDSCs through sub-conjunctival injection, which may improve the odds of direct interaction. During the process of rejection, lymphatic vessels and neovascular tissues are important factors to support the immune and inflammation response, as donor antigens, inflammatory cells, and pro-inflammatory cytokines could be delivered through these vessels to the graft. For corneal graft survival, reducing neovascularization and lymphangiogenesis is vital [16], and such reduction was confirmed in our high-risk mouse corneal grafts

6）参考文献（References）

1.Yang L, DeBusk LM, Fukuda K, Fingleton B, Green-Jarvis B, Shyr Y, et al. Expansion of myeloid immune suppressor Gr+CD11b+ cells in tumor-bearing host directly promotes tumor angiogenesis. Cancer Cell. 2004;6:409-21.

2.Fujimura T, Mahnke K, Enk AH. Myeloid derived suppressor cells and their role in tolerance induction in cancer. J Dermatol Sci. 2010;59:1-6.

3.Liechtenstein T, Perez-Janices N, Gato M, Caliendo F, Kochan G, Blanco-Luquin I, et al. A highly efficient tumor-infiltrating MDSC differentiation system for discovery of anti-neoplastic targets, which circumvents the need for tumor establishment in mice. Oncotarget. 2014;5:7843-57.

4. Marigo I, Dolcetti L, Serafini P, Zanovello P, Bronte V. Tumor-induced tolerance and immune suppression by myeloid derived suppressor cells. Immunol Rev. 2008;222:162-79.

5.Jiang M, Chen J, Zhang W, Zhang R, Ye Y, Liu P, et al. Interleukin-6 Trans-Signaling Pathway Promotes Immunosuppressive Myeloid-Derived Suppressor Cells via Suppression of Suppressor of Cytokine Signaling 3 in Breast Cancer. Front Immunol. 2017;8:1840.

6. Park MY, Lim BG, Kim SY, Sohn HJ, Kim S, Kim TG. GM-CSF Promotes the Expansion and Differentiation of Cord Blood Myeloid-Derived Suppressor Cells, Which Attenuate Xenogeneic Graft-vs.-Host Disease. Front Immunol. 2019;10:183.

7. Zea AH, Rodriguez PC, Atkins MB, Hernandez C, Signoretti S, Zabaleta J, et al. Arginase-producing myeloid suppressor cells in renal cell carcinoma patients: a mechanism of tumor evasion. Cancer Res. 2005;65:3044-8.

8. Bian Z, Abdelaal AM, Shi L, Liang H, Xiong L, Kidder K, et al. Arginase-1 is neither constitutively expressed in nor required for myeloid-derived suppressor cell-mediated inhibition of T-cell proliferation. Eur J Immunol. 2018;48:1046-58.

9. Hegde S, Beauregard C, Mayhew E, Niederkorn JY. CD4(+) T-cell-mediated mechanisms of corneal allograft rejection: role of Fas-induced apoptosis. Transplantation. 2005;79:23-31.

10. Braun MY, Desalle F, Le Moine A, Pretolani M, Matthys P, Kiss R, et al. IL-5 and eosinophils mediate the rejection of fully histoincompatible vascularized cardiac allografts: regulatory role of alloreactive CD8(+) T lymphocytes and IFN-gamma. Eur J Immunol. 2000;30:1290-6.

11. Sakaguchi S, Vignali DA, Rudensky AY, Niec RE, Waldmann H. The plasticity and stability of regulatory T cells. Nat Rev Immunol. 2013;13:461-7.

12. Huang B, Pan PY, Li Q, Sato AI, Levy DE, Bromberg J, et al. Gr-1+CD115+ immature myeloid suppressor cells mediate the development of tumor-induced T regulatory cells and T-cell anergy in tumor-bearing host. Cancer Res. 2006;66:1123-31.

13. Tahvildari M, Inomata T, Amouzegar A, Dana R. Regulatory T cell modulation of cytokine and cellular networks in corneal graft rejection. Curr Ophthalmol Rep. 2018;6:266-74.

14. Tahvildari M, Omoto M, Chen Y, Emami-Naeini P, Inomata T, Dohlman TH, et al. In Vivo Expansion of Regulatory T Cells by Low-Dose Interleukin-2 Treatment Increases Allograft Survival in Corneal Transplantation. Transplantation. 2016;100:525-32.

15. Dana MR. Angiogenesis and lymphangiogenesis-implications for corneal immunity. Semin Ophthalmol. 2006;21:19-22.

16. Di Zazzo A, Lee S-M, Sung J, Niutta M, Coassin M, Mashaghi A, et al. Variable Responses to Corneal Grafts: Insights from Immunology and Systems Biology. Journal of Clinical Medicine. 2020;9

２．執筆論文 Publication of thesis　※記載した論文を添付してください。Attach all of the papers listed below.

論文名1 Title	Report of Four Cases of Endogenous Klebsiella Pneumoniae Endophthalmitis Originated from Liver Abscess with Eye Complaints as the Initial Presentations					
掲載誌名 Published journal	Ocular Immunology Inflammation					
	2020 年 8 月	Epub 巻（号）	頁 ～ 頁	言語 Language	English	
第1著者名 First author	ZHU JUN	第2著者名 Second author	Chen Fang	第3著者名 Third author	Xie Zhenggao	
その他著者名 Other authors						

論文名2 Title						
掲載誌名 Published journal						
	年 月	巻（号）	頁 ～ 頁	言語 Language		
第1著者名 First author		第2著者名 Second author		第3著者名 Third author		
その他著者名 Other authors						

論文名3 Title						
掲載誌名 Published journal						
	年 月	巻（号）	頁 ～ 頁	言語 Language		
第1著者名 First author		第2著者名 Second author		第3著者名 Third author		
その他著者名 Other authors						

論文名4 Title						
掲載誌名 Published journal						
	年 月	巻（号）	頁 ～ 頁	言語 Language		
第1著者名 First author		第2著者名 Second author		第3著者名 Third author		
その他著者名 Other authors						

論文名5 Title						
掲載誌名 Published journal						
	年 月	巻（号）	頁 ～ 頁	言語 Language		
第1著者名 First author		第2著者名 Second author		第3著者名 Third author		
その他著者名 Other authors						

3．学会発表 Conference presentation　※筆頭演者とし　て総会国際学会を含む主な学会で発表し　たものを記載し　てください。

※Describe your presentation as the principal presenter in major academic meetings including general meetings or international meetings.

学会名 Conference	角膜カンファランス2021　第45回日本角膜学会総会/第37回日本角膜移植学会						
演　題 Topic	角膜移植における体外培養骨髄由来免疫抑制細胞を用いた新規免疫抑制療法の検討						
開催日 date	2021　　年　　2　月　　11　日		開催地 venue	Online			
形式　method	☑ 口頭発表　O ral　　□ ポスター発表　P ostr	言語　Language	□ 日本語	☑ 英語	□ 中国語		
共同演者名 Co-presenter							
学会名 Conference	第40回日本眼薬理学会						
演　題 Topic	骨髄由来免疫抑制細胞による免疫抑制効果の検討						
開催日 date	2021　　年　　2　月　　17　日		開催地 venue	Onlinえ			
形式　method	☑ 口頭発表　Oral　　□ ポスター発表　P ster	言語　anguage	□ 日本語	☑ 英語	□ 中国語		
共同演者名 Co-presenter							
学会名 Conference							
演　題 Topic							
開催日 date	年　　　　月　　　　日		開催地 venue				
形式　method	□ 口頭発表　O al　　□ ポスター発表　P oster	言語　Language	□ 日本語	□ 英語	□ 中国語		
共同演者名 Co-presenter							
学会名 Conference							
演　題 Topic							
開催日 date	年　　　　月　　　　日		開催地 venue				
形式　method	□ 口頭発表　O ral　　□ ポスター発表　P ster	言語　Language	□ 日本語	□ 英語	□ 中国語		
共同演者名 Co-oresenter							

4．受賞（研究業績）Award (Research achievement)

名　称 Award name	国名 Country name		受賞年 Year of award	年　　　　月
名　称 Award name	国名 Country name		受賞年 Year of award	年　　　　月

５．本研究テーマに関わる他の研究助成金受給 Other research grants concerned with your resarch theme

受給実績 Receipt record	□ 有　　　　□ 無				
助成機関名称 Funding agency					
助成金名称 Grant name					
受給期間 Supported period	年　　　　月　～　　　　年　　　　月				
受給額 Amount received	円				
受給実績 Receipt record	□ 有　　　　□ 無				
助成機関名称 Funding agency					
助成金名称 Grant name					
受給期間 Supported period	年　　　　月　～　　　　年　　　　月				
受給額 Amount received	円				

６．他の奨学金受給 Another awarded scholarship

受給実績 Receipt record	□ 有　　　　□ 無
助成機関名称 Funding agency	
奨学金名称 Scholarship name	
受給期間 Supported period	年　　　　月　～　　　　年　　　　月
受給額 Amount received	円

７．研究活動に関する報道発表 Press release concerned with your research activities

※記載した記事を添付してください。 Attach a copy of the article described below

報道発表 Press release	□ 有　　　　□ 無	発表年月日 Date of release	
発表機関 Released medium			
発表形式 Release method	・新聞　・雑誌　・Web site　・記者発表　・その他（　　　　　　　　　　　　）		
発表タイトル Released title			

８．本研究テーマに関する特許出願予定 Patent application concerned with your research theme

出願予定 Scheduled application	□ 有　　　　□ 無	出願国 Application country	
出願内容（概要） Application contents			
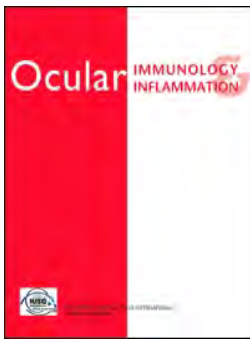
９．その他 Others

指導責任者（署名）　_[signature]_　㊞

Report of Four Cases of Endogenous *Klebsiella Pneumoniae* Endophthalmitis Originated from Liver Abscess with Eye Complaints as the Initial Presentations

Jun Zhu , Fang Chen & Zhenggao Xie

Taylor & Francis
Taylor & Francis Group

Check for updates

Report of Four Cases of Endogenous *Klebsiella Pneumoniae* Endophthalmitis Originated from Liver Abscess with Eye Complaints as the Initial Presentations

Jun Zhu, MD[a], Fang Chen, MD, Ph. D[a], and Zhenggao Xie, MD, Ph. D[b]

[a]Department of Ophthalmology, Subei People's Hospital Affiliated to Yangzhou University, Yangzhou, Jiangsu Province, China; [b]Department of Ophthalmology, Nanjing Drum Tower Hospital, the Affiliated Hospital of Nanjing University Medical School, Nanjing, Jiangsu Province, China

ABSTRACT

Purpose: To report four cases of endogenous endophthalmitis (EE) secondary to *Klebsiella pneumoniae* liver abscess, and discuss their clinic features and outcomes.

Methods: Clinical data were collected by reviewing the medical records of four patients diagnosed with endogenous *Klebsiella Pneumoniae* endophthalmitis (EKPE) secondary to liver abscess.

Results: Four patients were diagnosed with EE. Two males and two females, with ages ranging from 33 to 63 years old. All patients presented with ocular symptoms initially. Liver abscesses were diagnosed during hospitalization. All cases were caused by Klebsiella Pneumoniae confirmed by blood or tissue cultures. All patients were treated with intravitreal antibiotic injection, and two of the patients had vitrectomy. At the end, all affected eyes underwent evisceration. One patient died of septic shock with multiple organ failures.

Conclusion: EE secondary to liver abscess with metastatic spread is a severe sight-threatening condition. The delayed discovery of liver abscess may hinder the diagnosis and treatment of the disease, which may be related to poor prognosis.

Endogenous endophthalmitis (EE) is a metastatic infection of intraocular tissues. It is estimated that EE accounts for 2% to 15% of all cases of endophthalmitis.[1] In Asian population, especially in East Asia, Gram-negative organisms, particularly *Klebsiella Pneumoniae*, are the major cause of endogenous bacterial endophthalmitis.[2–4] According to a systematic review of 342 cases of endogenous bacterial endophthalmitis, the most common site of infection was the liver (19%).[5] Endogenous *Klebsiella Pneumoniae* endophthalmitis (EKPE) is associated with very poor visual outcomes, including a high rate of enucleation or evisceration.[4] There were numerous case reports about EKPE coming from preexisting liver abscess, but most of them had obvious systemic symptoms before having ocular manifestations.[6–8] We hereby report four cases of EKPE that presented with ocular symptoms as the initial presentations. As the diagnosis of liver abscess was delayed, they resulted in permanent blindness, or even death.

Case 1

A 51-year-old male with 15-year history of diabetes presented with blurry vision and pain in the left eye for 3 days. Before his eye symptoms, he had fever and chills. He was diagnosed with Uveitis by the local hospital. On examination, his visual acuity (VA) was hand motion (HM) in the left eye. Left eye examination revealed corneal edema, severe hypopyon in the anterior chamber, and vitreous opacity. The fundus of the left eye was cloudy. The diagnosis was suspected to be EE in the

left eye. His surgical risk was high as his platelet counts were low (10 × 10⁹/L), and therefore, intravitreal antibiotic injection (IVAI) of ceftazidime 2.25 mg/0.1 ml and vancomycin 1 mg/0.1 ml was performed immediately after admission. The patient was referred to the hematology department for the treatment of thrombocytopenia and systemic anti-infection therapy. His abdominal B-scan ultrasonography showed non-uniform fatty liver (Figure 1a). A further enhanced magnetic resonance imaging (MRI) demonstrated a round lesion in the liver and a liver abscess was highly suspected (Figure 1b). Computerized tomography (CT) for chest showed pneumonia. A liver abscess aspiration was performed urgently and the patient's overall condition improved significantly. One week later, his platelet counts rose to 54 × 10⁹/L; then, a pars plana vitrectomy (PPV) was performed. Although the patient's blood culture turned negative with antibiotic treatment, recurred hypopyon and vitreous abscess could not be controlled even after receiving multiple IVAIs. With no choice, evisceration was performed 2 weeks after the PPV. The patient's blood culture, vitreous culture, and the culture of aspirated fluid for the liver abscess were all positive for *Klebsiella Pneumoniae*.

Case 2

A 63-year-old female with a 4-year history of diabetes was admitted to our hospital with blurred vision in the right eye with high fever for 10 days. She denied any other systemic
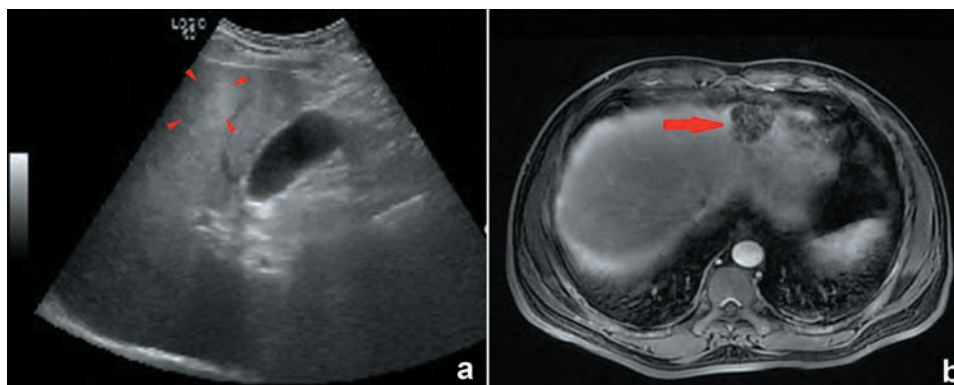
Figure 1. A: Abdominal B-scan ultrasonography showed non-uniform fatty liver (arrows head); b: An enhanced MRI demonstrated a round lesion in the liver and a liver abscess was highly suspected (arrow).

diseases or trauma. She was diagnosed with uveitis by her local clinic and received intravenous antibiotics and corticosteroid therapy. Her fever got better, but her VA decreased from 20/40 to counting finger (CF). On the first day of admission, her vision (VA) was HM. Ophthalmic examinations revealed moderate corneal edema, hypopyon, and vitreous opacity, which made the fundus hard to view. She was diagnosed with EE in the right eye, and empirical treatment with IVAI and systemic anti-infection were initiated. A PPV was performed on the third day, and the bacterial culture of the vitreous was positive for *Klebsiella Pneumoniae*. However, hypopyon recurred on the fifth postoperative day; then, a repeated IVAI was performed. The patient finally underwent evisceration on the tenth day after the surgery because of corneal perforation. While in the hospital, the patient's abdominal ultrasonographic examination revealed a liver cyst. Staphylococcus epidermidis was found in the blood but other primary lesions were not observed. On the fifth day after evisceration, the patient's condition worsened abruptly with mental confusion. She was immediately transferred to intensive care unit (ICU). The abdominal ultrasonography revealed hepatic abscesses. The cultures of blood and cerebrospinal fluid were found *Klebsiella Pneumoniae* positive. Unfortunately, she died of central nervous system infection, with septic shock and multiple organ dysfunction syndromes (MODS).

Case 3

A 61-year-old female was hospitalized for left eye pain and decreased vision for 5 days. She was diagnosed with panuveitis and secondary glaucoma by the local hospital. She had some cold-like symptoms briefly prior to her admission. On examination, her initial VA in the left eye was light perception (LP). The left eye had conjunctival injection, diffuse corneal edema, and hypopyon in the anterior chamber, but the fundus was not viewable. B-scan ultrasonography showed a hyperechoic mass in the posterior vitreous and sub-retinal space (Figure 2a). Orbit MRI showed intraocular exudates (Figure 2b). She was diagnosed with EE, and IVAI was performed. The patient had altered mental status on the second day. She was diagnosed with

sepsis with septic shock, and immediately transferred to the ICU. The patient's abdominal ultrasonographic examination revealed a heterogeneous echo with a clear boundary in liver (Figure 2c). Abdominal computed tomography (CT) scan revealed a large liver abscess (Figure 2d). A blood culture showed Gram-negative *klebsiella pneumoniae*. An ultrasound-guided liver aspiration was performed. After 2 weeks of antibiotic therapy, a PPV was performed under general anesthesia. However, the patient's scleral had melted (Figure 2e) and eventually she underwent an evisceration. Bacterial cultures of the discharged pus and vitreous were positive for *klebsiella pneumoniae* (Figure 2f).

Case 4

A 33-year-old male was transferred to our hospital with right eye pain and decreased eyesight for 3 days. One week earlier, he had symptoms of common cold with fatigue, but no fever. The local hospital diagnosed him with iritis. The patient had been diabetic for 3 years, with no history of surgery or trauma. On arrival, the vision in his right eye was LP. Ophthalmic examinations revealed a 1.5 mm hypopyon in the anterior chamber, and vitreous opacity, which blocked the view to the fundus. Ultrasonography revealed a hyperechoic mass in the vitreous and retinal detachment. A diagnosis of right eye EE was made and we performed IVAI and systemic antibiotics. On the third day of hospitalization, the patient developed high fever with chills, the laboratory test showed increased blood glucose of 31 mmol/L. Abdominal CT revealed low-density lesions in the right lobe of the liver with a clear margin, chest CT showed multiple round lesions in the right lung with bilateral pleural effusion. Infection was highly suspected. Considering that patient had liver abscess, sepsis, and hyperglycemic, we transferred him to the endocrine department for glucose control and systemic anti-infection treatment. Two weeks later, his general conditions improved but hypopyon and vitreous abscess worsened. His VA was LP. As the prognosis is poor even with PPV, the patient decided to have evisceration instead. The patient realized a poor prognosis was inevitable, and insisted on undergoing evisceration rather than PPV. Cultures of blood and vitreous humor were positive for *klebsiella pneumoniae*.
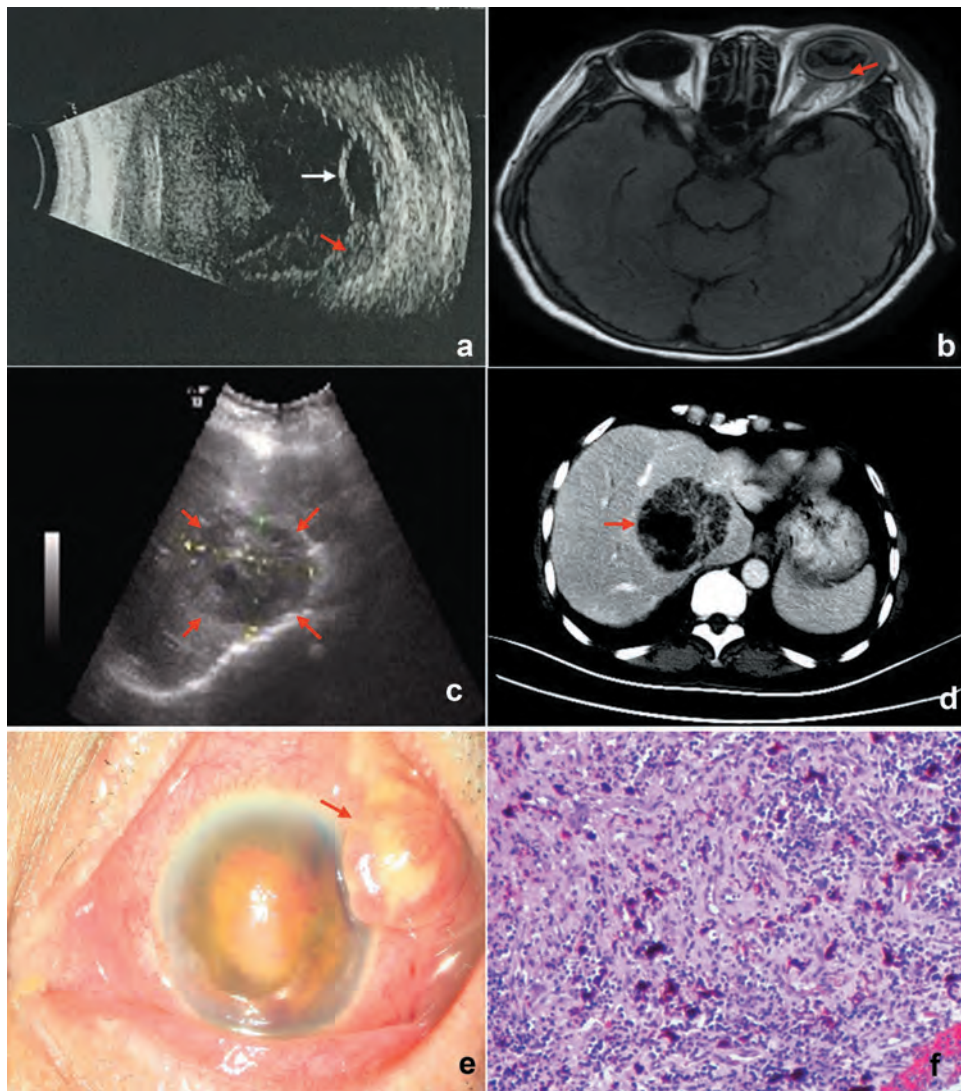
Figure 2. A: B-scan ultrasonogram showed extensive infiltrations in the vitreous cavity, retinal detachment (white arrow) and inferior unclear structure as presumed intraocular abscess (red arrow); b: Orbital MRI showed abnormal orbit tissue enhancement. Intraocular T1 weighted signal demonstrated intraocular exudates (red arrow); c: Abdominal B-scan ultrasonography showed heterogeneous echo graph (75 × 63 × 61 mm) with clear margin in the liver (red arrows), with no color doppler flow imaging signal; d: Arterial phase of the abdominal enhanced CT showed a large round lesion of the liver abscess (red arrow); e: Photo of panophthalmitis showed injected conjunctiva and chemosis. Anterior chamber filled with hemorrhagic hypopyon. The temporal swollen tissue was scleral abscess with perforation (red arrow); f: Post-operative intraocular tissues pathology, hematoxylin-eosin staining section noted the collection of acute inflammatory cells including neutrophils and lymphocytes, as well as necrosis combined with exudates. H&E × 200.

In summary, all patients had eye problems as the initial complaints and were diagnosed with EE with liver abscess as the primary lesion. The common underlining condition of these patients was diabetes. They all had symptoms of common cold in varying degrees like fever, chills, or fatigue at the onset. Confirming the initial diagnosis of EE was not hard but it was not straightforward to locate the primary lesion. None of the abdominal ultrasonography suggested liver abscesses. Abdominal enhanced CT and MRI were essential to establish the diagnosis. Hypoproteinemia presented in all patients. All patients had sepsis and two of them even suffered from complicated septic shock. Except for case 3, the other patients were referred to relevant department (ICU or endocrine department) for further treatment, so PPV was not performed promptly. Eventually, three patients underwent PPV including one patient, whose sclera had melted and she underwent evisceration instead of PPV. Unfortunately, the inflammation still could not be controlled in the rest of the two patients after PPV so they eventually underwent evisceration (Table 1).

Discussion

In East Asia, EE caused by *Klebsiella Pneumoniae* strains mostly develop from a primary liver abscess.[9] Comparing to other organisms, *Klebsiella Pneumoniae* is 100 times more likely to have metastatic spread.[10] Metastatic extrahepatic complications secondary to *Klebsiella Pneumoniae* liver abscess were termed as invasive liver abscess syndrome by Siu *et al.*[11] It could compromise lungs, central nerve system, resulting in pneumonia, meningitis, and endogenous endophthalmitis. Its high visual morbidity requires ophthalmologists to diagnose and treat EE urgently.

Most endogenous bacterial endophthalmitis occurs after the onset of systemic illness, but occasionally, it may develop

Table 1. Summary of the four cases.

Case	No. 1	No.2	No. 3	No. 4
Age (years)/Gender (M/F)/Eye (R/L)	51/M/L	63/F/R	61/F/L	33/M/R
Onset time (days)	3	10	5	3
Presenting vision	HM	FC/BE	LP	LP
Diagnosis at local clinic	Uveitis	Uveitis	Panuveitis; Secondary glaucoma	Iritis
Systemic symptoms	Fever; Chill	Fever	Influenza-like symptoms	Cold followed high fever
Abdominal ultrasonography	Non-uniform fatty liver; Pneumonia	Liver cyst	Heterogeneous echo (75*63*61 mm) with clear boundary near the caudate lobe of liver, no CDFI signal	Hyperechoic lesion with clear boundary in the right lobe of the liver
Abdominal CT/MRI	Low density lesion; Within the right lobe of the liver, likely; Representing hepatic abscesses	Non-performing	Abnormal signal; Probably liver abscess; Abdominal signal likely representing hepatic abscesses	Multiple lesions in which the maximum length is 61*52 mm and local abdominal effusion in the right lobe of the liver, considering an infectious process.
Systemic complications	Sepsis; Thrombocytopenia; Pneumonia	Septic shock; MODS; Intracranial infection	Septic shock ; Lung infection	Lung infection; Sepsis; Hyperglycemia
Interdisciplinary cooperation	Hematology	ICU	ICU	Internal, Endocrinology
IVAI after onset (days)	4	10	6	4
PPV	Yes	Yes	No	No
Time to perform PPV (days)	10	16	21 (Found scleral melting in exploration of the vitreous)	-
Outcome	Evisceration	Evisceration/Death	Evisceration	Evisceration

Abbreviations: CT, computed tomography; MRI, magnetic resonance imaging; HM, hand motion; IVAI, intravitreal antibiotic injection; ICU, intensive care unit; LP, light perception; MODS, multiple organ dysfunction syndrome; PPV, pars plana vitrectomy; M, male; F, female; R, right; L, left; FC, finger counting; BE, before eye; CDFI, color Doppler flow imaging.

in a month or more after the onset of sepsis.[12] In our cases, chief complaints were mostly eye problems rather than systemic issues. These patients were treated for several days at local clinics before referred to a comprehensive hospital. After thorough examinations, the original infection sites were confirmed as liver abscess. Even with our maximal efforts, all of them lost their eyesight. In one case, patient died of MODS. There are several issues we wish to discuss regarding the diagnosis and the management of these patients:

First, there was not enough evidence for systemic concerns and the patients were misdiagnosed at the initial presentation. As a rare condition, the underlining systemic conditions may be undiagnosed at presentation. Jackson *et al.* reported that 33% of 75 cases appeared to have (a) delayed diagnosis or (an) initial misdiagnosis.[13] Symptoms of EKPE in the early stage may be diverse and nonspecific. The presence of atypical systemic symptoms accompanying uveitis, such as fever and cold-like symptoms may raise a clinical suspicion for systemic involvement. A research of 124-eye cases on EKPE reported that fever was significantly associated with EKPE originating from liver abscess (*OR*, 3.5; 95% *CI*, 1.2–10.2; *P* = .015) compared with EKPE not originating from liver abscess.[14] However, in three of our four cases, treatment with antibiotics and steroids in the local clinics provided only transient relief, obscuring the underlying condition, thus misleading the treating ophthalmologists to focus their attention on the ocular symptoms mostly. The insidious onset of liver abscess in patients with EKPE may lead to diagnostic difficulties and treatment delays, which lead to a poor prognosis.[14] Thus, it is necessary for physicians, especially at the initial onset, to keep alert for all possible intraocular inflammatory conditions with minor systemic symptoms.

Secondly, the imaging results were not intuitive, which make it hard to find the source of infection at the early stage. EKPE originated from liver abscess needs diagnostic imaging of liver, such as B-ultrasonic, CT, or MRI, to exclude other original infection sites. Bacterial culture is the golden standard for the diagnosis, so the consistency between intraocular fluid culture and blood culture confirms this metastatic infection. However, this could be difficult as the appearance of liver abscesses on ultrasound and CT was not consistent.[15] For example, in case 1, at first, the abdominal CT showed a low-density lesion in the liver, whereas abdominal B-ultrasonic scan reported non-uniform fatty liver. It took us another 3 days to confirm the original infection site after the admission of patients. With the progression of the liver lesion, MRI and repeated B-scan eventually showed that it was a liver abscess. In case 2, with the alarmingly increased white blood cell count, the sepsis was soon confirmed, and blood culture found staphylococcus epidermidis. With the administration of broad-spectrum antibiotics, the repeated blood culture turned to negative. Although the PPV and silicone oil tamponade were performed, the patient finally underwent evisceration because of recurred hypopyon and corneal perforation. Due to the source of infection was not found, the treatments did not stop the deterioration of patient's condition. The symptoms, such as altered mental status, agitation, and confusion, indicated intracranial infection. Repeated abdominal ultrasonography confirmed liver abscess which

previously categorized as liver cyst. Therefore, in the seeking of the original infection site, we should be cautious about the imaging findings with ambiguous results. It is necessary to utilize adjunctive CT or MRI. Also, we should be aware that EE could not be excluded by a negative result of blood culture. According to report, the ratio of positive blood culture is 72% in EE cases, and there are 20% to 30% of EE presenting a negative intraocular fluid culture.[16]

Thirdly, the management for multiple systemic illnesses and the antibacterial therapy was delayed. The delayed diagnosis and insufficient use of antibiotics could relate to the uncontrolled infection. In these patients, three had diabetes mellitus (DM), with HbA1 c level indicating poor control. All four patients had hypoalbuminemia, and all developed sepsis and two had septic shock. Diabetes is a significant risk factor for EE, as the ratio of EKPE caused by liver abscess in DM patients was 3.6 to 11.0 folds of those without DM.[17] Therefore, interdisciplinary cooperation is necessary for solving the problems with abscess aspiration, antibiotic selection, glucose control, and nutrition support. As a severe infection, EE may need multiple therapeutic agents to cover a wide spectrum of pathogens, especially when waiting for the drug sensitivity testing reports. In our cases, three patients were treated with intravenous antibiotics for several days; one patient received topical antibiotic eyedrops at local clinics. With abscess aspiration and organism-sensitive antibiotics, three of them finally overcame this life-threatening condition.

Fourthly, intravitreal injection and vitrectomy intervention were delayed. A study shows that *Klebsiella pneumoniae* and its lipopolysaccharide exert a strong pro-inflammatory effect on retinal epithelial cells.[18] In the animal model of experimental Klebsiella-induced endophthalmitis, retinal photoreceptors could be permanently damaged in 48 hours after infection.[19] Early intravitreal antibiotics could cross the blood-eye barrier, giving an intraocular concentration higher than those through intravenous route. Therefore, it is the most direct and rapid way to give antibiotic treatments. PPV can do both diagnosis and treatment, but the timing of PPV is not clearly defined. Even though there are still controversies about the visual outcome after PPV for EKPE, the chance of enucleation decreases indeed. According to a Korean research by Yoon *et al.*,[20] 10 eyes of seven consecutive EKPE patients had their retina attached in all eyes (100%) after 6 months of PPV, and vision was CF or better in five eyes (50%). They suggested that early vitrectomy for EKPE could improve the noteworthy outcomes. In principle, when an EKPE was diagnosed, PPV should be performed as soon as possible. However, it is necessary to consider whether patients could endure such a surgery with poor systemic conditions. For those who are intolerable or inaccessible to PPV, the intravitreal injection would be the first choice. In case 1, the patient had an extremely low level of platelet count which increased the bleeding risk of surgery; in case 2 and 3, septic shock, lung infection threatened patients' lives and both of them had to be moved to ICU for a life-supporting treatment; in case 4, the patient had a hyperglycemic crisis. All of these were obstacles to a PPV, which inevitably led to destructive enucleation or evisceration.

Conclusion

When the patients with EE come to an eye clinic, detecting the primary lesion is particularly important. Though un-liquefied lesions may not be detected by ultrasonography in the early stage of liver abscess, we should not give up but utilize alternative examinations such as abdominal CT or MRI. An identical pathogenic microorganism cultured from blood, vitreous, or aqueous humor may confirm the diagnosis, but it cannot be excluded by a negative result. After the early diagnosis of EKPE, PPV should be performed as soon as possible. Both the ophthalmologists and the hepatobiliary surgeons should co-manage this disease. Prompt diagnosis and treatment can help to preserve the patients' globe and residual vision, as delayed treatment may lead to panophthalmitis, even death.

Declaration of Interest

Fang Chen has no financial/conflicting interests to disclose.
Zhenggao Xie has no financial/conflicting interests to disclose.

Funding

References

1. Puliafito CA, Baker AS, Haaf J, Foster CS. Infectious endophthalmitis. Review of 36 cases. *Ophthalmology*. 1982;89:921–929. doi:10.1016/S0161-6420(82)34704-1. PMID:6982445.

2. Jackson TL, Eykyn SJ, Graham EM, Stanford MR. Endogenous bacterial endophthalmitis: a 17-year prospective series and review of 267 reported cases. *Surv Ophthalmol*. 2003;48:403–423. doi:10.1016/s0039-6257(03)00054-7. PMID:12850229.

3. Connell PP, O'Neill EC, Fabinyi D, et al. Endogenous endophthalmitis: 10-year experience at a tertiary referral centre. *Eye (Lond)*. 2011;25:66–72. doi:10.1038/eye.2010.145. PMID:20966972.

4. Okada AA, Johnson RP, Liles WC, D'Amico DJ, Baker AS. Endogenous bacterial endophthalmitis. Report of a ten-year retrospective study. *Ophthalmology*. 1994;101:832–838. doi:10.1016/S0161-6420(13)31255-X. PMID:8190467.

5. Jackson TL, Paraskevopoulos T, Georgalas I. Systematic review of 342 cases of endogenous bacterial endophthalmitis. *Surv Ophthalmol*. 2014;59:627–635. doi:10.1016/j.survophthal.2014.06.002. PMID:25113611.

6. Yang CS, Tsai HY, Sung CS, Lin KH, Lee FL, Hsu WM. Endogenous Klebsiella endophthalmitis associated with pyogenic liver abscess. *Ophthalmology*. 2007;114:876–880. doi:10.1016/j.ophtha.2006.12.035. PMID: 17467526.

7. Wang F, Tao Y, Sun B, Tong ZH. Endogenous Klebsiella pneumoniae endophthalmitis associated with Klebsiella pneumoniae pneumonia: 3 cases report and literature review. *Zhonghua Jie He He Hu Xi Za Zhi*. 2019;42:438–443. Chinese. doi:10.3760/cma.j..1001-0939.2019.06.007. PMID: 31189230.

8. Fujita M, Takahashi A, Imaizumi H, et al. Endogenous endophthalmitis associated with pyogenic liver abscess caused by Klebsiella pneumoniae. *Intern Med*. 2019;58:2507–2514. doi:10.2169/internalmedicine.2684-19. PMID: 31118392.

9. Chung CY, Wong ES, Liu CCH, Wong MOM, Li KKW. Clinical features and prognostic factors of Klebsiella endophthalmitis—10-year experience in an endemic region. *Eye (Lond)*. 2017;31:1569–1575. doi:10.1038/eye.2017.92. PMID:28622312.

10. Kashani AH, Eliott D. The emergence of Klebsiella pneumoniae endogenous endophthalmitis in the USA: basic and clinical advances. *J Ophthalmic Inflamm Infect*. 2013; (3). 28. doi:10.1186/1869-5760-3-28. PMID:23514342.

11. Siu K, Yeh KM, Lin JC, Fung CP, Chang FY. Klebsiella pneumoniae liver abscess: a new invasive syndrome. *Lancet Infect Dis*. 2012;12:881–887. PMID:23514342.

12. Wong JS, Chan TK, Lee HM, Chee SP. Endogenous bacterial endophthalmitis. An East Asian experience and a reappraisal of a severe ocular affliction. *Ophthalmology*. 2000;107:1483–1491. doi:10.1016/s0161-6420(00)00216-5. PMID:10919895.

13. Jackson TL, Paraskevopoulos T, Georgalas I. Systematic. Review of 342 cases of endogenous bacterial endophthalmitis. *Surv Ophthalmol*. 2014;59:627–635. doi:10.1016/j.survophthal.2014.06.002. PMID:25113611.

14. Li YH, Chen YH, Chen KJ, et al. Infectious sources, prognostic factors, and visual outcomes of endogenous Klebsiella pneumoniae endophthalmitis. *Ophthalmol Retina*. 2018;2:771–778. doi:10.1016/j.oret.2017.11.013. PMID:31047528.

15. Bächler P, Baladron MJ, Menias C, et al. Multimodality imaging of liver infections: differential diagnosis and potential pitfalls. *Radiographics*. 2016;36:1001–1023. doi:10.1148/rg.2016150196. PMID:27232504.

16. Ma WJ, Zhang H, Zhao SZ. Laboratory diagnosis of infectious endophthalmitis. *Int J Ophthalmol*. 2011;4:100–102. doi:10.3980/j..2222-3959.2011.01.23. PMID: 22553620.

17. Sheu SJ, Kung YH, Wu TT, Chang FP, Horng YH. Risk factors for endogenous endophthalmitis secondary to klebsiella pneumoniae liver abscess: 20-year experience in Southern Taiwan. *Retina*. 2011;31:2026–2031. doi:10.1097/IAE.0b013e31820d3f9e. PMID:21499189.

18. Pollreisz A, Rafferty B, Kozarov E, Lalla E. Klebsiella pneumoniae induces an inflammatory response in human retinal-pigmented epithelial cells. *Biochem Biophys Res Commun*. 2012;418:33–37. doi:10.1016/j.bbrc.2011.12.102. PMID:22226964.

19. Meyers-Elliot RH, Dethlefs BA. Experimental Klebsiella-induced endophthalmitis in the rabbit. *Arch Ophthalmol*. 1982;100:1959–1963. doi:10.1001/archopht.1982.01030040939015. PMID:6983340.

20. Yoon YH, Lee SU, Sohn JH, Lee SE. Result of early vitrectomy for endogenous Klebsiella pneumoniae endophthalmitis. *Retina*. 2003;23:366–370. doi:10.1097/000c06982-200306000-00013. PMID: 12824838.

第 41 期	研究者番号： G4104			作成日 ： 2021 年 3 月　日	
氏　名	孟　雪	MENG　XUE	性別	F	生年月日 1986.08.23

所属機関（役職）	中国医大附属盛京医院口腔科（主治医師）
研究先（指導教官）	順天堂大学大学院医学研究科　耳鼻咽喉科学（池田　勝久教授）
研究テーマ	次世代シークエンサーを用いた頭頸部癌の特異的癌遺伝子の創出 Detection of cancer-specific genes of head and neck carcinoma using next generation sequencer

専攻種別	☑論文博士	☐課程博士

研究者評価（指導教官記入欄）

成績状況	優	取得単位数 取得単位数／取得すべき単位総数
学生本人が行った研究の概要	202 例の頭頸部扁平上皮癌症例に対して Tissue micro array を用いて bullous pemphigoid antigen II（BP180）遺伝子のタンパク発現を免疫組織化学染色（IHC）で検証した。また、その発現状況を Kaplan-Meier 法と Cox 回帰分析を用いて臨床情報との予後解析を行った。本研究を Anticancer research に投稿しアクセプトされた。現在 in press である	
総合評価	【良かった点】 現在のところまで勤勉に研究・実験にとりくんでいる。 指導教官への報告も漏れなく定期的に行っている。 研究成果をまとめ論文投稿しアクセプトすることができた	
	【改善すべき点】 現在のところ大きな問題なし	
	【今後の展望】 今後は順天堂大学への学位審査を受ける予定である	
学位取得見込	本年度中に取得できる見込みである	

評価者（指導教官名）　　松本文彦　　㊞

日中笹川医学奨学金制度(学位取得コース)報告書
研究者用

Supported by
日本財団
THE NIPPON
FOUNDATION

第41期　　　　研究者番号： G4104　　　　作成日：2021年2月16日

氏名	Meng Xue	孟 雪	性別	F	生年月日 1986. 08. 23
所属機関(役職)	中国医大附属盛京医院口腔科(主治医師)				
研究先(指導教官)	順天堂大学大学院医学研究科　耳鼻咽喉科学(池田 勝久教授)				
研究テーマ	次世代シークエンサーを用いた頭頚部癌の特異的癌遺伝子の創出 Detection of cancer-specific genes of head and neck carcinoma using next generation sequencer				
専攻種別	論文博士		☑	課程博士	☐

1．研究概要(1)

1)目的(Goal)

Head and neck squamous cell carcinoma (HNSCC) is the most lethal malignant head and neck cancer. Prognosis plays a vital role in patient management and decision-making. Bullous pemphigoid antigen II (BP180; also called collagen XVII, BPA-2 or BPAg2) is not only an epithelial transmembrane protein, but also a hemidesmosome transmembrane adhesion molecule, and likely participates in keratinocyte-matrix interactions in both physiological and pathological conditions. Although many cancers are reportedly associated with BP180, clinical prognostic relationships have not yet been described. The identification of prognostic factor BP180 was required in HNSCC.

2)戦略(Approach)

TMA construction. TMAs were prepared from formalin-fixed, paraffin-embedded pathological blocks as previously described. The blocks were sectioned at a thickness of 4 μM and subjected to immunohistochemical analyses.
Immunohistochemistry (IHC). Serial 4-μM-thick sections were incubated with the mouse monoclonal anti-human BP180 antibody established by our laboratory (collagen XVII) (1:1000, NCC-Lu-226 (immunoglobulin (Ig) G1, K), National Cancer Center Research Institute, Tokyo, Japan) using the Ventana DABMap detection kit and automated slide stainer (Discovery XT) (Ventana Medical Systems, Tucson, AZ, USA). Head and neck normal tissues stained positively for BP180 antibody were recognized as controls. Expression levels of BP180 protein were used to classify two groups. The first was a BP180-negative group in which no tumor cells were stained with BP180 antibody, tumor cells were stained at weaker intensity compared with normal tissue staining, or some tumor cells were more intense compared with normal tissue staining, but comprised less than 10% of the tumor cell area. The other was a BP180-positive group, comprised all other findings. Staining patterns were evaluated by two independent investigators blinded to clinical information.

3)材料と方法(Materials and methods)

Protein expression of bullous pemphigoid antigen II (BP180) was verified by immunohistochemistry (IHC) in a tissue microarray study of 202 cases. Prognostic significance was analyzed with Kaplan-Meier methods and Cox regression analyses IHC analysis were used. This study investigated 202 tumor specimens from 202 patients who underwent surgical resection with curative intention for head and neck carcinoma at the National Cancer Center Hospital (Tokyo, Japan) between 2006 and 2016. Clinicopathological records were retrospectively reviewed. In this cohort, median follow-up of the 202 patients was 34 months (range=2-74 months). Formalin-fixed paraffin-embedded tissue specimens of the 202 HNSCCs were collected according to the World Health Organization classification (4th edition) of HNSCC. All study protocols were approved by the ethics committee of the National Cancer Center (approval #2013-247).

4)実験結果(Results)

Kaplan-Meier methods and Cox regression analyses IHC analysis revealed that protein expression of BP180 among HNSCC patients differed significantly in the presence and absence of neural invasion, and according to T status in laryngeal and pharyngeal cancer subgroups (P<0.05). In overall survival analysis and multivariate analysis, we found that positive BP180 IHC and advanced clinical stage were significant independent positive predictors of mortality in HNSCC patients (P<0.05). In addition, in the oral squamous cell carcinoma subgroup, independent positive predictors were positive BP180 IHC, advanced N status and neural invasion. In patients with laryngeal or pharyngeal cancer, predictors were positive BP180 IHC and advanced clinical stage (P<0.05). In the present cohort, the mean 5-year survival rate for BP180-positive patients (42.8±7.7%) was lower than that for negative patients (69.0±7.3%). Compared with different subgroups, oral cancer patients showed a slightly higher survival rate (57.5±6.8%) than laryngeal and pharyngeal cancer patients (52.1±6.7%).

5)考察(Discussion)

In this retrospective study, BP180 (collagen XVII) was identified as a novel biomarker for predicting the prognosis of HNSCC, OSCC and laryngeal and pharyngeal cancer. To the best of our knowledge, this is the first study to investigate BP180 as an effective prognostic factor for HNSCC.
　　BP180 was identified as a prognostic factor in HNSCC, and BP180 expression was also closely associated with OS in HNSCC patients (p=0.0005), OSCC patients (p=0.006) and laryngeal and pharyngeal cancer patients (p=0.024). In particular, positive associations with OS were observed for the clinical late stage (III+IV) of these pathologies.

1. 研究概要（2）

Our findings show that BP180 is strongly predictive of tumor malignancy in HNSCC. DFS was also analyzed in our study, showing significant differences in the status of BP180 IHC in HNSCC and OSCC, but not in laryngeal and pharyngeal cancer. A key finding was that analysis of OS in laryngeal and pharyngeal cancer revealed a significant difference in the status of BP180 IHC. The possible reason is that there are many relapsed hypopharyngeal cancer patients due to alcohol.

The immunohistochemical staining of BP180 in cancers is typical. Immunohistochemically, using a mouse monoclonal anti-human BP180 antibody linear staining along the basement membrane and faint cytoplasmic staining in the basal layer of squamous epithelium in limited normal tissues was revealed. BP180 was distributed irregularly or scattered only in layers of the epithelium. Parikka et al. found similar results in a study of the transformation of oral epithelium to dysplasia and carcinoma, identifying intense staining in carcinoma cells at the invasive front in Grade II OSCC, with signals mainly missing from basal cells and strong signals restricted to the epithelium in cases of dysplasia. In our study, the same immune reaction was evident in normal tissues and squamous cell carcinomas. Some studies have proposed that BP180 serves as a cell-matrix adhesion molecule by stabilizing the hemidesmosome complex and mediating anchorage to the underlying basement membranes. Beyond any structural roles, BP180 is presumed to play a role in cell migration and differentiation to pathological states in malignant tumors.

Head and neck cancer is a wide disease classification that includes oral, salivary gland, thyroid, nasopharyngeal, laryngeal, oropharyngeal and hypopharyngeal cancers. In addition, oral cancers can arise from squamous epithelium of the tongue, gingiva, palate, buccal mucosa, and mouth floor. The present report offers a first demonstration of the expression profile of BP180 in different primary sites. BP180 positivity rates were 57.1–83.3%, with no marked differences apparent between primary sites of HNSCC (p=0.643, Fisher's exact test), but a tendency toward higher expression was noted in the current OSCC cohort (p=0.084, Fisher's exact test). We were surprised to observe that comparing OSCC with laryngeal and pharyngeal cancer, BP180 positivity was 74.5% for OSCC and 50.5% for laryngeal and pharyngeal cancer (p=0.001, Pearson's chi-square test). We hypothesize that BP180 expression in HNSCC correlates with anatomical localization. In a TMA of 124 HNSCCs, BP180 expression was found to be higher in the oral cavity (85.7%) than in other anatomical localizations. We found differences in BP180 positivity in some anatomical areas as novel data, and attributed this to differences in mucosal structure and function. The mucous membrane in the oral cavity is mostly used for maintaining an environment suitable for chewing and ingesting food, whereas the mucous membranes of the pharynx and larynx play important roles in immune function and vocalization. These results provide a clinical basis for future research into the pathological mechanisms of and drug-targeted therapies for HNSCC.

Based on the current research, a possible tumorigenesis mechanism is that the structural extracellular domain (ECD) of BP180 connects cytoplasmic structural components with the extracellular matrix (ECM). The ECD is essential for proper basement membrane formation. In the absence of normal regulation, changes in the ECM may contribute to the first steps toward cancer. Recent data have demonstrated that alterations in BP180 exert profound effects on cancer tumorigenesis, progression, invasion and migration in different kinds of cancers, as mentioned above. Our findings provide clinical data in support of this notion that BP180 is a factor associated with poor prognosis. However, several potential limitations must be considered. First, the sample size was quite limited and data from more cases is needed. In addition, the molecular mechanisms underlying the effects of BP180 on HNSCC need to be clarified. At last, we didn't have an in-depth analysis of surgical related factors.

In conclusion, the present study suggests that BP180 is a prognostic factor for HNSCC. Moreover, multivariate analysis suggested BP180 as a significant independent prognostic factor along with clinical stage in patients with HNSCC. Overall, the prognostic value of BP180 expression in this study provides an important experimental foundation for closer examination of this potentially significant biomarker in targeted treatments for patients with HNSCC.

6）参考文献（References）
1 Bray F, Ferlay J, Soerjomataram I, Siegel RL, Torre LA and Jemal A: Global cancer statistics 2018: Globocan estimates of incidence and mortality worldwide for 36 cancers in 185 countries. CA Cancer J Clin 68(6): 394-424, 2018. PMID: 30207593. DOI: 10.3322/caac.21492
2 Pfister DG, Spencer S, Brizel DM, Burtness B, Busse PM, Caudell JJ, Cmelak AJ, Colevas AD, Dunphy F, Eisele DW, Gilbert J, Gillison ML, Haddad RI, Haughey BH, Hicks WL, Jr., Hitchcock YJ, Jimeno A, Kies MS, Lydiatt WM, Maghami E, Martins R, McCaffrey T, Mell LK, Mittal BB, Pinto HA, Ridge JA, Rodriguez CP, Samant S, Schuller DE, Shah JP, Weber RS, Wolf GT, Worden F, Yom SS, McMillian NR and Hughes M: Head and neck cancers, version 2.2014. Clinical practice guidelines in oncology. J Natl Compr Canc Netw 12(10): 1454-1487, 2014. PMID: 25313184. DOI: 10.6004/jnccn.2014.0142
3 Chow LQM: Head and neck cancer. N Engl J Med 382(1): 60-72, 2020. PMID: 31893516. DOI: 10.1056/NEJMra1715715
4 Braakhuis BJ, Brakenhoff RH and Leemans CR: Treatment choice for locally advanced head and neck cancers on the basis of risk factors: Biological risk factors. Ann Oncol 23: x173-177, 2012. PMID:22987957. DOI: 10.1093/annonc/mds299
5 Parikka M, Kainulainen T, Tasanen K, Bruckner-Tuderman L and Salo T: Altered expression of collagen XVII in ameloblastomas and basal cell carcinomas. J Oral Pathol Med 30(10): 589-595, 2001. PMID: 11722708. DOI: 10.1034/j.1600-0714.2001.301003.x
6 Hammers CM and Stanley JR: Mechanisms of disease: Pemphigus and bullous pemphigoid. Annu Rev Pathol 11: 175-197, 2016. PMID: 26907530. DOI: 10.1146/annurev-pathol-012615-044313
7 Jones VA, Patel PM, Gibson FT, Cordova A and Amber KT: The role of collagen XVII in cancer: Squamous cell carcinoma and beyond. Front Oncol 10: 352, 2020. PMID: 32266137. DOI: 10.3389/fonc.2020.00352
8 Walko G, Castañón MJ and Wiche G: Molecular architecture and function of the hemidesmosome. Cell Tissue Res 360(3): 529-544, 2015. PMID: 26017636. DOI: 10.1007/s00441-015-2216-69 De Pascalis C and Etienne-Manneville S: Single and collective cell migration: The mechanics of adhesions. Mol Biol Cell 28(14): 1833-1846, 2017. PMID: 28684609. DOI: 10.1091/mbc.E17-03-01349
9 De Pascalis C and Etienne-Manneville S: Single and collective cell migration: The mechanics of adhesions. Mol Biol Cell 28(14): 1833-1846, 2017. PMID: 28684609. DOI: 10.1091/mbc.E17-03-0134
10 Walker C, Mojares E and Del Río Hernández A: Role of extracellular matrix in development and cancer progression. Int J Mol Sci 19(10): 3028, 2018. PMID: 30287763. DOI: 10.3390/ijms19103028
11-42 please see the details in the published paper.

1．研究概要（3）

11 Moilanen JM, Löffek S, Kokkonen N, Salo S, Väyrynen JP, Hurskainen T, Manninen A, Riihilä P, Heljasvaara R, Franzke CW, Kähäri VM, Salo T, Mäkinen MJ and Tasanen K: Significant role of collagen XVII and integrin β4 in migration and invasion of the less aggressive squamous cell carcinoma cells. Sci Rep 7: 45057, 2017. PMID: 28327550. DOI: 10.1038/srep45057

12 Stelkovics E, Korom I, Marczinovits I, Molnar J, Rasky K, Raso E, Ficsor L, Molnar B, Kopper L and Krenacs T: Collagen XVII/BP180 protein expression in squamous cell carcinoma of the skin detected with novel monoclonal antibodies in archived tissues using tissue microarrays and digital microscopy. Appl Immunohistochem Mol Morphol 16(5): 433–441, 2008. PMID: 18633319. DOI: 10.1097/PAI.0b013e318162f8aa

13 Yamada T, Endo R, Tsukagoshi K, Fujita S, Honda K, Kinoshita M, Hasebe T and Hirohashi S: Aberrant expression of a hemidesmosomal protein, bullous pemphigoid antigen 2, in human squamous cell carcinoma. Lab Invest 75(4): 589–600, 1996. PMID: 8874389

14 Parikka M, Kainulainen T, Tasanen K, Väänänen A, Bruckner-Tuderman L and Salo T: Alterations of collagen XVII expression during transformation of oral epithelium to dysplasia and carcinoma. J Histochem Cytochem 51(7): 921–929, 2003. PMID: 12810842. DOI: 10.1177/002215540305100707

15 Löffek S, Hurskainen T, Jackow J, Sigloch FC, Schilling O, Tasanen K, Bruckner-Tuderman L and Franzke CW: Transmembrane collagen XVII modulates integrin dependent keratinocyte migration via PI3K/RAC1 signaling. PLoS One 9(2): e87263, 2014. PMID: 24505282. DOI: 10.1371/journal.pone.0087263

16 Moilanen JM, Kokkonen N, Löffek S, Väyrynen JP, Syväniemi E, Hurskainen T, Mäkinen M, Klintrup K, Mäkelä J, Sormunen R, Bruckner-Tuderman L, Autio-Harmainen H and Tasanen K: Collagen XVII expression correlates with the invasion and metastasis of colorectal cancer. Hum Pathol 46(3): 434–442, 2015. PMID: 25623077. DOI: 10.1016/j.humpath.2014.11.020

17 Liu CC, Lin SP, Hsu HS, Yang SH, Lin CH, Yang MH, Hung MC and Hung SC: Suspension survival mediated by pp2a-stat3-col XVII determines tumour initiation and metastasis in cancer stem cells. Nat Commun 7: 11798, 2016. PMID: 27306323. DOI: 10.1038/ncomms11798

18 Hsu HS, Liu CC, Lin JH, Hsu TW, Hsu JW, Li AF and Hung SC: Involvement of collagen XVII in pluripotency gene expression and metabolic reprogramming of lung cancer stem cells. J Biomed Sci 27(1): 5, 2020. PMID: 31928533. DOI: 10.1186/s12929-019-0593-y

19 Liu CC, Lin JH, Hsu TW, Hsu JW, Chang JW, Su K, Hsu HS and Hung SC: Collagen XVII/Laminin-5 activates epithelial-to-mesenchymal transition and is associated with poor prognosis in lung cancer. Oncotarget 9(2): 1656–1672, 2018. PMID: 29416721. DOI: 10.18632/oncotarget.11208

20 Otsubo K, Goto H, Nishio M, Kawamura K, Yanagi S, Nishie W, Sasaki T, Maehama T, Nishina H, Mimori K, Nakano T, Shimizu H, Mak TW, Nakao K, Nakanishi Y and Suzuki A: MOB1-YAP1/TAZ-NKX2.1 axis controls bronchioalveolar cell differentiation, adhesion and tumour formation. Oncogene 36(29): 4201–4211, 2017. PMID: 28346423. DOI: 10.1038/onc.2017.58

21 Thangavelu PU, Krenács T, Dray E and Duijf PH: In epithelial cancers, aberrant COL17A1 promoter methylation predicts its misexpression and increased invasion. Clin Epigenetics 8: 120, 2016. PMID: 27891193. DOI: 10.1186/s13148-016-0290-6

22 Krenacs T, Kiszner G, Stelkovics E, Balla P, Teleki I, Nemeth I, Varga E, Korom I, Barbai T, Plotar V, Timar J and Raso E: Collagen XVII is expressed in malignant but not in benign melanocytic tumors and it can mediate antibody induced melanoma apoptosis. Histochem Cell Biol 138(4): 653–667, 2012. PMID: 22688676. DOI: 10.1007/s00418-012-0981-9

23 Bergstraesser LM, Srinivasan G, Jones JC, Stahl S and Weitzman SA: Expression of hemidesmosomes and component proteins is lost by invasive breast cancer cells. Am J Pathol 147(6): 1823–1839, 1995. PMID: 7495306.

24 Lo AK, Yuen PW, Liu Y, Wang XH, Cheung AL, Wong YC and Tsao SW: Downregulation of hemidesmosomal proteins in nasopharyngeal carcinoma cells. Cancer Lett 163(1): 117–123, 2001. PMID: 11163115. DOI: 10.1016/s0304-3835(00)00683-2

25 Kim SH, Carey TE, Liebert M, Yoo SJ, Kwon HJ and Kim SY: Characterization of AMC-HN-9, a cell line established from an undifferentiated carcinoma of the parotid gland: Expression of alpha6beta4 with the absence of BP180 and 230. Acta Otolaryngol 120(5): 660–666, 2000. PMID: 11039880. DOI: 10.1080/000164800750000513

26 Aho S and Uitto J: 180-kd bullous pemphigoid antigen/type XVII collagen: Tissue-specific expression and molecular interactions with keratin 18. J Cell Biochem 72(3): 356–367, 1999. PMID: 10022517. DOI: 10.1002/(sici)1097-4644(19990301)72:3<356::aid-jcb5>3.0.co;2-m

27 El-Naggar AK, Chan JKCC, Grandis JR, Takata T and Slootweg PJ: WHO classification of head and neck tumours, 4th Edition, 2017.

28 Ohtomo R, Mori T, Shibata S, Tsuta K, Maeshima AM, Akazawa C, Watabe Y, Honda K, Yamada T, Yoshimoto S, Asai M, Okano H, Kanai Y and Tsuda H: SOX10 is a novel marker of acinus and intercalated duct differentiation in salivary gland tumors: A clue to the histogenesis for tumor diagnosis. Mod Pathol 26(8): 1041–1050, 2013. PMID: 23558573. DOI: 10.1038/modpathol.2013.54

29 Watabe Y, Mori T, Yoshimoto S, Nomura T, Shibahara T, Yamada T and Honda K: Copy number increase of ACTN4 is a prognostic indicator in salivary gland carcinoma. Cancer Med 3(3): 613–622, 2014. PMID: 24574362. DOI: 10.1002/cam4.214

30 Watanabe T, Ueno H, Watabe Y, Hiraoka N, Morizane C, Itami J, Okusaka T, Miura N, Kakizaki T, Kakuya T, Kamita M, Tsuchida A, Nagakawa Y, Wilber H, Yamada T and Honda K: ACTN4 copy number increase as a predictive biomarker for chemoradiotherapy of locally advanced pancreatic cancer. Br J Cancer 112(4): 704–713, 2015. PMID: 25602965. DOI: 10.1038/bjc.2014.623

31 Liu Y, Li L and Xia Y: BP180 is critical in the autoimmunity of bullous pemphigoid. Front Immunol 8: 1752, 2017. PMID: 29276517. DOI: 10.3389/fimmu.2017.01752

32 Monshi B, Gulz L, Piringer B, Wiala A, Kivaranovic D, Schmidt M, Sesti A, Heil T, Vujic I, Posch C and Rappersberger K: Anti-BP180 autoantibody levels at diagnosis correlate with 1-year mortality rates in patients with bullous pemphigoid. J Eur Acad Dermatol Venereol 34(7): 1583–1589, 2020. PMID: 32170780. DOI: 10.1111/jdv.16363

33 Zhou XP, Liu B, Xu Q, Yang Y, He CX, Zuo YG and Liu YH: Serum levels of immunoglobulins G1 and G4 targeting the non-collagenous 16A domain of BP180 reflect bullous pemphigoid activity and predict bad prognosis. J Dermatol 43(2): 141–148, 2016. PMID: 26300465. DOI: 10.1111/1346-8138.13051

34 Bourdon-Lanoy E, Roujeau JC, Joly P, Guillaume JC, Bernard P, Prost C, Tancrède-Bohin E, Delaporte E, Picard-Dahan C, Albes B, Bedane C, Doutre MS, Chosidow O, Lok C, Pauwels C, Chevrand-Breton J, Sassolas B and Richard MA: Bullous pemphigoid in young patients: A retrospective study of 74 cases. Ann Dermatol Venereol 132(2): 115–122, 2005. PMID: 15798559. DOI: 10.1016/s0151-9638(05)79220-6

1．研究概要（4）

35 Bernard P, Reguiai Z, Tancrède-Bohin E, Cordel N, Plantin P, Pauwels C, Vaillant L, Grange F, Richard-Lallemand MA, Sassolas B, Roujeau JC, Lok C, Picard-Dahan C, Chosidow O, Vitry F and Joly P: Risk factors for relapse in patients with bullous pemphigoid in clinical remission: A multicenter, prospective, cohort study. Arch Dermatol 145(5): 537-542, 2009. PMID: 19451497. DOI: 10.1001/archdermatol.2009.53

36 Powell AM, Sakuma-Oyama Y, Oyama N and Black MM: Collagen XVII/BP180: A collagenous transmembrane protein and component of the dermoepidermal anchoring complex. Clin Exp Dermatol 30(6): 682-687, 2005. PMID: 16197389. DOI: 10.1111/j.1365-2230.2005.01937.x

37 Tanimura S, Tadokoro Y, Inomata K, Binh NT, Nishie W, Yamazaki S, Nakauchi H, Tanaka Y, McMillan JR, Sawamura D, Yancey K, Shimizu H and Nishimura EK: Hair follicle stem cells provide a functional niche for melanocyte stem cells. Cell Stem Cell 8(2): 177-187, 2011. PMID: 29033351. DOI: 10.1016/j.stem.2010.11.029

38 Laval S, Laklai H, Fanjul M, Pucelle M, Laurell H, Billon-Galés A, Le Guellec S, Delisle MB, Sonnenberg A, Susini C, Pyronnet S and Bousquet C: Dual roles of hemidesmosomal proteins in the pancreatic epithelium: The phosphoinositide 3-kinase decides. Oncogene 33(15): 1934-1944, 2014. PMID: 23624916. DOI: 10.1038/onc.2013.146

39 Tamás L, Szentkúti G, Eros M, Dános K, Brauswetter D, Szende B, Zsákovics I and Krenács T: Differential biomarker expression in head and neck cancer correlates with anatomical localization. Pathol Oncol Res 17(3): 721-727, 2011. PMID: 21487776. DOI: 10.1007/s12253-011-9376-9

40 Nishie W, Kiritsi D, Nyström A, Hofmann SC and Bruckner-Tuderman L: Dynamic interactions of epidermal collagen XVII with the extracellular matrix: Laminin 332 as a major binding partner. Am J Pathol 179(2): 829-837, 2011. PMID: 21801871. DOI: 10.1016/j.ajpath.2011.04.019

41 Franzke CW, Tasanen K, Schäcke H, Zhou Z, Tryggvason K, Mauch C, Zigrino P, Sunnarborg S, Lee DC, Fahrenholz F and Bruckner-Tuderman L: Transmembrane collagen XVII, an epithelial adhesion protein, is shed from the cell surface by ADAMs. Embo J 21(19): 5026-5035, 2002. PMID: 12356719. DOI: 10.1093/emboj/cdf532

42 Nishimura M, Nishie W, Shirafuji Y, Shinkuma S, Natsuga K, Nakamura H, Sawamura D, Iwatsuki K and Shimizu H: Extracellular cleavage of collagen XVII is essential for correct cutaneous basement membrane formation. Hum Mol Genet 25(2): 328-339, 2016. PMID: 26604146. DOI: 10.1093/hmg/ddv478

2. 執筆論文　Publication of thesis　※記載した論文を添付してください。Attach all of the papers listed below.

論文名 1 Title	Mandibular Malignant Fibrous Histiocytoma:a Case Report					
掲載誌名 Published journal	Journal of China Medical University					
	2019 年 9 月	48(9) 巻（号）	859 頁 ～ 861 頁	言語 Language	Chinese	
第1著者名 First author	Ye Li	第2著者名 Second author	Haiyang Yu	第3著者名 Third author	Qiuxu Wang	
その他著者名 Other authors	Weixian Liu, Corresponding author: Xue Meng					
論文名 2 Title	LncRNA DANCR promotes the proliferation, migration, and invasion of tongue squamous cell carcinoma cells through miR-135a-5p/KLF8 axis					
掲載誌名 Published journal	Cancer Cell Int					
	2019 年 11 月	19 巻（号）	302 頁 ～ 316 頁	言語 Language	English	
第1著者名 First author	Zheng Y	第2著者名 Second author	Zheng B	第3著者名 Third author	Meng X	
その他著者名 Other authors	Yan Y, He J, Corresponding author: Liu Y					
論文名 3 Title	The Effects of HBXIP on the Biological Functions of TSCCa Cells and correlation with PI3K/Akt					
掲載誌名 Published journal	Translational Cancer Research					
	2020 年 3 月	9(5) 巻（号）	3375 頁 ～ 3384 頁	言語 Language	English	
第1著者名 First author	Xue Meng	第2著者名 Second author		第3著者名 Third author		
その他著者名 Other authors	Corresponding author: Weixian Liu					
論文名 4 Title	BP180 Is a Prognostic Factor in Head and Neck Squamous Cell Carcinoma					
掲載誌名 Published journal	ANTICANCER RESEARCH					
	2021 年 2 月	41 巻（号）	1089 頁 ～ 1099 頁	言語 Language	English	
第1著者名 First author	XUE MENG	第2著者名 Second author	FUMIHIKO MATSUMOTO	第3著者名 Third author	TAISUKE MORI	
その他著者名 Other authors	NAMI MIURA,YOSHINORI INO, KAORU ONIDANI, KENYA KOBAYASHI, YUSUKE MATSUZAKI, SEIICHI YOSHIMOTO, KATSUHISA IKEDA and KAZUFUMI HONDA					
論文名 5 Title	Hepatitis B X-interacting protein, involved in increasing proliferation and cell migration, is a prognostic marker in head and neck squamous cell carcinoma					
掲載誌名 Published journal	Oral Science International（Accept）					
	2021 年 2 月	巻（号）	頁 ～ 頁	言語 Language	English	
第1著者名 First author	Xue Meng	第2著者名 Second author	Taisuke Mori	第3著者名 Third author	Fumihiko Matsumoto	
その他著者名 Other authors	Nami Miura, Kaoru Onidani, Kenya Kobayashi, Yusuke Matsuzaki, Seiichi Yoshimoto, Katsuhisa Ikeda, Kazufumi Honda					

3．学会発表　Conference presentation　※筆頭演者として総会・国際学会を含む主な学会で発表したものを記載してくだ

※Describe your presentation as the principal presenter in major academic meetings including general meetings or international me

学会名 Conference	15th Japan-Taiwan Conference on Otolaryngology-Head and Neck Surgery				
演　題 Topic	The effects of HBXIP on the Biological Functions of TSCCa Cell Line and the correlation with PI3K/Akt				
開催日 date	2019　年　　12　月　　6　　日	開催地 venue	福岡		
形式　method	☐　口頭発表　Oral　　☑　ポスター発表　Poster	言語　Language	☐　日本語　☑　英語　☐　中国語		
共同演者名 Co-presenter	Katsuhisa Ikeda, Fumihiko Matsumoto, Weixian Liu				
学会名 Conference	第38回日本耳鼻咽喉科免疫アレルギー学会総会・学術講演会				
演　題 Topic	The effects of HBXIP on the Biological Functions of TSCCa Cell Line and the correlation with PI3K/Akt				
開催日 date	2020　年　　9　月　　15　日	開催地 venue	横浜（Online）		
形式　method	☑　口頭発表　Oral　　☐　ポスター発表　Poster	言語　Language	☐　日本語　☑　英語　☐　中国語		
共同演者名 Co-presenter	Katsuhisa Ikeda, Fumihiko Matsumoto, Weixian Liu				
学会名 Conference	第18回日本臨床腫瘍学会学術集会				
演　題 Topic	HBXIP predicts a poor prognosis in HNSCC and shows its effects on the biological functions of squamous cell lines				
開催日 date	2021　年　　2　月　　18　日	開催地 venue	京都（Online）		
形式　method	☐　口頭発表　Oral　　☑　ポスター発表　Poster	言語　Language	☐　日本語　☑　英語　☐　中国語		
共同演者名 Co-presenter					
学会名 Conference					
演　題 Topic					
開催日 date	年　　　月　　　日	開催地 venue			
形式　method	☐　口頭発表　Oral　　☐　ポスター発表　Poster	言語　Language	☐　日本語　☐　英語　☐　中国語		
共同演者名 Co-presenter					

4．受賞（研究業績）Award（Research achievement）

名　称 Award name				受賞年 Year of	年　　　　月
	国名 Country				
名　称 Award name				受賞年 Year of	年　　　　月
	国名 Country				

5. 本研究テーマに関わる他の研究助成金受給 Other research grants concerned with your resarch theme

受給実績 Receipt record	■ 有　□ 無		
助成機関名称 Funding agency	公益財団法人国際耳鼻咽喉科学振興会		
助成金名称 Grant name	Society for Promotion of International Oto-Rhino-Laryngology（SPIO）		
受給期間 Supported period	2020　年　4　月　～　　2021　年　3　月		
受給額 Amount received	2,500,000 円		
受給実績 Receipt record	□ 有　□ 無		
助成機関名称 Funding agency			
助成金名称 Grant name			
受給期間 Supported period	年　　月　～　　　年　　月		
受給額 Amount received	円		

6. 他の奨学金受給 Another awarded scholarship

受給実績 Receipt record	□ 有　□ 無		
助成機関名称 Funding agency			
奨学金名称 Scholarship name			
受給期間 Supported period	年　　月　～　　　年　　月		
受給額 Amount received	円		

7. 研究活動に関する報道発表 Press release concerned with your research activities

※記載した記事を添付してください。Attach a copy of the article described below

報道発表 Press release	□ 有　□ 無	発表年月日 Date of release	
発表機関 Released medium			
発表形式 Release method	・新聞　・雑誌　・Web site　・記者発表　・その他（　　　　　　　　　　　）		
発表タイトル Released title			

8. 本研究テーマに関する特許出願予定 Patent application concerned with your research theme

出願予定 Scheduled	□ 有　□ 無	出願国 Application	
出願内容（概要） Application contents			

9. その他 Others

指導責任者（署名）　池田 勝久

- 305 -

· 短篇论著 ·

下颌骨恶性纤维组织细胞瘤1例报告

Mandibular Malignant Fibrous Histiocytoma：a Case Report

李野[1]，于海洋[2]，王秋旭[2]，刘维贤[2]，孟雪[2]

(1.北京大学深圳医院口腔科,广东 深圳 518046;2.中国医科大学附属盛京医院口腔颌面外科,沈阳 110004)

摘要 恶性纤维组织细胞瘤(MFH)是老年人最常见的恶性肿瘤之一。MFH常见于四肢软组织和腹膜后,位于下颌骨者极为罕见。手术切除是MFH患者的首选治疗方法,放疗和化疗可能有效。本文报告1例下颌骨MFH,并结合相关文献进行分析。

关键词 恶性纤维组织细胞瘤；颌骨；罕见肉瘤

纤维组织细胞瘤是细胞分化成纤维细胞和组织细胞而形成的肿瘤。其中只有一小部分表现为恶性,称为恶性纤维组织细胞瘤(malignant fibrous histiocytoma,MFH)[1],也称为未分化多形性肉瘤,是最常见的成人软组织肉瘤[2],由多形性纺锤和上皮样细胞组成,有少量多核细胞[3]。MFH可发生于广泛的年龄范围,常见于50~70岁年龄组,男性多见,在少数情况下,MFH发生于儿童,但侵略性较差。MFH好发部位为四肢软组织和腹膜后[4],发生在头部和颈部相对较少,发病率约3%~10%,可影响鼻腔、颅骨、喉部和颈部的软组织[5]。研究[6]表明,头颈部最常见的部位是上颌窦(5/15)、颈(4/15)和颞下窝(2/15),发生于下颌骨的MHF比较少见,仅占所有MFH骨病变的3%[7-8]。现回顾中国医科大学附属盛京医院口腔颌面外科收治的1例下颌骨MFH患者的诊治经过,总结其治疗经验和体会。

1 临床资料

患者,女,62岁,2016年9月因头疼就医。完善颈椎CT时发现右下后牙区破坏。数日后颈部淋巴结肿大,口服抗生素,症状缓解。同年10月,右下唇皮肤有麻木感,右下后牙咬合痛。入院检查口内可见右下第一磨牙根方舌侧黏膜隆起约0.5 cm× 0.5 cm,

表面光滑,质韧,界限清楚,无触压痛。颈部未触及肿大淋巴结。无全身系统性疾病。CT显示右下颌骨局部略膨胀,内见软组织密度影,边界欠清,冠状面长径约33 mm,骨皮质膨胀变薄、局部显示不清,提示右下颌骨占位性病变,见图1。

完善术前检查后,患者在全身麻醉下行下颌骨部分切除术+自体骨移植术(右髂前上棘)+下颌骨缺损钛板坚固内固定术。术后常规抗炎、换药及护理治疗,术区及供区愈合良好并顺利出院。术后45 d术区出现感染症状,反复肿胀和疼痛,皮肤出现瘘道,给予换药,明显好转。术后2个月,因意外的外力打击导致钛板折断,但未出现明显移位,且植入区断端可见明显新生骨质形成,继续给予局部冲洗、换药及抗生素治疗,半年后,感染完全消失,窦道愈合。术后随访1年,未再次出现肿胀及疼痛等相关感染症状,骨折断端愈合良好。见图2。

病理检查显示,光镜下可见瘤组织,由呈束状、密集排列的梭形瘤细胞构成,局部变性,未见坏死,每10个高倍视野约有26个分裂细胞。免疫组化：Vimentin(+)；CD68(+)；Ki-67(约20%+)；SMA(−)；Desmin(−)；CD34(血管−)；S-100(−)。见图3。

2 讨论

MFH是一种最常见的软组织肉瘤[9]。MFH通常分为多形性、黏液性、巨细胞、血管瘤性和炎症亚型5种组织学类型,预后较好的为黏液性及血管瘤性,而与巨细胞变异相关的预后较差[10]。在1个病灶

作者简介:李野(1992−),女,医师,硕士.

通信作者:孟雪,E−mail:mengx@sj-hospital.org
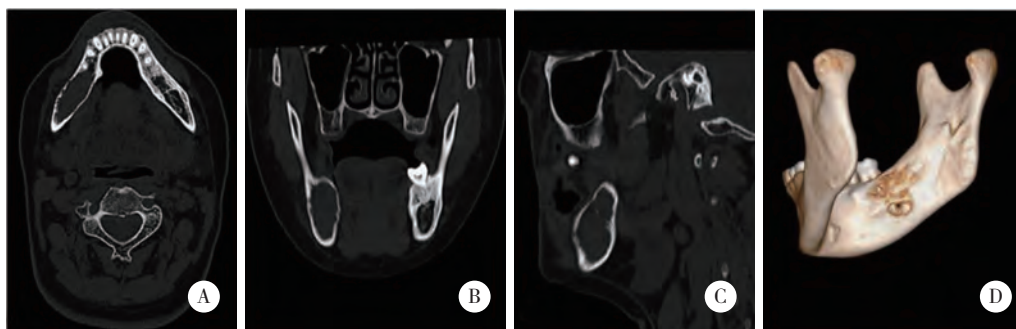
A,横断位;B,冠状位;C,矢状位;D,三维重建CT.

图1　CT检查结果
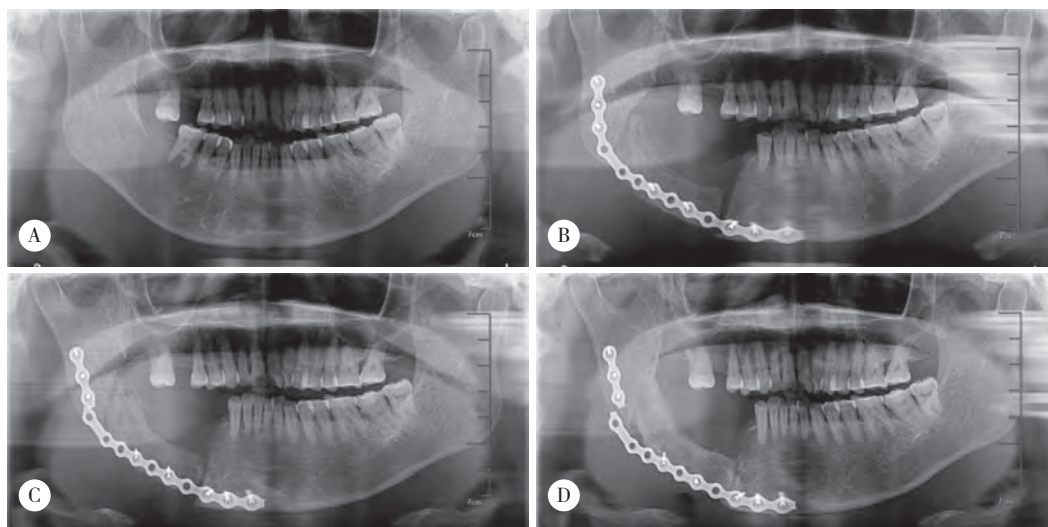
A,术前;B,术后1个月;C,术后2个月,患者受外力打击致钛板折断;D,术后1年,植骨断端可见明显新生骨质形成.

图2　术前及术后CT结果
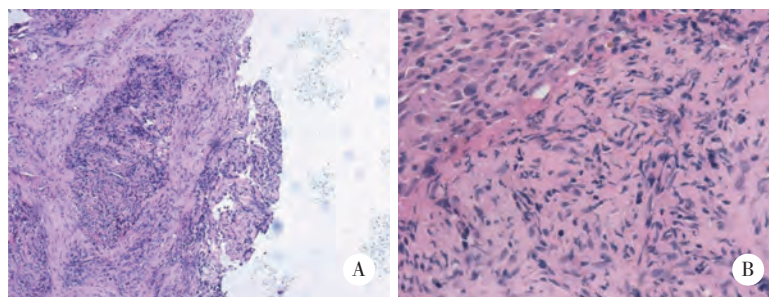
A,×10;B,×40.

图3　病理光镜下HE染色结果

内常可见到几种组织学类型同时存在,这可能与细胞分化优势有关[11]。尽管MFH诊断率很高,但仍然未确定其真正的起源细胞[8]。MFH的发病原因目前也尚未完全确定,据报道,MFH是头部和颈部区域最常见的辐射诱发肉瘤,CAI等[12]描述了59例头部和颈部的辐射诱发肉瘤,其中包括10例(16.9%)MFH。也有学者认为MFH是放射治疗、慢性术后修复、创伤、手术切口或烧伤疤痕后的并发症。此外,MFH与血液系统疾病有关,如非霍奇金淋巴瘤、霍奇金淋巴瘤、多发性骨髓瘤和恶性组织细胞增生症,大约20%的病例有创伤史。颌骨MFH最常见的症状是肿胀,疼痛,出血,伴分泌物[8]。MFH影像学无特异性表现,软组织侵犯和骨组织破坏比较常见,在头颈部的MFH中,可能会出现明显而长期的

增强信号。如果患者有放射治疗史,则应考虑MFH的诊断[13]。MFH没有标准的治疗指南。手术切除肿瘤是主要的治疗方法,所有接受手术切除的患者5年生存率为67.2%[14],未切除MFH患者的5年生存率<10%[15]。对于远处转移的高级别肿瘤,结合放射治疗和辅助化疗在内的多模式治疗可能会取得更好的结果[16-17]。晚期MFH的标准治疗方法是化疗,主要以阿霉素和异环磷酰胺作为一线治疗药物,单独或联合治疗[18]。MFH联合化疗的药物毒性常常导致治疗停止,尤其常见于老年患者[19]。另外,阿帕替尼可能为MFH的治疗提供了一个额外的选择[20]。MFH可通过血行播散,主要发生在肺部(82%),转移和复发的决定因素是组织学和肿瘤大小[21]。非黏液性MFH较黏液性MFH的转移倾向高,非黏液样病变超过5.0 cm的患者有出现转移的危险[22]。综上所述,手术治疗以及放化疗需要考虑到患者的年龄、并发症及肿瘤组织分型。如果肿瘤化学敏感,毗邻重要器官,术前可化疗[23]。不同类型的MFH化学敏感性和预后不同,MFH的风险分层对于治疗适应证尤其重要[24]。

参考文献:

[1] SENEL FC,BEKTAS D,CAYLAN R,et al. Malignant fibrous histi-ocytoma of the mandible [J]. Dentomaxillofac Radiol,2006,35(2):125-128. DOI:10.1259/dmfr/24174954.

[2] GOUNDER P,LAM M,VINCIULLO C,et al. Malignant fibrous his-tiocytoma masquerading as pyogenic granuloma [J]. Orbit,2017,36(2):122-123. DOI:10.1080/01676830.2017.1279652.

[3] SUN J,LIU R,WANG W,et al. Primary cardiac malignant fibrous histiocytoma with vulvar metastases:a case report [J]. Oncol Lett,2015,10(5):3153-3156. DOI:10.3892/ol.2015.3683.

[4] VIJAYALAKSHMI D,FATHIMA S,RAMAKRISHNAN K,et al. Malignant fibrous histiocytoma of the gingiva [J]. BMJ Case Reports,2012,2012:bcr2012007400. DOI:10.1136/bcr-2012-007400.

[5] SHELLENBERGER TD,STURGIS EM. Sarcomas of the head and neck region [J]. Curr Oncol Rep,2009,11(2):135-142.

[6] LI J,GENG ZJ,LV XF,et al. Computed tomography and magnet-ic resonance imaging findings of malignant fibrous histiocytoma of the head and neck [J]. Mol Clin Oncol,2016,4(5):888-892. DOI:10.3892/mco.2016.811.

[7] AL-SALIHI KA,SAMSUDIN AR. Malignant fibrous histiocytoma (MFH) of the mandible and submandibular salivary gland:report of a case [J]. Oral Oncol Extra,2004,40(10):123-125. DOI:10.1016/j.ooe.2004.07.002.

[8] LAMBADE PN,LAMBADE D,SAHA TK,et al. Malignant fibrous histiocytoma:an uncommon sarcoma with pathological fracture of mandible [J]. J Maxillofac Oral Surg,2015,14(Suppl 1):283-287. DOI:10.1007/s12663-013-0491-x.

[9] NIIMI R,MATSUMINE A,IINO T,et al. The expression of hDlg as a biomarker of the outcome in malignant fibrous histiocytomas [J]. On-col Rep,2010,23(3):631-638. DOI:10.3892/or_00000678.

[10] BALI A,SINGH MP,PADMAVATHI,et al. Malignant fibrous histiocytoma-an unusual transformation from benign to malignant [J]. J Canc Sci Ther,2010,2(2):53-57. DOI:10.4172/1948-5956.1000023.

[11] ANAVI Y,HERMAN GE,GRAYBILL S,et al. Malignant fibrous histiocytoma of the mandible [J]. Surg Med Pa,1989,68(4):436-443.

[12] CAI PQ,WU YP,LI L,et al. CT and MRI of radiation-induced sarcomas of the head and neck following radiotherapy for naso-pharyngeal carcinoma [J]. Clin Radiol,2013,68(7):683-689. DOI:10.1016/j.crad.2013.01.004.

[13] JAIN S,KAUR R,KOUL R. Malignant fibrous histiocytoma of max-illary sinus- a diagnostic challenge [J]. Indian J Surg Oncol,2015,6(3):259. DOI:10.1007/s13193-015-0384-1.

[14] OGURA K,GOTO T,IMANISHI J,et al. Neoadjuvant and adjuvant chemotherapy with modified mesna,adriamycin,ifosfamide,and da-carbazine(MAID)regimen for adult high-grade non-small round cell soft tissue sarcomas [J]. Int J Clin Oncol,2013,18(1):170-176. DOI:10.1007/s10147-011-0360-x.

[15] SHERMAN KL,WAYNE JD,CHUNG J,et al. Assessment of multi-modality therapy use for extremity sarcoma in the United States [J]. J Surg Oncol,2014,109(5):395. DOI:10.1002/jso.23520.

[16] OH SJ,YEOM SY,KIM KH. Clinical implication of surgical re-section for the rare cardiac tumors involving heart and great ves-sels [J]. J Korean Med Sci,2013,28(5):717-724. DOI:10.3346/jkms.2013.28.5.717.

[17] HARDSION SA,DAVIS PL 3RD,BROWNE JD. Malignant fibrous histiocytoma of the head and neck:a case series [J]. Am J Otolaryn-gol,2013,34(1):10-15. DOI:10.1016/j.amjoto.2012.06.010.

[18] SERENO M,MERINO M,AGUAYO C,et al. A major response to trabectedin in metastatic malignant fibrous histiocytoma of the ver-tebra:a case report and review of the literature [J]. Tumori,2013,9(22):e43-e48. DOI:10.1700/1283.14206.

[19] JI G,HONG L,YANG P. Successful treatment of advanced malig-nant fibrous histiocytoma of the right forearm with apatinib:a case report [J]. Onco Targets Ther,2016,9:643-647. DOI:10.2147/OTT.S96133.

[20] KIKUTA K,MORIOKA H,KAWAI A,et al. Global protein-expres-sion profiling for reclassification of malignant fibrous histiocytoma [J]. Biochim Biophys Acta,2015,1854(6):696-701. DOI:10.1016/j.bbapap.2014.08.012.

[21] DONG J,AN W,MA W,et al. Primary hepatic malignant brous histiocytoma mimicking hepatocellular carcinoma:a report of two cases [J]. Oncol Lett,2014,8(5):2150-2154. DOI:10.3892/ol.2014.2483.

[22] JI W,ZHONG M,YOU Y,et al. Primary malignant fibrous histiocy-toma of the colon:a case report and review of the literature [J]. Mol Clin Oncol,2016,4(6):1006-1008. DOI:10.3892/mco.2016.849.

[23] HSIAO PJ,CHEN GH,CHANG YH,et al. An unresectable retro-peritoneal malignant fibrous histiocytoma:a case report [J]. Oncol Lett,2016,11(4):2403-2407. DOI:10.3892/ol.2016.4283.

[24] RAJENDRA R,JONES R,POLLACK SM. Targeted treatment for advanced soft tissue sarcoma:profile of pazopanib [J]. Oncol Targets Ther,2013,6:217-222. DOI:10.2147/OTT.S32200.

（编辑　王又冬）

PRIMARY RESEARCH

Open Access

LncRNA DANCR promotes the proliferation, migration, and invasion of tongue squamous cell carcinoma cells through miR-135a-5p/KLF8 axis

Ying Zheng[1], Bowen Zheng[1], Xue Meng[2], Yuwen Yan[1], Jia He[1] and Yi Liu[1*]

Abstract

Background: Tongue squamous cell carcinoma (TSCC) is a most invasive cancer with high mortality and poor prognosis. It is reported that lncRNA DANCR has implications in multiple types of cancers. However, its biological role and underlying mechanism in TSCC progress are not well elucidated.

Methods: Our present study first investigated the function of DANCR on the proliferation, migration and invasion of TSCC cells by silencing or overexpressing DANCR. Further, the miR-135a-5p-Kruppel-like Factor 8 (KLF8) axis was focused on to explore the regulatory mechanism of DANCR on TSCC cell malignant phenotypes. Xenografted tumor growth using nude mice was performed to examine the role of DANCR in vivo.

Results: DANCR knockdown reduced the viability and inhibited the migration and invasion of TSCC cells in vitro, while ectopic expression of DANCR induced opposite effects. In vivo, the tumor growth and the expression of matrix metalloproteinase (MMP)-2/9 and KLF8 were also blocked by DANCR inhibition. In addition, we found that miR-135-5p directly targeted DANCR, which was negatively correlated with DANCR on TSCC progression. Its inhibition reversed the beneficial effects of DANCR silence on TSCC malignancies. Furthermore, the expression of KLF8 evidently altered by both DANCR and miR-135a-5p. Silencing KLF8 using its specific siRNA showed that KLF8 was responsible for the induction of miR-135a-5p inhibitor on TSCC cell malignancies and MMP-2/9 expression.

Conclusions: These findings, for the first time, suggest that DANCR plays an oncogenic role in TSCC progression via targeting miR-135a-5p/KLF8 axis, which provides a promising biomarker and treatment approach for preventing TSCC.

Keywords: DANCR, Tongue squamous cell carcinoma, miR-135a-5p, KLF8, MMP

Background

Tongue squamous cell carcinoma (TSCC) is a major type of head and neck squamous cell carcinoma (HNSCC) with high recurrence rates, increased proliferation and metastasis, and poor prognosis [1, 2]. Despite of significant advances in the prevention and treatment, the survival rates of TSCC patients are still low [3]. It is identified

that the invasion and migration mainly contribute to the progression of tumors. Therefore, it is urgent that developing novel therapeutic strategies for TSCC through the exploration of the underlying molecular mechanisms.

LncRNAs are a group of long non-coding RNAs with more than 200 nucleotides in length. Numerous reports has shown that lncRNAs play important roles in wide ranges of biological processes, including cell proliferation, differentiation, apoptosis, migration and invasion [4–6]. Especially, multiple lncRNAs has been found to be closely implicated in the tumorigenesis and progression of TSCC. For example, high-expression of lncRNA

*Correspondence: liuyi@cmu.edu.cn
[1] Department of Orthodontics, School of Stomatology, China Medical University, 117 North Nanjing Street, Shenyang 110002, People's Republic of China
Full list of author information is available at the end of the article

Zheng *et al. Cancer Cell Int*   (2019) 19:302

Page 2 of 14

AFAP1-AS1 in TSCC tumor tissues enhances tumor progression via the activation of Wnt/β-catenin signaling pathway [7]. NKILA serves as a crucial determinant of TSCC metastasis to reduce the migratory and invasive cells through inhibiting the process of epithelial–mesenchymal transition (EMT) [8]. Interestingly, lncRNA DANCR (differentiation antagonizing non-protein coding RNA) has been noticed to suppress epidermal cell differentiation [9] and improve hepatocellular carcinoma self-renewal [10]. DANCR is also taken as an oncogenic lncRNA for several cancers, such as prostate cancer [11], gastric cancer [12] and colorectal cancer [13]. However, the distinct function of DANCR in TSCC was not well understood.

MicroRNAs (miRNAs), a class of small non-coding RNAs, are shown to modulate the expression of target genes. Recent studies have revealed that miR-135a-5p is the main regulator of tumor invasion and metastasis [14, 15]. In non-small cell lung cancer (NSCLC), miR-135a-5p is demonstrated to inhibit cell migration and invasion through targeting Kruppel-like Factor 8 (KLF8) [16]. As we know, KLF8 has been widely confirmed to participate in the regulation of cell cycle progression, transformation, EMT and invasion [17–21]. Given that DANCR was predicted to have putative binding sites with miR-135a-5p through the analysis of online bioinformatics, we thus speculated that DANCR might affect the development and progression of TSCC by regulating miR-135a-5p/KLF8 axis.

To improve the understanding of DANCR effects on TSCC malignancies, CAL-27 and TCa-8113 cells with DANCR silence, and SCC9 and TSCCA cells with DANCR overexpression were constructed. Then the effects of DANCR on the proliferation, migration and invasion of TSCC cells were determined. Further, miR-135a-5p/KLF8 axis was focused to explore the molecular mechanism by which DANCR promoted TSCC progression.

Methods

Cell culture and reagents

In our experiments, four human TSCC cell lines (SCC9, TSCCA, TCa-8113 and CAL-27 cells) were used. SCC9 cells (Cellcook, Guangzhou, China) were cultured in DMEM/F12 medium supplemented with 10% fetal bovine serum (FBS; SH30084.03, Hyclone, South Logan, UT, USA); TSCCA cells (Procell, Wuhan, China) were maintained in DMEM medium (12100-46, Gibco) containing with 10% FBS; TCa-8113 and CAL-27 cell lines (Procell, Wuhan, China) were cultured in RPMI-1640 medium (31800-014, Gibco, Gaithersburg, MD, USA) supplemented with 10% FBS. All these cell lines were cultured in a standard environment at 37 °C with 5% CO_2.

MiR-135a-5p mimics/inhibitor and corresponding negative control (NC) mimics/inhibitor were purchased from JTS Scientific (Beijing, China).

Construction of siRNAs and shRNAs

The sequences of siRNAs (5′–3′) targeting human DANCR were designed as follows: si-DANCR-1 sense GUUGACAACUACAGGCACATT and antisense UGU GCCUGUAGUUGUCAACTT; si-DANCR-2 sense CUA GAGCAGUGACAAUGCUTT and antisense AGCAUU GUCACUGCUCUAGTT. The NC siRNA sequences (5′–3′) were: sense UUCUCCGAACGUGUCACGUTT and antisense ACGUGACACGUUCGGAGAATT. Then shRNAs targeting DANCR and corresponding NC were constructed by pRNAH1.1 plasmid vectors (Genscript, Nanjing, China).

Furthermore, we also designed the interfering sequences (5′–3′) for human KLF8 as follows: si-KLF8 sense CGAUAUGGAUAAACUCAUATT and antisense UAUGAGUUUAUCCAUAUCGAC. The corresponding NC siRNA sequences (5′–3′) were designed as follows: si-NC sense UUCUCCGAACGUGUCACGUTT and antisense ACGUGACACGUUCGGAGAATT.

Construction of overexpression plasmids

A pair of specific primers (forward 5′-CAAGGATCC GCCCTTGCCCAGAGTCTTCC-3′ and reverse 5′-CCG CTCGAGGTCAGGCCAAGTAAGTTTAT-3′) was used to amplify human DANCR (NR_024031.2). Then the amplified products were inserted into pcDNA3.1 plasmids (V790-20, Invitrogen, Carlsbad, CA, USA) between BamHI and XhoI restriction enzyme sites to induce the overexpression of DANCR. The empty pcDNA3.1 vector was used as control.

Cell transfection

When cells reached at 70% of confluence, siRNAs or shRNAs targeting DANCR were transfected into CAL-27 and TCa-8113 cells, and ectopic expression of DANCR were transfected into SCC9 and TSCCA cells by the mediation of Lipofectamine 2000 reagent (11668-019, Invitrogen) following the manufacturer's instructions. All experiments were performed at 48 h post transfection.

In addition, miR-135a-5p mimics or NC mimics was transfected into CAL-27 or TCa-8113 cells, and its inhibitor or NC inhibitor was transfected into SCC9 cells as mentioned above to overexpress or silence miR-135a-5p. Furthermore, the co-transfection of miR-135a-5p inhibitor and si-DANCR or si-KLF8 was also mediated by Lipofectamine 2000.

Zheng *et al. Cancer Cell Int*   (2019) 19:302

Page 3 of 14

Quantitative real-time polymerase chain reaction (qRT-PCR)

Total RNAs in TSCC cell lines were extracted with RNAsimple Total RNA Kit (DP419, TIANGEN, Beijing, China) and reverse-transcribed into cDNA templates using M-MLV reverse transcriptase (NG212, TIANGEN). The designed specific primer sequences were synthesized by Sangon Biotech (Shanghai, China) and shown as follows (5′−3′): miR-135a-5p, RT GTTGGCTCTGGT GCAGGGTCCGAGGTATTCGCACCAGAGCCAACT CACAT, forward GCCGTATGGCTTTTTATTCCTA and reverse GGTGCAGGGTCCGAGGTATT; U6, RT GTTGGCTCTGGTGCAGGGTCCGAGGTATTCGCA CCAGAGCCAACAAAATATGG, forward GCTTCG GCAGCACATATACT and reverse GGTGCAGGGTCC GAGGTATT; DANCR forward ACCCTCCTGCTT CCCTC and reverse CCCGAAACCCGCTACAT; KLF8 forward TCATTGGAGGAGATGGTAA and reverse GCTGCTGGTTCTTGCTGT; GAPDH forward GAC CTGACCTGCCGTCTAG and reverse AGGAGTGGG TGTCGCTGT. Subsequently, the mixture of cDNA templates, specific primers, SYBR Green reagent (SY1020, Solarbio, Beijing, China) and Taq PCR MasterMix (KT201, TIANGEN) were used to amplify target genes by qRT-PCR analysis on Exicycler 96 PCR system (Bioneer, Daejeon, Korea). GAPDH was normalized for DANCR and KLF8 expression, and U6 was normalized for miR-135a-5p expression. Relative expression was calculated using the $2^{-\Delta\Delta CT}$ method.

MTT assay

TSCC cells were seeded in 96-well plates at the density of 4×10^3 cells/well for 0, 24, 48 or 72 h, respectively. Then cells were incubated in a complete medium containing 0.5 mg/ml MTT (KGA311, KeyGEN, Nanjing, China) for 4 h. After dissolving in DMSO (ST038, Beyotime), the viable cells were determined using microplate reader (ELX-800, BIOTEK, Winooski, VT, USA) at the optical density of 570 nm.

Wound healing assay

The wound healing assay was used to assess cell migratory ability. Cells were treated with mitomycin C (M0503, Sigma) for 1 h in a serum-free medium. Then a wound scratch was made by a 200 μl pipette tip in the culture plate and recorded it by phase-contrast microscopy (IX53, Olympus, Tokyo, Japan) under 100× magnification. Twenty-four hours later, the migratory distances were measured with Image Pro Plus Software (Media Cybernetics, Silver Springs, MD, USA) to calculate the capacity of cell migration.

Transwell assay

Transwell assay was utilized to evaluate the invasive ability of cells. Briefly, cell suspensions (2×10^4 cells/well) were seeded in the upper chamber of 24-well Transwell inserts (3422, Corning Incorporated, Corning, NY, USA) pre-coated with Matrigel (356234, BD Biosciences, San Jose, CA, USA) with serum-free medium. The lower chamber was filled with the medium containing with 30% FBS. After 48 h of incubation, cells in the upper chamber were removed and washed in PBS twice. Then cells were fixed in 4% paraformaldehyde and stained with 0.4% crystal violet (0528, Amresco, Solon, OH, USA). The number of cells in the lower chamber was observed by phase-contrast microscope under 200× magnification. Five fields in each image were randomly selected to count and the invasive cell ratio was normalized to control.

Luciferase reporter assay

Bioinformatics analysis predicted that lncRNA DANCR had putative binding sites with miR-135a-5p. The pmir-GLO vector (E133A, Promega, Madison, WI, USA) containing NheI and SalI restriction enzyme sites was applied to construct wild type (wt) or mutant type (mut) luciferase reporter vectors for DANCR. The site-directed mutation of DANCR was used to verify the target effects between DANCR and miR-135a-5p. Then 293T cells (ZhongQiaoXinZhou Bio, Shanghai, China) were seeded in 12-well plates and co-transfected with wt-DANCR, or mut-DANCR together with miR-135a-5p or NC mimics using Lipofectamine 2000. Finally, the binding activity was tested with a dual luciferase reporter assay kit (E1910, Promega) by the calculation of Firefly luciferase activity/ Renilla luciferase activity at 48 h post-transfection.

Western blot

Total proteins from TSCC cell lines or tumor tissues were isolated using RIPA lysate (R0010, Solarbio) containing PMSF (P0100, Solarbio) and quantified using BCA assay kit (PC0020, Solarbio). Then equal proteins were loaded on the Sodium dodecylsulphate polyacrylamide gel electrophoresis (SDS-PAGE) gel, and transferred onto PVDF membrane (IPVH00010, Millipore, Billerica, MA, USA). After washing in TBST, the membrane was incubated with one of the following specific primary antibodies overnight at 4 °C: MMP-2 antibody (1:500; 10373-2-AP, Proteintech, Wuhan, China), MMP-9 antibody (1:500; ab38898, Abcam, Cambridge, UK), KLF8 antibody (1:1000; A16321, Abclonal, Wuhan, China) and GAPDH (1:10,000; 60004-1-Ig, Proteintech). Subsequently, horseradish peroxidase (HRP)-conjugated goat anti-rabbit antibody (1:3000; SE134, Solarbio) or HRP-conjugated goat anti-mouse antibody (1:3000; SE131, Solarbio) was

Zheng *et al. Cancer Cell Int*   (2019) 19:302

Page 4 of 14

used to incubate with the membrane for 1 h at 37 °C. Protein signals were developed with ECL kit (PE0010, Solarbio) and quantified using Gel-Pro-Analyzer Software (Media Cybernetics, Silver Springs, MD, USA). GAPDH was used as internal control.

Xenograft tumor model analysis

The ethical approval was obtained from School of Stomatology, China Medical University Committee (No. G2018007) in this study. All animal experimental procedures were performed according to the Guide for the Care and Use of Laboratory Animals. The Balb/c-nude mice (4–5 weeks, 18–20 g) were purchased from HuaFu-Kang Bioscience Co. lnc (Beijing, China) and housed in a standard environment. Stably transfected cells with sh-DANCR or sh-NC were selected using G418 antibiotics (A1720, Sigma, St. Louis, MO, USA). Then, CAL-27 cells or TCa-8113 cells with sh-DANCR or sh-NC stable transfections were subcutaneously injected into the right side of axilla at the density of 1×10^6 cells per animal. Tumor volume was measured using the caliper every 4 days following the formula: tumor volume $(mm^3) = (length \times width^2)/2$. Tumor weight was measured when mice were killed after 25 days.

Immunofluorescence

For immunofluorescence staining, the collected tumor tissues were fixed in paraformaldehyde, embedded with paraffin and sectioned into 5 μm-thickness slides. Then paraffin slides were incubated with specific primary antibody against KLF8 (NBP2-57740, NOVUS, Centennial, CO, USA) overnight at 4 °C, and conjugated with FITC-labeled goat anti-rabbit secondary antibody (A0562, Beyotime) at room temperature for 60 min. After counterstaining with DAPI, the immunopositive materials were visualized using optical microscope (BX53, Olympus) at the magnification of $400 \times$ and captured using digital camera (DP73, Olympus).

Statistical analysis

Data were expressed as mean $\pm$ SD and analyzed using GraphPad Prism software (San Diego, CA, USA). The comparisons were performed using t-test or one-way ANOVA following Bonferroni's test. $p < 0.05$ was identified to indicate a significant difference statistically.

Results

DANCR knockdown suppressed the proliferation, migration and invasion of TSCC cell lines

In four different TSCC cell lines, the expression profile of DANCR was first detected as shown in Fig. 1a. From this chart, it was apparent that DANCR expression was higher in CAL-27 and TCa-8113 cells than in SCC9 and

TSCCA cells. Thus in further experiments, CAL-27 and TCa-8113 cells were used to inhibit DANCR, while SCC9 and TSCCA cells were forced to express DANCR. As expectation, specific siRNAs targeting DANCR significantly decreased its levels in CAL-27 and TCa-8113 cells (Fig. 1b).

Then the effects of si-DANCRs on the proliferation, migration and invasion of TSCC cells were first assessed. MTT assay was considered to indicate cell proliferation, and the results showed that DANCR knockdown reduced the viable number of CAL-27 and TCa-8113 cells (Fig. 1c). Furthermore, it seemed that inhibition of DANCR significantly decreased the migratory and invasive ability of TSCC cells using wound healing assay and transwell invasion assay (Fig. 1d, e). These results indicate that DANCR knockdown may attenuate TSCC malignancies in vitro.

DANCR overexpression promoted the proliferation, migration and invasion of TSCC cell lines

Further, the forced expression of DANCR was used to investigate its biological function in SCC9 and TSCCA cells. We observed a marked increase of DANCR expression by its overexpression plasmids in SCC9 and TSCCA cells (Fig. 2a). Functional analysis from SCC9 and TSCCA cells indicated that the ectopic expression of DANCR induced increments of cell viability, migratory distance and invasive cell number (Fig. 2b–d). Our data show that DANCR can enhance the proliferation, migration and invasion of TSCC cells in vitro.

DANCR targeted miR-135a-5p to regulate KLF8 expression in TSCC cell lines

As shown in Fig. 3a, the bioinformatics predicted that DANCR was complementary with miR-135a-5p (Fig. 3a), which was confirmed by dual luciferase reporter assay. The results demonstrated that miR-135a-5p mimics significantly inhibited the luciferase activity of wt-DANCR, but not mut-DANCR (Fig. 3b). Then we observed a marked increase of miR-135a-5p level in CAL-27 and TCa-8113 cells transfected with si-DANCR (Fig. 3c, d), but a significant reduction of miR-135a-5p in SCC9 and TSCCA cells transfected with pcDNA3.1-DANCR (Fig. 3e, f). In addition, KLF8 mRNA was down-expressed by knockdown of DANCR in CAL-27 (Fig. 3g) and TCa-8113 cells (Fig. 3h), but increased by DANCR overexpression in SCC9 (Fig. 3i) and TSCCA cells (Fig. 3j). These data suggest that miR-135a-5p is a direct target of DANCR, and KLF8 may participate in DANCR-mediated regulation of TSCC malignant phenotypes.
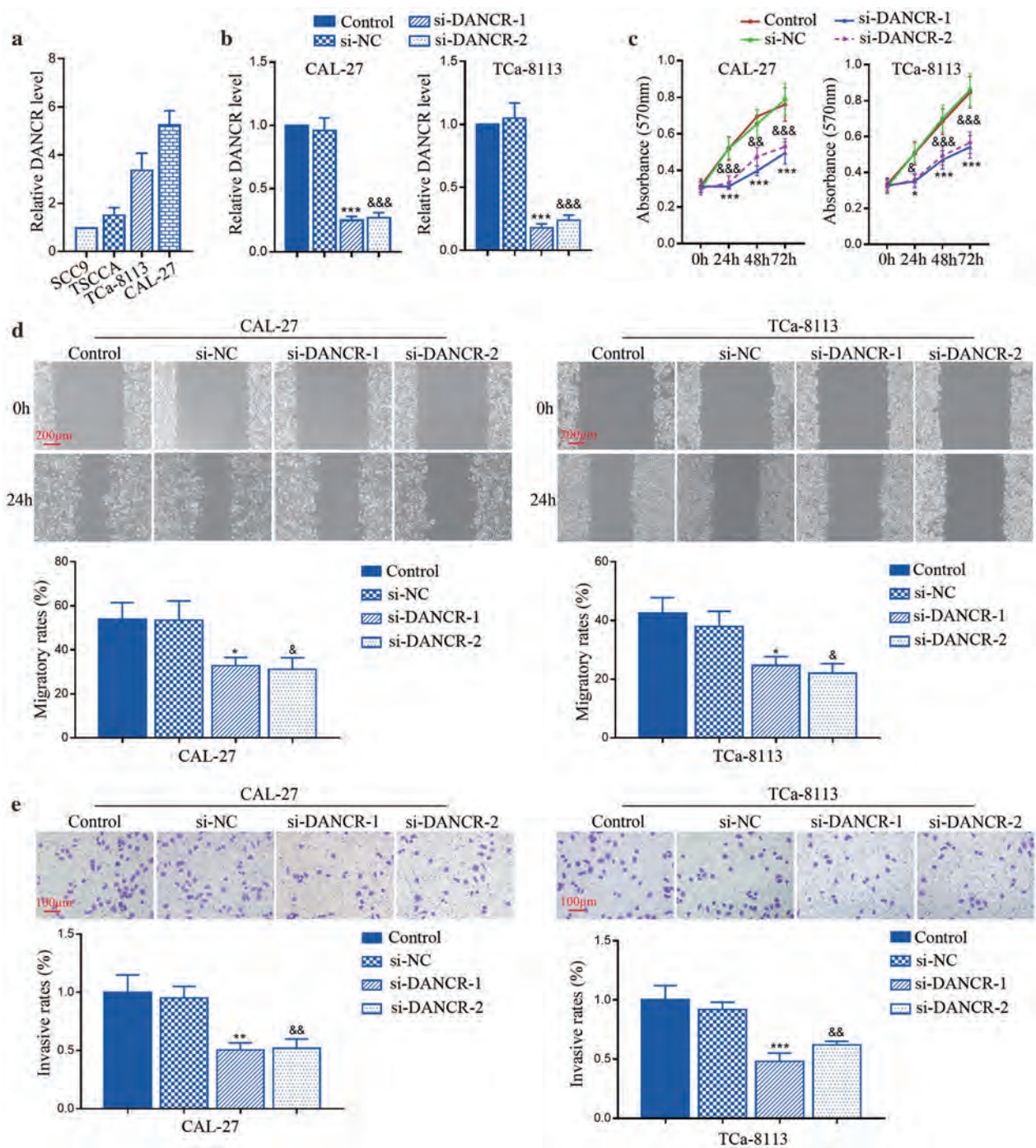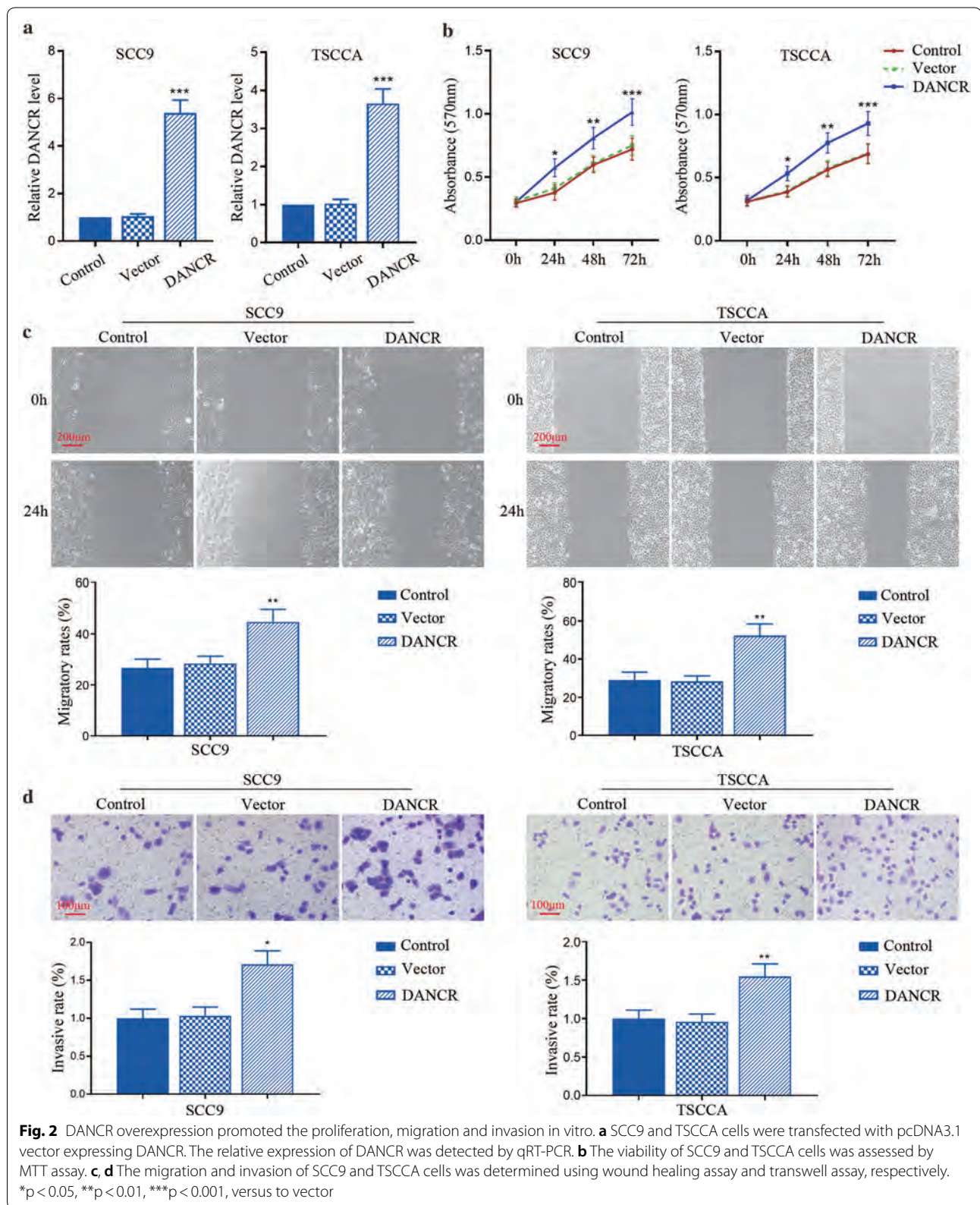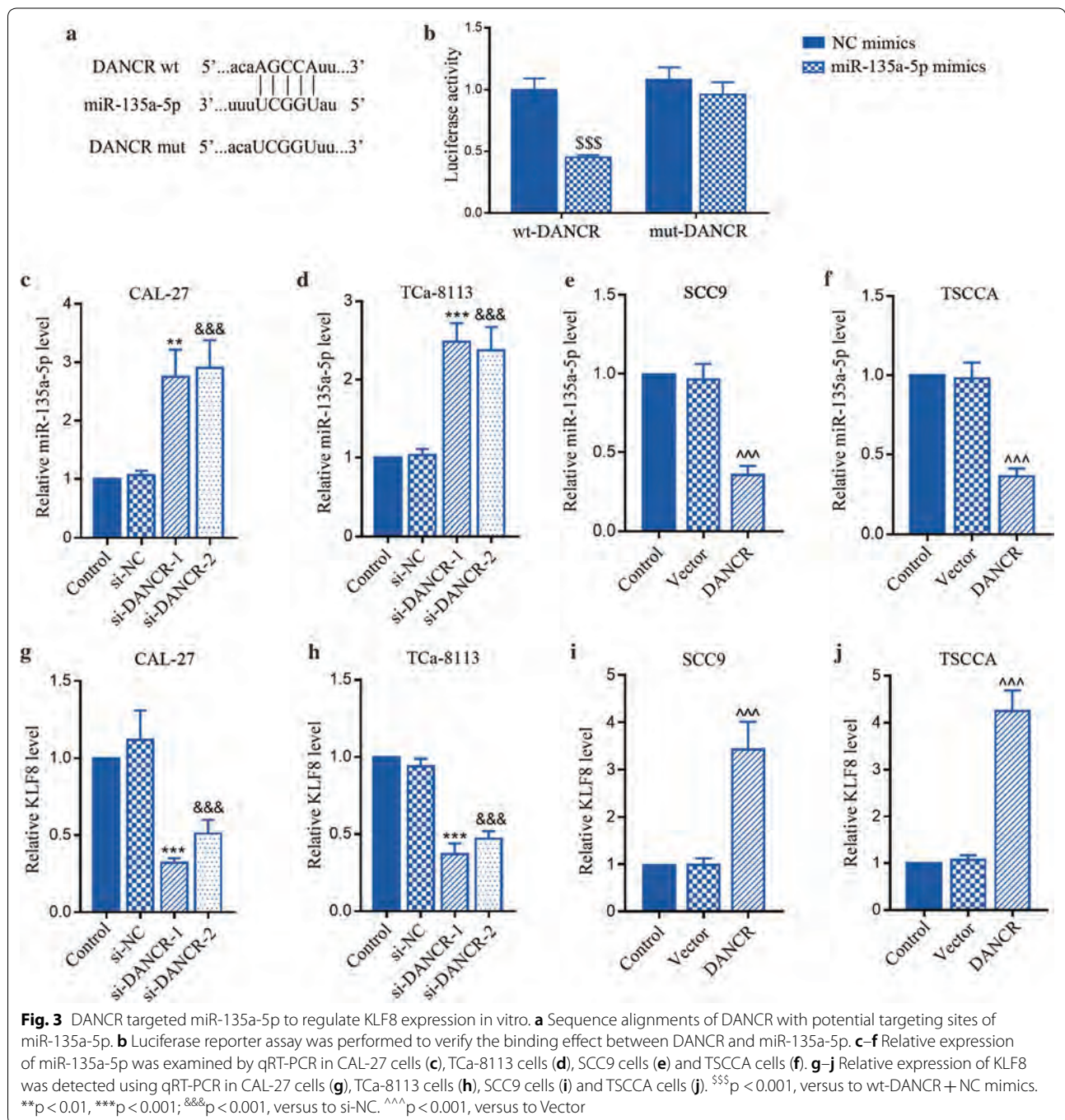
Fig. 1 DANCR knockdown suppressed the proliferation, migration and invasion in vitro. **a** Relative expression of DANCR was detected by qRT-PCR in different TSCC cell lines. **b** CAL-27 and TCa-8113 cells were transfected with siRNAs against DANCR. The relative expression of DANCR was detected by qRT-PCR. **c** The viability of CAL-27 and TCa-8113 cells was assessed by MTT assay. **d**, **e** The migration and invasion of CAL-27 and TCa-8113 cells was determined using wound healing assay and transwell assay, respectively. *$p < 0.05$, **$p < 0.01$, ***$p < 0.001$; &$p < 0.05$, &&$p < 0.01$, &&&$p < 0.001$, versus to si-NC

Zheng *et al. Cancer Cell Int*   (2019) 19:302

Page 6 of 14

Fig. 2 DANCR overexpression promoted the proliferation, migration and invasion in vitro. **a** SCC9 and TSCCA cells were transfected with pcDNA3.1 vector expressing DANCR. The relative expression of DANCR was detected by qRT-PCR. **b** The viability of SCC9 and TSCCA cells was assessed by MTT assay. **c**, **d** The migration and invasion of SCC9 and TSCCA cells was determined using wound healing assay and transwell assay, respectively. *p < 0.05, **p < 0.01, ***p < 0.001, versus to vector

Fig. 3 DANCR targeted miR-135a-5p to regulate KLF8 expression in vitro. **a** Sequence alignments of DANCR with potential targeting sites of miR-135a-5p. **b** Luciferase reporter assay was performed to verify the binding effect between DANCR and miR-135a-5p. **c**–**f** Relative expression of miR-135a-5p was examined by qRT-PCR in CAL-27 cells (**c**), TCa-8113 cells (**d**), SCC9 cells (**e**) and TSCCA cells (**f**). **g**–**j** Relative expression of KLF8 was detected using qRT-PCR in CAL-27 cells (**g**), TCa-8113 cells (**h**), SCC9 cells (**i**) and TSCCA cells (**j**). $^{\$\$\$}p < 0.001$, versus to wt-DANCR + NC mimics. $^{**}p < 0.01$, $^{***}p < 0.001$; $^{\&\&\&}p < 0.001$, versus to si-NC. $^{\wedge\wedge\wedge}p < 0.001$, versus to Vector

MiR-135a-5p overexpression suppressed tumor cell progression and KLF8 expression in TSCC cell lines

Then we found that miR-135a-5p expression in SCC9 and TSCCA cells was higher than that in TCa-8113 and CAL-27 cells (Fig. 4a). To further investigate the role of miR-135a-5p, its specific mimics were further carried out. It obviously confirmed that miR-135a-5p expression was increased by its mimics in CAL-27 and TCa-8113 cells (Fig. 4b). The results in Fig. 4c–e showed that overexpression of miR-135a-5p reduced viable cells, shortened migratory distance and decreased invasive cells in CAL-27 cells and TCa-8113 cells. In addition, KLF8 mRNA and protein expression were also suppressed by miR-135a-5p (Fig. 4f, g). All results indicate that miR-135a-5p may protect against TSCC malignant phenotypes with the involvement of KLF8 suppression.

Zheng *et al. Cancer Cell Int*   (2019) 19:302

Page 8 of 14

(See figure on next page.)
Fig. 4 MiR-135a-5p overexpression suppressed tumor cell progression and KLF8 expression in vitro. **a** Relative expression of miR-135a-5p in different TSCC cell lines was examined using qRT-PCR. **b** Relative expression of miR-135a-5p was measured in CAL-27 and TCa-8113 cells transfected with miR-135a-5p mimics by qRT-PCR. **c** The viability of CAL-27 and TCa-8113 cells was measured using MTT assay. **d**, **e** The migration and invasion of CAL-27 and TCa-8113 cells was examined using wound healing assay and transwell assay, respectively. **f** Relative expression of KLF8 mRNA was detected in CAL-27 and TCa-8113 cells using qRT-PCR. **g** Relative expression of KLF8 protein was measured using western blot in CAL-27 and TCa-8113 cells. *p < 0.05, **p < 0.01, ***p < 0.001, versus to NC mimics

DANCR knockdown repressed tumor cell progression and KLF8 expression by targeting miR-135a-5p in TSCC cell lines

Although miR-135a-5p had been identified to target DANCR and be beneficial for TSCC progress, whether miR-135a-5p was responsible for the effects of DANCR on tumor malignancies was unclear. As illustrated in Fig. 5a, the reduction of viable cells by DANCR knockdown was enhanced by miR-135a-5p inhibitor. Furthermore, inhibition of miR-135a-5p reversed si-DANCR-mediated suppression of cell migration and invasion (Fig. 5b, c). It is well-known that matrix metalloproteinase (MMP) family proteins are main biomarkers for tumor invasion and metastasis. Results in Fig. 5d showed that the decrease of MMP-2 and MMP-9 protein levels induced by DANCR silence was partially increased by miR-135a-5p inhibitor. In addition, we found that the reduction of KLF8 in si-DANCR cells was increased by miR-135a-5p inhibitor (Fig. 5e). Together the results further suggest that DANCR/miR-135a-5p may modulate TSCC progression by the regulation of KLF8.

MiR-135a-5p inhibition exacerbated tumor cell progression through activating KLF8 in TSCC cell lines

Next, we further elucidated whether KLF8 was responsible for the regulatory function of DANCR/miR-135a-5p in SCC9 cells using its specific siRNA. Expectedly, miR-135a-5p inhibitor-induced increase of KLF8 was suppressed by the siRNA of KLF8 itself (Fig. 6a). Knockdown of KLF8 attenuated the effects of miR-135a-5p inhibitor on the proliferation, migration and invasion of SCC9 cells (Fig. 6b–d). Similarly, the indicators for tumor development and progression, MMP-2 and MMP-9 were also inhibited by KLF8 silencing (Fig. 6e), which just proved the alterations of tumor malignancies at molecular level. Collectively, these findings demonstrate that KLF8 is responsible for the regulation of DANCR/miR-135a-5p on TSCC progression.

DANCR knockdown blocked the tumor formation in vivo involving KLF8 activation
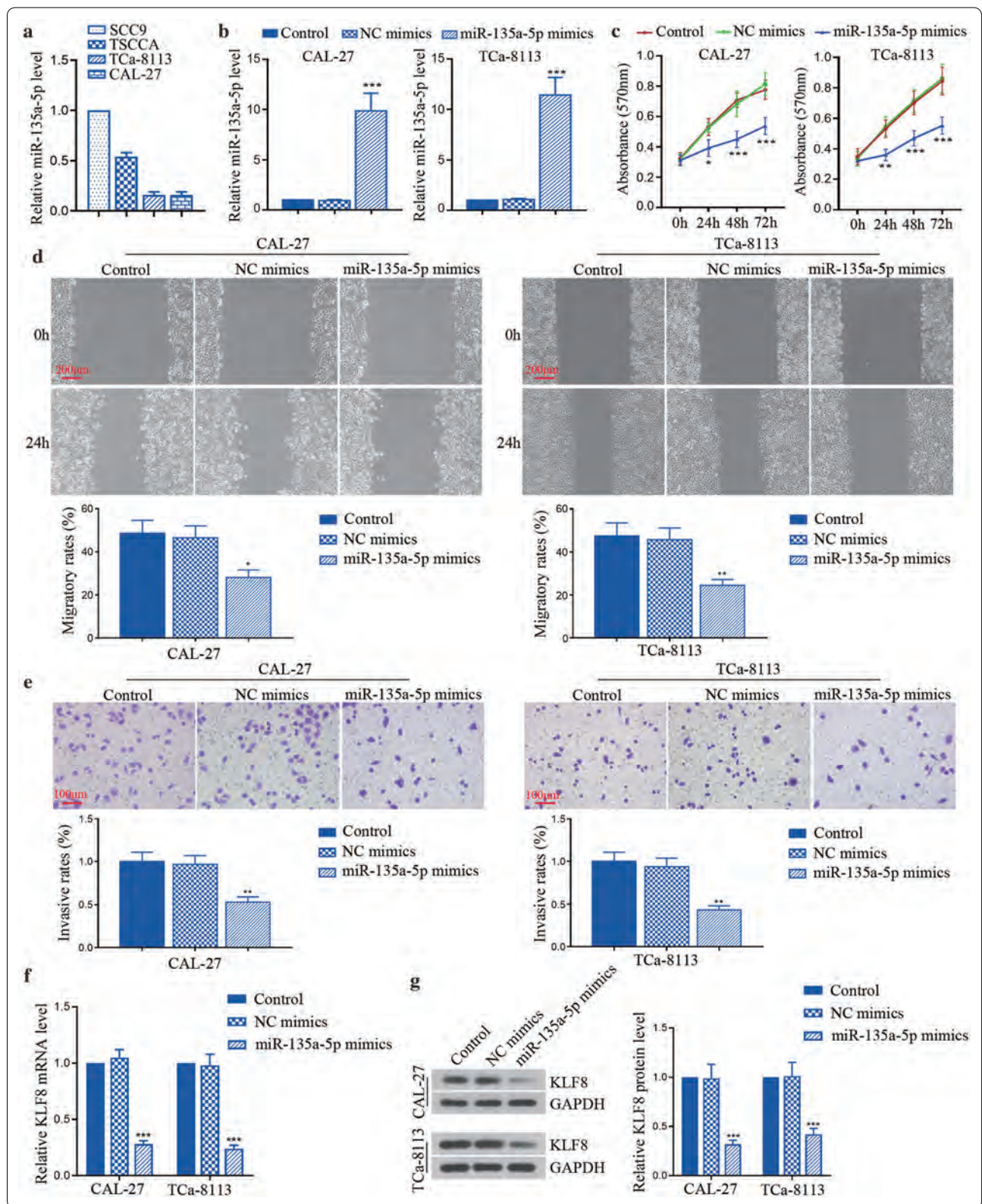
To test the role of DANCR in tumor growth in vivo, CAL-27 or TCa-8113 cells were stably transfected with shRNAs and injected subcutaneously into the right flank of axilla of nude mice. As shown in Fig. 7a, b, it showed

that the tumor size and weight could be suppressed by knockdown of DANCR. At molecular level, the expression of MMP-2 and MMP-9 in tumor tissues was also reduced by DANCR inhibition (Fig. 7c). In addition, as shown in Fig. 7d, e, both western blot and immunofluorescence staining demonstrated that a remarkable downregulation of KLF8 was induced in tumor tissues stably transfected with DANCR shRNA. Overall, these in vivo results show that DANCR may activate the expression of KLF8 and MMPs to affect TSCC tumor growth.

Discussion

Increasing lncRNAs have been revealed to be implicated in the development and progression of various cancers, including TSCC [7, 8, 22]. In this work, DANCR was showed to act as an oncogenic gene to facilitate the proliferation, migration and invasion of TSCC cells through the loss or gain of DANCR. Furthermore, miR-135a-5p was demonstrated to be complementary with DANCR and negatively regulated by DANCR. Overexpression of miR-135a-5p prevented the malignant phenotypes of TSCC cells and reduced the expression of KLF8. Inhibition of miR-135a-5p mediated the protective effects of DANCR silence on TSCC cells. KLF8 was responsible for the regulatory role of miR-135a-5p through modulating MMP-2/9 expression.

Previous reports showed that lncRNA DANCR was high-expressed in esophageal cancer [23], liver cancer [10], colorectal cancer [24], prostate cancer [11], retinoblastoma [25] and so on, which indicated its potential correlation with the poor prognosis of patients. Evidence demonstrated that DANCR enhanced the migration and invasion of prostate cancer cells or gastric cancer cells through impeding TIMP2/3 expression [11] or lncRNA-LET [26]. Jiang et al. suggested that the initiation and progression of osteosarcoma was affected by DANCR via competitively binding to miR-33a-5p [27]. In NSCLC cells, DANCR was found to target miR-758-3p to regulate cell proliferation, migration and invasion [28]. However, up to now, the functional significance of DANCR in the progression of TSCC still requires to be clarified. In this study, the gain- and loss-of-function experiments showed that DANCR could enhance the proliferation, migration and invasion of TSCC cells. The in vivo results further demonstrated that inhibition of DANCR prevented
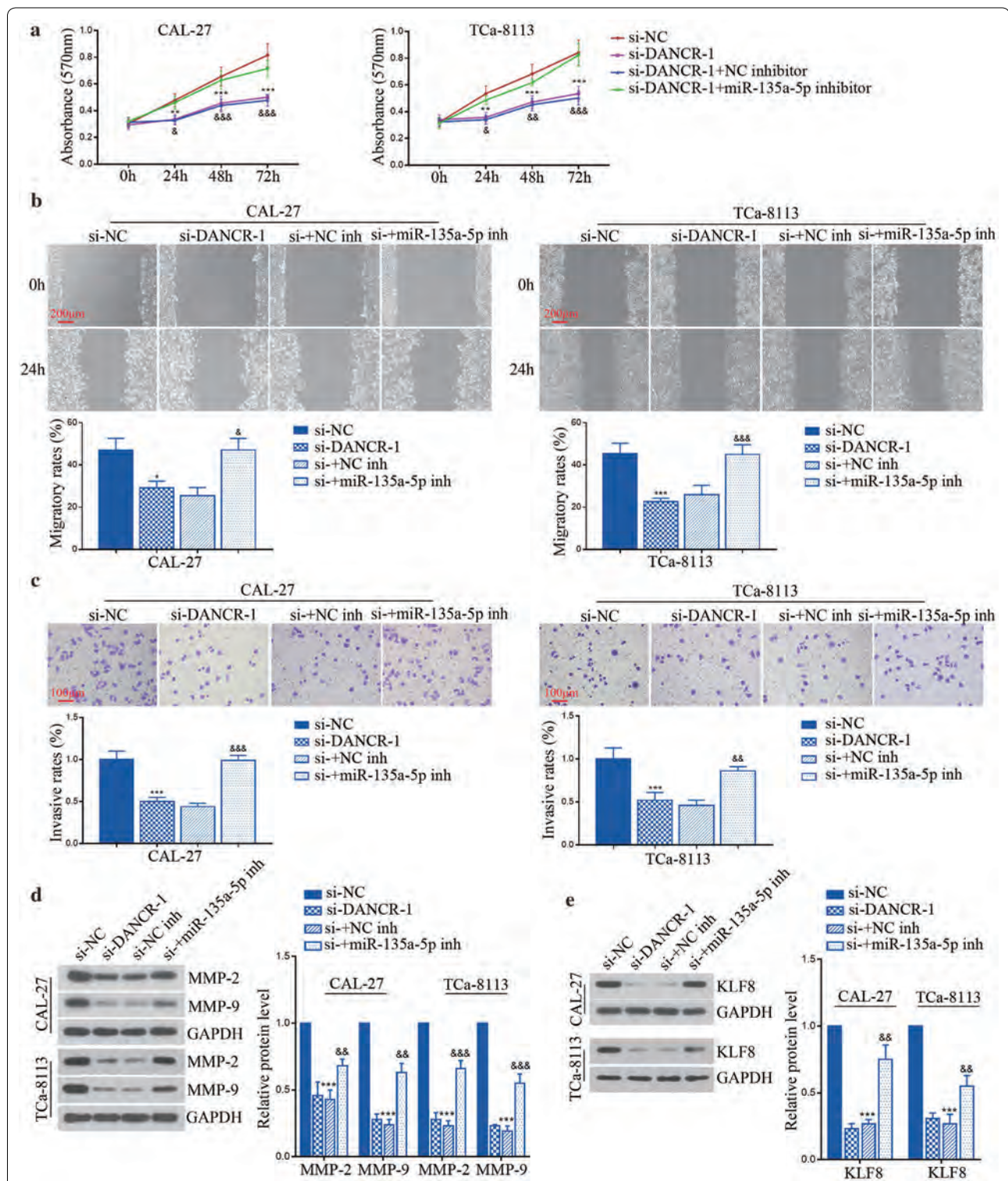
Zheng *et al. Cancer Cell Int*   (2019) 19:302

Page 9 of 14

Zheng *et al. Cancer Cell Int*   (2019) 19:302

Page 10 of 14

Fig. 5 DANCR knockdown repressed tumor cell progression and KLF8 expression by targeting miR-135a-5p in vitro. **a** The viability of CAL-27 and TCa-8113 cells was measured using MTT assay. **b**, **c** The migration and invasion of CAL-27 and TCa-8113 cells were detected by wound healing assay and transwell assay, respectively. **d** Relative expression of MMP-2 and MMP-9 protein was determined by western blot in CAL-27 and TCa-8113 cells. **e** Relative expression of KLF8 protein was detected using western blot in CAL-27 and TCa-8113 cells. *p < 0.05, **p < 0.01, ***p < 0.001, versus to si-NC; &p < 0.05, &&p < 0.01, &&&p < 0.001, versus to si-DANCR-1 + NC inhibitor
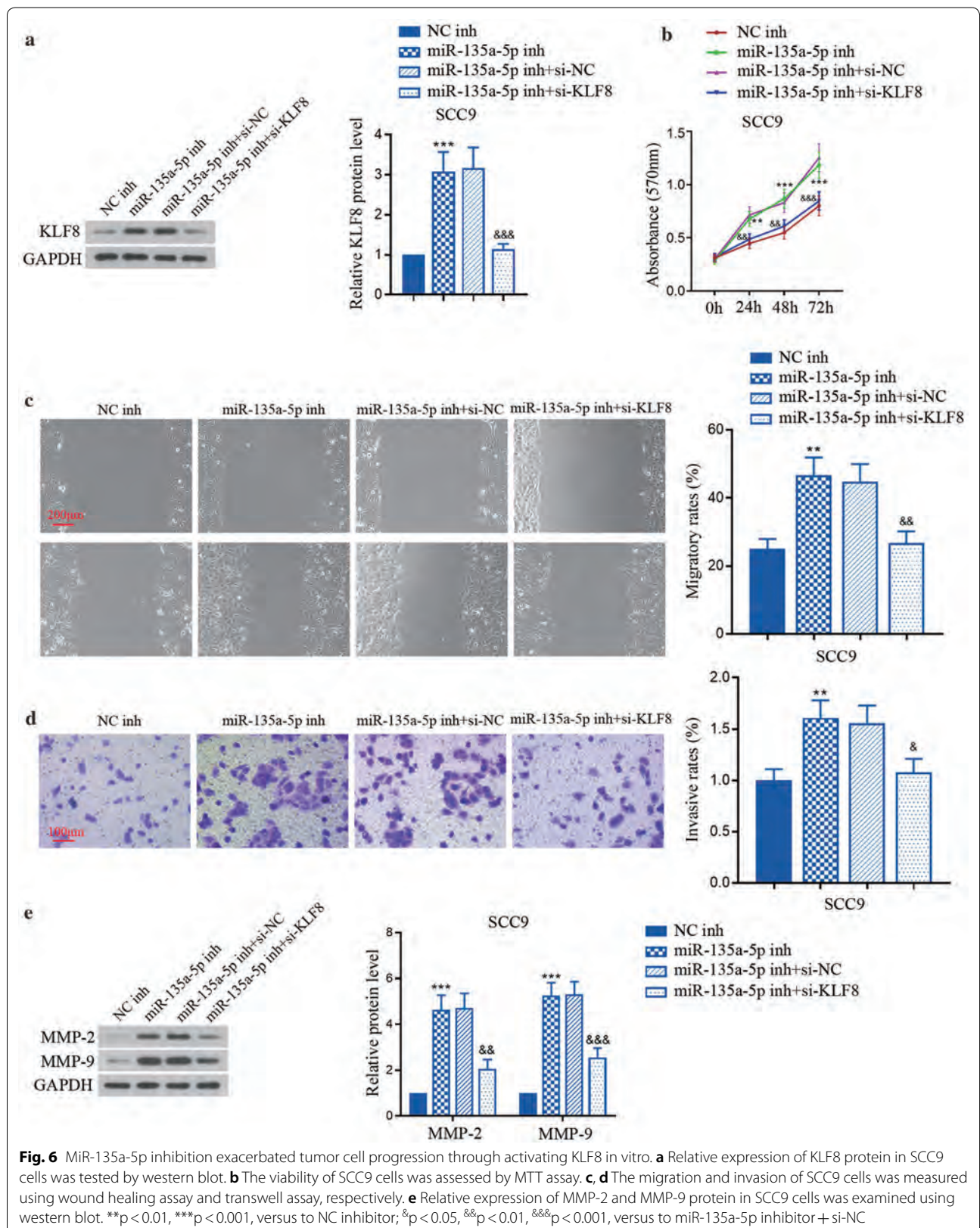
Fig. 6 MiR-135a-5p inhibition exacerbated tumor cell progression through activating KLF8 in vitro. **a** Relative expression of KLF8 protein in SCC9 cells was tested by western blot. **b** The viability of SCC9 cells was assessed by MTT assay. **c**, **d** The migration and invasion of SCC9 cells was measured using wound healing assay and transwell assay, respectively. **e** Relative expression of MMP-2 and MMP-9 protein in SCC9 cells was examined using western blot. **p < 0.01, ***p < 0.001, versus to NC inhibitor; &p < 0.05, &&p < 0.01, &&&p < 0.001, versus to miR-135a-5p inhibitor + si-NC

Zheng *et al. Cancer Cell Int* (2019) 19:302

Page 12 of 14
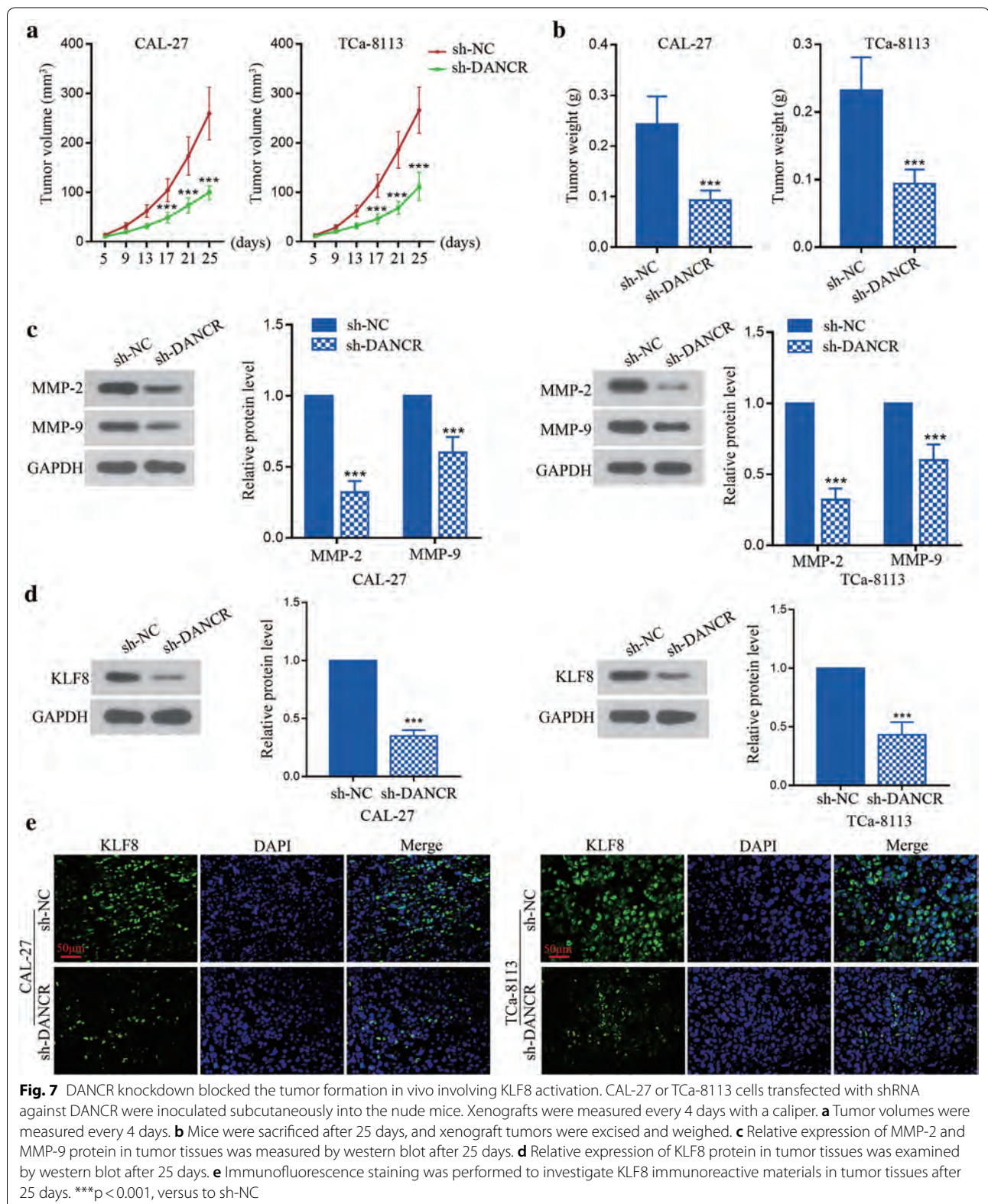
Fig. 7 DANCR knockdown blocked the tumor formation in vivo involving KLF8 activation. CAL-27 or TCa-8113 cells transfected with shRNA against DANCR were inoculated subcutaneously into the nude mice. Xenografts were measured every 4 days with a caliper. **a** Tumor volumes were measured every 4 days. **b** Mice were sacrificed after 25 days, and xenograft tumors were excised and weighed. **c** Relative expression of MMP-2 and MMP-9 protein in tumor tissues was measured by western blot after 25 days. **d** Relative expression of KLF8 protein in tumor tissues was examined by western blot after 25 days. **e** Immunofluorescence staining was performed to investigate KLF8 immunoreactive materials in tumor tissues after 25 days. ***p < 0.001, versus to sh-NC

Zheng *et al. Cancer Cell Int*   (2019) 19:302

Page 13 of 14

the tumor growth, which indicates the oncogenic role of DANCR in TSCC tumorigenesis.

To the best of our knowledge, this was the first report about the role of DANCR in the progression of TSCC. Emerging references suggested that lncRNAs might function as "sponge" of miRNAs to participate in multiple biological processes. For instance, lncRNA ZFAS1 activated the expression of ZEB1, MMP-14 and MMP-16 to promote tumor growth and metastasis by sponging miR-150 in hepatocellular carcinoma [29]. Wang et al. reported that DANCR facilitated ROCK1-mediated malignant biological behaviors through decoying both miR-335-5p and miR-1972 in osteosarcoma [30]. In this current study, functional experiments indicated that miR-135a-5p overexpression protected against the proliferation, migration and invasion of TSCC cells in vitro, which was showed to directly target DANCR. The inhibitory effects of DANCR silence on TSCC progress could be rescued by silencing miR-135a-5p. Altogether, this study shows that miR-135a-5p serves as a "sponge" miRNA of DANCR to prevent the progression of TSCC.

MiRNAs modulate gene transcription and expression by directly targeting the 3′ UTR of mRNAs, and lncRNAs may exhibit sponging effects on miRNAs during tumor progression. DANCR had been described to competitively bind miR-149 to positively regulate MSI2 expression and promote tumor malignant phenotypes in the pathogenesis of bladder cancer [31]. Although KLF8 expression was altered by DANCR and miR-135a-5p, whether KLF8 was the downstream effector of DANCR/miR-135a-5p to mediate the regulation of TSCC progression was not well understood. Knockdown of KLF8 attenuated the effect of miR-135a-5p inhibitor on TSCC cell proliferation, migration and invasion. More importantly, KLF8 was reported to be a direct target of miR-135a-5p to inhibit NSCLC cell migration, invasion and EMT process by Shi et al. [16]. Together, these results suggest that DANCR/miR-135a-5p axis affects the malignancies of TSCC by the regulation of KLF8.

In addition, MMP is a classical zinc-dependent endopeptidase to affect cell proliferation, angiogenesis, and tumor invasion and metastasis through the degradation of extracellular matrix [32, 33]. MMP-2 and MMP-9 had been demonstrated to be important prognostic biomarkers in diverse cancers, such as breast cancer, colorectal cancer, and NSCLC [34–36]. Considering that KLF8 was highlighted to bind the promoter of MMP-9 to induce its expression and stimulate cancer invasion [37, 38], thus we further examined the alterations of MMPs in the downstream of KLF8. Our data showed that the expression of MMP-9 and MMP-2 was altered by DANCR/miR-135a-5p/KLF8 axis, which just further proved the regulatory network on tumor malignancies from the

point of molecular level. Therefore, we conclude that DANCR serves as a "sponge" of miR-135a-5p to activate KLF8/MMP-2/9 signaling pathway, thus stimulating the development and progression of TSCC.

Conclusion

In conclusion, this present study develops a novel insight that the TSCC tumor progression may be regulated by DANCR/miR-135a-5p/KLF8 axis. To the best of our knowledge, DANCR is suggested to function as a diagnostic biomarker of TSCC for the first time, which may provide new therapeutic targets for the prevention and treatment of TSCC.

Author details
¹ Department of Orthodontics, School of Stomatology, China Medical University, 117 North Nanjing Street, Shenyang 110002, People's Republic of China. ² Department of Stomatology, Shengjing Hospital of China Medical University, Shenyang 110004, People's Republic of China.

References
1. Lydiatt DD, Robbins KT, Byers RM, Wolf PF. Treatment of stage I and II oral tongue cancer. Head Neck. 1993;15(4):308–12.

Zheng *et al. Cancer Cell Int*   (2019) 19:302

Page 14 of 14

2. Yuen AP, Lam KY, Chan AC, Wei WI, Lam LK, Ho WK, et al. Clinicopathological analysis of elective neck dissection for N0 neck of early oral tongue carcinoma. Am J Surg. 1999;177(1):90–2.

3. Siegel RL, Miller KD, Jemal A. Cancer statistics, 2019. CA Cancer J Clin. 2019;69(1):7–34.

4. Gibb EA, Brown CJ, Lam WL. The functional role of long non-coding RNA in human carcinomas. Mol Cancer. 2011;10:38.

5. Gupta RA, Shah N, Wang KC, Kim J, Horlings HM, Wong DJ, et al. Long non-coding RNA HOTAIR reprograms chromatin state to promote cancer metastasis. Nature. 2010;464(7291):1071–6.

6. Guttman M, Donaghey J, Carey BW, Garber M, Grenier JK, Munson G, et al. LincRNAs act in the circuitry controlling pluripotency and differentiation. Nature. 2011;477(7364):295–300.

7. Wang ZY, Hu M, Dai MH, Xiong J, Zhang S, Wu HJ, et al. Upregulation of the long non-coding RNA AFAP1-AS1 affects the proliferation, invasion and survival of tongue squamous cell carcinoma via the Wnt/beta-catenin signaling pathway. Mol Cancer. 2018;17(1):3.

8. Huang W, Cui X, Chen J, Feng Y, Song E, Li J, et al. Long non-coding RNA NKILA inhibits migration and invasion of tongue squamous cell carcinoma cells via suppressing epithelial–mesenchymal transition. Oncotarget. 2016;7(38):62520–32.

9. Kretz M, Webster DE, Flockhart RJ, Lee CS, Zehnder A, Lopez-Pajares V, et al. Suppression of progenitor differentiation requires the long noncoding RNA ANCR. Genes Dev. 2012;26(4):338–43.

10. Yuan SX, Wang J, Yang F, Tao QF, Zhang J, Wang LL, et al. Long noncoding RNA DANCR increases stemness features of hepatocellular carcinoma by derepression of CTNNB1. Hepatology. 2016;63(2):499–511.

11. Jia J, Li F, Tang XS, Xu S, Gao Y, Shi Q, et al. Long noncoding RNA DANCR promotes invasion of prostate cancer through epigenetically silencing expression of TIMP2/3. Oncotarget. 2016;7(25):37868–81.

12. Pan L, Liang W, Gu J, Zang X, Huang Z, Shi H, et al. Long noncoding RNA DANCR is activated by SALL4 and promotes the proliferation and invasion of gastric cancer cells. Oncotarget. 2018;9(2):1915–30.

13. Zhu J, Wang S, Liang Y, Xu X. Inhibition of microRNA-505 suppressed MPP+-induced cytotoxicity of SHSY5Y cells in an in vitro Parkinson's disease model. Eur J Pharmacol. 2018;835:11–8.

14. Tribollet V, Barenton B, Kroiss A, Vincent S, Zhang L, Forcet C, et al. MiR-135a inhibits the invasion of cancer cells via suppression of ERRα. PLoS ONE. 2016;11(5):e0156445.

15. Cheng Z, Liu F, Zhang H, Li X, Li Y, Li J, et al. MiR-135a inhibits tumor metastasis and angiogenesis by targeting FAK pathway. Oncotarget. 2017;8(19):31153–68.

16. Shi H, Ji Y, Zhang D, Liu Y, Fang P. MiR-135a inhibits migration and invasion and regulates EMT-related marker genes by targeting KLF8 in lung cancer cells. Biochem Biophys Res Commun. 2015;465(1):125–30.

17. Chen G, Yang W, Jin W, Wang Y, Tao C, Yu Z. Lentivirus-mediated gene silencing of KLF8 reduced the proliferation and invasion of gastric cancer cells. Mol Biol Rep. 2012;39(10):9809–15.

18. Lu H, Wang X, Urvalek AM, Li T, Xie H, Yu L, et al. Transformation of human ovarian surface epithelial cells by Kruppel-like factor 8. Oncogene. 2014;33(1):10–8.

19. Wang X, Zhao J. KLF8 transcription factor participates in oncogenic transformation. Oncogene. 2007;26(3):456–61.

20. Wang X, Zheng M, Liu G, Xia W, McKeown-Longo PJ, Hung MC, et al. Kruppel-like factor 8 induces epithelial to mesenchymal transition and epithelial cell invasion. Cancer Res. 2007;67(15):7184–93.

21. Wei H, Wang X, Gan B, Urvalek AM, Melkoumian ZK, Guan JL, et al. Sumoylation delimits KLF8 transcriptional activity associated with the cell cycle regulation. J Biol Chem. 2006;281(24):16664–71.

22. Yu J, Liu Y, Guo C, Zhang S, Gong Z, Tang Y, et al. Upregulated long non-coding RNA LINC00152 expression is associated with progression and poor prognosis of tongue squamous cell carcinoma. J Cancer. 2017;8(4):523–30.

23. Shi H, Shi J, Zhang Y, Guan C, Zhu J, Wang F, et al. Long non-coding RNA DANCR promotes cell proliferation, migration, invasion and resistance to apoptosis in esophageal cancer. J Thorac Dis. 2018;10(5):2573–82.

24. Liu Y, Zhang M, Liang L, Li J, Chen YX. Over-expression of lncRNA DANCR is associated with advanced tumor progression and poor prognosis in patients with colorectal cancer. Int J Clin Exp Pathol. 2015;8(9):11480–4.

25. Wang JX, Yang Y, Li K. Long noncoding RNA DANCR aggravates retinoblastoma through miR-34c and miR-613 by targeting MMP-9. J Cell Physiol. 2018;233(10):6986–95.

26. Mao Z, Li H, Du B, Cui K, Xing Y, Zhao X, et al. LncRNA DANCR promotes migration and invasion through suppression of lncRNA-LET in gastric cancer cells. Biosci Rep. 2017. https://doi.org/10.1042/BSR20171070.

27. Jiang N, Wang X, Xie X, Liao Y, Liu N, Liu J, et al. lncRNA DANCR promotes tumor progression and cancer stemness features in osteosarcoma by upregulating AXL via miR-33a-5p inhibition. Cancer Lett. 2017;405:46–55.

28. Wang S, Jiang M. The long non-coding RNA-DANCR exerts oncogenic functions in non-small cell lung cancer via miR-758-3p. Biomed Pharmacother. 2018;103:94–100.

29. Li T, Xie J, Shen C, Cheng D, Shi Y, Wu Z, et al. Amplification of long noncoding RNA ZFAS1 promotes metastasis in hepatocellular carcinoma. Cancer Res. 2015;75(15):3181–91.

30. Wang Y, Zeng X, Wang N, Zhao W, Zhang X, Teng S, et al. Long noncoding RNA DANCR, working as a competitive endogenous RNA, promotes ROCK1-mediated proliferation and metastasis via decoying of miR-335-5p and miR-1972 in osteosarcoma. Mol Cancer. 2018;17(1):89.

31. Zhan Y, Chen Z, Li Y, He A, He S, Gong Y, et al. Long non-coding RNA DANCR promotes malignant phenotypes of bladder cancer cells by modulating the miR-149/MSI2 axis as a ceRNA. J Exp Clin Cancer Res. 2018;37(1):273.

32. Zhao J, Guan JL. Signal transduction by focal adhesion kinase in cancer. Cancer Metastasis Rev. 2009;28(1–2):35–49.

33. Polette M, Nawrocki-Raby B, Gilles C, Clavel C, Birembaut P. Tumour invasion and matrix metalloproteinases. Crit Rev Oncol Hematol. 2004;49(3):179–86.

34. Dong H, Diao H, Zhao Y, Xu H, Pei S, Gao J, et al. Overexpression of matrix metalloproteinase-9 in breast cancer cell lines remarkably increases the cell malignancy largely via activation of transforming growth factor beta/SMAD signalling. Cell Prolif. 2019;52:e12633.

35. Fan L, Wu Y, Wang J, He J, Han X. Sevoflurane inhibits the migration and invasion of colorectal cancer cells through regulating ERK/MMP-9 pathway by up-regulating miR-203. Eur J Pharmacol. 2019;850:43–52.

36. Dong QZ, Wang Y, Tang ZP, Fu L, Li QC, Wang ED, et al. Derlin-1 is overexpressed in non-small cell lung cancer and promotes cancer cell invasion via EGFR–ERK-mediated up-regulation of MMP-2 and MMP-9. Am J Pathol. 2013;182(3):954–64.

37. Wang X, Lu H, Urvalek AM, Li T, Yu L, Lamar J, et al. KLF8 promotes human breast cancer cell invasion and metastasis by transcriptional activation of MMP9. Oncogene. 2011;30(16):1901–11.

38. Guo Y, Chen D, Su X, Chen J, Li Y. The lncRNA ELF3-AS1 promotes bladder cancer progression by interaction with Kruppel-like factor 8. Biochem Biophys Res Commun. 2019;508(3):762–8.

Publisher's Note

Springer Nature remains neutral with regard to jurisdictional claims in published maps and institutional affiliations.

The effects of HBXIP on the biological functions of tongue squamous cell carcinoma cells and correlation with PI3K/Akt

Xue Meng, Weixian Liu

Department of Oral and Maxillofacial Surgery, Shengjing Hospital of China Medical University, Shenyang 110004, China

Contributions: (I) Conception and design: All authors; (II) Administrative support: W Liu; (III) Provision of study materials or patients: W Liu; (IV) Collection and assembly of data: X Meng; (V) Data analysis and interpretation: X Meng; (VI) Manuscript writing: All authors; (VII) Final approval of manuscript: All authors.

Correspondence to: Prof. Weixian Liu. Department of Oral and Maxillofacial Surgery, Shengjing Hospital of China Medical University, 36# Sanhao Street, Heping District, Shenyang 110004, China. Email: liuwx@sj-hospital.org.

Background: Tongue squamous cell carcinoma (TSCC) is the most malignant oral cancer, having a high mortality rate.

Methods: The effects of hepatitis B X-interacting protein (HBXIP) overexpression on the proliferation, migration, and invasion of TSCC cells were measured by micro-culture tetrazolium assay (MTT) assay, transwell assay and scratch test, respectively, and the effects of HBXIP mRNA overexpression on the protein expression levels of AKT, p-AKT, PI3K, p-PI3K and S100A4 were detected by western blotting.

Results: MTT assay showed that there were significantly more proliferating cells than in the experimental group. In the scratch test and transwell assay, the migration rate and the number of invading cells were remarkably greater in the experimental group. The expression levels of p-AKT, p-PI3K and S100A4 were increased in the experimental group after HBXIP overexpression.

Conclusions: HBXIP mRNA overexpression can influence the proliferation, invasion, and migration of TSCC cells and promote their proliferation and migration by increasing the protein expression levels of p-AKT, p-PI3K and S100A4.

Keywords: Hepatitis B X-interacting protein (HBXIP); tongue squamous cell carcinoma (TSCC); biological function; PI3K/Akt; S100A4

Introduction

Tongue squamous cell carcinoma (TSCC) is one of the most common malignant tumors in the head and neck, accounting for 3% of all malignant tumors (1). It has high malignancy, easily develops early metastasis; its overall 5-year survival rate ranges between 45–55% (2), which has hardly changed during the past 30 years (3,4). Surgical treatment predominates, and the available adjuvant therapies include radiotherapy and chemotherapy. Although the surgical techniques have remained unchanged for many years, every doctor strives to improve the quality of surgery. A new study found that an ultrasonic coagulation device was effective in providing safe and adequate margins in operations for carcinoma tongue (5). Due to the lack of highly effective treatment options, most TSCC patients experience recurrence and metastasis after operation and those in the advanced stage have lower survival.

Hepatitis B X-interacting protein (HBXIP), an oncoprotein encoded by 91 amino acids, can decrease the activity of HBX by binding to the terminal C of HBX, thereby altering the replication cycle of hepatitis B virus (HBV) (6). Moreover, it can inhibit the transactivation of HBX by binding to the promoters or enhancers of

activator protein 1 and endogenous HBV, thereby affecting the replication cycle of HBV (7,8). It has been recently discovered that HBXIP mRNA expression is present in the myocardium, skeletal muscles and uteruses of human fetuses and mice, and HBXIP can promote the proliferation and migration of liver and breast cancer cells (9-15). There have been no reports on the correlation between HBXIP and TSCC or the mechanism thereof.

S100 calcium-binding protein A4 (S100A4), a gene closely related to tumor metastasis, is a member of the S100 calcium-binding protein family that interacts with other proteins in a calcium-dependent manner (16), and has a low molecular weight of 10–12 kDa (17,18). S100A4 is largely involved in diverse cellular functions, such as cell growth and differentiation, cell metabolism, cell cycle regulation, signal transduction and so on (19,20). Recent studies have suggested that S100A4 is associated with infiltration and metastasis in breast cancer, pancreatic cancer, colorectal cancer, bladder cancer, ovarian cancer, thyroid cancer and brain cancer (21-29), there only a few reports describing its relationship with TSCC (30,31). The phosphoinositide 3-kinase (PI3K)/ Akt signaling pathway plays an important role in the occurrence, development, and treatment of malignant tumors and participates in cellular growth, proliferation, and differentiation signaling pathways (32). Furthermore, PI3K/Akt phosphorylation can activate the aforementioned differentiation signaling pathway (33). This study aimed to explore the effects of HBXIP mRNA on the biological functions of TSCC cells and the possible mechanisms thereof. HBXIP may be a new target for treating TSCC.

Methods

Eukaryotic expression vector and cell strain

The eukaryotic expression vector pEGFP-N1, liposome 2000 and the TSCC cell line were purchased from the Cell Collection Center of Wuhan University (Wuhan, China).

Primer design

The primers designed for HBXIP nucleotide sequence (NM_006402) were: HBXIP-F, 5'-GGAGCAGCACT TGGAAGACA-3'; HBXIP-R, 5'-TCAGTGGGGTC AGAGGTTAG-3'. The primers designed for β-actin were: β-actin-F, 5'-CTTAGTTGCGTTACACC CTTTCTTG-3'; β-actin-R, 5'-CTGTCACCTTCAC CGTTCCAGTTT-3'. All primers were synthesized by

Shenyang Wanlei Biological Co., Ltd (Shenyang, China).

Reagents

RPMI-1640 culture medium was obtained from Gibco (Thermo Fisher Scientific, Waltham, MA, USA); fetal bovine serum (FBS) was obtained from HyClone Laboratories (Logan, UT, USA); the eukaryotic expression vector pEGFP-N1 and liposome 2000 were obtained from Invitrogen (Carlsbad, CA, USA); Super Moloney murine leukemia virus (M-MLV) reverse transcriptase was obtained from BioTeke (Beijing, China); RNA Simple Total RNA Kit and Total RNA Extraction Kit were obtained from Tiangen Biotech (Beijing, China); MTT reagent was obtained from Sigma-Aldrich (St. Louis, MO, USA); NP-40 lysis buffer, bicinchoninic acid (BCA) Protein Assay Kit and phenylmethylsulfonyl fluoride (PMSF) were obtained from Beyotime Biotechnology (Jiangsu, China); and electrochemiluminescence (ECL) luminescence reagent from 7sea Biotech (Shanghai, China).

Cell culture

TSCC cells were cultured with RPMI-1640 culture medium containing 10% FBS, 100 U/mL penicillin and 100 μg/mL streptomycin sulfate in a 37 ℃, 5% CO_2 incubator.

Construction of the eukaryotic expression vector

The eukaryotic expression vector pEGFP-N1-HBXIP was constructed using HBXIP mRNA as the template and by embedding pEGFP-N1 using recombination. pEGFP-N1-HBXIP was transfected into competent cells and then positive clones were screened, followed by vector analysis using restriction endonucleases and sequencing.

Transient transfection

The pEGFP-N1-HBXIP plasmid was constructed by Shenyang Wanlei Biological Co., Ltd. TSCC cells were transiently transfected with pEGFP-N1-HBXIP plasmid to serve as the experimental group and with pEGFP-N1 to serve as the vector group, and untransfected cells served as the control group. The transfection procedure was performed using Lipofectamine2000 according to the manufacturer's instructions. Briefly, cells were passaged 24 h before transfection, the culture medium in the 6-well plate was replaced with the serum-free minimal culture medium to treat the cells for 1 h, and then the transfection was

conducted. Successful transfection was detected using an electronic microscope and immunofluorescence techniques. Forty-eight hours after transfection, the cells in various groups were collected from the 6-well plates for mRNA and protein analysis.

HBXIP mRNA and protein expression levels in TSCC cells (RT-PCR)

Total RNA was extracted from the transfection, non-transfection and vector groups with TRIzol reagent, and its concentration was measured by UV spectrophotometry. First-strand cDNA was synthesized with Super M-MLV reverse transcriptase, then PCR was performed using the cDNA as template, and the non-transfection and vector groups served as references. The PCR products were subjected to agarose gel electrophoresis and evenly stained with Gold View stain, and then the stained gel was photographed using a gel imaging system. The experiment was repeated three times, densitometry analysis was performed using Quantity One software, and the HBXIP mRNA expression levels were compared between the groups.

Effects of HBXIP overexpression on the growth of TSCC cells (MTT assay)

Twenty-four hours after transfection, the cells from each group were counted and seeded into a 96-well plate at a density of 2×10^3 cells/well. Five replicate wells were seeded per group, and zeroing wells (culture medium, MTT, and DMSO) were added. Then, the cells were cultured in a 37 ℃, 5% CO_2 incubator for 24, 48, 72 or 96 h, and an MTT assay was performed. MTT (0.2 mg/mL) was added to the appropriate wells at the corresponding time points and then the plates were incubated in a 37 ℃ incubator for 4 h. After the supernatant was carefully removed 200 µL DMSO were added to dissolve the purple crystals formed by cells, and the optimal density (OD) was measured at 490 nm by a microplate reader. The measurement was repeated five times and the measurement results were averaged for analysis.

Scratch test

Twenty-four hours after transfection, the cells from each group were enumerated and seeded into 3 replicate wells of a 6-well plate at a density of 2×10^3 cells/well. After vertically scratching the monolayers with a 200 µL pipette tip, serum-free culture medium was added and the cells were cultured

in a 37 ℃, 5% CO_2 incubator for 16 h. The cells were then photographed; the photography and distance measurements were repeated three times at 0 h and at 16 h, and the results were averaged for analysis.

Transwell assay

Twenty-four hours after transfection, the cells in each group were enumerated and diluted with serum-free culture medium at a ratio of 1:10, then suspensions of 100 µL Matrigel and 100 µL cells were added into the upper chamber of a Transwell insert in a 24-well plate. After 24 h culture in the 37 ℃, 5% CO_2 incubator, the cells were removed from the upper chamber, the membrane was excised, and cells adhering to the bottom surface of the membrane were detected. The experiment was repeated five times and the results were averaged for analysis.

Western blotting

The protein expression levels of HBXIP, AKT, p-AKT, PI3K, p-PI3K and S100A4 were determined in each group. NP-40 lysis buffer was thawed at room temperature in advance and then mixed into PMSF to a final dilution of 1% for use. The cells were added to the corresponding volume of NP-40 lysis buffer and vortexed to suspend the cells. The cell suspension was then incubated on ice for 5 min and centrifuged at 12,000 rpm and 4 ℃ for 10 min, and the supernatant was collected for quantitative analysis. Total protein (40 µg) was subjected to 10% SDS-PAGE electrophoresis and then transferred onto a PVDF membrane. The PVDF membrane was blocked with 5% (M/V) skim milk powder and incubated at room temperature for 2 h; thereafter, it was incubated with primary antibody overnight at 4 ℃ and washed with TTBS. Next, it was incubated with donkey anti-goat IgG-HRP (HBXIP) or goat anti-rabbit IgG-HRP (AKT, p-AKT, PI3K, p-PI3K, and S100A4) at 37 ℃ for 45 min, washed with TTBS, then exposed to enhanced ECL reagent and developed in a dark room. The experiment was repeated three times, the films were scanned, and the optical densities (ODs) of target bands were analyzed using a gel image processing system (Gel-Pro-Analyzer software, Beijing Liuyi Biotechnology CO., WD-9413B).

Statistical analysis

SPSS 18.0 statistical software was used for analysis, and the data are presented as x±s. Inter-group comparisons were performed using the Student's *t*-test. P<0.05 indicated that a
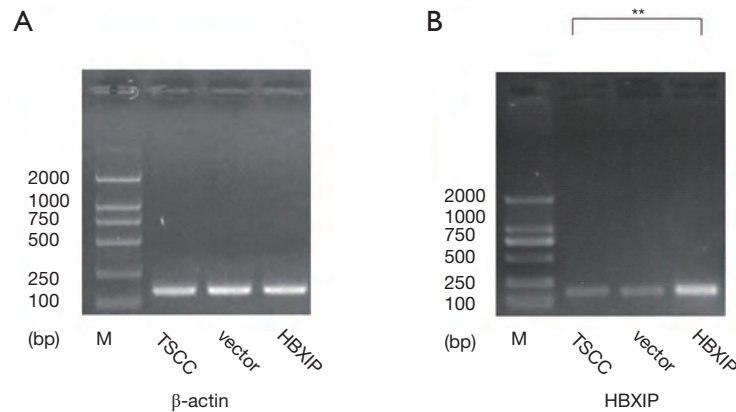
Figure 1 Expression of HBXIP mRNA in the experiment and control groups. (A) The expression of β-actin mRNA in three groups; (B) The mRNA level of HBXIP was examined by RT-PCR analysis after overexpression in three groups. **, P<0.01 *vs.* control groups. Student's *t*-test. HBXIP: transfection group, TSCC cells were transfected with pEGFP-N1-HBXIP; vector, vector group, TSCC cells with pEGFP-N1 only; TSCC: non-transfection group, only with non-transfected TSCC cells. TSCC, tongue squamous cell carcinoma cells; HBXIP, hepatitis B X-interacting protein.
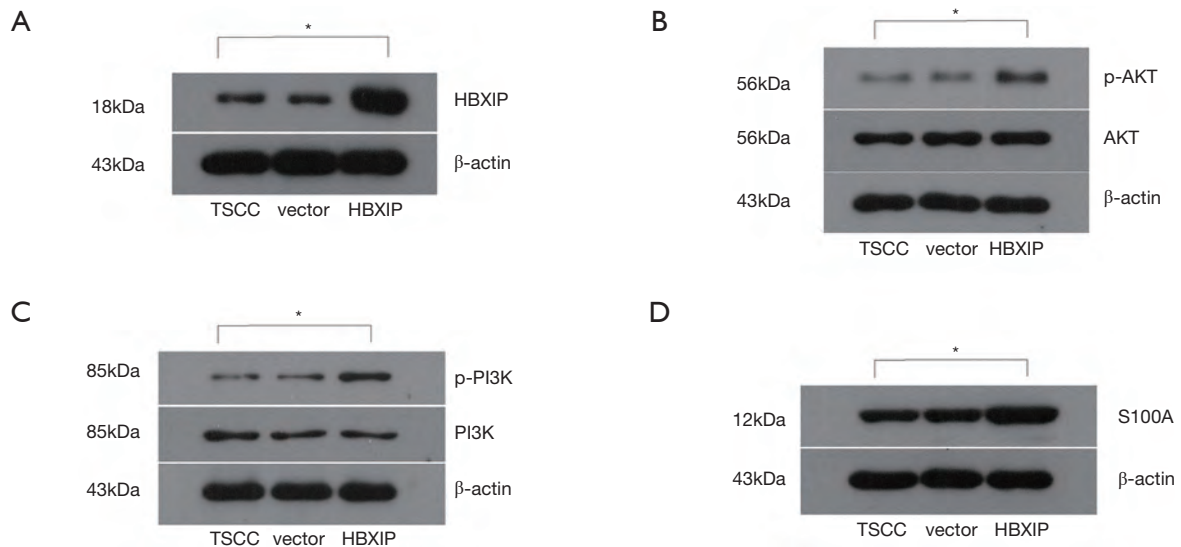
Figure 2 Protein expression of HBXIP, AKT, p-AKT, PI3K, p-PI3K and S100A4 by western blotting. (A) Protein expression of HBXIP in the experiment and control groups after HBXIP overexpression. (B) Protein expression of AKT and p-AKT. (C) Protein expression of PI3K and p-PI3K. (D) Protein expression of S100A4. *, P<0.05 *vs.* control groups. Student's *t*-test. HBXIP. HBXIP, hepatitis B X-interacting protein.

difference was statistically significant.

Results

HBXIP expression in TSCC cells

The PCR results showed that HBXIP expression was detected in the experimental group and the control groups (vector group and non-transfection group), the relative expressions were 3.01, 0.96 and 1.00, respectively, the difference was statistically significant (P<0.01, *Figure 1*). HBXIP expression was also detected by western blotting, and its relative expression level was 3.51 in the experimental group, which represented a statistically significant difference from the control groups (0.88, 1.00) (P<0.01, *Figure 2*).
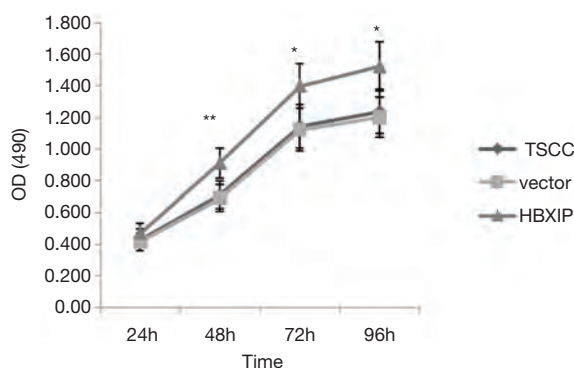
Figure 3 Cell proliferation in the experiment and control groups at 24, 48, 72, and 96 h by MTT assay. The y-axis represents the OD value and the x-axis represents time. Cell growth was determined via MTT assay at 24, 48, 72, and 96 h. *, P<0.05 and **, P<0.01 vs. control groups. Student's t-test. Each experiment was repeated five times, the average value was determined. OD, optimal density; MTT, micro-culture tetrazolium.
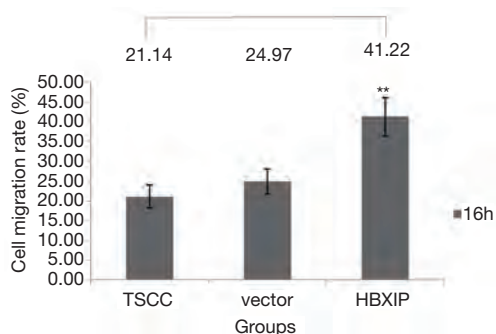

Figure 4 The cell migration rates in the experiment and control groups at 16 h by scratch test. The y-axis represents the cell migration rate and the x-axis represents the experiment and control groups. Cell migration was determined via scratch test at 16 h. **, P<0.01 vs. control groups. Student's t-test. Each experiment was repeated three times, the average value was determined.

The effects of HBXIP mRNA overexpression on the proliferation of TSCC cells

The cell proliferation rate in the experimental group and the control groups were detected via MTT assay. After each experiment was repeated five times, the average value was determined. The results showed that, at 24, 48, 72, and 96 h after transfection, the OD average value was 0.472±0.059, 0.911±0.094, 1.400±0.142, and 1.522±0.156, respectively,

in the experimental group (*Figure 3*). The vector group (0.415±0.054, 0.691±0.082, 1.122±0.135, 1.202±0.125) and untransfected group (0.429±0.068, 0.710±0.087, 1.143±0.138, 1.238±0.142), respectively, in the control groups; at 48, 72 and 96 h, the difference between the experimental and control groups was statistically significant (P<0.05).

Effects of HBXIP mRNA overexpression on the migration of TSCC cells

The results of the scratch test indicated that, after 16 h of observation, the cell migration average rates in the experimental group (transfection group), the vector control group and the non-transfection control group were 41.22±4.80, 24.97±3.10 and, 21.14±2.95, respectively; the differences among the three groups were statistically significant (P<0.01) (*Figures 4,5*). After each experiment was repeated three times, the average value was determined.

Effects of HBXIP mRNA overexpression on the invasion of TSCC cells

As shown by the results of the Transwell assay, the average numbers of invading cells in the experimental group (transfection group), the vector control group and the non-transfection control group after 24 h of observation were 137.60±14.01, 91.00±10.84 and 92.00±9.70, respectively; the differences between the experimental and the control groups were statistically significant (P<0.001) (*Figures 6,7*). After each experiment was repeated five times, the average value was determined.

Effects of HBXIP mRNA overexpression on the PI3K/Akt signaling pathway (Western blotting)

The protein expression levels of HBXIP, AKT, p-AKT, PI3K, p-PI3K, and S100A4 in the experimental and control groups were detected by western blotting. The results of the relative protein expression demonstrated that HBXIP protein expression was significantly higher after HBXIP mRNA overexpression than before transfection; after HBXIP mRNA overexpression, the relative protein expression levels of p-AKT, p-PI3K and S100A4 in the experimental group were 1.60, 2.46 and 1.72, which were all increased, and the differences were statistically significant
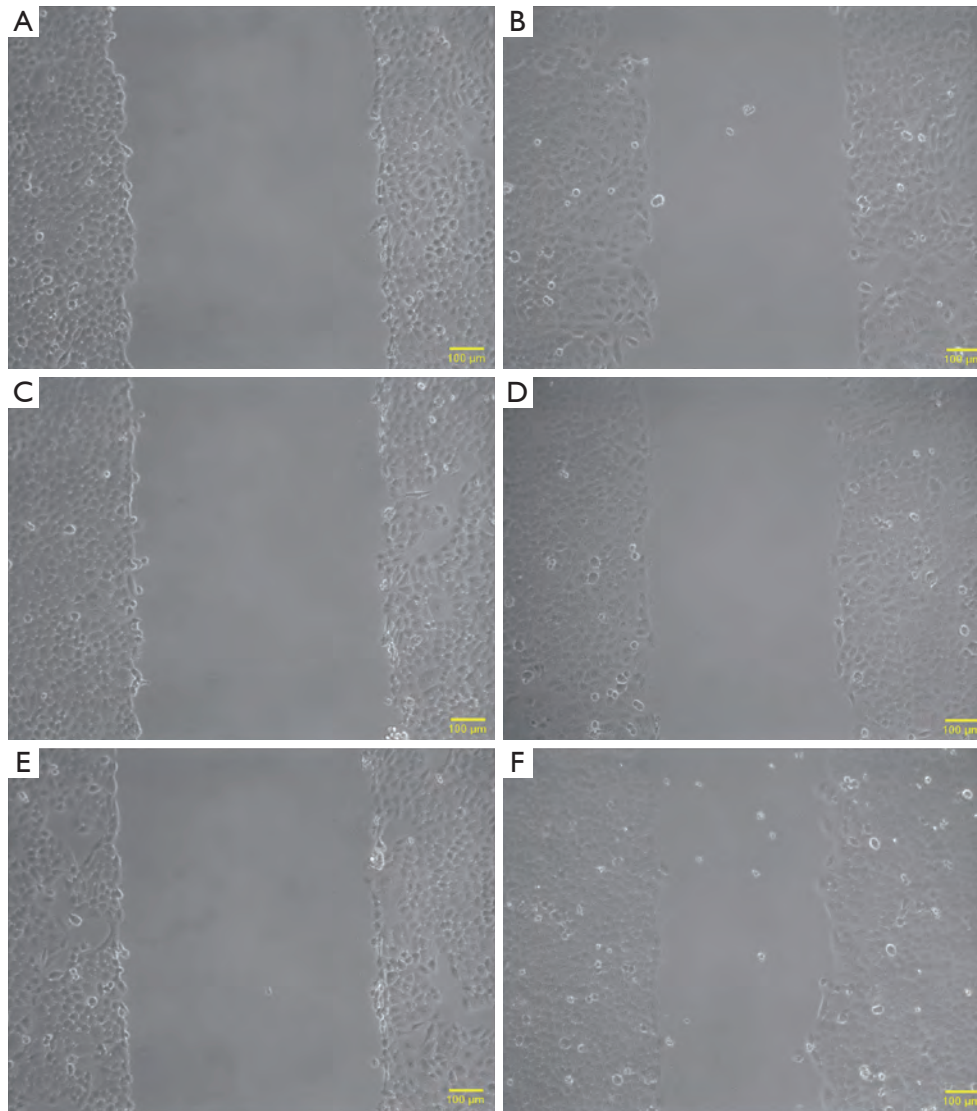
Figure 5 Comparison of cell migration between the experiment group and the control groups using an electronic microscope. (A) Control group (non-transfection group), 0 h; (B) control group (non-transfection group), 16 h; (C) control group (vector group), 0 h; (D) control group (vector group), 16 h; (E) experiment group (transfection group), 0 h; (F)** experiment group (transfection group), 16 h. Student's *t*-test. **, P<0.01 *vs.* control groups. Each experiment was repeated three times, the average value was determined.

(P<0.05) (*Figure 2*).

Discussion

HBXIP was first cloned from HepG2 cells by Melegari *et al.* in 1998 (6). Previous studies have shown that HBXIP can promote the proliferation and migration of tumor cells via various pathways and mechanisms, and that it plays a role in regulating the cell cycle and forming protein complexes. It

may be a candidate molecular prognostic marker for ESCC (34-36).

In our preliminary study, we detected HBXIP protein in several cell lines derived from oral and maxillofacial tumors and found that it was expressed at a low level in the TSCC cell line. Based on this preliminary study, the present study aimed to further clarify the effects of HBXIP on TSCC cells and to specifically investigate the effects of HBXIP mRNA overexpression on the proliferation, invasion, and metastasis
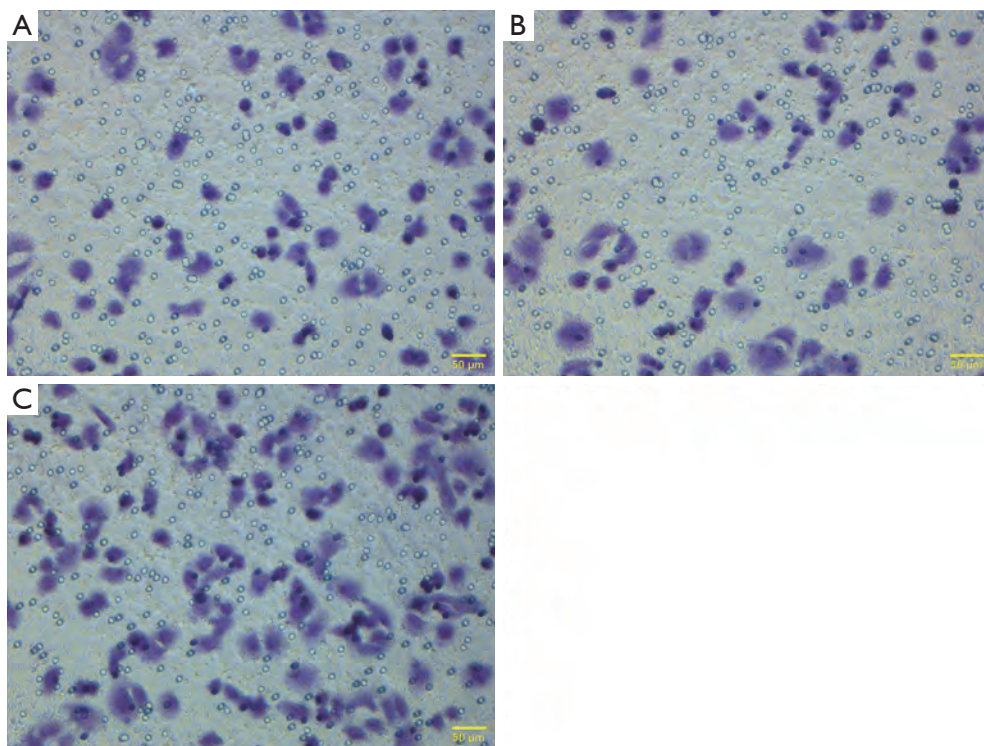
Figure 6 Comparison of cell invasion between the experimental group and control groups in the transwell test. (A) Control group (non-transfection group); (B) control group (vector group); (C)** experiment group (transfection group). **, P<0.001 *vs.* control groups. Each experiment was repeated five times, the average value was determined. Diff-Quick stain.
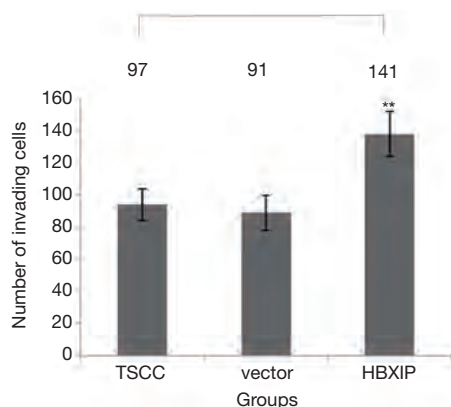

Figure 7 Comparison of the numbers of invading cells between the experiment group and the control groups at 24 h. The y-axis represents the number of invading cells and the x-axis represents the experiment and control groups. The number of invading cells was determined by transwell test after 24 h. **, P<0.001 *vs.* control groups. Student's *t*-test. Each experiment was repeated five times, the average value was determined.

of TSCC cells and on the PI3K/Akt signaling pathway. In the present study, plasmid construction and cell transfection were first performed, and then the cells were divided into the experimental group (transfected with pEGFP-N1-HBXIP), the control group (non-transfected) and the vector control group (transfected with pEGFP-N1). HBXIP expression was determined by RT-PCR in the experimental and control groups, and the ability of HBXIP to promote TSCC cell proliferation was measured via MTT assay, which showed that HBXIP overexpression could promote cell proliferation. Furthermore, the ability of HBXIP to promote the migration and invasion of TSCC cells was detected by scratch test and transwell assay, respectively, and the results suggested that HBXIP overexpression could promote cell migration and invasion. The above findings indicate that HBXIP overexpression can facilitate the biological behaviors (proliferation, migration, and invasion) of TSCC cells. Some studies have demonstrated that HBXIP promotes the proliferation and migration of breast

cancer cells, pancreatic cancer, and also oral squamous cell carcinoma by regulating S100A4 expression (17,21,37). In this study, HBXIP enhanced cell migration by increasing S100A4 protein expression.

Since the gene regulatory process in cells is a complex, dynamic network, we tried to identify the mechanisms by which HBXIP regulates PI3K/Akt. HBXIP was able to active AKT signaling in HepG2 cells (32). Wang found that activation of the PI3K/Akt signaling pathway is involved in S100A4 and induces viability and migration in colorectal cancer cells (37). The PI3K/Akt signaling pathway is activated by AKT phosphorylation; total AKT protein is constant in cells, and only its phosphorylation level varies. AKT is the core effector of the PI3K/Akt signaling pathway, while PI3K is an important upstream protein that plays a role in several biological processes, including cell metabolism, cell cycle regulation, cell growth, and apoptosis. In this study, we detected the protein expression levels of AKT, p-AKT, PI3K and p-PI3K by western blotting and found an remarkable increase in phosphorylation; the differences were statistically significant. These findings reveal that HBXIP overexpression can promote the phosphorylation of AKT and PI3K, the activation of PI3K/Akt signaling pathway, and the biological activities of TSCC cells.

Collectively, our results indicate that HBXIP can influence the biological functions of TSCC cells by activating the PI3K/Akt signaling pathway via phosphorylation of pI3K and AKT and by inducing S100A4 protein expression. This study provides an important experimental foundation for the targeted treatment of TSCC.

Conclusions

HBXIP mRNA overexpression can influence the proliferation, invasion, and migration of TSCC cells and promote their proliferation and migration by increasing the protein expression levels of p-AKT, p-PI3K and S100A4.

Acknowledgments

Footnote

References

1. Wu Y, Wang J, Zhao J, et al. Gene regulation analysis of the effects of evodiamine on tongue squamous cell carcinoma. J Cell Biochem 2019;120:15933-40.
2. Jehn P, Dittmann J, Zimmerer R, et al. Survival Rates According to Tumour Location in Patients with Surgically Treated Oral and Oropharyngeal Squamous Cell Carcinoma. Anticancer Res 2019;39:2527-33.
3. Bray F, Ferlay J, Soerjomataram I, et al. Global cancer statistics 2018: GLOBOCAN estimates of incidence and mortality worldwide for 36 cancers in 185 countries. CA Cancer J Clin 2018;68:394-424.
4. Siegel RL, Miller KD, Jemal A. Cancer statistics, 2019. CA Cancer J Clin 2019;69:7-34.
5. Rao KN, Jagade M, Kale VD, et al. Margin Status and Duration of Surgery in Resection of Tongue Carcinoma with Ultrasound Coagulation Device: a Comparative Study. Indian J Surg Oncol 2018;9:501-4.
6. Melegari M, Scaglioni PP, Wands JR. Cloning and characterization of a novel hepatitis B virus x binding protein that inhibits viral replication. J Virol 1998;72:1737-43.

7. Fei H, Zhou Y, Li R, et al. HBXIP, a binding protein of HBx, regulates maintenance of the G2/M phase checkpoint induced by DNA damage and enhances sensitivity to doxorubicin-induced cytotoxicity. Cell Cycle 2017;16:468-76.

8. Rawat S, Bouchard MJ. The hepatitis B virus (HBV) HBx protein activates AKT to simultaneously regulate HBV replication and hepatocyte survival. J Virol 2015;89:999-1012.

9. Liu BW, Wang TJ, Li LL, et al. Oncoprotein HBXIP induces PKM2 via transcription factor E2F1 to promote cell proliferation in ER-positive breast cancer. Acta Pharmacol Sin 2019;40:530-8.

10. Al-Anazi MR, Nazir N, Colak D, et al. Deletion and Functional Analysis of Hepatitis B Virus X Protein: Evidence for an Effect on Cell Cycle Regulators. Cell Physiol Biochem 2018;49:1987-98.

11. Fei HR, Li ZJ, Ying Z, et al. HBXIP regulates etoposide-induced cell cycle checkpoints and apoptosis in MCF-7 human breast carcinoma cells. Gene 2018;647:39-47.

12. Wang Y, Fang R, Cui M, et al. The oncoprotein HBXIP up-regulates YAP through activation of transcription factor c-Myb to promote growth of liver cancer. Cancer Lett 2017;385:234-42.

13. Li H, Wang Z, Jiang M, et al. The oncoprotein HBXIP promotes human breast cancer growth through down-regulating p53 via miR-18b/MDM2 and pAKT/MDM2 pathways. Acta Pharmacol Sin 2018;39:1787-96.

14. Cheng ST, Ren JH, Cai XF, et al. HBx-elevated SIRT2 promotes HBV replication and hepatocarcinogenesis. Biochem Biophys Res Commun 2018;496:904-10.

15. Zhang W, Lu Z, Kong G, et al. Hepatitis B virus X protein accelerates hepatocarcinogenesis with partner survivin through modulating miR-520b and HBXIP. Mol Cancer 2014;13:128.

16. Fei F, Qu J, Li C, et al. Role of metastasis-induced protein S100A4 in human non-tumor pathophysiologies. Cell Biosci 2017;7:64.

17. Natarajan J, Hunter K, Mutalik VS, et al. Overexpression of S100A4 as a biomarker of metastasis and recurrence in oral squamous cell carcinoma. J Appl Oral Sci 2014;22:426-33.

18. Huang S, Zheng J, Huang Y, et al. Impact of S100A4 Expression on Clinicopathological Characteristics and Prognosis in Pancreatic Cancer: A Meta-Analysis. Dis Markers 2016;2016:8137378.

19. Ambartsumian N, Klingelhöfer J, Grigorian M. The Multifaceted S100A4 Protein in Cancer and Inflammation.

20. Qu S, Wu J, Bao Q, et al. Osterix promotes the migration and angiogenesis of breast cancer by upregulation of S100A4 expression. J Cell Mol Med 2019;23:1116-27.

21. Zhou Y, Li Z, Ding Y, et al. Overexpression of S100A4 protein may be associated with the development and progression of pancreatic cancer. J Cancer Res Ther 2018;14:S159-66.

22. Fei F, Qu J, Zhang M, et al. S100A4 in cancer progression and metastasis: A systematic review. Oncotarget 2017;8:73219-39.

23. Tahara S, Nojima S, Ohshima K, et al. S100A4 accelerates the proliferation and invasion of endometrioid carcinoma and is associated with the "MELF" pattern. Cancer Sci 2016;107:1345-52.

24. Lv Y, Niu Z, Guo X, et al. Serum S100 calcium binding protein A4 (S100A4, metatasin) as a diagnostic and prognostic biomarker in epithelial ovarian cancer. Br J Biomed Sci 2018;75:88-91.

25. Zhang Q, Zhao Z, Ma Y, et al. Combined expression of S100A4 and Annexin A2 predicts disease progression and overall survival in patients with urothelial carcinoma. Urol Oncol 2014;32:798-805.

26. Yan W, Chen J, Chen Z, et al. Deregulated miR-296/S100A4 axis promotes tumor invasion by inducing epithelial-mesenchymal transition in human ovarian cancer. Am J Cancer Res 2016;6:260-9.

27. Jin T, Zhang Z, Yang XF, et al. S100A4 expression is closely linked to genesis and progression of glioma by regulating proliferation, apoptosis, migration and invasion. Asian Pac J Cancer Prev 2015;16:2883-7.

28. Zhai X, Zhu H, Wang W, et al. Abnormal expression of EMT-related proteins, S100A4, vimentin and E-cadherin, is correlated with clinicopathological features and prognosis in HCC. Med Oncol 2014;31:970.

29. Zhang K, Liu X, Hao F, et al. Targeting TGF-β1 inhibits invasion of anaplastic thyroid carcinoma cell through SMAD2-dependent S100A4-MMP-2/9 signalling. Am J Transl Res 2016;8:2196-209.

30. Ma L, Chen Y, Han R, et al. Benzyl isothiocyanate inhibits invasion and induces apoptosis via reducing S100A4 expression and increases PUMA expression in oral squamous cell carcinoma cells. Braz J Med Biol Res 2019;52:e8409.

31. Hu FW, Lee SS, Yang LC, et al. Knockdown of S100A4 impairs arecoline-induced invasiveness of oral squamous cell carcinomas. Oral Oncol 2015;51:690-7.

32. Shi H, Fang R, Li Y, et al. The oncoprotein HBXIP

Methods Mol Biol 2019;1929:339-65.

suppresses gluconeogenesis through modulating PCK1 to enhance the growth of hepatoma cells. Cancer Lett. 2016;382:147-56.

33. Cerniglia GJ, Dey S, Gallagher-Colombo SM, et al. The PI3K/Akt Pathway Regulates Oxygen Metabolism via Pyruvate Dehydrogenase (PDH)-E1α Phosphorylation. Mol Cancer Ther 2015;14:1928-38.

34. You X, Liu F, Zhang T, et al. Hepatitis B virus X protein upregulates Lin28A/Lin28B through Sp-1/c-Myc to enhance the proliferation of hepatoma cells. Oncogene 2014;33:449-60.

35. Zhou XL, Zhu CY, Wu ZG, et al. The oncoprotein

HBXIP competitively binds KEAP1 to activate NRF2 and enhance breast cancer cell growth and metastasis. Oncogene 2019;38:4028-46.

36. Xia H, Ma L, Li J, et al. Elevated HBXIP expression is associated with aggressive phenotype and poor prognosis in esophageal squamous cell carcinoma. Am J Cancer Res 2017;7:2190-8.

37. Wang H, Duan L, Zou Z, et al. Activation of the PI3K/Akt/mTOR/p70S6K pathway is involved in S100A4-induced viability and migration in colorectal cancer cells. Int J Med Sci 2014;11:841-9.

Transl Cancer Res 2020;9(5):3375-3384 | http://dx.doi.org/10.21037/tcr-19-2102

BP180 Is a Prognostic Factor in Head and Neck Squamous Cell Carcinoma

XUE MENG[1,2,3,4], FUMIHIKO MATSUMOTO[2], TAISUKE MORI[5,6], NAMI MIURA[1,4],
YOSHINORI INO[6], KAORU ONIDANI[1], KENYA KOBAYASHI[7], YUSUKE MATSUZAKI[1,4],
SEIICHI YOSHIMOTO[7], KATSUHISA IKEDA[2] and KAZUFUMI HONDA[1,4]

[1]Department of Biomarkers for Early Detection of Cancer,
National Cancer Center Research Institute, Tokyo, Japan;
[2]Department of Otorhinolaryngology, Juntendo University Faculty of Medicine, Tokyo, Japan;
[3]Department of Oral and Maxillofacial Surgery,
Shengjing Hospital of China Medical University, Shenyang, P.R. China;
[4]Department of Bioregulation, Graduate School of Medicine, Nippon Medical School, Tokyo, Japan;
[5]Department of Diagnostic Pathology, National Cancer Center Hospital, Tokyo, Japan;
[6]Division of Molecular Pathology, National Cancer Center Research Institute, Tokyo, Japan;
[7]Department of Head and Neck Surgery, National Cancer Center Hospital, Tokyo, Japan

Abstract. *Background/Aim: Prognosis plays a vital role in head and neck squamous cell carcinoma (HNSCC) patient management and decision-making. This study aimed to identify the role of BP180 as a prognostic factor in HNSCC. Patients and Methods: Protein expression of bullous pemphigoid antigen II (BP180) was verified by immunohistochemistry (IHC) in a tissue microarray study of 202 cases. Results: IHC analysis revealed that protein expression of BP180 among HNSCC patients differed significantly in the presence and absence of neural invasion, and according to T status in laryngeal and pharyngeal cancer subgroups. Overall survival and multivariate analysis showed that positive BP180-IHC and advanced clinical stage were significant independent positive predictors of mortality in HNSCC patients. In addition, in the oral cancer subgroup, independent positive predictors were positive BP180-IHC, advanced N status and neural invasion. In laryngeal and pharyngeal cancer subgroups, predictors were positive BP180-IHC and advanced clinical stage. Conclusion: BP180 is a prognostic factor in head and neck squamous cell carcinoma.*

Correspondence to: Kazufumi Honda, Department of Bioregulation, Graduate of Medicine, Nippon Medical School, 1-1-5 Sendagi Bunkyo-ku, Tokyo 113-8603, Japan. Tel: +81 358146835, Fax: +81 358146879, e-mail: k-honda@nms.ac.jp

Head and neck cancer was reported as the 7th most common cancer worldwide in 2018, and the vast majority of malignant head and neck cancers are head and neck squamous cell carcinomas (HNSCCs) (1). Squamous cell carcinoma (SCC) affects the oral cavity, nasopharynx, oropharynx, hypopharynx and larynx. Early-stage patients with stage I or II disease can be cured with surgery alone and/or adjuvant therapies, improving long-term survival rates in approximately 70-90% of patients (2). About 60% of HNSCC patients present with stage III or IV disease (3). Such locally advanced disease shows high malignancy, easily develops early metastasis, and carries a poor prognosis with an overall 5-year survival rate below 50%. This pathology also displays a local recurrence rate of 15-40% and frequent distant metastasis (4).

Bullous pemphigoid antigen II (BP180; also called collagen XVII, BPA-2 or BPAg2) is not only an epithelial transmembrane protein, but also a hemidesmosome transmembrane adhesion molecule, and likely participates in keratinocyte-matrix interactions in both physiological and pathological conditions (5, 6). The intracellular domain contains binding sites for plectin, integrin b4, and BP230 (7). Hemidesmosomes are adhesion complexes connecting keratin intermediate filaments of stratified and complex epithelia to extracellular matrix components (EMCs) (8, 9). EMCs are responsible for cell communications, adhesion and proliferation, and has also been recognized as playing key roles in both progression and tumor initiation (10). Aberrant expression of BP180 has been reported in many malignant tumors, such as skin (11, 12), esophageal (13), oral (14), pancreatic (11, 15), colorectal (16, 17), lung (18-20), cervical (12, 21, 22), breast (21, 23), nasopharyngeal (24) and

1089

salivary gland cancer (25, 26). A murine monoclonal antibody designated NCC-Lu-226 [immunoglobulin (Ig) G1, K] was obtained from NCC (National Cancer Center, Tokyo, Japan) has been used in previous studies that found aberrant expression of BP180 in solar keratosis, Bowen's disease, invasive skin squamous cell carcinoma, lung squamous cell carcinoma, esophageal squamous cell carcinoma and cervix squamous cell carcinoma (13). According to recent research using BP180 overexpression and knock-out models, this protein is presumed to play roles in cell migration and differentiation under pathological conditions (5, 7). Although many cancers are reportedly associated with BP180, clinical prognostic relationships have not yet been described.

This study evaluated protein expression levels of BP180 immunohistochemically using tissue microarrays (TMAs) for 202 surgical specimens of HNSCC and normal squamous epithelium. In addition, data on prognosis were analyzed using data for overall survival (OS), disease-free survival (DFS) and multivariate analysis. This study may contribute to understanding the prognostic influence of BP180 in malignant phenotypes of HNSCC.

Patients and Methods

Patients and tissue samples. This study investigated 202 tumor specimens from 202 patients who underwent surgical resection with curative intention for head and neck carcinoma at the National Cancer Center Hospital (Tokyo, Japan) between 2006 and 2016. Clinicopathological records were retrospectively reviewed. In this cohort, median follow-up of the 202 patients was 34 months (range=2-74 months). Formalin-fixed paraffin-embedded tissue specimens of the 202 HNSCCs were collected according to the World Health Organization classification (4th edition) (27) of HNSCC (Table I). All study protocols were approved by the ethics committee of the National Cancer Center (approval #2013-247).

TMA construction. TMAs were prepared from formalin-fixed, paraffin-embedded pathological blocks as previously described (28). The blocks were sectioned at a thickness of 4 μM and subjected to immunohistochemical analyses.

Immunohistochemistry (IHC). Serial 4-μM-thick sections were incubated with the mouse monoclonal anti-human BP180 antibody established by our laboratory (collagen XVII) [1:1000, NCC-Lu-226 (immunoglobulin (Ig) G1, K), National Cancer Center Research Institute, Tokyo, Japan] (13) using the Ventana DABMap detection kit and automated slide stainer (Discovery XT) (Ventana Medical Systems, Tucson, AZ, USA) (29, 30). Head and neck normal tissues stained positively for BP180 antibody were recognized as controls. Expression levels of BP180 protein were used to classify two groups. The first was a BP180-negative group in which no tumor cells were stained with BP180 antibody, tumor cells were stained at weaker intensity compared with normal tissue staining, or some tumor cells were more intense compared with normal tissue staining, but comprised less than 10% of the tumor cell area. The other was a BP180-positive group, comprised all other findings. Staining patterns were evaluated by two independent investigators

Table I. *Baseline characteristics of HNSCC patients with positive/negative IHC staining for BP180.*

	Number of cases (%)	BP180 IHC		p-Value
		Negative	Positive	
Total	202	79 (39.1)	123 (60.9)	
Age, years				
Median (range)	68.0 (29-95)			0.387
<68	94 (46.5)	40	54	
≥68	108 (53.5)	39	69	
Gender				0.058
Male	156 (77.2)	67	89	
Female	46 (22.8)	12	34	
Smoking status				0.248
No	90 (44.6)	31	59	
Yes	112 (55.4)	48	64	
Drinking status				0.146
No	114 (56.4)	50	64	
Yes	88 (43.6)	29	59	
Disease				0.643#
Oral cancer	98 (48.5)	25 (25.5)	73 (74.5)	0.084#
Tongue cancer	58 (59.2)	11 (19.0)	47 (81.0)	
Mouth floor cancer	12 (12.2)	2 (16.7)	10 (83.3)	
Gingival cancer	17 (17.3)	8 (47.1)	9 (52.9)	
Others	11 (11.3)	4 (36.4)	7 (63.6)	
Laryngeal cancer	14 (6.9)	8 (57.1)	6 (42.9)	
Oropharyngeal cancer	42 (20.8)	20 (47.6)	22 (52.4)	
Hypopharyngeal cancer	41 (20.3)	20 (48.8)	21 (51.2)	
Other	7 (3.5)	6 (85.7)	1 (14.3)	

IHC: Immunohistochemistry; HNSCC: head and neck squamous cell cancer; BP180: also known as collagen XVII, BPA-2 or BPAg2; #Fisher's exact test.

blinded to clinical information. Representative staining patterns are shown in Figure 1.

Statistical analysis. SPSS version 23.0 statistical software (IBM, Armonk, NY, USA) was used for analysis. Values of $p < 0.05$ were taken as indicating statistically significant results. Significant differences were detected using Student's *t*-test, Pearson's chi-square test or Fisher's exact test. OS and DFS were measured as the period from surgery to date of death or recurrence as estimated by the Kaplan–Meier log-rank test. Uni- and multivariate analyses were performed by Cox proportional regression hazard modeling.

Results

Protein expression of BP180 and baseline characteristics in HNSCC patients. Examples of positive expression of BP180 in HNSCC are shown in Figure 1. BP180-positive staining was evident in tumor cell membranes and faintly in the cytoplasm (Figure 1C, D, F, G), and also as linear staining along the basement membrane in normal tissues (Figure 1H, I). BP180-positive cases usually showed aberrant non-basal expression, such as immunoreaction mainly restricted to the peripheral cells of tumor nests and the invasive front (Figure

1090
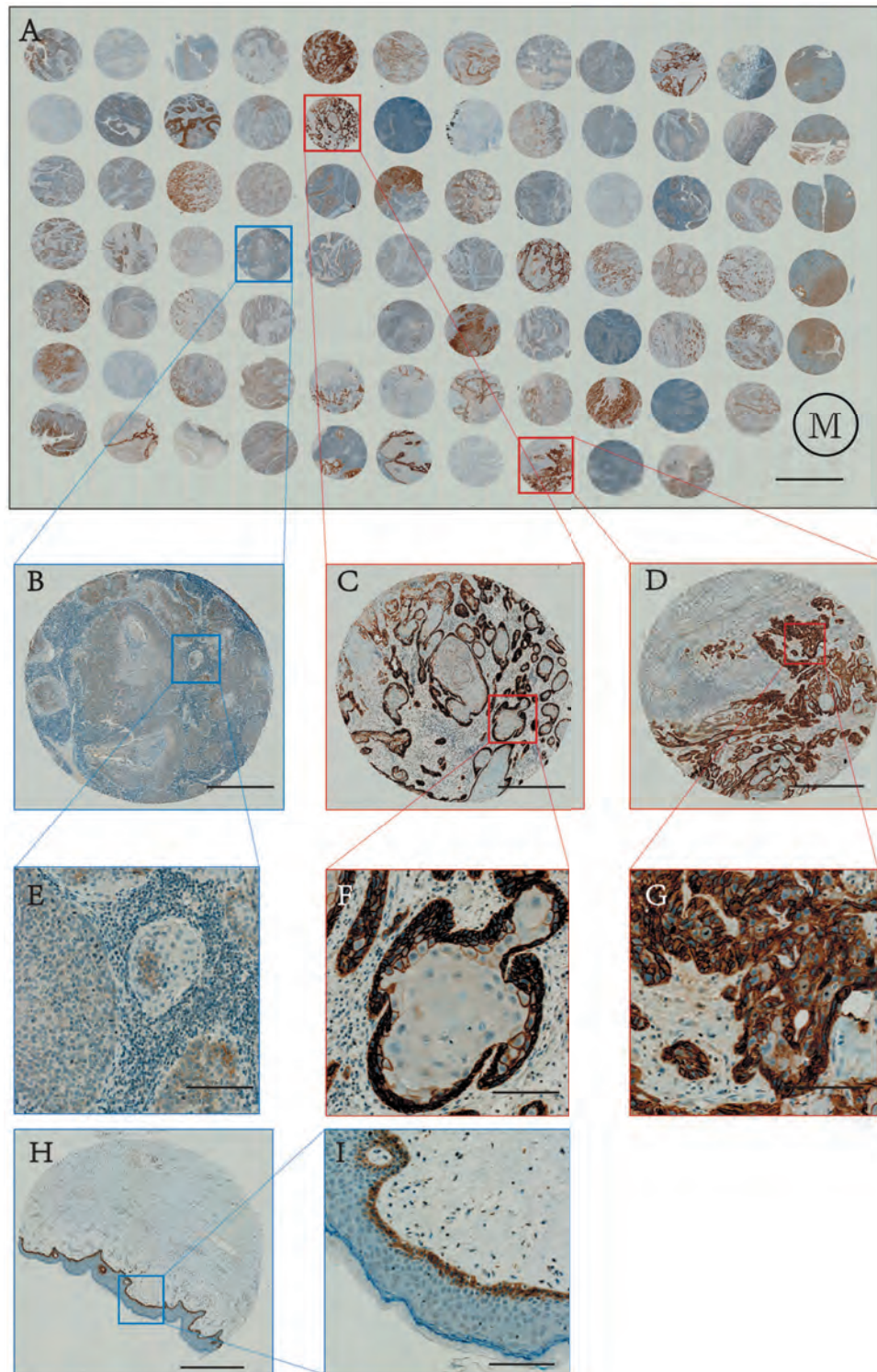
Figure 1. *Immunohistochemistry of BP180 protein expression. A) Representative BP180 protein expression in one HNSCC TMA slide (bar, 5 mm). M, TMA slide marker. B, E) Representative negative expressions of BP180 (bars: 500 μm in B, 100 μm in E). C, D, F, G) Representative positive expressions of BP180 (F: immunoreaction restricted to peripheral cells of cancer nest; G: immunoreaction at invasion front; bars: 500 μm in C and D, 100 μm in F and G). H, I) Representative BP180 protein expression in normal tissue as a positive control (linear staining along basement membrane; bars: 500 μm in H, 100 μm in I).*

1091

Table II. *Association between BP180 IHC status and clinicopathological characteristics in HNSCC patients.*

	Number of cases (%)	BP180 IHC		*p*-Value
		Negative	Positive	
Total	202	79 (39.1)	123 (60.9)	
Clinical stage[a]				0.440
I, II	63 (31.2)	22	41	
III, IV	139 (68.8)	57	82	
N status				1.000
N0	105 (52.0)	41	64	
N1, N2, N3	97 (48.0)	38	59	
T status				0.885
T1, T2	108 (53.5)	43	65	
T3, T4	94 (46.5)	36	58	
Lymphatic invasion				0.301
Absent	123 (60.9)	52	71	
Present	79 (39.1)	27	52	
Neural invasion				0.025*
Absent	156 (77.2)	68	88	
Present	46 (22.8)	11	35	
Vascular invasion				0.925
Absent	98 (48.5)	38	60	
Present	104 (51.5)	41	63	

IHC: Immunohistochemistry; HNSCC: head and neck squamous cell cancer; BP180: also known as collagen XVII, BPA-2 or BPAg2; [a]According to the International Union Against Cancer (UICC) TNM Classification of Malignant Tumors, 7th edition; *$p<0.05$.

Table III. *Association between BP180 IHC status and clinicopathological characteristics in OSCC patients.*

	Number of cases (%)	BP180 IHC		*p*-Value
		Negative	Positive	
Total	98	25 (25.5)	73 (74.5)	
Age, years				
Median (range)	70 (29-95)			0.490
<70	48 (49.0)	14	34	
≥70	50 (51.0)	11	39	
Gender				0.812
Male	64 (65.3)	17	47	
Female	34 (34.7)	8	26	
Smoking status				0.639
No	57 (58.2)	16	41	
Yes	41 (41.8)	9	32	
Drinking status				0.141
No	65 (66.3)	20	45	
Yes	33 (33.7)	5	28	
Clinical stage				1.000
I, II	43 (43.9)	11	32	
III, IV	55 (56.1)	14	41	
N status				0.129
N0	70 (71.4)	21	49	
N1-N3	28 (28.6)	4	24	
T status				0.163
T1, T2	59 (60.2)	12	47	
T3, T4	39 (39.8)	13	26	
Lymphatic invasion				0.129
Absent	70 (71.4)	21	49	
Present	28 (28.6)	4	24	
Neural invasion				0.195
Absent	71 (72.4)	21	50	
Present	27 (27.6)	4	23	
Vascular invasion				0.154
Absent	62 (63.3)	19	43	
Present	36 (36.7)	6	30	

IHC: Immunohistochemistry; OSCC: oral squamous cell carcinoma; BP180: also known as collagen XVII, BPA-2 or BPAg2.

1F, G). In BP180-negative cases, either no tumor cells or less than 10% of tumor cells were stained (Figure 1B, E).

Clinical characteristics of the 202 enrolled HNSCC patients (46 females, 156 males) are shown in Table I. Median age was 68 years (range=29-95 years). In the overall cohort, 79 patients (39.1%) were BP180-negative and 123 (60.9%) were BP180-positive. One hundred and twelve patients (55.4%) were smokers, defined as those currently smoking >20 packs/year of cigarettes. 88 patients were drinkers (43.6%), defined as those currently drinking >10 bottles/week. Rates of BP180 positivity in head and neck cancer types, comprising oral, laryngeal, oropharyngeal and hypopharyngeal cancer, were 74.5% (73/98), 42.9% (6/14), 52.4% (22/42) and 51.2% (21/41), respectively (Table I). In the oral squamous cell carcinoma (OSCC) subgroup, rates of BP180 positivity for tongue cancer and mouth floor cancer were 81.0% (47/58) and 83.3% (10/12), higher than for other anatomical localizations of HNSCC. No significant associations were observed between baseline characteristics of HNSCC patients and BP180 positivity.

Association between BP180 IHC and clinicopathological characteristics in HNSCC patients. IHC was conducted to detect BP180 expression in 202 HNSCC patients. Correlations

between clinicopathological characteristics and BP180 expression are summarized in Table II. A significant difference was observed in neural invasion in HNSCC (*p*=0.025) (Table II), but not in clinical stage, N status, T status, lymphatic invasion or vascular invasion. The HNSCCs studied could be classified into two broad subgroups: OSCC (comprising tongue, mouth floor and gingival cancer), and laryngeal/pharyngeal cancer (comprising laryngeal, oropharyngeal and hypopharyngeal cancer). The rate of BP180 positivity in the OSCC group was 74.5% (73/98), higher than that in laryngeal and pharyngeal cancers 50.5% (49/97) (Tables III and IV). In the laryngeal and pharyngeal cancer subgroup, a significant difference in the status of BP180 IHC was observed according to T status (*p*=0.026) (Table IV). However, the OSCC subgroup showed no significant associations in the status of BP180 IHC.

1092

Table IV. *Association between BP180 IHC status and clinicopathological characteristics in laryngeal and pharyngeal cancer patients.*

	Number of cases (%)	BP180 IHC		*p*-Value
		Negative	Positive	
Total	97	48 (49.5)	49 (50.5)	
Age, years				
Median (range)	68 (42-87)			1.000
<68	48 (49.5)	24	24	
≥68	49 (50.5)	24	25	
Gender				0.199
Male	86 (88.7)	45	41	
Female	11 (11.3)	3	8	
Smoking status				0.511
No	30 (30.9)	13	17	
Yes	67 (69.1)	35	32	
Drinking status				0.156
No	45 (46.4)	26	19	
Yes	52 (53.6)	22	30	
Clinical stage				0.803
I, II	19 (19.6)	10	9	
III, IV	78 (80.4)	38	40	
N status				0.664
N0	30 (30.9)	16	14	
N1-N3	67 (69.1)	32	35	
T status				0.026*
T1, T2	47 (48.5)	29	18	
T3, T4	50 (51.5)	19	31	
Lymphatic invasion				0.545
Absent	47 (48.5)	25	22	
Present	50 (51.5)	23	27	
Neural invasion				0.286
Absent	80 (82.5)	42	38	
Present	17 (17.5)	6	11	
Vascular invasion				0.830
Absent	32 (33.0)	15	17	
Present	65 (67.0)	33	32	

IHC: Immunohistochemistry; BP180: also known as collagen XVII, BPA-2 or BPAg2. **p*<0.05.

Hazard ratios (HRs) for death in HNSCC patients. We calculated HRs for the same factors, including age (median, 68 years), sex, smoking status, drinking status, clinical stage, BP180 positivity, N status, T status, lymphatic invasion, neural invasion and vascular invasion using uni- and multivariate Cox regression analysis.

Univariate Cox regression analyses revealed clinical stage [HR=2.644; 95% confidence interval (CI)=1.444-4.843], BP180 positivity (HR=2.508; 95%CI=1.463-4.300), N status (HR=1.987; 95%CI=1.236-3.194), T status (HR=1.656; 95%CI=1.036-2.645), lymphatic invasion (HR=1.701; 95%CI=1.060-2.729), neural invasion (HR=2.288; 95%CI=1.385-3.778) and vascular invasion (HR=1.730; 95%CI=1.071-2.794) as factors significantly associated with risk of mortality. All significant factors

from univariate analyses were entered into multivariate analysis. Multivariate Cox regression analysis indicated clinical stage (HR=2.854; 95%CI=1.558-5.228) and BP180 positivity (HR=2.690; 95%CI=1.569-4.609) remained as significant risk factors for death (Table V).

In the OSCC subgroup, univariate Cox regression analysis showed significant differences in clinical stage, BP180 positivity, N status, smoking status, neural invasion and vascular invasion. Multivariate analysis revealed BP180 positivity (HR=3.936; 95%CI=1.283-12.076), N status (HR=2.492; 95%CI=1.172-5.297) and neural invasion (HR=2.173; 95%CI=1.010-4.675) as prognostic factors for death in OSCC patients (Table VI). In the laryngeal and pharyngeal cancer subgroup, univariate Cox regression analysis, significant differences were found for BP180 positivity (HR=2.146; 95%CI=1.085-4.234) and clinical stage (HR=3.370; 95%CI=1.032-11.005). Multivariate analysis revealed BP180 positivity (HR=2.184; 95%CI=1.103-4.322) and clinical stage (HR=3.442; 95%CI=1.053-11.247) as significant risk factors for death (Table VII).

Prognostic significance of BP180 positivity in HNSCC patients. Kaplan–Meier analysis showed significant difference in OS and DFS in the 202 HNSCC patients, who were classified according to BP180 IHC positivity and negativity (*p*=0.0005, HR=2.317, 95%CI=1.443-3.720; *p*=0.020, HR=1.536, 95%CI=1.011-2.333; log-rank test) (Figure 2A, D). In the 98 OSCC subgroup of patients, the same positive results for OS and DFS were found (*p*=0.006, HR=3.700, 95%CI= 1.798-7.611; *p*=0.010, HR=2.349, 95%CI=1.270-4.343; log-rank test), respectively (Figure 2B, E). However, significant results for the 97 patients in the laryngeal and pharyngeal cancer subgroups were only observed in OS (*p*=0.024, HR=2.138, 95%CI=1.109-4.122; log-rank test), not in DFS (Figure 2C, F).

Prognostic significance of BP180 positivity in the late clinical stage. Clinical stages were divided into early (I+II) or late (III+IV). Further OS analysis was carried out in HNSCC patients, OSCC patients and laryngeal and pharyngeal cancer patients (Figure 3). All patient groups showed significant differences in OS between early and late clinical stages (*p*=0.0002, HR=2.967, 95%CI=1.773-4.966; *p*=0.015, HR=4.979, 95%CI=2.076-11.940; *p*=0.009, HR=2.511, 95%CI=1.263-4.989, respectively, log-rank test). In the OSCC subgroup, BP180-positive patients showed a high risk of death (HR=4.979) compared to others.

Five-year survival rates in HNSCC patients. In the present study HNSCC cohort, the mean 5-year overall survival (OS) rate for BP180-positive patients was 42.8±7.7%, lower than that for BP180-negative patients (69.0±7.3%). Compared with different subgroups, OSCC patients showed a slightly

1093

- 337-

Table V. *Clinicopathological factors and their effect on HNSCC patient mortality and overall survival (OS) by Cox proportional hazards regression modeling.*

	Univariate analysis			Multivariate analysis		
	HR	95%CI	*p*-Value	HR	95%CI	*p*-Value
Age (years)						
≥68 *vs.* <68	1.011	0.634-1.612	0.964			
Gender						
Male *vs.* Female	0.947	0.549-1.633	0.844			
Smoking status						
Yes *vs.* No	1.475	0.913-2.383	0.112			
Drinking status						
Yes *vs.* No	1.215	0.762-1.939	0.413			
Clinical stage						
III, IV *vs.* I, II	2.644	1.444-4.843	0.002**	2.854	1.558-5.228	0.001**
BP180 protein expression						
Positive *vs.* Negative	2.508	1.463-4.300	0.001**	2.690	1.569-4.609	<0.001**
N status						
N1-N3 *vs.* N0	1.987	1.236-3.194	0.005**			
T status						
T3, T4 *vs.* T1, T2	1.656	1.036-2.645	0.035*			
Lymphatic invasion						
Present *vs.* Absent	1.701	1.060-2.729	0.028*			
Neural invasion						
Present *vs.* Absent	2.288	1.385-3.778	0.001**			
Vascular invasion						
Present *vs.* Absent	1.730	1.071-2.794	0.025*			

HR: Hazard ratio; CI: confidence interval; HNSCC: head and neck squamous cell cancer; BP180: also known as collagen XVII, BPA-2 or BPAg2. Age 68 years was used as a cutoff because this was the median age. Values showing *p*<0.05 were entered into multivariate analysis. *p<0.05; **p<0.01.

Table VI. *Clinicopathological factors and their effects on OSCC patient mortality and overall survival (OS) by Cox proportional hazards regression modeling.*

	Univariate analysis			Multivariate analysis		
	HR	95%CI	*p*-Value	HR	95%CI	*p*-Value
Age (years)						
≥70 *vs.* <70	1.000	0.505-1.982	0.999			
Gender						
Male *vs.* Female	1.116	0.541-2.304	0.766			
Smoking status						
Yes *vs.* No	2.370	1.184-4.742	0.015*			
Drinking status						
Yes *vs.* No	1.606	0.803-3.210	0.180			
Clinical stage						
III, IV *vs.* I, II	2.338	1.108-4.935	0.026*			
BP180 protein expression						
Positive *vs.* Negative	4.267	1.413-12.882	0.010*	3.936	1.283-12.076	0.017*
N status						
N1-N3 *vs.* N0	3.437	1.709-6.910	0.001**	2.492	1.172-5.297	0.018*
T status						
T3, T4 *vs.* T1, T2	1.722	0.868-3.416	0.120			
Lymphatic invasion						
Present *vs.* Absent	1.790	0.858-3.736	0.121			
Neural invasion						
Present *vs.* Absent	3.226	1.580-6.587	0.001**	2.173	1.010-4.675	0.047*
Vascular invasion						
Present *vs.* Absent	2.035	1.012-4.093	0.046*			

HR: Hazard ratio; CI: confidence interval; OSCC: oral squamous cell cancer; BP180: also known as collagen XVII, BPA-2 or BPAg2. Age 70 years was used as a cutoff because this was the median age. Values showing *p*<0.05 were entered into multivariate analysis. *p<0.05; **p<0.01.

1094

Table VII. *Clinicopathological factors and their effects on laryngeal/pharyngeal cancer patient mortality and overall survival (OS) by Cox proportional hazards regression modeling.*

	Univariate analysis			Multivariate analysis		
	HR	95%CI	*p*-Value	HR	95%CI	*p*-Value
Age (years)						
≥68 *vs*. <68	0.926	0.480-1.785	0.818			
Gender						
Male *vs*. Female	0.478	0.198-1.154	0.101			
Smoking status						
Yes *vs*. No	0.829	0.413-1.662	0.596			
Drinking status						
Yes *vs*. No	1.258	0.654-2.423	0.491			
Clinical stage						
III, IV *vs*. I, II	3.370	1.032-11.005	0.044*	3.442	1.053-11.247	0.041*
BP180 protein expression						
Positive *vs*. Negative	2.146	1.085-4.243	0.028*	2.184	1.103-4.322	0.025*
N status						
N1-N3 *vs*. N0	1.157	0.569-2.354	0.687			
T status						
T3, T4 *vs*. T1, T2	1.783	0.911-3.491	0.091			
Lymphatic invasion						
Present *vs*. Absent	1.462	0.754-2.836	0.261			
Neural invasion						
Present *vs*. Absent	1.250	0.547-2.855	0.597			
Vascular invasion						
Present *vs*. Absent	1.227	0.591-2.546	0.583			

HR: Hazard ratio; CI: confidence interval; BP180: also known as collagen XVII, BPA-2 or BPAg2. Age 68 years was used as a cutoff because this was the median age. Values showing *p*<0.05 were entered into multivariate analysis. *p<0.05.

higher survival rate (57.5±6.8%) than laryngeal and pharyngeal cancer patients (52.1±6.7%). With clinical stage disease from I to IV, 5-year survival rates were 65.6±19.9%, 63.1±9.8%, 52.6±10.4% and 51.5±5.9%, respectively.

Discussion

In this retrospective study, BP180 (collagen XVII) was identified as a novel biomarker for predicting the prognosis of HNSCC, OSCC and laryngeal and pharyngeal cancer. To the best of our knowledge, this is the first study to investigate BP180 as an effective prognostic factor for HNSCC.

BP180 was identified as a prognostic factor in HNSCC, and BP180 expression was also closely associated with OS in HNSCC patients (*p*=0.0005), OSCC patients (*p*=0.006) and laryngeal and pharyngeal cancer patients (*p*=0.024). In particular, positive associations with OS were observed for the clinical late stage (III+IV) of these pathologies. Our findings show that BP180 is strongly predictive of tumor malignancy in HNSCC. BP180 was first found in bullous pemphigoid (BP), which is by far the most common autoimmune blistering dermatosis and mainly occurs in the elderly. BP180 is a transmembrane glycoprotein that acts as a significant

autoantigen and is highly immunodominant in BP (31). Our group first reported the relationship between BP180 expression and cancers in 1996 (13). Many studies have focused on the mechanisms of the relationship between BP180 and tumorigenesis, invasion and metastasis in different kinds of cancers, but no studies have investigated BP180 as a biomarker for cancer prognosis. However, many reports have examined the relationship between BP180 and prognosis of BP. In BP, patients with serum concentrations of BP180 autoantibodies ≥61 U/ml showed a 2.4-fold increase in the risk of early death compared with the general population (95%CI=1.81-3.81; *p*<0.0001) (32). Serum levels of IgG1 and IgG4 targeting BP180NC16A were both independent prognostic factors for early death from BP (33). In a retrospective study of BP in 74 young patients, higher expression of anti-BP180 autoantibodies represented a marker of poor prognosis (34). Another multicenter prospective cohort study showed high-titer anti-BP180 ELISA (enzyme-linked immunosorbent assay) score as a predictor of BP recurrence (35). These three studies (33-35) identified high expression of BP180 as a marker of poor prognosis. Such evidence provides some support for our conclusion about prognosis in HNSCC. DFS was also analyzed in our study, showing significant differences in the status of BP180 IHC in HNSCC and OSCC,
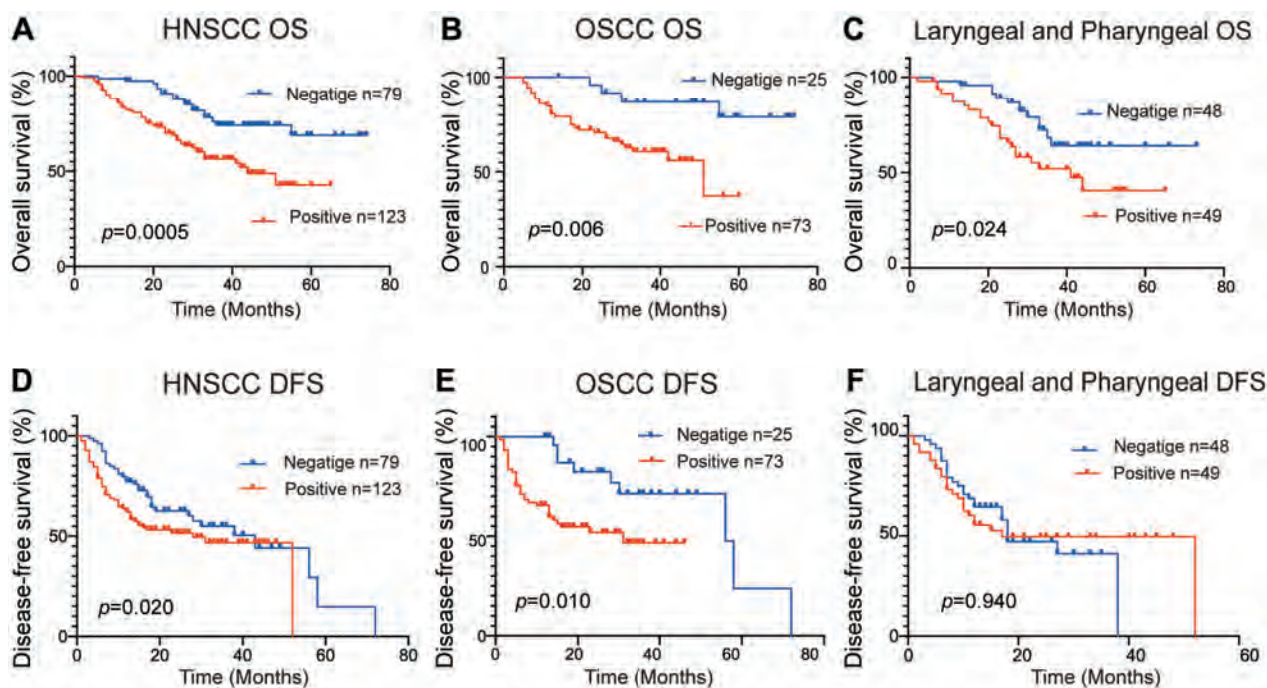
1095

Figure 2. *Kaplan–Meier analyses for overall survival (OS) and disease-free survival (DFS) in 202 HNSCC patients. A) OS curves of 202 HNSCC patients for BP180-positive cases (red line, n=123) and BP180-negative cases (blue line, n=79). B) OS curves of OSCC patients for BP180-positive cases (red line, n=73) and BP180-negative cases (blue line, n=25). C) OS curves of laryngeal and pharyngeal cancer patients for BP180-positive cases (red line, n=49) and BP180-negative cases (blue line, n=48). D) DFS curves of 202 HNSCC patients for BP180-positive cases (red line, n=123) and BP180-negative cases (blue line, n=79). E) DFS curves of OSCC patients for BP180-positive cases (red line, n=73) and BP180-negative cases (blue line, n=25). F) DFS curves of laryngeal and pharyngeal cancer patients for BP180-positive cases (red line, n=49) and BP180-negative cases (blue line, n=48). Values of p<0.05 are considered statistically significant.*

but not in laryngeal and pharyngeal cancer. A key finding was that analysis of OS in laryngeal and pharyngeal cancer revealed a significant difference in the status of BP180 IHC. The possible reason is that there are many relapsed hypopharyngeal cancer patients due to alcohol.

Immunohistochemically, using a mouse monoclonal anti-human BP180 antibody linear staining along the basement membrane and faint cytoplasmic staining in the basal layer of squamous epithelium in limited normal tissues was revealed. BP180 was distributed irregularly or scattered only in layers of the epithelium (13). Parikka *et al.* found similar results in a study of the transformation of oral epithelium to dysplasia and carcinoma, identifying intense staining in carcinoma cells at the invasive front in Grade II OSCC, with signals mainly missing from basal cells and strong signals restricted to the epithelium in cases of dysplasia (5, 14). In our study, the same immune reaction was evident in normal tissues and squamous cell carcinomas. Some studies have proposed that BP180 serves as a cell-matrix adhesion molecule by stabilizing the hemidesmosome complex and mediating anchorage to the underlying basement membranes. Beyond any structural roles, BP180 is presumed to play a

role in cell migration and differentiation to pathological states in malignant tumors (5, 7, 36-38).

Head and neck cancer is a wide disease classification that includes oral, salivary gland, thyroid, nasopharyngeal, laryngeal, oropharyngeal and hypopharyngeal cancers. In addition, oral cancers can arise from squamous epithelium of the tongue, gingiva, palate, buccal mucosa, and mouth floor. The present report offers a first demonstration of the expression profile of BP180 in different primary sites. BP180 positivity rates were 57.1-83.3%, with no marked differences apparent between primary sites of HNSCC ($p=0.643$, Fisher's exact test), but a tendency toward higher expression was noted in the current OSCC cohort ($p=0.084$, Fisher's exact test). We were surprised to observe that comparing OSCC with laryngeal and pharyngeal cancer, BP180 positivity was 74.5% for OSCC and 50.5% for laryngeal and pharyngeal cancer ($p=0.001$, Pearson's chi-square test) (Tables III and IV). We hypothesize that BP180 expression in HNSCC correlates with anatomical localization. In a TMA of 124 HNSCCs, BP180 expression was found to be higher in the oral cavity (85.7%) than in other anatomical localizations (39). We found differences in BP180 positivity in some anatomical areas as
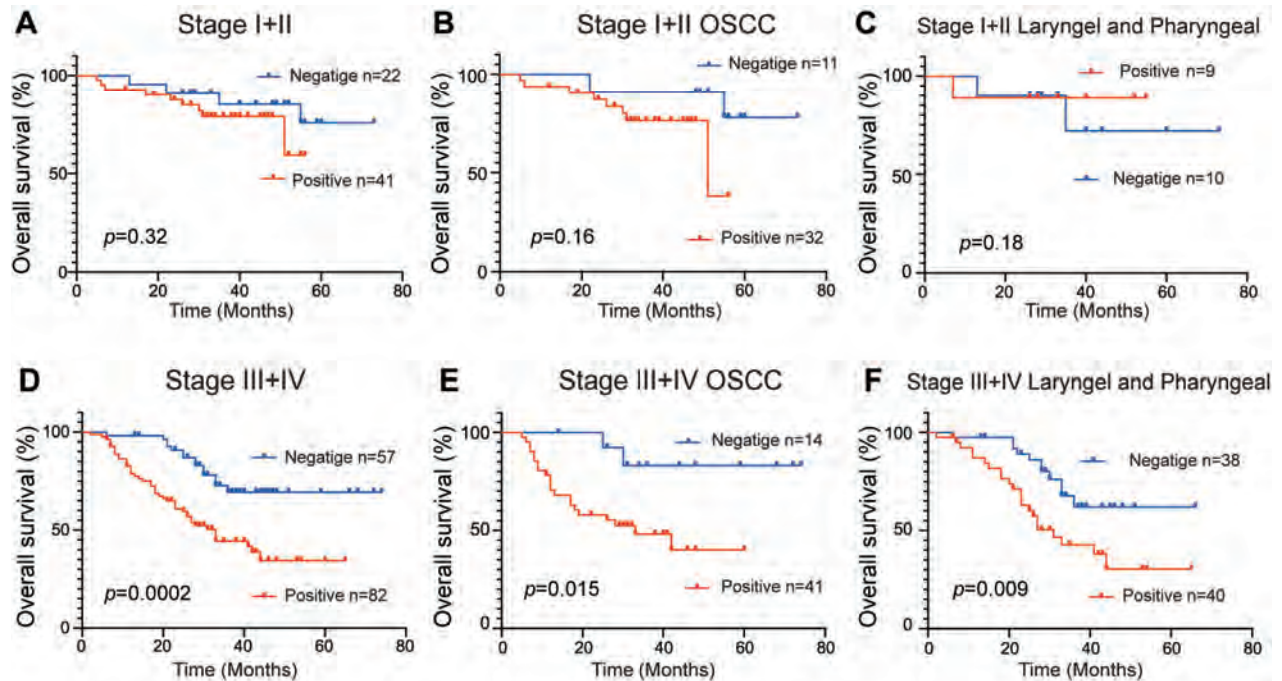
1096

Figure 3. *Kaplan–Meier analyses for overall survival (OS) in early and late clinical stage HNSCC patients. A) OS curves of 63 HNSCC patients in stage I+II for BP180-positive cases (red line, n=41) and BP180-negative cases (blue line, n=22). B) OS curves of 43 OSCC patients in stage I+II for BP180-positive cases (red line, n=32) and BP180-negative cases (blue line, n=11). C) OS curves of 19 laryngeal and pharyngeal cancer patients in stage I+II for BP180-positive cases (red line, n=9) and BP180-negative cases (blue line, n=10). D) OS curves of 139 HNSCC patients in stage III+IV for BP180-positive cases (red line, n=82) and BP180-negative cases (blue line, n=57). E) OS curves of 55 OSCC patients in stage III+IV for BP180-positive cases (red line, n=41) and BP180-negative cases (blue line, n=14). F) OS curves of 78 laryngeal and pharyngeal cancer patients in stage III+IV for BP180-positive cases (red line, n=40) and BP180-negative cases (blue line, n=38). Values of p<0.05 are considered statistically significant.*

novel data, and attributed this to differences in mucosal structure and function. The mucous membrane in the oral cavity is mostly used for maintaining an environment suitable for chewing and ingesting food, whereas the mucous membranes of the pharynx and larynx play important roles in immune function and vocalization. These results provide a clinical basis for future research into the pathological mechanisms of and drug-targeted therapies for HNSCC.

Based on the current research, a possible tumorigenesis mechanism is that the structural extracellular domain (ECD) of BP180 connects cytoplasmic structural components with the extracellular matrix (ECM). The ECD is essential for proper basement membrane formation. In the absence of normal regulation, changes in the ECM may contribute to the first steps toward cancer. Recent data have demonstrated that alterations in BP180 exert profound effects on cancer tumorigenesis, progression, invasion and migration in different kinds of cancers, as mentioned above (40-42). Our findings provide clinical data in support of this notion that BP180 is a factor associated with poor prognosis. However, several potential limitations must be considered. First, the

sample size was quite limited and data from more cases is needed. In addition, the molecular mechanisms underlying the effects of BP180 on HNSCC need to be clarified. At last, we did not have an in-depth analysis of surgical related factors.

In conclusion, the present study suggests that BP180 is a prognostic factor for HNSCC. Moreover, multivariate analysis suggested BP180 as a significant independent prognostic factor along with clinical stage in patients with HNSCC. Overall, the prognostic value of BP180 expression in this study provides an important experimental foundation for closer examination of this potentially significant biomarker in targeted treatments for patients with HNSCC.

Conflicts of Interest

The Authors declare that there are no conflicts of interest in relation to this study.

Authors' Contributions

X.M. performed experiments, analyzed the data and wrote the article. F.M. and K.I. analyzed the data and revised the article. T.M.

1097

References

1 Bray F, Ferlay J, Soerjomataram I, Siegel RL, Torre LA and Jemal A: Global cancer statistics 2018: Globocan estimates of incidence and mortality worldwide for 36 cancers in 185 countries. CA Cancer J Clin 68(6): 394-424, 2018. PMID: 30207593. DOI: 10.3322/caac.21492

2 Pfister DG, Spencer S, Brizel DM, Burtness B, Busse PM, Caudell JJ, Cmelak AJ, Colevas AD, Dunphy F, Eisele DW, Gilbert J, Gillison ML, Haddad RI, Haughey BH, Hicks WL, Jr., Hitchcock YJ, Jimeno A, Kies MS, Lydiatt WM, Maghami E, Martins R, McCaffrey T, Mell LK, Mittal BB, Pinto HA, Ridge JA, Rodriguez CP, Samant S, Schuller DE, Shah JP, Weber RS, Wolf GT, Worden F, Yom SS, McMillian NR and Hughes M: Head and neck cancers, version 2.2014. Clinical practice guidelines in oncology. J Natl Compr Canc Netw 12(10): 1454-1487, 2014. PMID: 25313184. DOI: 10.6004/jnccn.2014.0142

3 Chow LQM: Head and neck cancer. N Engl J Med 382(1): 60-72, 2020. PMID: 31893516. DOI: 10.1056/NEJMra1715715

4 Braakhuis BJ, Brakenhoff RH and Leemans CR: Treatment choice for locally advanced head and neck cancers on the basis of risk factors: Biological risk factors. Ann Oncol 23: x173-177, 2012. PMID: 22987957. DOI: 10.1093/annonc/mds299

5 Parikka M, Kainulainen T, Tasanen K, Bruckner-Tuderman L and Salo T: Altered expression of collagen XVII in ameloblastomas and basal cell carcinomas. J Oral Pathol Med 30(10): 589-595, 2001. PMID: 11722708. DOI: 10.1034/j.1600-0714.2001.301003.x

6 Hammers CM and Stanley JR: Mechanisms of disease: Pemphigus and bullous pemphigoid. Annu Rev Pathol 11: 175-197, 2016. PMID: 26907530. DOI: 10.1146/annurev-pathol-012615-044313

7 Jones VA, Patel PM, Gibson FT, Cordova A and Amber KT: The role of collagen XVII in cancer: Squamous cell carcinoma and beyond. Front Oncol 10: 352, 2020. PMID: 32266137. DOI: 10.3389/fonc.2020.00352

8 Walko G, Castañón MJ and Wiche G: Molecular architecture and function of the hemidesmosome. Cell Tissue Res 360(3): 529-544, 2015. PMID: 26017636. DOI: 10.1007/s00441-015-2216-6

9 De Pascalis C and Etienne-Manneville S: Single and collective cell migration: The mechanics of adhesions. Mol Biol Cell 28(14): 1833-1846, 2017. PMID: 28684609. DOI: 10.1091/mbc.E17-03-0134

10 Walker C, Mojares E and Del Río Hernández A: Role of extracellular matrix in development and cancer progression. Int J Mol Sci 19(10): 3028, 2018. PMID: 30287763. DOI: 10.3390/ijms19103028

11 Moilanen JM, Löffek S, Kokkonen N, Salo S, Väyrynen JP, Hurskainen T, Manninen A, Riihilä P, Heljasvaara R, Franzke CW, Kähäri VM, Salo T, Mäkinen MJ and Tasanen K: Significant role of collagen XVII and integrin β4 in migration and invasion of the less aggressive squamous cell carcinoma cells. Sci Rep 7: 45057, 2017. PMID: 28327550. DOI: 10.1038/srep45057

12 Stelkovics E, Korom I, Marczinovits I, Molnar J, Rasky K, Raso E, Ficsor L, Molnar B, Kopper L and Krenacs T: Collagen XVII/BP180 protein expression in squamous cell carcinoma of the skin detected with novel monoclonal antibodies in archived tissues using tissue microarrays and digital microscopy. Appl Immunohistochem Mol Morphol 16(5): 433-441, 2008. PMID: 18633319. DOI: 10.1097/PAI.0b013e318162f8aa

13 Yamada T, Endo R, Tsukagoshi K, Fujita S, Honda K, Kinoshita M, Hasebe T and Hirohashi S: Aberrant expression of a hemidesmosomal protein, bullous pemphigoid antigen 2, in human squamous cell carcinoma. Lab Invest 75(4): 589-600, 1996. PMID: 8874389.

14 Parikka M, Kainulainen T, Tasanen K, Väänänen A, Bruckner-Tuderman L and Salo T: Alterations of collagen XVII expression during transformation of oral epithelium to dysplasia and carcinoma. J Histochem Cytochem 51(7): 921-929, 2003. PMID: 12810842. DOI: 10.1177/002215540305100707

15 Löffek S, Hurskainen T, Jackow J, Sigloch FC, Schilling O, Tasanen K, Bruckner-Tuderman L and Franzke CW: Transmembrane collagen XVII modulates integrin dependent keratinocyte migration via PI3K/RAC1 signaling. PLoS One 9(2): e87263, 2014. PMID: 24505282. DOI: 10.1371/journal.pone.0087263

16 Moilanen JM, Kokkonen N, Löffek S, Väyrynen JP, Syväniemi E, Hurskainen T, Mäkinen M, Klintrup K, Mäkelä J, Sormunen R, Bruckner-Tuderman L, Autio-Harmainen H and Tasanen K: Collagen XVII expression correlates with the invasion and metastasis of colorectal cancer. Hum Pathol 46(3): 434-442, 2015. PMID: 25623077. DOI: 10.1016/j.humpath.2014.11.020

17 Liu CC, Lin SP, Hsu HS, Yang SH, Lin CH, Yang MH, Hung MC and Hung SC: Suspension survival mediated by pp2a-stat3-col XVII determines tumour initiation and metastasis in cancer stem cells. Nat Commun 7: 11798, 2016. PMID: 27306323. DOI: 10.1038/ncomms11798

18 Hsu HS, Liu CC, Lin JH, Hsu TW, Hsu JW, Li AF and Hung SC: Involvement of collagen XVII in pluripotency gene expression and metabolic reprogramming of lung cancer stem cells. J Biomed Sci 27(1): 5, 2020. PMID: 31928533. DOI: 10.1186/s12929-019-0593-y

19 Liu CC, Lin JH, Hsu TW, Hsu JW, Chang JW, Su K, Hsu HS and Hung SC: Collagen XVII/Laminin-5 activates epithelial-to-mesenchymal transition and is associated with poor prognosis in lung cancer. Oncotarget 9(2): 1656-1672, 2018. PMID: 29416721. DOI: 10.18632/oncotarget.11208

20 Otsubo K, Goto H, Nishio M, Kawamura K, Yanagi S, Nishie W, Sasaki T, Maehama T, Nishina H, Mimori K, Nakano T, Shimizu H, Mak TW, Nakao K, Nakanishi Y and Suzuki A: MOB1-YAP1/TAZ-NKX2.1 axis controls bronchioalveolar cell differentiation, adhesion and tumour formation. Oncogene 36(29): 4201-4211, 2017. PMID: 28346423. DOI: 10.1038/onc.2017.58

1098

21 Thangavelu PU, Krenács T, Dray E and Duijf PH: In epithelial cancers, aberrant COL17A1 promoter methylation predicts its misexpression and increased invasion. Clin Epigenet *8*: 120, 2016. PMID: 27891193. DOI: 10.1186/s13148-016-0290-6

22 Krenacs T, Kiszner G, Stelkovics E, Balla P, Teleki I, Nemeth I, Varga E, Korom I, Barbai T, Plotar V, Timar J and Raso E: Collagen XVII is expressed in malignant but not in benign melanocytic tumors and it can mediate antibody induced melanoma apoptosis. Histochem Cell Biol *138(4)*: 653-667, 2012. PMID: 22688676. DOI: 10.1007/s00418-012-0981-9

23 Bergstraesser LM, Srinivasan G, Jones JC, Stahl S and Weitzman SA: Expression of hemidesmosomes and component proteins is lost by invasive breast cancer cells. Am J Pathol *147(6)*: 1823-1839, 1995. PMID: 7495306.

24 Lo AK, Yuen PW, Liu Y, Wang XH, Cheung AL, Wong YC and Tsao SW: Downregulation of hemidesmosomal proteins in nasopharyngeal carcinoma cells. Cancer Lett *163(1)*: 117-123, 2001. PMID: 11163115. DOI: 10.1016/s0304-3835(00)00683-2

25 Kim SH, Carey TE, Liebert M, Yoo SJ, Kwon HJ and Kim SY: Characterization of AMC-HN-9, a cell line established from an undifferentiated carcinoma of the parotid gland: Expression of alpha6beta4 with the absence of BP180 and 230. Acta Otolaryngol *120(5)*: 660-666, 2000. PMID: 11039880. DOI: 10.1080/000164800750000513

26 Aho S and Uitto J: 180-kd bullous pemphigoid antigen/type XVII collagen: Tissue-specific expression and molecular interactions with keratin 18. J Cell Biochem *72(3)*: 356-367, 1999. PMID: 10022517. DOI: 10.1002/(sici)1097-4644(19990301)72:3<356::aid-jcb5>3.0.co;2-m

27 El-Naggar AK, Chan JKCC, Grandis JR, Takata T and Slootweg PJ: WHO classification of head and neck tumours, 4th Edition, 2017.

28 Ohtomo R, Mori T, Shibata S, Tsuta K, Maeshima AM, Akazawa C, Watabe Y, Honda K, Yamada T, Yoshimoto S, Asai M, Okano H, Kanai Y and Tsuda H: SOX10 is a novel marker of acinus and intercalated duct differentiation in salivary gland tumors: A clue to the histogenesis for tumor diagnosis. Mod Pathol *26(8)*: 1041-1050, 2013. PMID: 23558573. DOI: 10.1038/modpathol.2013.54

29 Watabe Y, Mori T, Yoshimoto S, Nomura T, Shibahara T, Yamada T and Honda K: Copy number increase of ACTN4 is a prognostic indicator in salivary gland carcinoma. Cancer Med *3(3)*: 613-622, 2014. PMID: 24574362. DOI: 10.1002/cam4.214

30 Watanabe T, Ueno H, Watabe Y, Hiraoka N, Morizane C, Itami J, Okusaka T, Miura N, Kakizaki T, Kakuya T, Kamita M, Tsuchida A, Nagakawa Y, Wilber H, Yamada T and Honda K: ACTN4 copy number increase as a predictive biomarker for chemoradiotherapy of locally advanced pancreatic cancer. Br J Cancer *112(4)*: 704-713, 2015. PMID: 25602965. DOI: 10.1038/bjc.2014.623

31 Liu Y, Li L and Xia Y: BP180 is critical in the autoimmunity of bullous pemphigoid. Front Immunol *8*: 1752, 2017. PMID: 29276517. DOI: 10.3389/fimmu.2017.01752

32 Monshi B, Gulz L, Piringer B, Wiala A, Kivaranovic D, Schmidt M, Sesti A, Heil T, Vujic I, Posch C and Rappersberger K: Anti-BP180 autoantibody levels at diagnosis correlate with 1-year mortality rates in patients with bullous pemphigoid. J Eur Acad Dermatol Venereol *34(7)*: 1583-1589, 2020. PMID: 32170780. DOI: 10.1111/jdv.16363

33 Zhou XP, Liu B, Xu Q, Yang Y, He CX, Zuo YG and Liu YH: Serum levels of immunoglobulins G1 and G4 targeting the non-collagenous 16A domain of BP180 reflect bullous pemphigoid activity and predict bad prognosis. J Dermatol *43(2)*: 141-148, 2016. PMID: 26300465. DOI: 10.1111/1346-8138.13051

34 Bourdon-Lanoy E, Roujeau JC, Joly P, Guillaume JC, Bernard P, Prost C, Tancrède-Bohin E, Delaporte E, Picard-Dahan C, Albes B, Bedane C, Doutre MS, Chosidow O, Lok C, Pauwels C, Chevrand-Breton J, Sassolas B and Richard MA: Bullous pemphigoid in young patients: A retrospective study of 74 cases. Ann Dermatol Venereol *132(2)*: 115-122, 2005. PMID: 15798559. DOI: 10.1016/s0151-9638(05)79220-6

35 Bernard P, Reguiai Z, Tancrède-Bohin E, Cordel N, Plantin P, Pauwels C, Vaillant L, Grange F, Richard-Lallemand MA, Sassolas B, Roujeau JC, Lok C, Picard-Dahan C, Chosidow O, Vitry F and Joly P: Risk factors for relapse in patients with bullous pemphigoid in clinical remission: A multicenter, prospective, cohort study. Arch Dermatol *145(5)*: 537-542, 2009. PMID: 19451497. DOI: 10.1001/archdermatol.2009.53

36 Powell AM, Sakuma-Oyama Y, Oyama N and Black MM: Collagen XVII/BP180: A collagenous transmembrane protein and component of the dermoepidermal anchoring complex. Clin Exp Dermatol *30(6)*: 682-687, 2005. PMID: 16197389. DOI: 10.1111/j.1365-2230.2005.01937.x

37 Tanimura S, Tadokoro Y, Inomata K, Binh NT, Nishie W, Yamazaki S, Nakauchi H, Tanaka Y, McMillan JR, Sawamura D, Yancey K, Shimizu H and Nishimura EK: Hair follicle stem cells provide a functional niche for melanocyte stem cells. Cell Stem Cell *8(2)*: 177-187, 2011. PMID: 29033351. DOI: 10.1016/j.stem.2010.11.029

38 Laval S, Laklai H, Fanjul M, Pucelle M, Laurell H, Billon-Galés A, Le Guellec S, Delisle MB, Sonnenberg A, Susini C, Pyronnet S and Bousquet C: Dual roles of hemidesmosomal proteins in the pancreatic epithelium: The phosphoinositide 3-kinase decides. Oncogene *33(15)*: 1934-1944, 2014. PMID: 23624916. DOI: 10.1038/onc.2013.146

39 Tamás L, Szentkúti G, Eros M, Dános K, Brauswetter D, Szende B, Zsákovics I and Krenács T: Differential biomarker expression in head and neck cancer correlates with anatomical localization. Pathol Oncol Res *17(3)*: 721-727, 2011. PMID: 21487776. DOI: 10.1007/s12253-011-9376-9

40 Nishie W, Kiritsi D, Nyström A, Hofmann SC and Bruckner-Tuderman L: Dynamic interactions of epidermal collagen XVII with the extracellular matrix: Laminin 332 as a major binding partner. Am J Pathol *179(2)*: 829-837, 2011. PMID: 21801871. DOI: 10.1016/j.ajpath.2011.04.019

41 Franzke CW, Tasanen K, Schäcke H, Zhou Z, Tryggvason K, Mauch C, Zigrino P, Sunnarborg S, Lee DC, Fahrenholz F and Bruckner-Tuderman L: Transmembrane collagen XVII, an epithelial adhesion protein, is shed from the cell surface by ADAMs. Embo J *21(19)*: 5026-5035, 2002. PMID: 12356719. DOI: 10.1093/emboj/cdf532

42 Nishimura M, Nishie W, Shirafuji Y, Shinkuma S, Natsuga K, Nakamura H, Sawamura D, Iwatsuki K and Shimizu H: Extracellular cleavage of collagen XVII is essential for correct cutaneous basement membrane formation. Hum Mol Genet *25(2)*: 328-339, 2016. PMID: 26604146. DOI: 10.1093/hmg/ddv478

傻傻的落寞

在广岛开学术会，买返程新干线票路上，突发心脏骤停的乘客，乘务员呼叫没有反应，我去摸了脉搏没有，CPR，黄金4分钟，30:2…真是日语同时方恨少，直接操作，和图片上黑衣服姐姐轮换，很快面色恢复了，3-5分钟消防救护和AED机器也迅速赶到，希望一切平安…

东京 · 顺天堂大学 医学部

1小时前

♡ A太郎🐺, 朔朔朔朔, 阿噗, 李高娃

袁世華: 孟雪，给你点赞。我们是笹川奖学金研究员，无论何时何地，不会忘记感恩。我们是医务工作者，无论何时何地，不会见死不救。

李高娃 回复 袁世華: 袁老师说出了我的心声👍

孟さんは学術会議に参加するため、広島へ行きました。今回の緊急救助活動は、会議終了後、10月2日夕方ぐらいホテルから広島駅へ移動中にあったことです。孟さんは広島電鉄2号線に乗車して、終点の広島駅に到着する手前に、同車両の後部座席に座っていた40-50代の男性は意識が無くなったことを巡回していた乗務員に発見され、何回も声かけても、まったく返事がなかったです。孟さんは心臓停止の可能性があると判断し、即時に男性の脈を確認したところ、既に脈はなくなりました。心臓停止の最初の4分間に救助を施すことはとても重要だと思われ、孟さんは躊躇なく、その後に同じく救助のために近づいてきた黒い服の女性と交代でCPR（心肺蘇生法）を実施し、男性の顔色はようやく紫色よりだんだん正常の肌色に回復してきました。

5分ぐらい経ってから救助隊も来て、男性を車両より搬出しました。